INFORMATION TO USERS

This manuscript has been reproduced from the microfilm master. UMI films the text directly from the original or copy submitted. Thus, some thesis and dissertation copies are in typewriter face, while others may be from any type of computer printer.

The quality of this reproduction is dependent upon the quality of the copy submitted. Broken or indistinct print, colored or poor quality illustrations and photographs, print bleedthrough, substandard margins, and improper alignment can adversely affect reproduction.

In the unlikely event that the author did not send UMI a complete manuscript and there are missing pages, these will be noted. Also, if unauthorized copyright material had to be removed, a note will indicate the deletion.

Oversize materials (e.g., maps, drawings, charts) are reproduced by sectioning the original, beginning at the upper left-hand corner and continuing from left to right in equal sections with small overlaps. Each original is also photographed in one exposure and is included in reduced form at the back of the book.

Photographs included in the original manuscript have been reproduced xerographically in this copy. Higher quality 6" x 9" black and white photographic prints are available for any photographs or illustrations appearing in this copy for an additional charge. Contact UMI directly to order.

UMI

A Bell & Howell Information Company
300 North Zeeb Road, Ann Arbor MI 48106-1346 USA
313/761-4700   800/521-0600

COMPUTER-AIDED ENGINEERING OF
ADVANCED MULTILAYER CERAMIC CAPACITORS

By

VINAY SRINIVAS

A DISSERTATION PRESENTED TO THE GRADUATE SCHOOL
OF THE UNIVERSITY OF FLORIDA IN PARTIAL FULFILLMENT
OF THE REQUIREMENTS FOR THE DEGREE OF
DOCTOR OF PHILOSOPHY

UNIVERSITY OF FLORIDA

1996

UMI Number: 9703614

UMI

300 North Zeeb Road
Ann Arbor, MI 48103

To my parents ... ...

without their encouragement and confidence this would not have been possible.

From a long view of the history of mankind—seen from, say, 10,000 years from now—there can be little doubt that the most significant event of the 19th century will be judged as Maxwell's discovery of the laws of electrodynamics. The American Civil War will pale into provincial insignificance in comparison with this important scientific event of the same decade.

Richard P. Feynman

ACKNOWLEDGEMENTS

TABLE OF CONTENTS

vi

viii

KEY TO SYMBOLS

Roman alphabets

$\mathbf{A}$: Magnetic vector potential

$\mathbf{A}^*$: Electric vector potential defined with $\mathbf{D}$

$\tilde{\mathcal{A}}$: Column matrix containing the degrees of freedom corresponding to $\mathbf{A}$

$\mathbf{B}$: Magnetic induction

B : "Damping" matrix; related to conductivity σ

$\mathcal{B}$: "Damping" matrix before imposing the essential boundary condition

$\mathbb{C}$: A space containing all the complex numbers

C : Capacitance

$\mathbf{D}$: Electric induction

$\{d\}$: Unknown coefficients in the Finite Element formulation

$\mathbf{E}$: Electric field

$\hat{\mathbf{e}}_1, \hat{\mathbf{e}}_2, \hat{\mathbf{e}}_3$

   : Unit basis vectors in Cartesian co-ordinate axes

$\mathbf{F}$: Force

$\mathbf{f}$: A general function or force per unit volume

f : Frequency ($f = \omega/(2\pi)$)

$\mathcal{G}_b$: Energy associated with the "damping" term in the transient problem

$\mathcal{G}_f$: Energy associated with the "force" term in the transient problem

$\mathcal{G}_k$: Energy associated with the "stiffness" term in the transient problem

ix

$\mathcal{G}_m$: Energy associated with the "mass" term in the transient problem

$\mathcal{G}_{f_0}$: Energy associated with the "force" term in the static problem

$\mathcal{G}_{k_0}$: Energy associated with the "stiffness" term in the static problem

$\mathcal{G}_{m_0}$: Energy associated with the "mass" term in the static problem

$\bar{\mathcal{G}}_b$: Energy associated with the "damping" term in the time-harmonic problem

$\bar{\mathcal{G}}_f$: Energy associated with the "force" term in the time-harmonic problem

$\bar{\mathcal{G}}_k$: Energy associated with the "stiffness" term in the time-harmonic problem

$\bar{\mathcal{G}}_m$: Energy associated with the "mass" term in the time-harmonic problem

$\mathbf{H}$: Magnetic field

$\mathcal{H}^k$: Sobolev space of functions that are square integrable upto k^{th} order partial derivatives

$\mathbf{H}_m$: Homogeneous part of the magnetic field $\mathbf{H}$ (i.e., with $\mathbf{J}_f = 0$)

$\mathbf{H}_s$: Particular part of the magnetic field $\mathbf{H}$ (i.e., with $\mathbf{J}_f \neq 0$)

I : Current

i : Equal to $\sqrt{-1}$

$\mathbf{J}_f$: Volumetric free-current density, induced by electric field $\mathbf{E}$

$\mathbf{J}_a$: Applied free-current volume density

K : "Stiffness" matrix; related to permeability μ

$\mathcal{K}$: "Stiffness" matrix before imposing the essential boundary condition

$\mathbf{K}_a$: Applied free-current surface density

$\mathbf{K}_f$: Induced free-current surface density

$\mathcal{L}$: A curve

L : Inductance

L_2 : Hilbert space of square integrable functions $(= \mathcal{H}^0)$

x

$\mathbf{M}$: Magnetization vector

$\mathfrak{M}$: Mutual induction.

M : "Mass" matrix; related to permittivity ϵ.

$\mathcal{M}$: "Mass" matrix before imposing the essential boundary condition

$\aleph$: Number of nodes in the finite element mesh

$\mathbf{N}$: Weighting function

N : A matrix of the basis functions corresponding to $\mathbf{A}$ and ψ

N_A : A matrix of the basis functions corresponding to $\mathbf{A}$

N_ψ : A matrix of the basis functions corresponding to ψ

N_i : The ith component of the weighting function

n_A : Number of nodes at which $\mathbf{A}$ has to be determined

n_ψ : Number of nodes at which ψ has to be determined

$\hat{\mathbf{n}}$: Unit normal

$\mathcal{P}$: Power

$\mathcal{P}_E$: Power due to the displacement current

$\mathcal{P}_H$: Power due to the magnetic field

$\mathcal{P}_J$: Power due to the electric current

$\mathbf{P}$: Electric polarization

p : Machine precision (e.g., single, double, etc)

$\flat$: Penalty parameter for the Coulomb gauge

Q : Dimensionless parameter

$\mathbf{R}$: A space containing all the real numbers

R : Resistance

$\mathcal{T}_h$: Finite element triangulation

$\mathbf{T}$: Electric vector potential defined with $\mathbf{J}_f$

$\hat{t}$: A unit tangent vector

$\mathbf{u}$: The U-field used to define the algebraic gauge

$\mathcal{V}_A$: Space of weighting functions $\mathbf{W}_A$ corresponding to the $\mathbf{A}$ potential
      (Transient problem)

$\mathcal{V}_{A_0}$: Space of weighting functions $\mathbf{W}_A$ corresponding to the $\mathbf{A}$ potential
      (Static problem)

$\bar{\mathcal{V}}_A$: Space of weighting functions $\bar{\mathbf{W}}_A$ corresponding to the $\mathbf{A}$ potential
      (Time-harmonic problem)

$\mathcal{V}_\psi$: Space of weighting functions W_ψ corresponding to the ψ potential
      (Transient problem)

$\mathcal{V}_{\psi_0}$: Space of weighting functions W_ψ corresponding to the ψ potential
      (Static problem)

$\bar{\mathcal{V}}_\psi$: Space of weighting functions $\bar{W}_\psi$ corresponding to the ψ potential
      (Time-harmonic problem)

V : Voltage

v : Velocity of the electromagnetic wave

$\mathbf{W}$: Weighting function for Ampere's law and the time integrated continuity
      equation combined (Transient and static problem)

$\bar{\mathbf{W}}$: Weighting function for Ampere's law and the time integrated continuity
      equation combined (Time-harmonic problem)

$\mathbf{w}$: The field used to define the algebraic gauge

$\mathbf{W}_A$: Weighting function for Ampere's law

W_ψ : Weighting function for the time integrated continuity equation

$\mathbf{x}$: A point in space $\mathbf{R}^3$

$\mathbf{x}'$: A point in space $\mathbf{R}^3$

Z : Impedance

<u>Greek alphabets</u>

α_x : Numerical scaling factor for length

α_x^{opt} : Optimal (least condition number) numerical scaling factor for length

Γ_{h_A} : The part of the boundary $\partial\Omega$ on which $(\mathbf{H} \times \hat{\mathbf{n}})_a$ is specified (Transient problem)

Γ_{g_A} : The part of the boundary $\partial\Omega$ on which $\mathbf{A}_a$ is specified (Transient problem)

$\Gamma_{h_{A_0}}$: The part of the boundary $\partial\Omega$ on which $(\mathbf{H}_0 \times \hat{\mathbf{n}})_a$ is specified (Static problem)

$\Gamma_{g_{A_0}}$: The part of the boundary $\partial\Omega$ on which $\mathbf{A}_{a_0}$ is specified (Static problem)

$\Gamma_{h_{A_r}}$: The part of the boundary $\partial\Omega$ on which $(\mathbf{H}_{0r} \times \hat{\mathbf{n}})_a$ is specified

(Time-harmonic problem)

$\Gamma_{g_{A_r}}$: The part of the boundary $\partial\Omega$ on which $\mathbf{A}_{ar}$ is specified

(Time-harmonic problem)

$\Gamma_{h_{A_i}}$: The part of the boundary $\partial\Omega$ on which $(\mathbf{H}_{0i} \times \hat{\mathbf{n}})_a$ is specified

(Time-harmonic problem)

$\Gamma_{g_{A_i}}$: The part of the boundary $\partial\Omega$ on which $\mathbf{A}_{ai}$ is specified

(Time-harmonic problem)

Γ_{h_ψ} : The part of the boundary $\partial\Omega$ on which $\left(\left(\dfrac{\partial\mathbf{D}}{\partial t} + \mathbf{J}_f\right) \times \hat{\mathbf{n}}\right)_a$ is specified

(Transient problem)

Γ_{g_ψ} : The part of the boundary $\partial\Omega$ on which ψ_a is specified (Transient problem)

$\Gamma_{h\dot{\psi}_0}$: The part of the boundary $\partial(\Omega \setminus \Omega_{cond})$ on which $\left(\left(\dfrac{\partial \mathbf{D}_0}{\partial t} + \mathbf{J}_{f_0}\right) \times \hat{\mathbf{n}}\right)_a$ is specified

(Static problem)

$\Gamma_{g\dot{\psi}_0}$: The part of the boundary $\partial(\Omega \setminus \Omega_{cond})$ on which $\dot{\psi}_{0_a}$ is specified (Static problem)

$\Gamma_{h\psi_r}$: The part of the boundary $\partial\Omega$ on which $\left(\left(-\omega\mathbf{D}_i + \mathbf{J}_{f_r}\right) \times \hat{\mathbf{n}}\right)_a$ is specified

(Time-harmonic problem)

$\Gamma_{g\psi_r}$: The part of the boundary $\partial\Omega$ on which ψ_{a_r} is specified (Time-harmonic problem)

$\Gamma_{h\psi_i}$: The part of the boundary $\partial\Omega$ on which $\left(\left(\omega\mathbf{D}_r + \mathbf{J}_{f_i}\right) \times \hat{\mathbf{n}}\right)_a$ is specified

(Time-harmonic problem)

$\Gamma_{g\psi_i}$: The part of the boundary $\partial\Omega$ on which ψ_{a_i} is specified (Time-harmonic problem)

Υ_0 : Combined potential for the static problem

δ : Skin depth

δ_{ij} : Kronecker delta. $\delta_{ij} = 0$ if $i \neq j$, and $\delta_{ii} = 1$

ϵ_0 : Permittivity of free space

ϵ : Permittivity of a material

ε_{ijk} : Permutation symbol

Λ : Wavelength of the electromagnetic wave

μ_0 : Permeability of free space

μ : Permeability of a material

Π : Combined potential, i.e., includes potentials ψ and $\mathbf{A}$

Π_0 : Combined potential for the static problem

ϖ : An integer, i.e., belongs to the set $\{1, 2, 3, \cdots\}$

ρ_a : Applied volume free-charge density

ρ_{a0} : Applied volume free-charge density at $t = 0$.

ρ_f : Induced volume free-charge density (due to the electric field)

ρ_{f0} : Induced volume free-charge density at $t = 0$.

σ : Conductivity of a material

σ_a : Applied surface free-charge density

σ_f : Induced surface free-charge density

τ : Machine base (e.g., binary, octal, etc)

ϕ : Electric scalar potential

ϕ^* : Magnetic scalar potential defined with $\mathbf{A}^*$

ϕ_m : Total magnetic scalar potential

ψ : Time-integrated electric scalar potential

ψ_m : Reduced scalar potential

$\tilde{\psi}$: Column matrix containing the degrees of freedom corresponding to ψ

Ω : Volume (domain of computation)

Ω : Magnetic scalar potential

Ω_{cond}: Domain of the conductors inside Ω, where $\sigma \neq 0$

Ω_{σ_a} : Volume in which ρ_a is imposed

$\partial\Omega$: Boundary of Ω (a closed surface)

$\partial\Omega_{\sigma_a}$: Part of $\partial\Omega$ on which σ_a is imposed

$d\Omega$: Infinitesimal volume element in volumetric integration

ω : Angular frequency ($\omega = 2\pi f$)

List of operators and other symbols

$< \dot{} >$: First time-derivative of $< >$

xv

$< \overset{..}{} >$: Second time-derivative of $< >$

$< \bar{} >$: Indicates $< >$ is a complex quantity

$< \bar{} >^{*}$: Indicates a complex conjugate of $< \bar{} >$

$< >_{r}$: Is the real part of $< \bar{} >$

$< >_{i}$: Is the imaginary part of $< \bar{} >$

$< >_{0}$: Indicates $< >$ is a independent of time t

$< >_{a}$: Indicates $< >$ is an applied (specified) quantity that is known

$^{CGS} < >$: Indicates $< >$ is unrationalized CGS units

$^{GEN} < >$: Indicates $< >$ is generalized units

$^{(l)} < >$: Indicates $< >$ for linear-isotropic materials

$^{RCGS} < >$: Indicates $< >$ is rationalized CGS units

$^{SI} < >$: Indicates $< >$ is SI units

$< >^{[k]}$: Indicates $< >$ is known, i.e., a prescribed in the problem

$< >^{[u]}$: Indicates $< >$ is unknown, and hence, to be computed

$\text{curl} < >$: Curl of vector $< >$

$\text{div} < >$: Divergence of vector $< >$

$\text{grad} < >$: Gradient of $< >$

$\beta_{<>}$: Dimensional multiplicative factor for converting $< >$ from the rationalized

CGS unit system to the generalized unit system

$\alpha_{<>}$: Non-dimensional multiplicative factor for converting a numerical value

$< >$ from the rationalized CGS unit system to the generalized unit system

xvi

Abstract of Dissertation Presented to the Graduate School
of the University of Florida in Partial Fulfillment of the
Requirements for the Degree of Doctor of Philosophy

COMPUTER-AIDED ENGINEERING OF
ADVANCED MULTILAYER CERAMIC CAPACITORS

By

Vinay Srinivas

May, 1996

Chairman: Loc Vu-Quoc
Major Department: Aerospace Engineering, Mechanics, and Engineering Science

The objective of this work is to analyze advanced Multi-Layer Ceramic Capacitors (MLCCs) using the Finite Element (FE) method. The focus is to study the behavior of the capacitor with changing frequency of excitation. In this work, the solution to the FE problem is used to compute the lumped circuit parameters, i.e., the capacitance C, resistance R, and the inductance L, for a range of frequencies.

We introduce a new multiple-scale technique to model electromagnetic systems. We non-dimensionalize and scale the Maxwell equations to a new *generalized* system of units. This decreases the condition number of the matrices in the FE solution, and we thereby reduce the errors significantly. The scaling parameter is decided by the geometry and material properties of the components in the capacitor. The multiple-scale technique permits a change in the scaling parameter, and hence, is easily adapted to components with a variety of geometrical shapes and material properties.

xvii

We introduce two algorithms to efficiently analyze the behavior of a capacitor with changing frequency: The low frequency (much below the self-resonant frequency (srf) of the capacitor) algorithm separates the effect of the electric and magnetic fields and reduces the computational effort required to solve the FE problem, whereas, the high frequency (close to, or above srf) algorithm couples the effect between the electric and the magnetic fields. The advanced MLCCs developed by Ngo [1990] are miniature in size with an intricate network of electrodes. We use these algorithms in conjunction with the multiple scale technique to effectively determine the small values of R, L, and C in MLCCs.

We develop a new FE code that incorporates the multiple-scale technique in conjunction with the low and high frequency algorithms. The code includes routines to compute the lumped parameters (i.e., the R, L, C) from the FE solution (potentials A and ψ). Special mesh generation routines are also developed to accurately describe the complex geometry of the capacitor.

FE analysis used in this work provides a significant improvement over the circuit models used in the past: The capacitance C is now accurately computed as opposed to being estimated from experimental values. The capacitance C computed using FE analysis for a $10\mu Farad$ MLCC developed by Ngo [1990] shows a 20% difference from the experimental value. This difference is attributed to changes in the geometry and the material properties during manufacturing. Unlike a linear distribution of current assumed in the circuit model proposed by Ngo [1992], we compute an accurate distribution of the current in the electrodes. As a consequence, the parasitic parameters R and L computed in this work using FE analysis are smaller than those computed by the circuit model. The proposed methodology and computer implementation can be applied to design and analyze other passive electromagnetic devices.

xviii

CHAPTER 1
INTRODUCTION

Fastest-growing sector of the capacitor industry are surface-mount capacitors
that are used in computers and telecommunication equipment. This high-tech sector
of the capacitor industry constitutes approximately 33% of the $14 billion capacitor
market, out of which $7 billion of capacitors are used by Japan. The demand for
these surface-mount capacitors is growing at a rate of 15% a year. United States
based capacitor manufacturers include AVX corporation, Vishay Intertechnology,
and KEMET. These three manufactures have established themselves in the man-
ufacture of surface-mount capacitors: AVX corporation has 17% ($683 million),
Vishay Intertechnology has 13% ($517 million), and KEMET has 11% ($455 mil-
lion) of the $4 billion global surface-mount capacitor market. AVX corporation is
the second-largest manufacturer in the world of surface-mount capacitors, next to
only Japan's Murata. DeFrancesco [1996] estimates that surface-mount capacitors
would account for 20% of capacitor sales by the year 2000.

Multilayer Ceramic Capacitors (MLCCs) is a surface-mount capacitor that has
seen an annual growth rate of 20% to 25% over the past 20 years. These capacitors
are used in a variety of applications ranging from house-hold devices to satellites.
A present trend in the design of electromagnetic devices is to miniaturize its com-
ponents. As a consequence, most modern electromagnetic devices have a complex
geometry and nonlinear material properties. An accurate computer model of these
devices is crucial to reduce their cost and to improve their design. In recent years,
Finite Element (FE) analysis has become a popular tool to design and analyze these

1

devices.[1] Simplicity in meshing complex geometries, better numerical accuracy, ever increasing number of available FE electromagnetic software, and increased computer resources have contributed to its success.

1.1. MultiLayer Ceramic Capacitors (MLCCs)

MLCCs have up to ten times the capacitance density of state of the art capacitors. Typically, a 10 μf MLCC is packaged in less than 0.15 cubic inch. The electrical performance of the capacitor is characterized by its impedance as a function of frequency. High-quality MLCCs are expected to have their equivalent series inductance (esl) in the order of picohenries. To improve the high-frequency performance of MLCCs, an advanced multilayer matrix capacitor geometry was introduced by Ngo [1990]. These advanced MLCCs consists of alternate electrodes with "positive" and "negative" polarity separated by dielectric sheets; see Figure 7.1 on page 140. These MLCCs are composed of cells, which have a footprint of 0.635cm × 0.635cm. The electrodes are 1.5μm thick, and the dielectric is 15μm thick. The positive electrodes are connected by positive vias. A positive via extends through holes in the dielectric layer and insulatingly through the negative electrodes. Similarly, we have negative vias connecting the negative electrodes. Unlike the conventional MLCC, these advanced MLCCs have terminations distributed on all four sides of the electrode, and therefore have lower equivalent series resistance (esr) and lower equivalent series inductance (esl). The esr and esl degrade the performance of the capacitor beyond the self-resonant frequency. However, low values of esr and esl, combined with high capacitance, increase the self-resonant frequency (srf) and improves the performance of the advanced MLCCs (Ngo [1992]). The MLCC shown

---

[1] FE analysis has been used to model a variety of electromagnetic devices, e.g., electrical machines (Brauer, Larkin, MacNeal and Ruehl [1991]), semi-conductors (Barnes and Lomax [1977]), and piezoelectric devices (Lerch [1990]).

in Figure 1.1 has 14 pairs of electrodes along the thickness, and 4×4 cells along the width of the capacitor; the figure is not drawn to scale. A detailed description of the complicated geometry of an advanced MLCC is given in Chapter 7.

1.2. Research Objectives

Prymak and Martin [1989] and others suggest that simple formulae such as those in Grover [1973] cannot be used for unconventional electrode geometries. However, circuit models have been developed by Ngo [1992] to simulate the behavior of the advanced MLCCs at low frequencies (in the order of megahertz). Figure 1.2 shows a single cell in a capacitor. The MLCC in Figure 1.1 is constructed by arranging these single cells in a novel architecture. The circuit model for the entire capacitor is constructed by connecting the equivalent circuits for all the 4×4 cells together. Discrepancies remain between the simulation and the experimental results. Anand [1993] attributes these discrepancies to a need for a better approximation to the current path and its distribution in the electrodes.

The objective of this work is to analyze MLCCs using the Finite Element (FE) method. The focus is on advanced MLCCs designed by Ngo [1990]. We compute the lumped parameters, i.e., the capacitance C, resistance R, and the inductance L, for a range of frequencies. These lumped parameters are then used to compute the *esr*, *esl* and *srf* of the MLCC. We employ a coupled formulation to compute the interaction between the electric and magnetic fields. We study the distribution of current inside the electrodes of the MLCC. We compare the FE solution to the circuit models. The formulation, the implementation, and the subsequent results demonstrate the efficacy of FE analysis and establishes a systematic methodology to design and analyze advanced electromagnetic components.
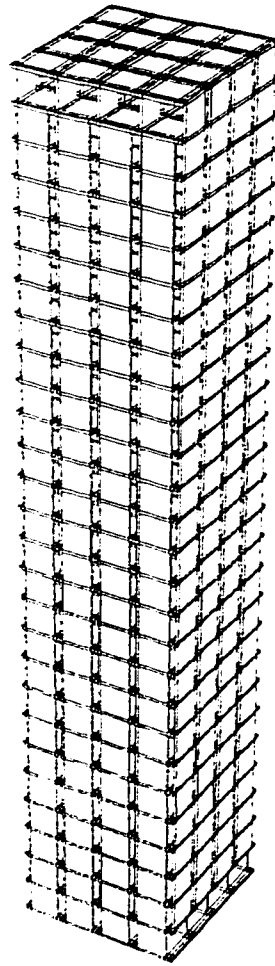
Figure 1.1. A 10 μ *Farad* advanced Multi Layer Ceramic Capacitor (MLCC) proposed by Ngo [1990]. The figure is not drawn to scale. The footprint of the capacitor is approximately 2.54×10^{-2} $m \times 2.54 \times 10^{-2}$ m, and the thickness (height) is approximately 4.5×10^{-4} m.
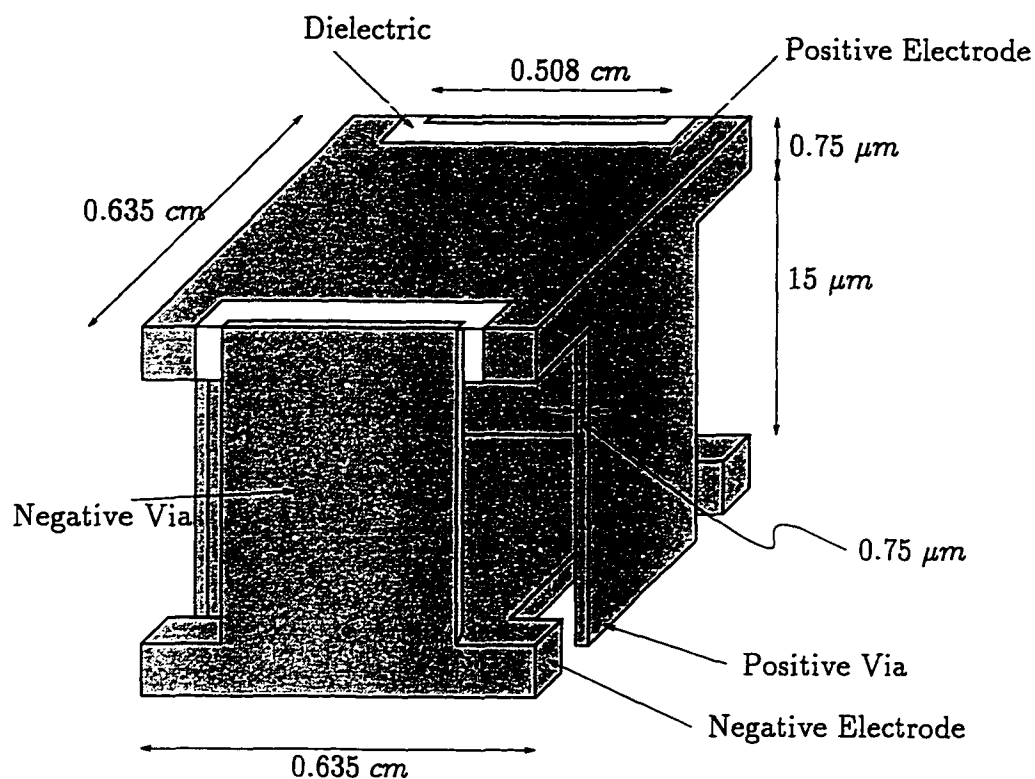
Figure 1.2. A typical single cell in the interior of a MLCC stack.

1.3. Overview

Use of FE analysis to model electromagnetic components is well established, see e.g., Silvester and Ferrari [1983]. FE analysis begins with a description of the problem geometry and material characteristics. The boundary conditions and the source for the electric and magnetic fields are specified. The sources are prescribed voltages and current densities. The region (i.e., a volume containing the electromagnetic component) of interest is then discretized in space into a mesh, and Maxwell equations are solved in a "weak" sense. Static and time-harmonic analysis is most popular; transient analysis is rarely attempted. The principle of virtual power for electromagnetics (Maugin [1980]) is the basis for the approximation. A detailed
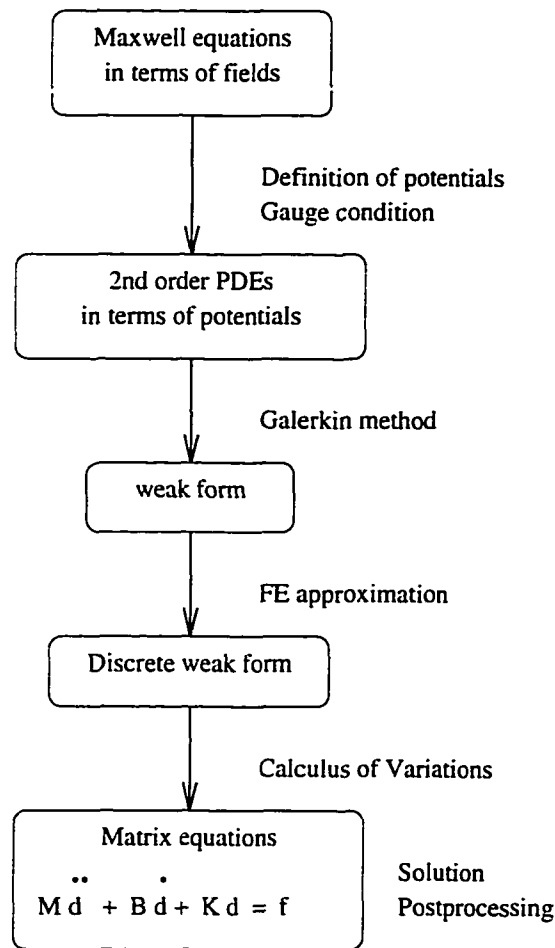
Figure 1.3.   The typical Finite Element (FE) procedure to solve Maxwell equations.

discussion of the FE procedure given in Figure 1.3 can be found in Hughes [1987] and Zienkiewicz and Taylor [1989].

The present formulation uses the magnetic vector potential $\mathbf{A}$ together with the time-integrated scalar potential ψ (MacNeal, Brauer and Coppolino [1990]). The partial differential equations (PDEs) are coupled, i.e., the terms related to the electric field are coupled with the terms related to the magnetic fields. Maxwell equations in terms of the field quantities and the potentials are explained in Chap-

ter 2. The discussion on the gauge condition explains the need for a gauge and the reasons for the choice of the Coulomb gauge in the present work. Chapter 3 transcribes the partial differential equations (PDEs) in Chapter 2 to a weak form via Galerkin projection. In Chapter 4, the weak form is discretized using first-order Lagrange isoparametric 8-noded brick elements. The matrix equations are derived. The entire procedure is repeated for electrostatic, magnetostatic, transient, and time-harmonic problems. The Coulomb gauge is implemented in the matrix equations via a penalty method. The use of selective reduced integration and the choice of a penalty parameter are explained in Sections 4.1.3 and 4.1.3.1, respectively.

In Chapter 5, a lumped parameter model for the MLCC is presented. The electric and magnetic field quantities of the continuum problem obtained via the FE solution are related to the lumped parameters of the circuit model, namely, the capacitance, the resistance and the inductance. The voltage and the current are related to the field quantities. These relations are derived for the static, transient, and time-harmonic solutions. The focus is on problems with an independent voltage source. A relation between the lumped parameters and the FE matrices is presented at the end of Chapter 5.

1.4. Contributions and Results

We introduce a new multiple-scale technique in Chapter 6 to transform Maxwell equations from the conventional *SI* unit system to the *generalized* unit system. The technique requires a set of scaling parameters that are determined by the physics of the electromagnetic problem. Suitable choice of the scaling parameters allows an effective interaction between different physical processes in the device. Previously intractable problems can be effectively solved by scaling. Scaling proves to be particularly useful to model electromagnetic devices having a complex geometry and a

mixture of regions of finite conductivity and zero conductivity. We demonstrate the efficacy of this scaling technique in a Finite Element(FE) model for a single cell of an advanced Multi Layer Ceramic capacitor. Scaling, motivated by the physics of the problem, decreases the condition[2] number of the matrices in the FE solution, and reduces the errors significantly. For example, the condition number of the solution to a single cell in a capacitor (in Figure 1.4(a)) with an applied voltage at the left end of the top electrode and the right end of the bottom electrode can be improved from $\mathcal{O}(10^{20})$ in the *SI* unit system to $\mathcal{O}(10^{13})$ in the optimal *generalized* system unit system. The relative error[3] improves from $\mathcal{O}(10^{-2})\%$ to $\mathcal{O}(10^{-11})\%$. A detailed study on the effects of scaling and other examples are presented in Chapter 8. The choice of the scaling parameter depends on the electromagnetic properties of the materials, and the frequency of excitation. The condition number and the relative errors also depend on the boundary conditions.

We introduce Algorithm 9.1 and Algorithm 9.2 to analyze the behavior of the capacitor with the change in frequency. These two algorithms in conjunction with the multiple-scale technique is implemented on the computer using FEAP[4] and MODULEF.[5] Figure 1.5 outlines the computer implementation. Static, transient,

---

[2] Condition number is defined using the 2-norm, i.e., the ratio of the largest to the smallest singular (eigen) value.

[3] Here, the numerical accuracy of the solution to a linear system of equations $\mathbf{K}\,d = f$ is estimated by the relative error

$$\frac{\|\,\mathbf{K}\,d - f\,\|_2}{\|\,f\,\|_2}\,,$$

where $\mathbf{K}$ is a square matrix and f is the right-hand side column vector. The computed solution is represented by column vector d. The symbol "$\|\cdot\|$" indicates a 2-norm; see Golub and van Loan [1987] for details.

[4] Finite Element Analysis Program (FEAP) was originally developed at the University of California, Berkeley. The structure of FEAP (©R.L. Taylor) and its macro command language are described in Chapter 15 of Zienkiewicz and Taylor [1989].

[5] MODUle Element Finis (MODULEF) club was founded by Institut National de Recherche en Informatique et an Automatique (INRIA), France, in 1974. MODULEF is a general purpose finite element library developed by the MODULEF club. See Bernadou, George, Hassim, Joly, Laug, Perronet, Saltel, Steer, Vanberborck and Vidrascu [1986] for further details regarding its

and time-harmonic solutions for Maxwell equations are implemented. Sophisticated mesh-generation routines are developed to mesh the the intricate network of electrodes and vias in the complicated three-dimensional structure of the advanced MLCC.

A solution at zero frequency, i.e., an electrostatic solution, to model the entire capacitor (i.e., $4 \times 4 \times 27 = 432$ cells) is presented in Chapter 7. A 20% difference is observed between the FE solution and the experimental values of capacitance C. This difference is attributed to changes in the geometry and the material properties during manufacturing.

Time-harmonic analysis increases the size of the matrix equations involved in the FE solution. The available computer resources limit the time-harmonic analysis to just a few ($2 \times 2 \times 3 = 12$) cells. In Chapter 9, we compare the FE solution for a few cells with its circuit model proposed by Ngo [1992]. Unlike the circuit model, FE analysis provides a detailed picture of the distribution of current in the electrodes. We observe that the distribution of current is not linear. The lumped parameters R and L computed using FE analysis is smaller than those predicted by Ngo [1992]'s circuit model.

The resistance, inductance, and capacitance for a MLCC are obtained by assuming simple linear isotropic constitutive relationships for the materials. However, high performance materials such as ferroelectric $BaTiO_3$ used in MLCCs require sophisticated constitutive models to account for the change in material properties with temperature and orientation of the material. A new methodology based on semi-infinite optimization is introduced to obtain, for the first time, accurate constitutive models for ferroelectric material. Appendix B outlines the proposed methodology. In the future, these accurate models can be used in conjunction with the FE proce-

---

program structure and its use.

dure to improve the accuracy of the solution.

The contents of the chapters in this dissertation are summarized as follows. In Chapter 2, we introduce Maxwell equations. We derive a concise mathematical statement of an electromagnetic problem for devices with static, transient, and time-harmonic excitations . In Chapter 3, we explain the weak form for these electromagnetic problems. The subsequent matrix equations are derived in Chapter 4 using first-order Lagrange isoparametric 8-nodes brick elements. In Chapter 5, we outline the procedure to calculate the lumped parameters R, L, and C from the FE solution (potentials $\mathbf{A}$ and ψ). A brief discussion on the equivalent circuit model is also presented. In Chapter 6, we propose the new multiple-scale technique, and explain the transformation from the *SI* unit system to the *generalized* unit system. The features and advantages of the multiple-scale technique are discussed.

The numerical results obtained using FE analysis for the capacitance C of the complete MLCC are shown in Chapter 7; the capacitance is calculated from a solution to an electrostatic problem. In Chapter 8, we explore solutions to benchmark time-dependent electromagnetic problems. The focus is on electromagnetic devices with time-harmonic excitations. The performance of solutions using the multiple-scale technique is evaluated. The frequency dependent characteristics of the cells inside the MLCC capacitor obtained using FE analysis are compared to its equivalent circuit model in Chapter 9. The use of a circuit simulator to study the behavior of the circuit models is discussed in Appendix A.

(a)

Condition number = 5.425006e+20 in SI
Rel. error = 2.171048e-02 in SI
Rel. error = 4.306341e-11 in Generalized

$\alpha_x^{opt} = 10^2$
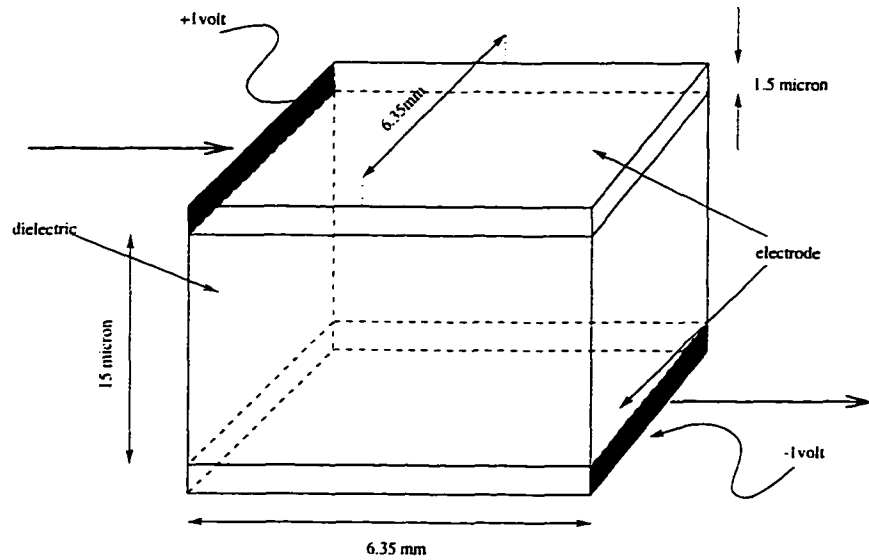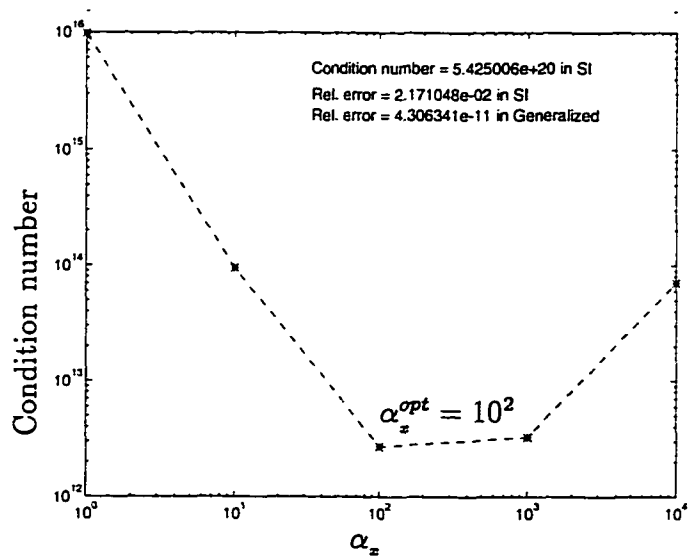
(b)

Figure 1.4. (a) A schematic of one cell in a MLCC. (Not drawn to scale.) The direction of the current flow is indicated by arrows. (b) Condition number vs. scaling parameter α_x.
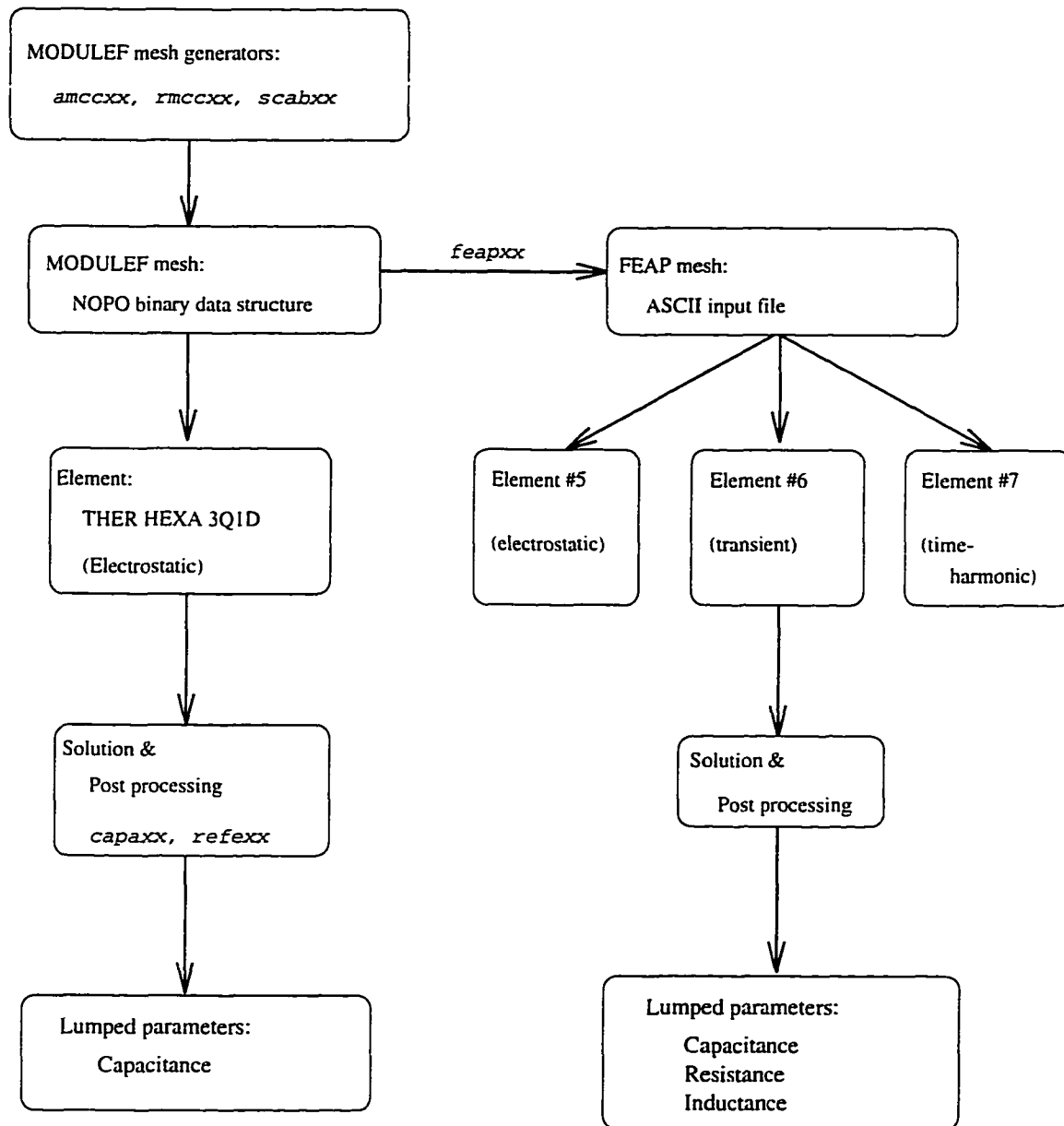
Figure 1.5.   Computer implementation of FE procedure to solve Maxwell equations. The processors amccxx, rmccxx, and scabxx are used to generate a mesh for the capacitor. The processor feapxx is used to convert the MODULEF mesh data structure to the FEAP mesh data structure. The flow chart on the left-hand side is implemented in MODULEF; and the flow chart on the right-hand side is implemented in FEAP.

CHAPTER 2
PROBLEM STATEMENT

This chapter begins with Maxwell equations. Mathematical statements are derived for problems with static, transient, and time-harmonic excitations. In solutions to problems with passive electromagnetic devices, use of intermediate functions termed as electromagnetic potentials reduce the computational effort, and is often more convenient. This chapter discusses the relation between the field quantities and the pair of potentials $\mathbf{A}$ and ψ, where $\mathbf{A}$ is the magnetic vector potential and ψ the electric scalar potential. The mathematical statement of the electromagnetic problems are expressed in terms of potentials $\mathbf{A}$ and ψ. The use of these potentials requires gauge conditions to ensure an unique solution. The gauge of choice in this document is the Coulomb gauge. Some aspects of uniqueness are also discussed. Albeit much of the discussion in this chapter can be found in the current literature, this review is used to develop the ensuing finite element formulation.

2.1. Problem Statement using Electromagnetic Fields

In the 1870's, Maxwell unified the theory of electricity and magnetism to explain the interaction between the different forces which lead to the unified Maxwell equations. These partial differential equations are a consequence of the Gauss's law, the Ampere's law, and the Faraday's law. A comprehensive account of the history of electromagnetics can be found in Hammond [1981]. Electric and magnetic fields in an electromagnetic device are solutions to the Maxwell equations.

13

2.1.1. Maxwell Equations in Terms of Fields

The governing partial differential equations (Maxwell equations) for electromagnetic problems are as follows:

$$\text{Faraday's law:} \qquad \frac{\partial \mathbf{B}}{\partial t} + \operatorname{curl} \mathbf{E} \qquad = \mathbf{0} \ , \qquad (2.1)$$

$$\text{Gauss's law for electric field:} \qquad \operatorname{div} \mathbf{D} - \rho_f \qquad = 0 \ , \qquad (2.2)$$

$$\text{Ampere's law:} \quad -\frac{\partial \mathbf{D}}{\partial t} + \operatorname{curl} \mathbf{H} - \mathbf{J}_f \quad = \mathbf{J}_a \ , \qquad (2.3)$$

$$\text{Gauss's law for magnetic induction:} \qquad \operatorname{div} \mathbf{B} \qquad = 0 \ , \qquad (2.4)$$

where the field quantities are the electric field $\mathbf{E}$, the magnetic induction $\mathbf{B}$, the electric induction $\mathbf{D}$, and the magnetic field $\mathbf{H}$. The quantities $\mathbf{J}_f$ and ρ_f are the field induced free-current volume density and free-charge volume density, respectively. In some electromagnetic problems an applied free-current volume density $\mathbf{J}_a$ and an applied free-charge volume density ρ_a are prescribed. The applied free-charge volume density ρ_a is imposed as an additional constraint equation

$$\boxed{\rho_f = \rho_a \qquad \text{in } \Omega_{\rho_a} \subset \Omega \ .} \qquad (2.5)$$

2.1.2. Constitutive Laws

The macroscopic behavior from the internal constitution of the material is described by constitutive laws. For the materials employed in MLCCs, the constitutive laws that relate $\mathbf{D}$, $\mathbf{H}$, and $\mathbf{J}_f$ to the field quantities $\mathbf{E}$ and $\mathbf{B}$ are

$$\mathbf{D} = \epsilon_0 \mathbf{E} + \mathbf{P}(\mathbf{E}) \ , \qquad \mathbf{H} = \frac{1}{\mu_0}\mathbf{B} - \mathbf{M}(\mathbf{B}) \ , \qquad \mathbf{J}_f \equiv \mathbf{J}_f(\mathbf{E}) \ , \qquad (2.6)$$

where the polarization $\mathbf{P}$ is a non-linear function of the electric field $\mathbf{E}$, and the magnetization $\mathbf{M}$ is a non-linear function of the magnetic induction $\mathbf{B}$. Note that the above constitutive equations characterize the behavior of most materials used in
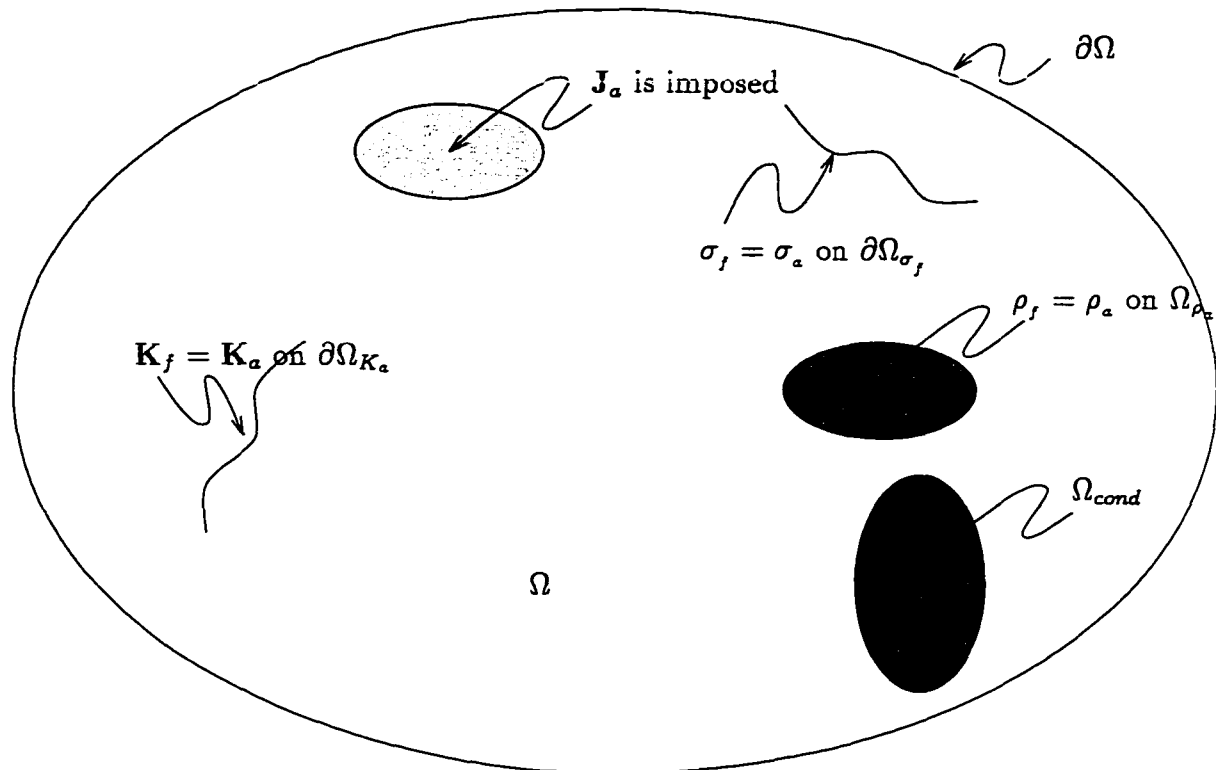
Figure 2.1. A typical electromagnetic problem

electromagnetic devices. Historically, the field quantities $\mathbf{E}$ and $\mathbf{B}$ are treated as the primary unknowns in an electromagnetic problem, i.e., all the other field quantities are calculated from $\mathbf{E}$ and $\mathbf{B}$.

The part of the volume Ω in which the current density $\mathbf{J}_f$ is not zero in the presence of a non-zero electric field $\mathbf{E}$ is characterized as a region of finite conductivity and is designated to be $\Omega_{cond} \subset \Omega$. As the focus of the present work does not apply to superconductors, we designate the remaining volume $(\Omega \setminus \Omega_{cond})$ to be the non-conductive region. Splitting the volume Ω into conductive and non-conductive regions is especially useful in solving for the initial conditions (2.14) and (2.15) (see Section 2.1.5 below).

2.1.3. Interface Conditions

Due to the abrupt change in the material behavior at the interface between two different materials, we find abrupt changes in the field quantities: The conditions at the interface between medium (i) and medium (j) can be shown to be (e.g., Wangsness [1986]) as follows.

Tangential component of $\mathbf{E}$ is continuous:

$$\hat{\mathbf{n}} \times \left(\mathbf{E}^{(j)} - \mathbf{E}^{(i)} \right) = \mathbf{0} \,. \qquad (2.7)$$

Normal component of $\mathbf{D}$ is discontinuous by the amount of surface charge σ_f:

$$\hat{\mathbf{n}} \cdot \left(\mathbf{D}^{(j)} - \mathbf{D}^{(i)} \right) = \sigma_f \,. \qquad (2.8)$$

Tangential component of $\mathbf{H}$ is discontinuous by the amount of surface current $\mathbf{K}_f$:

$$\hat{\mathbf{n}} \times \left(\mathbf{H}^{(j)} - \mathbf{H}^{(i)} \right) = \mathbf{K}_f \,. \qquad (2.9)$$

Normal component of $\mathbf{B}$ is continuous:

$$\hat{\mathbf{n}} \cdot \left(\mathbf{B}^{(j)} - \mathbf{B}^{(i)} \right) = \mathbf{0} \,. \qquad (2.10)$$

The unit normal vector $\hat{\mathbf{n}}$ to the surface of discontinuity is directed away from medium (i) into medium (j). The induced field quantities are the free-current surface density $\mathbf{K}_f$ and the free-charge surface density σ_f. However, in some electromagnetic problems, an applied free-current surface density $\mathbf{K}_a$ and a free-charge surface density σ_a are prescribed. They are imposed as additional constraint equations

$$\boxed{\begin{array}{ll} \mathbf{K}_f = \mathbf{K}_a & \text{in } \partial\Omega_{\mathbf{K}_a} \subset \Omega \,, \\ \sigma_f = \sigma_a & \text{in } \partial\Omega_{\sigma_a} \subset \Omega \,. \end{array}} \qquad (2.11)$$

2.1.4. Boundary Conditions

The formulation to be presented in this document apply to the following possibilities: (1) The domain Ω is bounded, (2) Ω is an unbounded region comprising of all space, and (3) Ω is an unbounded region from which certain regions are excluded.

2.1.4.1. Interior boundaries

For the boundaries that are close to "center" of the problem, we specify field quantities **E** and **B**. These interior boundaries are present only if we know the solution on the boundary a priori, e.g., if we exploit the symmetry in the problem.

2.1.4.2. Exterior boundaries

However, for an exact solution, we must also impose the Dirichlet or the Neumann boundary conditions at an infinite distance from the "center" of the problem as follows. The Dirichlet boundary conditions at infinity are

$$\left. \begin{array}{ll} \lim_{|\mathbf{x}|\to\infty} \mathbf{B}(\mathbf{x},t) &= \mathbf{0} \\[2mm] \lim_{|\mathbf{x}|\to\infty} \mathbf{E}(\mathbf{x},t) &= \mathbf{0} \end{array} \right\} \forall\, t \geq 0 \; . \tag{2.12}$$

The Neumann boundary conditions at infinity are

$$\left. \begin{array}{lll} \lim_{|\mathbf{x}|\to\infty} \dfrac{\partial \mathbf{H}}{\partial n}(\mathbf{x},t) &= \lim_{|\mathbf{x}|\to\infty} \operatorname{curl} \mathbf{H} \times \hat{\mathbf{n}} &= \mathbf{0} \\[3mm] \lim_{|\mathbf{x}|\to\infty} \dfrac{\partial \mathbf{D}}{\partial n}(\mathbf{x},t) &= \lim_{|\mathbf{x}|\to\infty} \operatorname{curl} \mathbf{D} \times \hat{\mathbf{n}} &= \mathbf{0} \end{array} \right\} \forall\, t \geq 0 \; . \tag{2.13}$$

In practice, we create an artificial boundary at a large finite distance from the "center" of the problem, thereby introducing errors in the solution. As this artificial boundary is made more distant, the errors are reduced. Any outgoing wave is reflected by the boundary. For a Neumann boundary condition, the reflected (incoming) wave is in phase with the incident (outgoing) wave, and conversely, for a Dirichlet boundary condition, the reflected wave is out of phase. See Remark 2.1 for an overview of the methods to handle exterior boundary problems.

Remark 2.1. Typically, the domain of an electromagnetic problem is infinite. We require infinite number of elements to discretize an infinite domain. However, the present day computer resources are finite. This contradiction requires alternative

procedures to deal with exterior regions (far from the "center" of the problem). Some of the popular methods are explained in Emson [1988], and the most popular methods, the method of truncation and the use of infinite elements, are explained below.

The method of choice in this work is the method of truncation, where the finite element mesh is truncated at a finite distance away from the "center" of the problem. As the distance of the artificial boundary is increased we expect better accuracy. However, the success of such a method depends on the physics of the problem. Care should be taken for 2-dimensional problems, where the 2-dimensional assumption introduces sources at infinity, and hence, a field at infinity. For 3-dimensional problems, the mesh should be constructed to make the excluded region source-free. Incoming and outgoing electromagnetic waves play havoc at the artificial boundary. For example, in scattering problems, the artificial boundary should be constructed such that it does not reflect any waves (wave absorbing boundaries).

Another popular method to model the boundary is the use of *infinite* elements. The infinite elements are of two types. The first type maps the local co-ordinates of one set of nodes to infinity. The second type uses a singular decay function in the basis polynomials. This ensures that the potentials, and consequently, the field quantities decay to zero. The success of the infinite elements is problem dependent. Care must be exercised in the choice of the mapping functions and the decay functions. See Penman, Grieve and Wilson [1986], Imhoff, Meunier and Sabonnadiere [1990] and Gratkowski and Ziolkowski [1992] for application of infinite elements to electromagnetic problems. Yet another method is the use of the Boundary Integral Method (BEM) to model the artificial boundary coupled with the FE method for the interior volume. This method couples all the nodes at the boundary and significantly increases the bandwidth of the matrix equation. The increase in the cost

for solution may outweigh the increase in accuracy. Ramahi and Mittra [1991] and McDonald and Wexler [1972] use only the Boundary Integral Method for the entire problem. Ren, Bouillault, Razek and Verite [1988] presents a comparison of different boundary integral methods when coupled with finite elements in three dimensions. For complicated geometries such as the advanced multi-layer capacitors, the use of truncation to establish artificial boundaries appears to be most cost effective. We use the method of truncation, which is not necessarily better than the use of infinite elements, however, is simple enough to allow us to focus on the main objectives of this work. ∎

2.1.5. Initial Conditions

In addition to the boundary conditions, we must specify the field quantities at the instant that we begin solving the PDEs: Let $\mathbf{E}_0$ be the electric field and $\mathbf{B}_0$ be the magnetic field at time $t = 0$. The solutions to an electrostatic and a magneto-static problems often serve as initial conditions to a time dependent electromagnetic problem. An electrostatic problem is with zero current inside the conductors, and hence, the electric field inside the conductors is zero. Therefore, the electrostatic equations that must be satisfied by $\mathbf{E}_0$ outside the conductive region are

$$
\begin{aligned}
\operatorname{curl} \mathbf{E}_0 &= 0 & \text{in } (\Omega \setminus \Omega_{cond}) , \\
\operatorname{div} \mathbf{D}_0 - \rho_{f0} &= 0 & \text{in } (\Omega \setminus \Omega_{cond}) , \\
\rho_{f0} &= \rho_{a0} & \text{in } (\Omega \setminus \Omega_{cond}) \cap \Omega_{\rho_{a0}} , \\
\rho_{f0} &= 0 & \text{in } (\Omega \setminus \Omega_{cond}) \setminus \Omega_{\rho_{a0}} ,
\end{aligned}
\tag{2.14}
$$

where the subscript "0" indicates quantities at time $t = 0$. The applied free-charge density ρ_{a0} is specified in a non-conductive region. A magnetostatic problem is with

time-independent magnetic field, i.e., the magnetic induction $\mathbf{B_0}$ must satisfy

$$
\begin{aligned}
\text{curl}\,\mathbf{H_0} &= \mathbf{J}_{a_0} \quad \text{in } \Omega \,, \\
\text{div}\,\mathbf{B_0} &= 0 \quad\;\; \text{in } \Omega \,.
\end{aligned}
\tag{2.15}
$$

See e.g., Stratton [1941] for details.

A typical electromagnetic problem involves calculating $\mathbf{E}$, $\mathbf{B}$, and ρ_f (total of seven unknowns) by solving Maxwell equations (2.1) to (2.4) together with appropriate constitutive laws (2.6), boundary conditions (2.12) or (2.13), initial conditions (2.14) and (2.15), and constraints (2.5) and (2.11).

2.2. Problem Statement using Electromagnetic Potentials

Electromagnetic fields are often calculated by using intermediate functions which are called potentials. Some of these potentials reduce the number of unknowns to be determined in the solution to Maxwell equations, thereby reducing the computational effort. Furthermore, potentials can be conveniently related to the circuit quantities. For example, in some problems with electromagnetic devices, the electric scalar potential ϕ is the voltage in a circuit. Many different sets of potentials have been defined to solve electromagnetic problems; see e.g., Hammond [1982]. A set of potentials is only applicable to a particular kind of electromagnetic problem. This is due to the fact that many simplifying assumptions were made in order to define these potentials. The potentials most commonly used in electromagnetic problems and their respective simplifying assumptions are listed in Tables 2.1 and 2.2. Note that the electromagnetic fields $\mathbf{E}$ and $\mathbf{B}$ can also be computed directly without calculating the potentials; see e.g., Bossavit [1989].

The most common potentials are the magnetic vector potential $\mathbf{A}$ and the electric scalar potential ϕ. However, in the past few years the use of the magnetic

Table 2.1. The potentials used in the formulation of electromagnetic problems. The assumptions required to simplify Maxwell equations are also listed.

Potentials	Assumptions	PDEs to be solved
$\mathbf{B} =: \operatorname{curl} \mathbf{A}$ $\mathbf{E} =: -\operatorname{grad} \phi - \dfrac{\partial \mathbf{A}}{\partial t}$ Carpenter [1977, p. 1027]	None	$\operatorname{curl} \mathbf{H} - \dfrac{\partial \mathbf{D}}{\partial t} - \mathbf{J}_f = 0$ $\operatorname{div} \mathbf{D} = \rho_f$
$\mathbf{B} =: \operatorname{curl} \mathbf{A}$ $\mathbf{E} =: -\operatorname{grad} \dfrac{\partial \psi}{\partial t} - \dfrac{\partial \mathbf{A}}{\partial t}$ MacNeal et al. [1990]	None	$\operatorname{curl} \mathbf{H} - \dfrac{\partial \mathbf{D}}{\partial t} - \mathbf{J}_f = 0$ $\operatorname{div} \mathbf{D} = \rho_f$
$\mathbf{J}_f =: \operatorname{curl} \mathbf{T}$ $\mathbf{H} =: \mathbf{T} - \operatorname{grad} \Omega$ Brown [1982, pp. 49–50]	$\dfrac{\partial \mathbf{D}}{\partial t} << \mathbf{J}_f$	$\operatorname{curl} \mathbf{E} - \dfrac{\partial \mathbf{B}}{\partial t} = 0$ $\operatorname{div} \mathbf{B} = 0$
$\mathbf{D} =: -\operatorname{curl} \mathbf{A}^*$ $\mathbf{H} =: -\dfrac{\partial \mathbf{A}^*}{\partial t} - \dfrac{\sigma}{\epsilon} \mathbf{A}^* - \operatorname{grad} \phi^*$ Stratton [1941]	$\rho_f = 0$ linear-isotropic homogeneous material	$\operatorname{curl} \mathbf{E} - \dfrac{\partial \mathbf{B}}{\partial t} = 0$ $\operatorname{div} \mathbf{B} = 0$
$\mathbf{E} =: -\operatorname{grad} \phi$ Hammond [1982, p. 107]	$\dfrac{\partial \mathbf{B}}{\partial t} = 0$ $\mathbf{J}_f = 0$ $\dfrac{\partial \mathbf{D}}{\partial t} = 0$	$\operatorname{div} \mathbf{D} = \rho_f$
$\mathbf{H} =: -\operatorname{grad} \phi_m$ Hammond [1982, p. 107] Albanese and Rubinacci [1990, p. 516]	$\dfrac{\partial \mathbf{B}}{\partial t} = 0$ $\mathbf{J}_f = 0$ $\dfrac{\partial \mathbf{D}}{\partial t} = 0$	$\operatorname{div} B = 0$

Table 2.2. The potentials used in the formulation of electromagnetic problems (continued).

Potentials	Assumptions	PDE's to be solved
$\mathbf{H} =: \mathbf{H}_s + \mathbf{H}_m$ $\mathbf{H}_m =: -\mathrm{grad}\,\psi_m$ $\mathbf{H}_s := \dfrac{1}{4\pi} \displaystyle\int_\Omega \dfrac{\mathbf{J}_f \times (\mathbf{x} - \mathbf{x}')}{\mid \mathbf{x} - \mathbf{x}' \mid^3} d\Omega'$ Hammond [1982, p. 107] Albanese and Rubinacci [1990, p. 516] Simkin and Trowbridge [1979]	$\dfrac{\partial \mathbf{B}}{\partial t} = \mathbf{0}$ $\mathbf{J}_f$ known $\dfrac{\partial \mathbf{D}}{\partial t} = \mathbf{0}$	$\mathrm{div}\,\mathbf{H}_m = 0$
$\mathbf{B} = \mathrm{curl}\,\mathbf{A}$ Hammond [1982, p. 107] Albanese and Rubinacci [1990, p. 516] Simkin and Trowbridge [1979]	$\dfrac{\partial \mathbf{B}}{\partial t} = \mathbf{0}$ $\mathbf{J}_f$ known $\dfrac{\partial \mathbf{D}}{\partial t} = \mathbf{0}$	$\mathrm{curl}\,(\mathbf{H}) = \mathbf{J}_f$

vector potential $\mathbf{A}$ together with the time-integrated scalar potential ψ has gained popularity (MacNeal et al. [1990]). The main advantage of using $\mathbf{A}$ and ψ is that the resulting FE matrices are symmetric and positive semi-definite. Hence, conventional numerical algorithms can be used to solve the resulting system of equations.

2.2.1. Maxwell Equations in Terms of Potentials

The formulation for electromagnetic problems presented here uses the time-integrated scalar potential ψ and the magnetic vector potential $\mathbf{A}$. The definition

of the potentials

$$
\boxed{
\begin{aligned}
\mathbf{B} &=: \text{curl } \mathbf{A} ,\\
\mathbf{E} &=: -\text{grad}\,\frac{\partial \psi}{\partial t} - \frac{\partial \mathbf{A}}{\partial t} ,
\end{aligned}
}
\tag{2.16}
$$

satisfy Faraday's law (2.1) and Gauss's law for magnetic induction (2.4) uniquely. The remaining two equations, i.e., Ampere's law (2.3)

$$
-\frac{\partial \mathbf{D}}{\partial t} + \text{curl } \mathbf{H} - \mathbf{J}_f = \mathbf{J}_a ,
$$

and Gauss's law for electric field (2.2)

$$
\text{div } \mathbf{D} - \rho_f = 0 ,
$$

are solved to determine the potentials $\mathbf{A}$ and ψ. Therefore, all the quantities in left-hand side of the equations (2.3) and (2.2) must be represented in terms of the potentials $\mathbf{A}$ and ψ.

To recapitulate, the PDEs to be solved for the electromagnetic problem formulated using potentials $\mathbf{A}$ and ψ are

$$
\boxed{
\begin{aligned}
\text{curl } \mathbf{H} - \frac{\partial \mathbf{D}}{\partial t} - \mathbf{J}_f &= \mathbf{J}_a ,\\
\text{div } \mathbf{D} - \rho_f &= 0 .
\end{aligned}
}
\tag{2.17}
$$

where all the expressions on the left-hand side can be represented in terms of potentials.[6]

2.2.2. Constitutive Laws

The field quantities $\mathbf{H}$, $\mathbf{D}$, and $\mathbf{J}_f$ are related to the potentials defined in (2.16) via the constitutive equation (2.6). The disadvantage in using these potentials in a

---

[6] The field quantities $\mathbf{H}$, $\mathbf{D}$, and $\mathbf{J}_f$ are related to the potentials via the constitutive equation (2.6). Equation (2.30) is used to represent ρ_f in terms of the potentials. $\mathbf{J}_a$ and ρ_a are applied sources, i.e., prescribed quantities.

numerical solution is the need to differentiate the potentials in order to determine the field quantities.

2.2.3. Boundary Conditions

2.2.3.1. Interior boundaries

For the boundaries that are close to "center" of the problem, we specify the potentials $\mathbf{A}$ and ψ. These interior boundaries are present only if we know the solution on the boundary a priori, e.g., in the case of existing symmetry in the problem. Typically, in electrostatic problems, we specify the quantity $\dot{\psi}_0$ (which is equivalent to the voltage) on the interface between the conductive and non-conductive regions. In magnetostatic problems, we could impose the analytical solution for the potential $\mathbf{A}_0 \cong 0$ at the interface between the conductive and non-conductive regions.

2.2.3.2. Exterior boundaries

By definition the field quantities $\mathbf{E}$ and $\mathbf{B}$, involve the derivatives of potentials $\mathbf{A}$ and ψ, and hence, imposing (2.12) and (2.13) is equivalent to imposing linear constraint equations on the derivatives of $\mathbf{A}$ and ψ, and hence is not computationally efficient. Therefore we choose to impose the following boundary conditions: Dirichlet boundary conditions

$$\left.\begin{array}{l} \lim_{|\mathbf{x}|\to\infty} \mathbf{A}(\mathbf{x},t) = 0 \\ \lim_{|\mathbf{x}|\to\infty} \psi(\mathbf{x},t) = 0 \end{array}\right\} \forall\, t \geq 0\,, \tag{2.18}$$

or the Neumann boundary conditions

$$\left.\begin{array}{l} \lim_{|\mathbf{x}|\to\infty} \dfrac{\partial \mathbf{A}}{\partial n}(\mathbf{x},t) = \lim_{|\mathbf{x}|\to\infty} \operatorname{curl}\mathbf{A}\times\hat{n} = 0 \\ \lim_{|\mathbf{x}|\to\infty} \dfrac{\partial \psi}{\partial n}(\mathbf{x},t) = \lim_{|\mathbf{x}|\to\infty} \operatorname{grad}\psi\cdot\hat{n} = 0 \end{array}\right\} \forall\, t \geq 0\,. \tag{2.19}$$

In the limit as $|\mathbf{x}| \to \infty$ the boundary conditions (2.12) and (2.13) are equivalent to (2.18) and (2.19). In practice, it is preferred to impose the Neumann boundary conditions (2.19) at a large finite distance from the center of the problem.

2.2.4. Initial Conditions

Initial conditions comprise of the potentials $(\mathbf{A}_0, \psi_0)$ and their first-time derivative $(\dot{\mathbf{A}}_0, \dot{\psi}_0)$. The potential $\mathbf{A}_0$ is a solution to (2.15), and the potential $\dot{\psi}_0$ is a solution to (2.14). Note that we have the electric field $\mathbf{E}$ to be zero inside the conductive region Ω_{cond}, and hence, a convenient choice is to set

$$\boxed{\dot{\psi}_0 := \text{constant} \qquad \text{in } \Omega_{cond} \, .} \tag{2.20}$$

The remaining potentials $\dot{\mathbf{A}}_0$ and ψ_0 are chosen as follows. The initial condition assumes a steady magnetic induction $\mathbf{B}$ everywhere in Ω, i.e,

$$\frac{\partial \mathbf{B}_0}{\partial t} = \mathbf{0} \quad \Rightarrow \quad \frac{\partial \text{curl} \, \mathbf{A}_0}{\partial t} = \mathbf{0} \, .$$

and hence, a convenient choice is

$$\boxed{\dot{\mathbf{A}}_0 := \mathbf{0} \qquad \text{in } \Omega \, ,} \tag{2.21}$$

As the field quantities at time $t = 0$ do not involve the scalar potential ψ_0, but only its time derivatives, we choose

$$\boxed{\psi_0 := 0 \qquad \text{in } \Omega \, .} \tag{2.22}$$

2.2.5. Typical Electromagnetic Problems

We present here a comprehensive statement for electromagnetic problems with static, transient, and time-harmonic excitations. Our focus is on passive electromagnetic devices such as capacitors. Before we look at the complicated transient problem, we present a simpler static problem with the following assumptions:

Assumption 2.1. The following assumptions are made to solve the electrostatic and magnetostatic problems:

1. For the electrostatic problem, all the electromagnetic quantities are independent of time.
2. For the magnetostatic problem, the magnetic quantities are independent of time; and any applied current is divergence free, i.e.,

$$\operatorname{div} \mathbf{J}_{f_0} \equiv 0 \ . \qquad \blacksquare$$

2.2.5.1. The electrostatic problems

We determine the electric scalar potential $\overset{\bullet}{\psi}_0$, and consequently, the electric field $\mathbf{E}_0$ inside a non-conductive region. With Assumption 2.1 we have (explained in Section 2.2.4)[7]

$$\psi_0 \equiv 0 \text{ and } \overset{\bullet\bullet}{\psi}_0 \equiv 0 \ , \text{ with } \overset{\bullet}{\psi}_0 = \overset{\bullet}{\psi}_{a_0} \text{ in } \Omega_{cond} \text{ and } \overset{\bullet}{\psi}_0 \neq 0 \text{ in } \Omega \setminus \Omega_{cond} \ ,$$

where $\overset{\bullet}{\psi}_{a_0}$ is the voltage applied to the conductors. Hence, we only need to solve for the potential $\overset{\bullet}{\psi}_0$ in the non-conductive region $\Omega \setminus \Omega_{cond}$, i.e.,

$$
\boxed{
\begin{aligned}
&\text{Find } \overset{\bullet}{\psi}_0 : \Omega \setminus \Omega_{cond} \to \mathbf{R} \text{ such that}\\
&\quad \operatorname{div} \mathbf{D}_0 - \rho_{f_0} = 0 && \text{in } (\Omega \setminus \Omega_{cond}) \ ,\\
&\quad \rho_{f_0} = \rho_{a0} && \text{in } (\Omega \setminus \Omega_{cond}) \cap \Omega_{\rho_{a0}} \ ,\\
&\quad \rho_{f_0} = 0 && \text{in } (\Omega \setminus \Omega_{cond}) \setminus \Omega_{\rho_{a0}} \ ,\\
&\quad \overset{\bullet}{\psi}_0 = \overset{\bullet}{\psi}_{a_0} && \text{on } \Gamma_{g\overset{\bullet}{\psi}_0}\\
&\quad \mathbf{D}_0 \cdot \hat{\mathbf{n}} = (\mathbf{D}_0 \cdot \hat{\mathbf{n}})_a && \text{on } \Gamma_{h\overset{\bullet}{\psi}_0}
\end{aligned}
}
\qquad (2.23)
$$

where $\mathbf{D}_0$ is related to $\mathbf{E}_0 = -\operatorname{grad} \overset{\bullet}{\psi}_0$, and hence $\overset{\bullet}{\psi}_0$, via the constitutive law (2.6). The symbol $\Omega_{\rho_{a0}}$ denotes the volume in which a charge of applied charge volume density ρ_{a0} is prescribed. The boundary $\partial\Omega =: \overline{\Gamma_{h\overset{\bullet}{\psi}_0} \cup \Gamma_{g\overset{\bullet}{\psi}_0}}$, where $\Gamma_{h\overset{\bullet}{\psi}_0}$ is the part of

---

[7] To emphasize the difference, the quantities that are independent of time t, have a subscript "0".

the boundary on which the $\mathbf{D}_0 \cdot \hat{\mathbf{n}}$ field is specified, and $\Gamma_{g\dot{\psi}_0}$ is the remaining part of the boundary on which $\dot{\psi}_0$ is specified. In Chapter 5, the quantity $\dot{\psi}_0$ is defined to be the voltage. For the part of the boundary close to the "center" of the problem, we either specify the voltage by setting the value of $\dot{\psi}_{a_0}$ on the boundary $\Gamma_{g\dot{\psi}_0}$, and/or the non-zero[8] field $(\mathbf{D}_0 \cdot \hat{\mathbf{n}})_a$ on the boundary $\Gamma_{h\dot{\psi}_0}$. For part of the boundaries far from the "center" of the problem, we impose a Dirichlet boundary condition

$$\dot{\psi}_0(\mathbf{x}) = 0 ,$$

by specifying $\psi_{a_0} \equiv 0$, and/or a Neumann boundary condition

$$\operatorname{grad}\dot{\psi}_0(\mathbf{x}) \cdot \hat{\mathbf{n}} = 0 ,$$

by specifying $(\mathbf{D}_0 \cdot \hat{\mathbf{n}})_a \equiv 0$.

2.2.5.2. The magnetostatic problems

We determine the magnetic vector potential $\mathbf{A}_0$, and consequently, the magnetic induction $\mathbf{B}_0$ inside the region Ω. For the magnetostatic problem, as explained in Section 2.2.4[7] we have

$$\dot{\mathbf{A}}_0 \equiv 0 \text{ and } \ddot{\mathbf{A}}_0 \equiv 0 , \text{ with } \mathbf{A}_0 \neq 0 \text{ in } \Omega .$$

We determine the potential $\mathbf{A}_0$ in the region Ω as follows:

$$
\begin{array}{|ll|}
\hline
\text{Find } \mathbf{A}_0 : \Omega \to \mathbf{R}^3 \text{ such that} & \\
\qquad \operatorname{curl} \mathbf{H}_0 = \mathbf{J}_a & \text{in } \Omega , \\
\qquad \mathbf{A}_0 = \mathbf{A}_{a_0} & \text{on } \Gamma_{g_{A_0}} \\
\qquad \mathbf{H}_0 \times \hat{\mathbf{n}} = (\mathbf{H}_0 \times \hat{\mathbf{n}})_a & \text{on } \Gamma_{h_{A_0}} \\
\hline
\end{array}
\qquad (2.24)
$$

where $\mathbf{H}_0$ is related to $\mathbf{B}_0 = \operatorname{curl} \mathbf{A}_0$, and hence $\mathbf{A}_0$, via the constitutive law (2.6). The boundary $\partial\Omega =: \overline{\Gamma_{h_{A_0}} \cup \Gamma_{g_{A_0}}}$, where $\Gamma_{h_{A_0}}$ is the part of the boundary on which

---

[8] A non-zero $\mathbf{D}_{a_0} \cdot \hat{\mathbf{n}}$ is equivalent to specifying an surface free-charge density σ_{a_0}; see (2.11).

the $\mathbf{H}_0 \times \hat{\mathbf{n}}$ field is specified, and $\Gamma_{g_{A_0}}$ is the remaining part of the boundary on which $\mathbf{A}_0$ is specified. For the part of the boundary close to the "center" of the problem, we either specify the value of $\mathbf{A}_{a_0}$ on the boundary $\Gamma_{g_{A_0}}$, and/or the field non-zero $(\mathbf{H}_0 \times \hat{\mathbf{n}})_a$ on the boundary $\Gamma_{h_{A_0}}$. For part of the boundary far from the "center" of the problem, we impose a Dirichlet boundary condition

$$\mathbf{A}_0(\mathbf{x}) = \mathbf{0}$$

by specifying $\mathbf{A}_{a_0} \equiv \mathbf{0}$, and/or a Neumann boundary condition

$$\operatorname{curl} \mathbf{A}_0(\mathbf{x}) \times \hat{\mathbf{n}} = \mathbf{0}$$

by specifying $(\mathbf{H}_0 \times \hat{\mathbf{n}})_a \equiv \mathbf{0}$.

2.2.5.3. The transient problems

A convenient formulation is to eliminate ρ_f in (2.17). This is done by differentiating $(2.17)^2$ with respect to time, and replacing ρ_f by using the continuity equation (2.28); see Remark 2.2 for details. The set of PDEs

$$\boxed{\begin{aligned} \operatorname{curl} \mathbf{H} - \frac{\partial \mathbf{D}}{\partial t} - \mathbf{J}_f &= \mathbf{J}_a\,, \\ \frac{\partial \{\operatorname{div} \mathbf{D}\}}{\partial t} + \operatorname{div} \mathbf{J}_f &= -\operatorname{div} \mathbf{J}_a\,, \end{aligned}} \tag{2.25}$$

which are used in the remainder of the present document, is equivalent to (2.17). Note that substituting $(2.17)_2$ by $(2.25)_2$ requires the satisfaction of $(2.17)_2$ at time $t = 0$; which is included as an initial condition to the electromagnetic problem. In the transient problem stated below we determine the electric and magnetic field quantities for a prescribed distribution of current (specified by $\mathbf{J}_a$ with appropriate boundary conditions. Note that the statement below does not permit a voltage to

be prescribed in the region Ω.

Given $\psi_0 \equiv 0$, $\dot{\mathbf{A}}_0 \equiv \mathbf{0}$, $\dot{\psi}_0$ that satisfies (2.23) and $\mathbf{A}_0$ that satisfies (2.24), find $\mathbf{A}(\mathbf{x}, t)$ and $\psi(\mathbf{x}, t)$ for all $\mathbf{x} \in \Omega$ and $t > 0$, such that we satisfy (2.25)

$$\operatorname{curl} \mathbf{H} - \frac{\partial \mathbf{D}}{\partial t} - \mathbf{J}_f = \mathbf{J}_a \qquad \forall\, \mathbf{x} \in \Omega \text{ and } t > 0 ,$$

$$\frac{\partial \{\operatorname{div} \mathbf{D}\}}{\partial t} + \operatorname{div} \mathbf{J}_f = -\operatorname{div} \mathbf{J}_a \qquad \forall\, \mathbf{x} \in \Omega \text{ and } t > 0 ,$$

with the volume constraint (2.5)

$$\rho_f = \rho_a \qquad \text{in } \Omega_{\rho_a} \subset \Omega ,$$

the interface constraints (2.11)

$$\mathbf{K}_f = \mathbf{K}_a \qquad \text{on } \partial\Omega_{\mathbf{K}_a} \subset \Omega ,$$

$$\sigma_f = \sigma_a \qquad \text{on } \partial\Omega_{\sigma_a} \subset \Omega ,$$

and the boundary conditions

$$\mathbf{A} = \mathbf{A}_a \qquad \text{on } \Gamma_{g_A} ,$$

$$\mathbf{H} \times \hat{\mathbf{n}} = (\mathbf{H} \times \hat{\mathbf{n}})_a \qquad \text{on } \Gamma_{h_A} ,$$

$$\psi = \psi_a \qquad \text{on } \Gamma_{g_\psi} ,$$

$$\left(\frac{\partial \mathbf{D}}{\partial t} + \mathbf{J}_f \right) \cdot \hat{\mathbf{n}} = \left(\left(\frac{\partial \mathbf{D}}{\partial t} + \mathbf{J}_f \right) \cdot \hat{\mathbf{n}} \right)_a \qquad \text{on } \Gamma_{h_\psi} .$$

$$(2.26)$$

In (2.26) the field quantities $\mathbf{H}$, $\mathbf{D}$, and $\mathbf{J}_f$ are related to the potentials $\mathbf{A}$ and ψ via the constitutive equations (2.6). The boundary $\partial\Omega =: \overline{\Gamma_{h_A} \cup \Gamma_{g_A}}$, where Γ_{h_A} is the part of the boundary where the $\mathbf{H} \times \hat{\mathbf{n}}$ field is specified, and Γ_{g_A} is the remaining part of the boundary where the vector potential $\mathbf{A}$ is specified. Also, the boundary $\partial\Omega =: \overline{\Gamma_{h_\psi} \cup \Gamma_{g_\psi}}$, where Γ_{h_ψ} is the part of the boundary where the $\left(\dfrac{\partial \mathbf{D}}{\partial t} + \mathbf{J}_f \right) \cdot \hat{\mathbf{n}}$ field is specified, and Γ_{g_ψ} is the remaining part of the boundary where the time integrated scalar potential ψ is specified. For the part of the boundary close to the "center" of the problem, we either specify the values $\mathbf{A}_a$ and ψ_a on the boundary, and/or the field $(\mathbf{H} \times \hat{\mathbf{n}})_a$ and $\left(\left(\dfrac{\partial \mathbf{D}}{\partial t} + \mathbf{J}_f \right) \cdot \hat{\mathbf{n}} \right)_a$. For part of the boundary far

from the "center" of the problem, we impose a Dirichlet boundary condition

$$\mathbf{A}(\mathbf{x}) = 0 \quad \text{and} \quad \psi(\mathbf{x}) = 0$$

by specifying $\mathbf{A}_a \equiv 0$ and $\psi_a \equiv 0$, and a Neumann boundary condition

$$\operatorname{curl} \mathbf{A}(\mathbf{x}) \times \hat{\mathbf{n}} = 0 \quad \text{and} \quad \operatorname{grad} \psi(\mathbf{x}) \cdot \hat{\mathbf{n}}$$

by specifying $(\mathbf{H} \times \hat{\mathbf{n}})_a \equiv 0$ and $\left(\left(\dfrac{\partial \mathbf{D}}{\partial t} + \mathbf{J}_f \right) \cdot \hat{\mathbf{n}} \right)_a \equiv 0.$

<u>Remark 2.2.</u> Differentiate (2.2) with respect to time t to obtain

$$\frac{\partial(\operatorname{div}\mathbf{D})}{\partial t} - \frac{\partial \rho_f}{\partial t} = 0 \ . \tag{2.27}$$

However, using the continuity equation

$$\frac{\partial \rho_f}{\partial t} + \operatorname{div}\,[\mathbf{J}_f + \mathbf{J}_a] = 0 \ , \tag{2.28}$$

we can eliminate ρ_f from (2.27) to get the time integrated continuity equation

$$\frac{\partial(\operatorname{div}\mathbf{D})}{\partial t} + \operatorname{div}\,[\mathbf{J}_f + \mathbf{J}_a] = 0 \ . \tag{2.29}$$

Moreover, an expression for ρ_f is obtained by integrating the continuity equation (2.28) with respect to time t :

$$\rho_f = \rho_{f0} - \int_{t_0}^{t} \operatorname{div}\,[\mathbf{J}_f + \mathbf{J}_a]\ dt \ , \tag{2.30}$$

where t_0 is the instant in time where we begin the analysis of the electromagnetic problem and ρ_{f0} is the free charge density at time t_0. ∎

2.2.5.4. The time-harmonic problems

In many practical electromagnetic problems, the driving forces, e.g., $\mathbf{J}_a$, ρ_a, $\mathbf{A}_a$, ψ_a, etc, are periodic sinusoidal functions of a particular frequency ω. As a

result, the induced fields and potentials are also sinusoidal function of the same frequency ω. A convenient formulation for such problems is to represent all the quantities as time-harmonic functions (see Definition 2.1 below) of the frequency ω. For a time-harmonic problem the potentials are

$$
\begin{aligned}
\mathbf{A}(\mathbf{x}, t) &:= \bar{\mathbf{A}}_0(\mathbf{x})e^{(i\omega t)}, \\
\psi(\mathbf{x}, t) &:= \bar{\psi}_0(\mathbf{x})e^{(i\omega t)}.
\end{aligned}
\tag{2.31}
$$

Hence, we now only need to calculate the complex functions $\bar{\mathbf{A}}_0$ and $\bar{\psi}_0$ that are independent of time t. An electromagnetic problem using these time harmonic representation is also called a quasi-static electromagnetic problem, which is formulated below.

<u>Definition 2.1.</u> A time-harmonic function $f(\mathbf{x}, t) : \Omega \times \mathsf{R}^+ \to \mathsf{C}$ (where R^+ denotes a set of positive real numbers) of frequency ω is defined as follows.

$$
f(\mathbf{x}, t) := \bar{f}_0(\mathbf{x})e^{(i\omega t)} := \left(f_{0_r}(\mathbf{x}) + i f_{0_i}(\mathbf{x}) \right) e^{(i\omega t)},
\tag{2.32}
$$

where $\bar{f}_0(\mathbf{x}) : \Omega \to \mathsf{C}$ is a complex function of the spatial co-ordiantes $\mathbf{x}$, and $f_{0_r}(\mathbf{x}) : \Omega \to \mathsf{R}$ and $f_{0_i}(\mathbf{x}) : \Omega \to \mathsf{R}$ are real functions of $\mathbf{x}$. The "$^-$" indicates a complex quantity, and the subscript "0" indicates that the quantity is independent of time. The complex quantity $\bar{f}_0(\mathbf{x})$ is popularly referred to as a "phasor." The angle

$$
\tan^{-1}\left(\frac{f_{0_i}(\mathbf{x})}{f_{0_r}(\mathbf{x})} \right),
$$

is called the phase angle. ∎

The quasi-static electromagnetic problem is formulated by substituting all the field quantities and the potentials in the transient problem (2.26) by their respective time harmonic representation. The term $e^{(i\omega t)}$ is then eliminated. In the

time-harmonic problem stated below we determine the electric and magnetic field quantities for a prescribed distribution of current (specified by $\bar{\mathbf{J}}_a$) and a prescribed voltage (specified by $-i\omega\bar{\psi}_{a_0}$), with appropriate boundary conditions.

Find $\bar{\mathbf{A}}_0(\mathbf{x}) : \Omega \to \mathbf{C}^3$ and $\bar{\psi}_0(\mathbf{x}) : \Omega \to \mathbf{C}$ forall $\mathbf{x} \in \Omega$, such that we satisfy

$$\mathrm{curl}\,\bar{\mathbf{H}}_0 - i\omega\bar{\mathbf{D}}_0 - \bar{\mathbf{J}}_{f_0} = \bar{\mathbf{J}}_{a_0} \qquad \forall\, \mathbf{x} \in \Omega ,$$

$$i\omega\left\{\mathrm{div}\,\bar{\mathbf{D}}_0\right\} + \mathrm{div}\,\bar{\mathbf{J}}_{f_0} = -\mathrm{div}\,\bar{\mathbf{J}}_{a_0} \qquad \forall\, \mathbf{x} \in \Omega ,$$

with the volume constraint

$$\bar{\rho}_{f_0} = \bar{\rho}_{a_0} \qquad \text{in } \Omega_{\rho_a} \subset \Omega ,$$

with the interface constraints

$$\bar{\mathbf{K}}_{f_0} = \bar{\mathbf{K}}_{a_0} \qquad \text{on } \partial\Omega_{\mathbf{K}_a} \subset \Omega ,$$

$$\bar{\sigma}_{f_0} = \bar{\sigma}_{a_0} \qquad \text{on } \partial\Omega_{\sigma_a} \subset \Omega ,$$

with the boundary conditions for the real part

$$Re\left\{\bar{\mathbf{A}}_0\right\} = Re\left\{\bar{\mathbf{A}}_{a_0}\right\} \qquad \text{on } \Gamma_{g_{A_r}} ,$$

$$Re\left\{\bar{\mathbf{H}}_0 \times \hat{\mathbf{n}}\right\} = Re\left\{\left(\bar{\mathbf{H}}_0 \times \hat{\mathbf{n}}\right)_a\right\} \qquad \text{on } \Gamma_{h_{A_r}} ,$$

$$Re\left\{\bar{\psi}_0\right\} = Re\left\{\bar{\psi}_{a_0}\right\} \qquad \text{on } \Gamma_{g_{\psi_r}} ,$$

$$Re\left\{\left(i\omega\bar{\mathbf{D}}_0 + \bar{\mathbf{J}}_{f_0}\right)\cdot\hat{\mathbf{n}}\right\} = Re\left\{\left(\left(i\omega\bar{\mathbf{D}}_0 + \bar{\mathbf{J}}_{f_0}\right)\cdot\hat{\mathbf{n}}\right)_a\right\} \quad \text{on } \Gamma_{h_{\psi_r}} ,$$

with the boundary conditions for the imaginary part

$$Im\left\{\bar{\mathbf{A}}_0\right\} = Im\left\{\bar{\mathbf{A}}_{a_0}\right\} \qquad \text{on } \Gamma_{g_{A_i}} ,$$

$$Im\left\{\bar{\mathbf{H}}_0 \times \hat{\mathbf{n}}\right\} = Im\left\{\left(\bar{\mathbf{H}}_0 \times \hat{\mathbf{n}}\right)_a\right\} \qquad \text{on } \Gamma_{h_{A_i}} ,$$

$$Im\left\{\bar{\psi}_0\right\} = Im\left\{\bar{\psi}_{a_0}\right\} \qquad \text{on } \Gamma_{g_{\psi_i}} ,$$

$$Im\left\{\left(i\omega\bar{\mathbf{D}}_0 + \bar{\mathbf{J}}_{f_0}\right)\cdot\hat{\mathbf{n}}\right\} = Im\left\{\left(\left(i\omega\bar{\mathbf{D}}_0 + \bar{\mathbf{J}}_{f_0}\right)\cdot\hat{\mathbf{n}}\right)_a\right\} \quad \text{on } \Gamma_{h_{\psi_i}} .$$

$$(2.33)$$

The boundary $\partial\Omega =: \overline{\Gamma_{h_{A_r}} \cup \Gamma_{g_{A_r}}}$, where $\Gamma_{h_{A_r}}$ is the part of the boundary with a $\mathbf{H}_r$ field specified, and $\Gamma_{g_{A_r}}$ is the remaining part of the boundary where the vector

potential $\mathbf{A}_r$ is specified. In addition, the boundary $\partial\Omega =: \overline{\Gamma_{h_{A_i}} \cup \Gamma_{g_{A_i}}}$, where $\Gamma_{h_{A_i}}$ is the part of the boundary with a $\mathbf{H}_i$ field is specified, and $\Gamma_{g_{A_i}}$ is the remaining part of the boundary where a vector potential $\mathbf{A}_i$ is specified. The boundary $\partial\Omega =: \overline{\Gamma_{h_{\psi_r}} \cup \Gamma_{g_{\psi_r}}}$, where $\Gamma_{h_{\psi_r}}$ is the part of the boundary with a $\left(-\omega\mathbf{D}_{0i} + \mathbf{J}_{f_{0r}}\right)$ field is specified, and $\Gamma_{g_{\psi_r}}$ is the remaining part of the boundary where a potential ψ_r is specified. In addition, the boundary $\partial\Omega =: \overline{\Gamma_{h_{\psi_i}} \cup \Gamma_{g_{\psi_i}}}$, with $\Gamma_{h_{\psi_i}}$ is the part of the boundary where a $\left(\omega\mathbf{D}_{0r} + \mathbf{J}_{f_{0i}}\right)$ is specified, and $\Gamma_{g_{\psi_i}}$ is the remaining part of the boundary where a potential ψ_i is specified.

2.3. Gauge Conditions.

The solution of the electromagnetic problems (2.23), (2.24), (2.26), and (2.33) in terms of the electromagnetic potentials $\mathbf{A}$ and ψ is not unique. If $(\mathbf{A}, \psi)$ is the solution of the electromagnetic problem, then a set of potentials $(\mathbf{A}', \psi')$ that are defined by

$$
\begin{aligned}
\mathbf{A}' &:= \mathbf{A} + \operatorname{grad} f , \\
\psi' &:= \psi - f ,
\end{aligned}
\tag{2.34}
$$

for any arbitrary scalar function $f : \Omega \to \mathbf{R}$ produces the same field via the definition (2.16). Hence, the problem does not have a unique solution. However, from a numerical standpoint, a unique solution is important (Williamson and Chan [1993]). It improves convergence, and in some cases, the accuracy of the solution. For eigenvalue problems, non-uniqueness can lead to spurious modes; see e.g., Kikuchi [1987], Bossavit [1989], and Bossavit [1990].

A simplistic viewpoint to explain the non-uniqueness of the potentials is based on relating $\mathbf{A}$ to the "motion" of a volume (MacNeal [1989]). Consider a cube in Figure 2.3. Uniqueness is achieved when the translation, the rotation (related to to the curl), the volume change (related to the divergence), and the "deformation" are specified. The curl $\mathbf{A}$ is specified by Ampere's law, i.e., by (2.3). The translation and

Translation

Curl (Rotation)

Divergence (volume change)
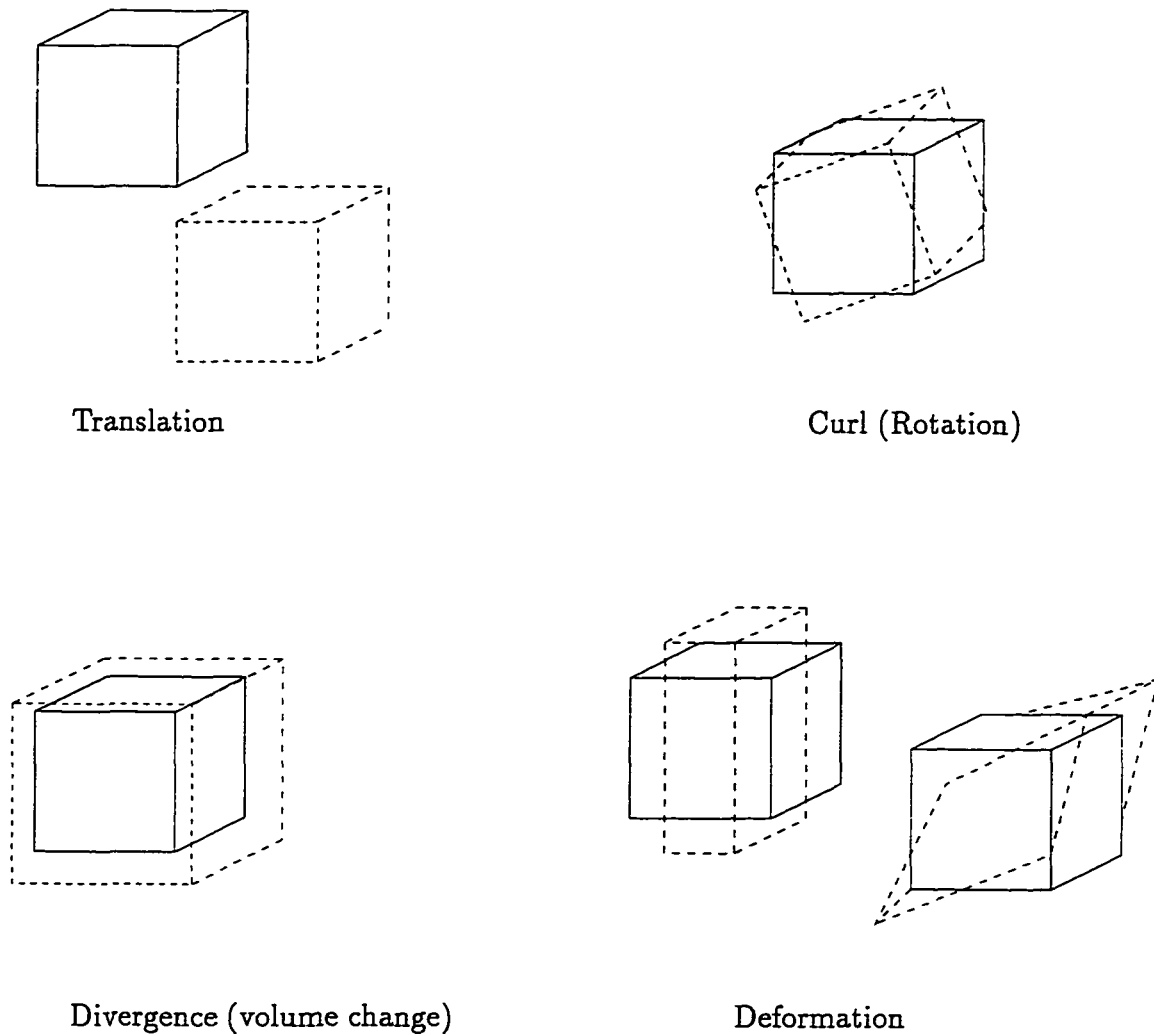
Deformation

Figure 2.2.   Vector potential **A** interpreted as "motion" with four primary parts: Translation, rotation, divergence, and deformation.

the "deformation" are specified by appropriate boundary conditions on **A**. However, the above problem formulations does not include any constraint (specification) for div **A**, and hence, the solution is not unique.

To make the solution unique we need additional constraints on the potentials $(\mathbf{A}, \psi)$. These constraints are termed *gauge* conditions. The word gauge refers to

the fact that the pair $(\mathbf{A}, \psi)$ can be calibrated (Lowther and Silvester [1986]). The popular gauge conditions can be categorized into *differential* gauges and *algebraic* gauges. Differential gauges include a constraint that involves the derivatives of the potentials. Coulomb gauge,[9] Lorentz gauge, London gauge, etc., are differential gauges (Hammond [1982]). Compared to the differential gauges, the development of algebraic gauges is recent (Carpenter [1977] and Brown [1982]). Algebraic gauges do not directly constrain the derivatives of the potential, and hence, are easier to implement in a FE solution. A popular algebraic gauge is to constrain the vector potential $\mathbf{A}$ using $\mathbf{A} \cdot \mathbf{w} = 0$, where $\mathbf{w}$ is a field without closed field lines. The gauge is effectively enforced for edge elements using a "tree" technique; see e.g., Albanese and Rubinacci [1990]. However, the formulation and implementation of algebraic gauges has been confined to magnetostatic and eddy-current problems. Its performance for problems with material properties changing with position is yet to be studied. Numerical results demonstrate that algebraic gauge overconstrains the vector potential $\mathbf{A}$ at material interfaces (Mesquita and Bastos [1992]). For the problems with capacitors, the Coulomb gauge is relatively easy to implement in the FE formulation, and is the gauge of choice for the remainder of the thesis.

Coulomb gauge[10] requires the constraint

$$\operatorname{div} \mathbf{A}(\mathbf{x}, t) = 0 , \tag{2.35}$$

to be satisfied for all time $t \in \mathbf{R}^+$ and at all points $\mathbf{x} \in \mathbf{R}^3$. Substituting the Coulomb gauge in (2.34), we obtain

$$\operatorname{div}(\operatorname{grad} f) = 0 .$$

---

[9] The Coulomb gauge is also referred to as the transverse gauge; see e.g., Jackson [1962, p. 141].

[10] For time-harmonic problems, the Coulomb gauge translates into two constraints, i.e, $\operatorname{div} \mathbf{A}_r = 0$ and $\operatorname{div} \mathbf{A}_i = 0$ for all time $t \in \mathbf{R}^+$ and at all points $\mathbf{x} \in \mathbf{R}^3$.

If the function f on the boundary is confined to zero, then using the Maximum Principle[11] (Courant and Hilbert [1962, p.255]) we can show that $f \equiv 0$ inside the domain of solution. Hence, the potentials $(\mathbf{A}, \psi)$ are unique. The above arguments do not hold true if the domain under consideration has discontinuous material properties, in particular, the permeability μ. For example, in a problem with a transformer, the core has a high permeability μ, and the surrounding air has low μ. In this case, the Coulomb gauge does not eliminate the nonuniqueness of the vector potential but rather "narrows" down the nonuniqueness (Mayergoyz [1993]). In such problems, a notion of "combined" gauges may be used, where additional constraints at the material interfaces are imposed; see e.g., Mayergoyz [1993]. In the discussions that follows, we use the Coulomb gauge combined with appropriate boundary conditions. Imposing the Coulomb gauge does not make the solution unique, but it does reduce the degree of nonuniqueness of the solution. Section 3.2.1 on page 40 discusses the enforcement of the Coulomb gauge in a FE solution.

Under the Coulomb gauge, the vector potential $\mathbf{A}$ still obeys the wave equation, however, the wave propagation effects are removed from the scalar potential ψ. Therefore, ψ is also called as the instantaneous potential. The dynamic (wave) effects of the electric field are now contained in the vector potential $\mathbf{A}$.

---

[11] The Maximum Principle can be stated as follows. Let the function f be regular and harmonic in a connected volume Ω and continuous up to and on the boundary $(\partial\Omega)$. Then its maximum and minimum are always attained on the boundary; the maximum and minimum are attained in the interior if and only if f is a constant.

In this chapter we formulate the weak (variational) counterpart of the static, transient, and time-harmonic problems formulated in Chapter 2. Problems (2.23), (2.24), (2.26), and (2.33) are second-order partial differential equations in terms of the potentials $(\mathbf{A}, \psi)$, and hence require $(\mathbf{A}, \psi)$ to be at least twice-differentiable. However, the solution to the the weak forms presented in this chapter, require $(\mathbf{A}, \psi)$ to be only once-differentiable. These weak forms are used to construct the matrix equations in Chapter 4.

3.1. Weak Form for the Electrostatic Problem

Let $W_\psi : (\Omega \setminus \Omega_{cond}) \to \mathbf{R}$ be a weighting function.[12] We transform problem (2.23) into a weighted residual form

$$\int_{\Omega \setminus \Omega_{cond}} W_\psi \left\{ \operatorname{div} \mathbf{D}_0 - \rho_{f0} \right\} \, d\Omega = 0 \quad \forall \, W_\psi \in \mathbf{R} \ . \tag{3.1}$$

Using the vector identity

$$W_\psi \left(\operatorname{div} \mathbf{D}_0 \right) = \operatorname{div} \left(W_\psi \mathbf{D}_0 \right) - \operatorname{grad} W_\psi \cdot \mathbf{D}_0$$

---

[12] The weighting function corresponding to the unknown $\dot{\psi}_0$ should be represented by $W_{\dot{\psi}_0}$. However, to improve the readability of the document we omit the dot " $\bullet$ " and the subscript zero "0".

and applying the divergence theorem[13] we obtain the weak form

$$
\text{Find } \dot{\psi}_0 \in \mathcal{S}_{\psi_0} \ , \ \forall\, \mathbf{x} \in (\Omega \setminus \Omega_{cond}), \text{ such that}
$$

$$
- \int_{\Omega \setminus \Omega_{cond}} \text{grad}\, W_\psi \cdot \mathbf{D}_0 \ d\Omega
$$

$$
= \int_{\Omega_{\rho_{a0}}} \rho_{a0} W_\psi \ d\Omega - \int_{\Gamma_{h\dot{\psi}_0}} W_\psi (\mathbf{D}_0 \cdot \hat{\mathbf{n}}) \ d(\partial\Omega) \ , \quad \forall\, W_\psi \in \mathcal{V}_{\psi_0} \ .
$$

$$(3.2)$$

As explained earlier, we split the boundary $\partial\Omega =: \overline{\Gamma_{h\dot{\psi}_0} \cup \Gamma_{g\dot{\psi}_0}}$, where $\Gamma_{h\dot{\psi}_0}$ is the part of the boundary on which the field $\mathbf{D}_0 \cdot \hat{\mathbf{n}}$ is specified, and $\Gamma_{g\dot{\psi}_0}$ is the remaining part of the boundary on which $\dot{\psi}_0$ is specified. Recall that $\mathbf{D}_0 = \epsilon_0 \mathbf{E}_0 + \mathbf{P}_0(\mathbf{E}_0) = -\epsilon_0 \text{grad}\, \dot{\psi}_0 + \mathbf{P}_0(-\text{grad}\, \dot{\psi}_0)$ using the constitutive law (2.6), where $\mathbf{P}_0$ is electric polarization.

The terms on the right-hand side of the equation are associated with the "known" quantities that are specified in the problem statement. The term on the left-hand side of the equation corresponds to the "mass"[14] matrix in the final matrix equation (4.23). The space $\mathcal{V}_{\psi_0}$ for the weighting functions is defined as

$$
\mathcal{V}_{\psi_0} := \left\{ W_\psi \in \mathcal{H}^1 (\Omega \setminus \Omega_{cond}) \ \middle|\ W_\psi(\mathbf{x}) = 0 \ , \ \forall\, \mathbf{x} \in \Gamma_{g\dot{\psi}_0} \right\} \ , \qquad (3.3)
$$

---

[13] Let $\mathbf{v} : \Omega \to \mathbf{R}^3$ be continuously differentiable vector field. Then the divergence theorem states that

$$
\int_\Omega (\text{div}\, \mathbf{v}) \ d\Omega \ = \ \int_{(\partial\Omega)} \mathbf{v} \cdot \hat{\mathbf{n}} \ d(\partial\Omega) \ ,
$$

where the surface $(\partial\Omega)$ is the boundary to the volume Ω, and $\hat{\mathbf{n}}$ is the unit outward normal to the surface $(\partial\Omega)$.

[14] The nomenclature "mass", "damping", and "stiffness" is adopted from mechanics. The "mass" is associated with the acceleration (second time-derivative of position), the "damping" is associated with the velocity (first time-derivative of position), and "stiffness" is associated with the displacement (position). In the matrix equation (4.53) for transient problems, we observe that the terms containing the permittivity ϵ are associated with the second time-derivative and hence are referred to as components of the "mass" matrix. Similarly, terms containing the conductivity σ and permeability μ are referred to as components of the "damping" matrix and the "stiffness" matrix, respectively.

where

$$\mathcal{H}^1(\Omega) := \left\{ w \mid w \in L_2(\Omega) \text{ and } \frac{\partial w}{\partial x} \in L_2(\Omega) \right\} , \tag{3.4}$$

and

$$L_2(\Omega) := \left\{ w \mid \int_\Omega w^2 d\Omega < +\infty \right\} \equiv \mathcal{H}^0(\Omega) .$$

The space $\mathcal{S}_{\psi_0}$ for the trial functions is defined as

$$\mathcal{S}_{\psi_0} := \left\{ W_\psi \in \mathcal{H}^1(\Omega \setminus \Omega_{cond}) \mid W_\psi(\mathbf{x}) = \dot{\psi}_{a_0} , \ \forall \ \mathbf{x} \in \Gamma_{h\dot{\psi}_0} \right\} . \tag{3.5}$$

Note that in the present document, character $\mathcal{S}$ is used for the space of trial solutions, and the character $\mathcal{V}$ is used for the space of weighting functions.

3.2. Weak Form for the Magnetostatic Problem

Let $\mathbf{W}_A : \Omega \to \mathbf{R}^3$ be a weighting vector field on Ω. We transform problem (2.24) into weighted residual form

$$\int_\Omega \mathbf{W}_A \cdot \{ \text{curl } \mathbf{H}_0 - \mathbf{J}_{a_0} \} \ d\Omega = 0 , \quad \forall \ \mathbf{W}_A \in \mathbf{R}^3 . \tag{3.6}$$

Using the vector identity

$$\mathbf{W}_A \cdot (\text{curl } \mathbf{H}_0) = -\text{div } (\mathbf{W}_A \times \mathbf{H}_0) + (\text{curl } \mathbf{W}_A) \cdot \mathbf{H}_0$$

and applying the divergence theorem we obtain the weak form

Find $\mathbf{A}_0 \in \mathcal{S}_{A_0}$ such that

$$\int_\Omega (\text{curl } \mathbf{W}_A) \cdot \mathbf{H}_0 \ d\Omega$$
$$= \int_\Omega \mathbf{W}_A \cdot \mathbf{J}_{a_0} \ d\Omega - \int_{\Gamma_{h_{A_0}}} \mathbf{W}_A \cdot (\mathbf{H}_0 \times \hat{\mathbf{n}}) \ d(\partial\Omega) , \quad \forall \ \mathbf{W}_A \in \mathcal{V}_{A_0} .$$

$$\tag{3.7}$$

The space $\mathcal{V}_{\psi_0}$ for the weighting functions is defined as

$$\mathcal{V}_{A_0} := \left\{ \mathbf{W}_A \in \mathcal{H}^1(\Omega) \;\middle|\; \mathbf{W}_A(\mathbf{x}) = \mathbf{0} \;,\; \forall\, \mathbf{x} \in \Gamma_{g_{A_0}} \right\} \;, \tag{3.8}$$

and the space of trial solutions

$$\mathcal{S}_{A_0} := \left\{ \mathbf{W}_A \in \mathcal{H}^1(\Omega) \;\middle|\; \mathbf{W}_A(\mathbf{x}) = \mathbf{A}_{a_0} \;,\; \forall\, \mathbf{x} \in \Gamma_{g_{A_0}} \right\} \;. \tag{3.9}$$

As explained earlier, we split the boundary $\partial\Omega =: \overline{\Gamma_{h_{A_0}} \cup \Gamma_{g_{A_0}}}$, where $\Gamma_{h_{A_0}}$ is the part of the boundary on which the $\mathbf{H}_0 \times \hat{\mathbf{n}}$ field is specified, and $\Gamma_{g_{A_0}}$ is the remaining part of the boundary on which $\mathbf{A}_0$ is specified. Recall that $\mathbf{H}_0 = \dfrac{1}{\mu_0}\mathbf{B}_0 + \mathbf{M}_0(\mathbf{B}_0) = \dfrac{1}{\mu_0}\mathrm{curl}\,\mathbf{A}_0 + \mathbf{M}_0(\mathrm{curl}\,\mathbf{A}_0)$ using the constitutive law (2.6), where $\mathbf{M}_0$ is magnetization.

The terms on the right-hand side of the equation are associated with the "known" quantities that are specified in the problem statement. The term on the left-hand side of the equation corresponds to the "stiffness" matrix in the final matrix equation (4.23).

3.2.1. Coulomb Gauge

Uniqueness is enforced on the admissible vector potential $\mathbf{A}_0 \in \mathcal{S}_{A_0}$ using the Coulomb gauge (2.35) via a penalty method (e.g., Williamson and Chan [1993]). The weak form in (3.7) is modified to find $\mathbf{A}_0 \in \mathcal{S}_{A_0}$ such that

$$\int_\Omega (\mathrm{curl}\,\mathbf{W}_A)\cdot\mathbf{H}_0\; d\Omega \;+\; \int_\Omega \flat\,(\mathrm{div}\,\mathbf{W}_A)(\mathrm{div}\,\mathbf{A}_0)\; d\Omega$$

$$= \int_\Omega \mathbf{W}_A\cdot\mathbf{J}_{a_0}\; d\Omega - \int_{\Gamma_{h_{A_0}}} \mathbf{W}_A\cdot(\mathbf{H}_0\times\hat{\mathbf{n}})\; d(\partial\Omega) \;,\quad \forall\,\mathbf{W}_A \in \mathcal{V}_{A_0} \;, \tag{3.10}$$

where $\flat(\mathbf{x}) : \Omega \to \mathbf{R}^+$ is the penalty parameter. The choice of the penalty parameter $\flat$ is crucial to the numerical accuracy of the ensuing solution. Choosing an extremely high value for $\flat$ leads to a trivial solution $\mathbf{A} \equiv 0$. This phenomenon of overconstraining the vector potential is called mesh locking. On the contrary, too

small a value of þ leads to a non-unique solution. In order to obtain an effective solution, the term

$$\int_\Omega þ\,(\mathrm{div}\,\mathbf{W}_A)(\mathrm{div}\,\mathbf{A}_0)\;d\Omega \tag{3.11}$$

is integrated using reduced integration (fewer Gauss integration points than the other integrals) with a suitably high þ. The reduced integration renders singular the FE matrix that corresponds to the Coulomb gauge. The penalty parameter þ is estimated by trials and errors. Williamson and Chan [1993] notes that the enforcement of the Coulomb gauge is not crucial if we use direct solvers (e.g., Gauss elimination), however, for iterative solvers, the Coulomb gauge must be strictly enforced. The no-gauge formulation is also effective for some electromagnetic problems see, e.g., Cendes, Weiss and Hoole [1982], Hoole, Rios and Yoganathan [1988], Nakata, Takahashi, Fujiwara and Shiraki [1990] and Morisue [1993]. The Coulomb gauge in electromagnetics is equivalent to the incompressibility constraint in elasticity. Most of the methods to enforce the Coulomb gauge have been derived from methods used in incompressible elasticity.

In addition to the penalty term in the weak form, it is imperative that the boundary of the electromagnetic problem does not excite div $\mathbf{A}$. This is enforced in an integral sense as follows:

$$\int_\Omega (\mathrm{div}\,\mathbf{A}_0)\;d\Omega \;=\; \int_{\partial\Omega} (\mathbf{A}_0\boldsymbol{\cdot}\hat{\mathbf{n}})\;d(\partial\Omega) \;=\; 0\;, \tag{3.12}$$

where $\partial\Omega$ is the surface boundary enclosing the volume Ω. A convenient choice to enforce the above condition is to choose $\mathbf{A}_0\boldsymbol{\cdot}\hat{\mathbf{n}} = 0$ on the boundary, where $\hat{\mathbf{n}}$ is the unit normal to the surface $\partial\Omega$. To recapitulate, the Coulomb gauge is enforced via the inclusion of the a penalty term (3.11) in the weak form, and a boundary condition $\mathbf{A}_0\boldsymbol{\cdot}\hat{\mathbf{n}} = 0$ on the exterior surface.

An alternative to the penalty method to enforce the Coulomb gauge is the use

of the Lagrange multiplier method. However, the Lagrange multiplier method requires the use of an additional variable, the Lagrange multiplier, and hence increases the number of unknowns to be determined (see e.g., Lee [1993]).

3.3. Weak Form for the Transient Problem

In the ensuing discussion, we focus on a simple case with Assumption 3.1. With this assumption we transcribe problem (2.26) into a weak form.

Assumption 3.1. The following assumptions are made to solve time-dependent problems: For all time $t > 0$, the Volume-charge density ρ_f is not prescribed anywhere in the volume Ω, and the surface current K_a and surface-charge density σ_a are not specified on any surface inside the volume Ω. ∎

3.3.1. Ampere's Law

Let $W_A : \Omega \to R^3$ be a weighting vector field Ω. The weighted residual form for the first equation in (2.26) is

$$\int_\Omega W_A \cdot \left\{ \text{curl}\, H - \frac{\partial D}{\partial t} - J_f - J_a \right\} \, d\Omega = 0 \, , \quad \forall\, W_A \in R^3 \, . \tag{3.13}$$

Using the vector identity

$$W_A \cdot (\text{curl}\, H) = \text{div}\,(W_A \times H) \, + \, (\text{curl}\, W_A) \cdot H$$

and applying the divergence theorem to (3.13) we obtain

$$\int_{\partial\Omega} W_A \cdot (H \times \hat{n}) \; d(\partial\Omega) + \int_\Omega (\text{curl}\, W_A) \cdot H \; d\Omega - \int_\Omega W_A \cdot \frac{\partial D}{\partial t} \; d\Omega$$
$$- \int_\Omega W_A \cdot J_a \; d\Omega - \int_\Omega W_A \cdot J_f \; d\Omega = 0 \, , \quad \forall\, W_A \in \mathcal{V}_A \, .$$

If the boundary $\partial\Omega =: \overline{\Gamma_{h_A} \cup \Gamma_{g_A}}$, where Γ_{h_A} is the part of the boundary with a H field specified, and Γ_{g_A} is the remaining part of the boundary with the vector

potential **A** specified. Then we can rewrite the above equation as follows

$$-\int_\Omega \mathbf{W}_A \cdot \frac{\partial \mathbf{D}}{\partial t} \, d\Omega - \int_\Omega \mathbf{W}_A \cdot \mathbf{J}_f \, d\Omega + \int_\Omega (\operatorname{curl} \mathbf{W}_A) \cdot \mathbf{H} \, d\Omega$$

$$= -\int_{\Gamma_{h_A}} \mathbf{W}_A \cdot (\mathbf{H} \times \hat{\mathbf{n}}) \, d(\partial\Omega) + \int_\Omega \mathbf{W}_A \cdot \mathbf{J}_a \, d\Omega \,, \qquad \forall \, \mathbf{W}_A \in \mathcal{V} \,.$$

(3.14)

The terms on the right-hand side of (3.14) are associated with the "known" quantities that are specified in the problem statement. The three terms on the left-hand side of the equation correspond to the "mass", "damping" and "stiffness" matrices, respectively, in the final matrix equation (4.53). The space $\mathcal{V}_A$ for the weighting functions is defined as

$$\mathcal{V}_A := \Big\{ \ \mathbf{W}_A = \big\{ W_A^1, \ W_A^2, \ W_A^3 \big\} \in \big(\mathcal{H}^1(\Omega)\big)^3$$

$$\Big| \ W_A^i \in \mathcal{H}^1(\Omega) \ \forall \, i = 1, 2, 3 \quad \text{and} \quad \mathbf{W}_A(\mathbf{x}) = 0 \,, \ \forall \, \mathbf{x} \in \Gamma_{g_A} \Big\} \,,$$

(3.15)

and the corresponding space of trial functions (used later)

$$\mathcal{S}_A := \Big\{ \ \mathbf{W}_A = \big\{ W_A^1, \ W_A^2, \ W_A^3 \big\} \in \big(\mathcal{H}^1(\Omega)\big)^3$$

$$\Big| \ W_A^i \in \mathcal{H}^1(\Omega) \ \forall \, i = 1, 2, 3 \quad \text{and} \quad \mathbf{W}_A(\mathbf{x}) = \mathbf{A}_a \,, \ \forall \, \mathbf{x} \in \Gamma_{g_A} \Big\} \,.$$

(3.16)

3.3.2. Time-integrated Continuity Equation

Let $W_\psi : \Omega \to \mathbf{R}$ be a weighting function. The weighted residual form $(2.26)_2$ is

$$\int_\Omega W_\psi \left\{ \frac{\partial \operatorname{div} \mathbf{D}}{\partial t} + \operatorname{div} \mathbf{J}_f + \operatorname{div} \mathbf{J}_a \right\} d\Omega = 0 \,, \qquad \forall \, W_\psi \in \mathbf{R} \,. \tag{3.17}$$

Using the vector identity

$$W_\psi \left(\operatorname{div} \mathbf{D} \right) = \operatorname{div} \left(W_\psi \mathbf{D} \right) \, - \, \operatorname{grad} W_\psi \cdot \mathbf{D}$$

and applying the divergence theorem we obtain

$$\int_{\partial\Omega} W_\psi \left(\frac{\partial \mathbf{D}}{\partial t}\cdot\hat{\mathbf{n}}\right)\, d(\partial\Omega) - \int_\Omega \operatorname{grad} W_\psi\cdot\frac{\partial \mathbf{D}}{\partial t}\, d\Omega + \int_\Omega W_\psi(\operatorname{div}\mathbf{J}_a)\, d\Omega$$

$$+ \int_{\partial\Omega} W_\psi\,(\mathbf{J}_f\cdot\hat{\mathbf{n}})\, d(\partial\Omega) - \int_\Omega \operatorname{grad} W_\psi\cdot\mathbf{J}_f\cdot\, d\Omega = 0, \quad \forall\, W_\psi \in \mathcal{V}_\psi.$$

The boundary $\partial\Omega =: \overline{\Gamma_{h\psi}\cup\Gamma_{g\psi}}$, where $\Gamma_{h\psi}$ is the part of the boundary where the $\left(\frac{\partial\mathbf{D}}{\partial t}+\mathbf{J}_f\right)$ field is specified, and $\Gamma_{g\psi}$ is the remaining part of the boundary where the time integrated scalar potential ψ is specified. Then we can rewrite the above equation as follows.

$$-\int_\Omega \operatorname{grad} W_\psi\cdot\frac{\partial\mathbf{D}}{\partial t}\, d\Omega - \int_\Omega \operatorname{grad} W_\psi\cdot\mathbf{J}_f\, d\Omega$$

$$= -\int_{\Gamma_{h\psi}} W_\psi\left(\frac{\partial\mathbf{D}}{\partial t}\cdot\hat{\mathbf{n}}\right)\, d(\partial\Omega) - \int_{\Gamma_{h\psi}} W_\psi\,(\mathbf{J}_f\cdot\hat{\mathbf{n}})\, d(\partial\Omega) + \int_\Omega W_\psi(\operatorname{div}\mathbf{J}_a)\, d\Omega,$$

$$\forall\, W_\psi \in \mathcal{V}_\psi.$$

$$(3.18)$$

The terms on the right-hand side of the equation (3.18) are associated with the "known" quantities that are specified in the problem statement. The two terms on the left-hand side of the equation correspond to the "mass" and "damping" matrices, respectively, in the final matrix equation (4.53). The space $\mathcal{V}_\psi$ of weighting functions is defined as

$$\mathcal{V}_\psi := \left\{ W_\psi \in \mathcal{H}^1(\Omega)\,\middle|\, W_\psi(\mathbf{x}) = 0,\ \forall\,\mathbf{x}\in\Gamma_{g\psi}\right\}, \qquad (3.19)$$

and the corresponding space of trial solutions (used later)

$$\mathcal{S}_\psi := \left\{ W_\psi \in \mathcal{H}^1(\Omega)\,\middle|\, W_\psi(\mathbf{x}) = \psi_a,\ \forall\,\mathbf{x}\in\Gamma_{g\psi}\right\}. \qquad (3.20)$$

3.3.3. Combined Weak Form

To state the weak form in a concise form, we define the following. Let the combination of the vector potential $\mathbf{A}$ and the scalar potential ψ be defined as

$$\mathbf{\Pi} := \left\{\mathbf{A}\,\middle|\,\psi\right\} \equiv \left\{A^1, A^2, A^3, \psi\right\}, \qquad (3.21)$$

where $\mathbf{\Pi} : \Omega \times R \rightarrow R^4$ is the combined potential. Let $\cdot \mathbf{W} : \Omega \rightarrow R^4$ be a weighting function

$$\mathbf{W} := \left\{ \mathbf{W}_A \,\middle|\, W_\psi \right\} \equiv \left\{ W_A^1, W_A^2, W_A^3, W_\psi \right\} . \tag{3.22}$$

Let the space $\mathcal{V}$ of trial functions be defined as

$$\mathcal{V} := \left\{ \begin{array}{l} \mathbf{W} = \left\{ W^1, W^2, W^3, W^4 \right\} \\[2mm] \;\middle|\; \left\{ W^1, W^2, W^3 \right\} \in \mathcal{V}_A \quad \text{and} \quad W^4 \in \mathcal{V}_\psi \end{array} \right\} , \tag{3.23}$$

and the space of trial solutions $\mathcal{S}$ be defined as

$$\mathcal{S} := \left\{ \begin{array}{l} \mathbf{W} = \left\{ W^1, W^2, W^3, W^4 \right\} \\[2mm] \;\middle|\; \left\{ W^1, W^2, W^3 \right\} \in \mathcal{S}_A \quad \text{and} \quad W^4 \in \mathcal{S}_\psi \end{array} \right\} . \tag{3.24}$$

The weak forms (3.14) and (3.18) are combined as follows.

Given $\mathbf{\Pi}_0(\mathbf{x})$ and $\dot{\mathbf{\Pi}}_0(\mathbf{x})$, find $\mathbf{\Pi} \in \mathcal{S}$ $\forall \, \mathbf{x} \in \Omega$ and $t > 0$ such that

$$\mathcal{G}_m(\mathbf{W}, \mathbf{\Pi}) + \mathcal{G}_b(\mathbf{W}, \mathbf{\Pi}) + \mathcal{G}_k(\mathbf{W}, \mathbf{\Pi}) = \mathcal{G}_f(\mathbf{W}) , \qquad \forall \, \mathbf{W} \in \mathcal{V} ,$$

$$\tag{3.25}$$

where the new operators are defined as follows.

$$\mathcal{G}_m(\mathbf{W}, \mathbf{\Pi}) \quad := -\int_\Omega \mathbf{W}_A \cdot \frac{\partial \mathbf{D}}{\partial t}\, d\Omega - \int_\Omega \operatorname{grad} W_\psi \cdot \frac{\partial \mathbf{D}}{\partial t}\, d\Omega , \tag{3.26}$$

$$\mathcal{G}_b(\mathbf{W}, \mathbf{\Pi}) \quad := -\int_\Omega \mathbf{W}_A \cdot \mathbf{J}_f\, d\Omega - \int_\Omega \operatorname{grad} W_\psi \cdot \mathbf{J}_f\, d\Omega , \tag{3.27}$$

$$\mathcal{G}_k(\mathbf{W}, \mathbf{\Pi}) \quad := \int_\Omega (\operatorname{curl} \mathbf{W}_A) \cdot \mathbf{H}\, d\Omega , \quad \text{and} \tag{3.28}$$

$$\begin{aligned} \mathcal{G}_f(\mathbf{W}) \quad &:= -\int_{\Gamma_{h_A}} \mathbf{W}_A \cdot (\mathbf{H} \times \hat{\mathbf{n}})\; d(\Omega) + \int_\Omega \mathbf{W}_A \cdot \mathbf{J}_a\, d\Omega \\[2mm] &\quad - \int_{\Gamma_{h_\psi}} W_\psi \left(\frac{\partial \mathbf{D}}{\partial t} \cdot \hat{\mathbf{n}} \right)\, d(\partial\Omega) - \int_{\Gamma_{h_\psi}} W_\psi (\mathbf{J}_f \cdot \hat{\mathbf{n}})\; d(\partial\Omega) \\[2mm] &\quad + \int_\Omega W_\psi (\operatorname{div} \mathbf{J}_a)\, d\Omega . \end{aligned} \tag{3.29}$$

The field quantities $\mathbf{D}$, $\mathbf{J}_f$ and $\mathbf{H}$ are related to the potential $\mathbf{\Pi}$ and its time and spatial derivatives via the constitutive equations (2.6). From (2.26), we have $\psi_0 = 0$ and $\dot{\mathbf{A}}_0 = \mathbf{0}$. The problem to determine the remaining initial values, i.e., $\dot{\psi}_0$ and $\mathbf{A}_0$ are are obtained by solving (3.7) and (3.2), which can be concisely stated as follows.

$$
\boxed{
\begin{aligned}
&\text{Find } \mathbf{\Pi}_0(\mathbf{x}) \in \mathcal{S}_0 \text{ and } \dot{\mathbf{\Pi}}_0(\mathbf{x}) \in \dot{\mathcal{S}}_0 \; \forall \, \mathbf{x} \in \Omega \text{ and } t > 0 \text{ such that} \\[2mm]
&\mathcal{G}_{m_0}(\mathbf{W}, \mathbf{\Pi}_0) + \mathcal{G}_{k_0}(\mathbf{W}, \mathbf{\Pi}_0) = \mathcal{G}_{f_0}(\mathbf{W}) , \qquad\qquad \forall \, \mathbf{W} \in \mathcal{V}_0 .
\end{aligned}
}
\tag{3.30}
$$

The space $\mathcal{V}_0$ is defined as

$$
\mathcal{V}_0 := \left\{ \; \mathbf{W} = \left\{ W^1, \; W^2, \; W^3, \; W^4 \right\} \; \middle| \; \left\{ W^1, \; W^2, \; W^3 \right\} \in \mathcal{V}_{A_0} \quad \text{and} \quad W^4 \in \mathcal{V}_{\psi_0} \right\} ,
\tag{3.31}
$$

and the spaces of trial solutions $\mathcal{S}_0$ and $\dot{\mathcal{S}}_0$ are defined to be

$$
\mathcal{S}_0 := \left\{ \; \mathbf{W} = \left\{ W^1, \; W^2, \; W^3, \; W^4 \right\} \; \middle| \; \left\{ W^1, \; W^2, \; W^3 \right\} \in \mathcal{S}_{A_0} \quad \text{and} \quad W^4 = 0 \right\} ,
\tag{3.32}
$$

$$
\dot{\mathcal{S}}_0 := \left\{ \; \mathbf{W} = \left\{ W^1, \; W^2, \; W^3, \; W^4 \right\} \; \middle| \; W^1 = 0 , \; W^2 = 0 , \; W^3 = 0 , \quad \text{and} \quad W^4 \in \mathcal{S}_{\psi_0} \right\} .
\tag{3.33}
$$

The operators are defined to be

$$
\mathcal{G}_{m_0}(\mathbf{W}, \mathbf{\Pi}_0) \quad := -\int_{\Omega \backslash \Omega_{cond}} \operatorname{grad} W_\psi \cdot \mathbf{D}_0 \; d\Omega ,
\tag{3.34}
$$

$$
\mathcal{G}_{k_0}(\mathbf{W}, \mathbf{\Pi}_0) \quad := \int_\Omega (\operatorname{curl} \mathbf{W}_A) \cdot \mathbf{H}_0 \; d\Omega , \quad \text{and}
\tag{3.35}
$$

$$
\mathcal{G}_{f_0}(\mathbf{W}) \quad := \int_{\Gamma_{h_{A_0}}} \mathbf{W}_A \cdot (\mathbf{H}_0 \times \hat{\mathbf{n}}) \; d(\Omega) + \int_\Omega \mathbf{W}_A \cdot \mathbf{J}_{a_0} \; d\Omega
$$

$$
- \int_{\Gamma_{h\dot{\psi}_0}} W_\psi (\mathbf{D} \cdot \hat{\mathbf{n}}) \; d(\partial\Omega) .
\tag{3.36}
$$

The field quantities $\mathbf{D}_0$ and $\mathbf{H}_0$ are related to the combined potential $\boldsymbol{\Pi}_0$ and its time and spatial derivatives via the constitutive equations (2.6). The Coulomb gauge is imposed similar to the magnetostatic case in Section 3.2.1 on page 40. The stiffness operators $\mathcal{G}_k$ and $\mathcal{G}_{k_0}$ are modified to include the penalty term.

3.4. Weak Form for the Time-Harmonic Problem

Again we focus on a simple case with Assumption 3.1. With these assumptions we split the problem (2.33) into a weak form for its real and imaginary parts as follows.

3.4.1. Ampere's Law

Let $\bar{\mathbf{W}}_A : \Omega \to \mathbf{C}^3$ be a weighting function. The weighted residual form for the first equation in (2.33) is

$$\left. \begin{array}{l} \displaystyle\int_\Omega \mathbf{W}_{Ar} \cdot \left\{ \operatorname{curl} \mathbf{H}_{0r} + \omega \mathbf{D}_{0i} - \mathbf{J}_{f_{0r}} - \mathbf{J}_{a_{0r}} \right\} \, d\Omega = 0 \\[2mm] \displaystyle\int_\Omega \mathbf{W}_{Ai} \cdot \left\{ \operatorname{curl} \mathbf{H}_{0i} - \omega \mathbf{D}_{0r} - \mathbf{J}_{f_{0i}} - \mathbf{J}_{a_{0i}} \right\} \, d\Omega = 0 \end{array} \right\} \quad \forall \, \bar{\mathbf{W}}_A \in \mathbf{C}^3 \, . \quad (3.37)$$

Similar to the transient case, we obtain

$$\int_{\partial\Omega} \mathbf{W}_{Ar} \cdot (\mathbf{H}_{0r} \times \hat{\mathbf{n}}) \cdot d(\partial\Omega) + \int_\Omega (\operatorname{curl} \mathbf{W}_{Ar}) \cdot \mathbf{H}_{0r} \, d\Omega + \omega \int_\Omega \mathbf{W}_{Ar} \cdot \mathbf{D}_{0i} \, d\Omega$$
$$- \int_\Omega \mathbf{W}_{Ar} \cdot \mathbf{J}_{a_{0r}} \, d\Omega - \int_\Omega \mathbf{W}_{Ar} \cdot \mathbf{J}_{f_{0r}} \, d\Omega = 0 \, , \qquad \forall \, \mathbf{W}_{Ar} \in \mathcal{V}_{Ar} \, ,$$

and

$$\int_{\partial\Omega} \mathbf{W}_{Ai} \cdot (\mathbf{H}_{0i} \times \hat{\mathbf{n}}) \, d(\partial\Omega) + \int_\Omega (\operatorname{curl} \mathbf{W}_{Ai}) \cdot \mathbf{H}_{0i} \, d\Omega - \omega \int_\Omega \mathbf{W}_{Ai} \cdot \mathbf{D}_{0r} \, d\Omega$$
$$- \int_\Omega \mathbf{W}_{Ai} \cdot \mathbf{J}_{a_{0i}} \, d\Omega - \int_\Omega \mathbf{W}_{Ai} \cdot \mathbf{J}_{f_{0i}} \, d\Omega = 0 \, , \qquad \forall \, \mathbf{W}_{Ai} \in \mathcal{V}_{Ai} \, .$$

The boundary $\partial\Omega =: \overline{\Gamma_{h_{A_r}} \cup \Gamma_{g_{A_r}}}$, where $\Gamma_{h_{A_r}}$ is the part of the boundary with a $\mathbf{H}_r$ field specified, and $\Gamma_{g_{A_r}}$ is the remaining part of the boundary where the vector potential $\mathbf{A}_r$ is specified. In addition, the boundary $\partial\Omega =: \overline{\Gamma_{h_{A_i}} \cup \Gamma_{g_{A_i}}}$, where $\Gamma_{h_{A_i}}$

is the part of the boundary with a $\mathbf{H}_i$ field is specified, and $\Gamma_{g_{A_i}}$ is the remaining part of the boundary where a vector potential $\mathbf{A}_i$ is specified. We can rewrite the above equations as follows.

$$
\begin{aligned}
+\omega \int_\Omega \mathbf{W}_{Ar} \cdot \mathbf{D}_{0i}\, d\Omega &- \int_\Omega \mathbf{W}_{Ar} \cdot \mathbf{J}_{f_{0r}}\, d\Omega + \int_\Omega (\operatorname{curl} \mathbf{W}_{Ar}) \cdot \mathbf{H}_{0r}\, d\Omega \\
&= \int_{\Gamma_{h_{Ar}}} \mathbf{W}_{Ar} \cdot (\mathbf{H}_{0r} \times \hat{n})\, d(\partial\Omega) + \int_\Omega \mathbf{W}_{Ar} \cdot \mathbf{J}_{a_{0r}}\, d\Omega\,, \quad \forall\, \mathbf{W}_{Ar} \in \mathcal{V}_{Ar}\,, \\
-\omega \int_\Omega \mathbf{W}_{Ai} \cdot \mathbf{D}_{0r}\, d\Omega &- \int_\Omega \mathbf{W}_{Ai} \cdot \mathbf{J}_{f_{0i}}\, d\Omega + \int_\Omega (\operatorname{curl} \mathbf{W}_{Ai}) \cdot \mathbf{H}_{0i}\, d\Omega \\
&= \int_{\Gamma_{h_{Ai}}} \mathbf{W}_{Ai} \cdot (\mathbf{H}_{0i} \times \hat{n})\, d(\partial\Omega) + \int_\Omega \mathbf{W}_{Ai} \cdot \mathbf{J}_{a_{0i}}\, d\Omega\,, \quad \forall\, \mathbf{W}_{Ai} \in \mathcal{V}_{Ai}\,.
\end{aligned}
$$

$$(3.38)$$

The terms on the right-hand side of (3.38) are associated with the "known" quantities that are specified in the problem statement. The spaces of weighting functions are defined as

$$
\begin{aligned}
\mathcal{V}_{Ar} &:= \left\{ \ \mathbf{W}_A = \left\{ W_A^1,\, W_A^2,\, W_A^3 \right\} \in \left(\mathcal{H}^1(\Omega) \right)^3 \right. \\
&\qquad \left. \left| \ \mathbf{W}_A(\mathbf{x}) = \mathbf{0}\,,\ \forall\, \mathbf{x} \in \Gamma_{g_{Ar}} \right\}\,, \right. \\
\mathcal{V}_{Ai} &:= \left\{ \ \mathbf{W}_A = \left\{ W_A^1,\, W_A^2,\, W_A^3 \right\} \in \left(\mathcal{H}^1(\Omega) \right)^3 \right. \\
&\qquad \left. \left| \ \mathbf{W}_A(\mathbf{x}) = \mathbf{0}\,,\ \forall\, \mathbf{x} \in \Gamma_{g_{Ai}} \right\}\,, \right. \\
\bar{\mathcal{V}}_A &:= \left\{ \ \bar{\mathbf{W}}_A = (\mathbf{W}_{Ar} + i\mathbf{W}_{Ai}) : \Omega \to \mathbb{C}^3 \ \middle|\ \mathbf{W}_{Ar} \in \mathcal{V}_{Ar} \ \text{ and } \ \mathbf{W}_{Ai} \in \mathcal{V}_{Ai} \right\}\,.
\end{aligned}
$$

$$(3.39)$$

The spaces of trial solutions are defined as

$$
\mathcal{S}_{Ar} := \left\{ \ \mathbf{W}_A = \left\{ W_A^1, \ W_A^2, \ W_A^3 \right\} \in \left(\mathcal{H}^1(\Omega) \right)^3 \ \Bigg| \ \mathbf{W}_A(\mathbf{x}) = \mathbf{A}_{a_{0r}} \ , \ \forall \, \mathbf{x} \in \Gamma_{g_{Ar}} \right\} ,
$$

$$
\mathcal{S}_{Ai} := \left\{ \ \mathbf{W}_A = \left\{ W_A^1, \ W_A^2, \ W_A^3 \right\} \in \left(\mathcal{H}^1(\Omega) \right)^3 \ \Bigg| \ \mathbf{W}_A(\mathbf{x}) = \mathbf{A}_{a_{0r}} \ , \ \forall \, \mathbf{x} \in \Gamma_{g_{Ai}} \right\} ,
$$

$$
\bar{\mathcal{S}}_A := \left\{ \ \bar{\mathbf{W}}_A = (\mathbf{W}_{Ar} + i\mathbf{W}_{Ai}) : \Omega \to \mathbf{C}^3 \ \Big| \ \mathbf{W}_{Ar} \in \mathcal{S}_{Ar} \quad \text{and} \quad \mathbf{W}_{Ai} \in \mathcal{S}_{Ai} \right\} . \tag{3.40}
$$

3.4.2. Time-integrated Continuity Equation

Let $\bar{W}_\psi : \Omega \to \mathbf{C}$ be a weighting function. The weighted residual form for the second equation in (2.33) is

$$
\left. \begin{aligned}
\int_\Omega W_{\psi_r} \left\{ -\operatorname{div} \mathbf{D}_{0i} + \operatorname{div} \mathbf{J}_{fo_r} + \operatorname{div} \mathbf{J}_{a_{0r}} \right\} d\Omega = 0 \\
\int_\Omega W_{\psi_i} \left\{ +\operatorname{div} \mathbf{D}_{0r} + \operatorname{div} \mathbf{J}_{fo_i} + \operatorname{div} \mathbf{J}_{a_{0i}} \right\} d\Omega = 0
\end{aligned} \right\} \quad \forall \, \bar{W}_\psi \in \mathbf{C} . \tag{3.41}
$$

Similar to the transient case, we obtain the expression for the weak form to be

$$
-\omega \int_{\partial\Omega} W_{\psi_r} (\mathbf{D}_{0i} \cdot \hat{\mathbf{n}}) \ d(\partial\Omega) + \omega \int_\Omega \operatorname{grad} W_{\psi_r} \cdot \mathbf{D}_{0i} \ d\Omega + \int_\Omega W_{\psi_r} (\operatorname{div} \mathbf{J}_{a_{0r}}) \ d\Omega
$$
$$
+ \int_{\partial\Omega} W_{\psi_r} \left(\mathbf{J}_{fo_r} \cdot \hat{\mathbf{n}} \right) \ d(\partial\Omega) - \int_\Omega \operatorname{grad} W_{\psi_r} \cdot \mathbf{J}_{fo_r} \ d\Omega = 0 \ , \qquad \forall \, W_{\psi_r} \in \mathcal{V}_{\psi_r} \ ,
$$

and

$$
+\omega \int_{\partial\Omega} W_{\psi_i} (\mathbf{D}_{0r} \cdot \hat{\mathbf{n}}) \ d(\partial\Omega) - \omega \int_\Omega \operatorname{grad} W_{\psi_i} \cdot \mathbf{D}_{0r} \ d\Omega + \int_\Omega W_{\psi_i} (\operatorname{div} \mathbf{J}_{a_{0i}}) \ d\Omega
$$
$$
+ \int_{\partial\Omega} W_{\psi_i} \left(\mathbf{J}_{fo_i} \cdot \hat{\mathbf{n}} \right) \ d(\partial\Omega) - \int_\Omega \operatorname{grad} W_{\psi_i} \cdot \mathbf{J}_{fo_i} \ d\Omega = 0 \ , \qquad \forall \, W_{\psi_i} \in \mathcal{V}_{\psi_i} \ .
$$

The boundary $\partial\Omega =: \overline{\Gamma_{h\psi_r} \cup \Gamma_{g\psi_r}}$, where $\Gamma_{h\psi_r}$ is the part of the boundary with a $\left(-\omega\mathbf{D}_{0i} + \mathbf{J}_{fo_r} \right)$ field is specified, and $\Gamma_{g\psi_r}$ is the remaining part of the boundary where a potential ψ_r is specified. In addition, the boundary $\partial\Omega =: \overline{\Gamma_{h\psi_i} \cup \Gamma_{g\psi_i}}$, with

$\Gamma_{h\psi_i}$ is the part of the boundary where a $\left(\omega \mathbf{D}_{0r} + \mathbf{J}_{f_{0i}}\right)$ is specified, and $\Gamma_{g\psi_i}$ is the remaining part of the boundary where a potential ψ_i is specified. Then we can rewrite the above equations as follows.

$$
\begin{aligned}
& -\int_\Omega \operatorname{grad} W_{\psi_r} \cdot \mathbf{J}_{f_{0r}} \, d\Omega + \omega \int_\Omega \operatorname{grad} W_{\psi_r} \cdot \mathbf{D}_{0i} \, d\Omega \\
& = \omega \int_{\Gamma_{h\psi_r}} W_{\psi_r} \left(\mathbf{D}_{0i} \cdot \hat{\mathbf{n}}\right) \, d(\partial\Omega) - \int_{\Gamma_{h\psi_r}} W_{\psi_r} \left(\mathbf{J}_{f_{0r}} \cdot \hat{\mathbf{n}}\right) \, d(\partial\Omega) + \int_\Omega W_{\psi_r} (\operatorname{div} \mathbf{J}_{a_{0r}}) \, d\Omega \; , \\
& \hspace{9cm} \forall \, W_{\psi_r} \in \mathcal{V}_{\psi_r} \; , \\
& -\int_\Omega \operatorname{grad} W_{\psi_i} \cdot \mathbf{J}_{f_{0i}} \, d\Omega - \omega \int_\Omega \operatorname{grad} W_{\psi_i} \cdot \mathbf{D}_{0r} \, d\Omega \\
& = -\omega \int_{\Gamma_{h\psi_r}} W_{\psi_i} \left(\mathbf{D}_{0r} \cdot \hat{\mathbf{n}}\right) \, d(\partial\Omega) - \int_{\Gamma_{h\psi_r}} W_{\psi_i} \left(\mathbf{J}_{f_{0i}} \cdot \hat{\mathbf{n}}\right) \, d(\partial\Omega) + \int_\Omega W_{\psi_i} (\operatorname{div} \mathbf{J}_{a_{0i}}) \, d\Omega \; , \\
& \hspace{9cm} \forall \, W_{\psi_i} \in \mathcal{V}_{\psi_i} \; ,
\end{aligned}
$$

(3.42)

The terms on the right-hand side of (3.42) are associated with the "known" quantities that are specified in the problem statement. The spaces of weighting functions are defined as

$$
\begin{aligned}
\mathcal{V}_{\psi_r} &:= \left\{ W_\psi \in \mathcal{H}^1(\Omega) \quad \text{and} \quad W_\psi(\mathbf{x}) = 0 \, , \, \forall \, \mathbf{x} \in \Gamma_{g\psi_r} \right\} \; , \\
\mathcal{V}_{\psi_i} &:= \left\{ W_\psi \in \mathcal{H}^1(\Omega) \quad \text{and} \quad W_\psi(\mathbf{x}) = 0 \, , \, \forall \, \mathbf{x} \in \Gamma_{g\psi_i} \right\} \; , \\
\bar{\mathcal{V}}_\psi &:= \left\{ \bar{W}_\psi = \left(W_{\psi_r} + i W_{\psi_i}\right) : \Omega \to \mathbb{C} \, \middle| \, W_{\psi_r} \in \mathcal{V}_{\psi_r} \quad \text{and} \quad W_{\psi_i} \in \mathcal{V}_{\psi_i} \right\} \; .
\end{aligned}
$$

(3.43)

The spaces of trial solutions are defined as

$$
\begin{aligned}
\mathcal{S}_{\psi_r} &:= \left\{ W_\psi \in \mathcal{H}^1(\Omega) \quad \text{and} \quad W_\psi(\mathbf{x}) = \psi_{a_{0r}} \, , \, \forall \, \mathbf{x} \in \Gamma_{g\psi_r} \right\} \; , \\
\mathcal{S}_{\psi_i} &:= \left\{ W_\psi \in \mathcal{H}^1(\Omega) \quad \text{and} \quad W_\psi(\mathbf{x}) = \psi_{a_{0i}} \, , \, \forall \, \mathbf{x} \in \Gamma_{g\psi_i} \right\} \; , \\
\bar{\mathcal{S}}_\psi &:= \left\{ \bar{W}_\psi = \left(W_{\psi_r} + i W_{\psi_i}\right) : \Omega \to \mathbb{C} \, \middle| \, W_{\psi_r} \in \mathcal{S}_{\psi_r} \quad \& \quad W_{\psi_i} \in \mathcal{S}_{\psi_i} \right\} \; .
\end{aligned}
$$

(3.44)

3.4.3. Combined Weak Form

To state the weak form concisely, we define the following. Let the combination of the vector potential $\bar{\mathbf{A}}_0$ and the scalar potential $\bar{\psi}_0$ be $\bar{\Pi}_0 : \Omega \to \mathbf{C}^4$ which is

$$\bar{\Pi}_0 := \Pi_{0_r} + i\Pi_{0_i} , \qquad (3.45)$$

where $\Pi_{0_r} : \Omega \to \mathbf{R}^4$ is

$$\Pi_{0_r} := \left\{ \mathbf{A}_r \,\middle|\, \psi_r \right\} \equiv \left\{ A^1{}_r, A^2{}_r, A^3{}_r, \psi_r \right\} ,$$

and $\Pi_{0_i} : \Omega \to \mathbf{R}^4$ is

$$\Pi_{0_i} := \left\{ \mathbf{A}_i \,\middle|\, \psi_i \right\} \equiv \left\{ A^1{}_i, A^2{}_i, A^3{}_i, \psi_i \right\} .$$

Let $\bar{\mathbf{W}}(\mathbf{x}) : \Omega \to \mathbf{C}^4$ be a weighting function that is defined to be

$$\bar{\mathbf{W}} := \mathbf{W}_r + i\mathbf{W}_i , \qquad (3.46)$$

where $\mathbf{W}_r : \Omega \to \mathbf{R}^4$ is

$$\mathbf{W}_r := \left\{ \mathbf{W}_{Ar} \,\middle|\, W_{\psi_r} \right\} \equiv \left\{ W^1_{Ar}, W^2_{Ar}, W^3_{Ar}, W_{\psi_r} \right\} , \qquad (3.47)$$

and $\mathbf{W}_i : \Omega \to \mathbf{R}^4$ is

$$\mathbf{W}_i := \left\{ \mathbf{W}_{Ai} \,\middle|\, W_{\psi_i} \right\} \equiv \left\{ W^1_{Ai}, W^2_{Ai}, W^3_{Ai}, W_{\psi_i} \right\} . \qquad (3.48)$$

Let the space $\bar{\mathcal{V}}$ be defined as

$$\bar{\mathcal{V}} := \left\{ \begin{array}{l} \bar{\mathbf{W}} = \mathbf{W}_r + i\mathbf{W}_i \Omega \to \mathbf{C}^4 \\[6pt] \text{where } \mathbf{W}_r \text{ and } \mathbf{W}_i \text{ are defined in (3.47) and (3.48)} \\[6pt] \left| \begin{array}{l} \mathbf{W}_{Ar} \in \mathcal{V}_{Ar} , \quad \mathbf{W}_{Ai} \in \mathcal{V}_{Ai} \\[6pt] W_{\psi_r} \in \mathcal{V}_{\psi_r} \quad \text{and} \quad W_{\psi_i} \in \mathcal{V}_{\psi_i} \end{array} \right. \end{array} \right\} , \qquad (3.49)$$

and the space of trial solutions $\bar{S}$ be defined as

$$\bar{S} := \left\{ \begin{array}{l} \bar{\mathbf{W}} = \mathbf{W}_r + i\mathbf{W}_i : \Omega \to \mathbb{C}^4 \\[2mm] \text{where } \mathbf{W}_r \text{ and } \mathbf{W}_i \text{ are defined in (3.47) and (3.48)} \\[2mm] \mathbf{W}_{Ar} \in S_{Ar} , \quad \mathbf{W}_{Ai} \in S_{Ai} \\[2mm] W_{\psi_r} \in S_{\psi_r} \quad \text{and} \quad W_{\psi_i} \in S_{\psi_i} \end{array} \right\} . \tag{3.50}$$

Now the weak form for the time harmonic problem can be stated as follows

$$\boxed{\begin{array}{l} \text{Find } \bar{\Pi}_0 \in \bar{S} \;\forall\; \mathbf{x} \in \Omega \text{ such that} \\[3mm] \bar{\mathcal{G}}_m(\bar{\mathbf{W}}, \bar{\Pi}_0) + \bar{\mathcal{G}}_b(\bar{\mathbf{W}}, \bar{\Pi}_0) + \bar{\mathcal{G}}_k(\bar{\mathbf{W}}, \bar{\Pi}_0) = \bar{\mathcal{G}}_f(\bar{\mathbf{W}}) , \qquad \forall\; \bar{\mathbf{W}} \in \bar{V} , \end{array}}$$
$$\tag{3.51}$$

where the operators $\bar{\mathcal{G}}_m =: \mathcal{G}_{mr} + i\mathcal{G}_{mi}$, $\bar{\mathcal{G}}_b =: \mathcal{G}_{br} + i\mathcal{G}_{bi}$, $\bar{\mathcal{G}}_k =: \mathcal{G}_{kr} + i\mathcal{G}_{ki}$, and $\bar{\mathcal{G}}_f =: \mathcal{G}_{f_r} + i\mathcal{G}_{f_i}$, are defined as follows.

$$\mathcal{G}_{mr}(\bar{\mathbf{W}}, \bar{\Pi}) \quad := +\omega \int_\Omega \mathbf{W}_{Ar} \cdot \mathbf{D}_{0i} \, d\Omega + \omega \int_\Omega \text{grad}\, W_{\psi_r} \cdot \mathbf{D}_{0i} \, d\Omega , \tag{3.52}$$

$$\mathcal{G}_{mi}(\bar{\mathbf{W}}, \bar{\Pi}) \quad := -\omega \int_\Omega \mathbf{W}_{Ai} \cdot \mathbf{D}_{0r} \, d\Omega - \omega \int_\Omega \text{grad}\, W_{\psi_i} \cdot \mathbf{D}_{0r} \, d\Omega , \tag{3.53}$$

$$\mathcal{G}_{br}(\bar{\mathbf{W}}, \bar{\Pi}) \quad := -\int_\Omega \mathbf{W}_{Ar} \cdot \mathbf{J}_{f_r} \, d\Omega - \int_\Omega \text{grad}\, W_{\psi_r} \cdot \mathbf{J}_{f_r} \, d\Omega , \tag{3.54}$$

$$\mathcal{G}_{bi}(\bar{\mathbf{W}}, \bar{\Pi}) \quad := -\int_\Omega \mathbf{W}_{Ai} \cdot \mathbf{J}_{f_i} \, d\Omega - \int_\Omega W_{\psi_i} \cdot \mathbf{J}_{f_i} \, d\Omega , \tag{3.55}$$

$$\mathcal{G}_{kr}(\bar{\mathbf{W}}, \bar{\Pi}) \quad := \int_\Omega (\text{curl}\, \mathbf{W}_{Ar}) \cdot \mathbf{H}_r \, d\Omega , \tag{3.56}$$

$$\mathcal{G}_{ki}(\bar{\mathbf{W}}, \bar{\Pi}) \quad := \int_\Omega (\text{curl}\, \mathbf{W}_{Ai}) \cdot \mathbf{H}_i \, d\Omega , \tag{3.57}$$

$$\mathcal{G}_{f_r}(\bar{\mathbf{W}}) \quad := \int_{\Gamma_{h_{Ar}}} \mathbf{W}_{Ar} \cdot (\mathbf{H}_{0r} \times \hat{\mathbf{n}}) \, d(\Omega) + \int_\Omega \mathbf{W}_{Ar} \cdot \mathbf{J}_{a_{0r}} \, d\Omega$$

$$+ \omega \int_{\Gamma_{h_{\psi_r}}} W_{\psi_r} \, (\mathbf{D}_{0i} \cdot \hat{\mathbf{n}}) \, d(\partial\Omega) - \int_{\Gamma_{h_{\psi_r}}} W_{\psi_r} \left(\mathbf{J}_{f_{0r}} \cdot \hat{\mathbf{n}} \right) d(\partial\Omega)$$

$$+ \int_\Omega W_{\psi_r} (\text{div}\, \mathbf{J}_{a_{0r}}) \, d\Omega , \quad \text{and} \tag{3.58}$$

$$\mathcal{G}_{f_i}(\bar{\mathbf{W}}) \quad := \quad \int_{\Gamma_{h_{A_i}}} \mathbf{W}_{A_i} \cdot (\mathbf{H}_{0_i} \times \hat{\mathbf{n}}) \ d(\Omega) + \int_{\Omega} \mathbf{W}_{A_i} \cdot \mathbf{J}_{a_{0_i}} \ d\Omega$$

$$- \omega \int_{\Gamma_{h_{\psi_i}}} W_{\psi_i} (\mathbf{D}_{0_r} \cdot \hat{\mathbf{n}}) \ d(\partial\Omega) - \int_{\Gamma_{h_{\psi_i}}} W_{\psi_i} \left(\mathbf{J}_{f_{0_i}} \cdot \hat{\mathbf{n}} \right) \ d(\partial\Omega)$$

$$+ \int_{\Omega} W_{\psi_r} (\operatorname{div} \mathbf{J}_{a_{0_i}}) \ d\Omega \ . \tag{3.59}$$

The field quantities $\bar{\mathbf{D}}_0$, $\bar{\mathbf{J}}_{f_0}$, and $\bar{\mathbf{H}}_0$ are related to the potential $\bar{\Pi}$ and its spatial derivatives via the constitutive equations (2.6). The Coulomb gauge can now be imposed in a similar fashion to the magnetostatic case in Section 3.2.1, page 40, i.e., include the penalty term

$$\int_{\Omega} \flat \, (\operatorname{div} \mathbf{W}_{A_r}) \, (\operatorname{div} \mathbf{A}_{0_r}) \ d\Omega$$

in the stiffness operators $\mathcal{G}_{k_r}$, and include the penalty term

$$\int_{\Omega} \flat \, (\operatorname{div} \mathbf{W}_{A_i}) \, (\operatorname{div} \mathbf{A}_{0_i}) \ d\Omega$$

in the operator $\mathcal{G}_{k_i}$.

CHAPTER 4
APPROXIMATION FOR LINEAR-ISOTROPIC MATERIALS

In this chapter we express the weak form (3.42) for static excitations, (3.25) for transient excitations, and (3.51) for time-harmonic excitations, as matrix equations (4.23), (4.53) and (4.67), respectively. To do so we use a first-order Lagrange isoprameteric 8-noded brick element. The formulation is limited to linear-isotropic materials, however, can be extended to materials with more complex constitutive laws.

Here, as a first approximation, we assume linear-isotropic constitutive relationships, i.e., the relations in (2.6) take the form

$$ \mathbf{D} = \epsilon(\mathbf{x})\,\mathbf{E}\ , \qquad \mathbf{H} = \frac{1}{\mu(\mathbf{x})}\,\mathbf{B}\ , \qquad \mathbf{J}_f = \sigma(\mathbf{x})\,\mathbf{E}\ , \qquad (4.1) $$

where the permittivity ϵ, permeability μ, and conductivity σ are only functions of position $\mathbf{x}$, but are *not* functions of time t or functions of the electromagnetic field quantities.

The accuracy of the FE solution depends on the data (geometry and material properties) available for the electrical component being analyzed. The manufacturing process, especially firing, changes the material properties (Morweiser, Meunier and Salze [1994]). The thin electrodes often develop numerous holes, thereby changing the conductivity. The dielectric properties of the final ceramic are different. Moreover, the geometry of the electrical component may be altered. Typically a shrinkage is observed, but not necessarily equal in all directions. The parasitic parameters, like the inductance of a capacitor depends on the permeability of the

54

ceramics. This information is usually not provided by the manufacturer. Hence, additional tests need to be done prior to numerical simulation.

Electromagnetic devices (a combination of various electrical components) generally have abrupt changes (i.e., discontinuities) in material properties across the material interfaces. Such material discontinuities induce the dicontinuities in certain components of the field quantities, thus requiring special elements and numerical algorithms to model interfaces (Monk [1993] and Lee and Masfen [1990]). As the focus of the present work is to model the global properties (the lumped parameters) of the device, we choose not to employ any special elements to treat the discontinuities at the material interfaces.

4.1. Static Problem

As a consequence of the linear-isotropic constitutive relationships (4.1), the potentials $\mathbf{A}_0$ and ψ_0 used in static problems are related to the field quantities $\mathbf{D}$ and $\mathbf{H}$ as follows:

$$\mathbf{D} = -\epsilon(\mathbf{x}) \operatorname{grad} \dot{\psi}_0 \qquad \text{and} \qquad \mathbf{H} = \frac{1}{\mu(\mathbf{x})} \operatorname{curl} \mathbf{A}_0 . \tag{4.2}$$

Recall that $\mathbf{J}_f \equiv 0$ in static problems.

4.1.1. Weak Form

Our goal is to transform (3.30) to a matrix equation. Because the combined potential $\Pi_0 \in S_0$ and $\dot{\Pi}_0 \in \dot{S}_0$, there are only *four* unknown quantities in (3.30), i.e., $\mathbf{A}_0$ and $\dot{\psi}_0$. As the problems are time-independent, the remaining quantities, i.e., $\dot{\mathbf{A}}_0$ and ψ_0, are set to zero prior to solution; see Section 2.2.4 in page 25 for details. For convenience, we define a new variable $\Upsilon_0 : \Omega \mapsto \mathbf{R}^4$ as follows:

$$\Upsilon_0 := \left\{ \mathbf{A}_0 \,\middle|\, \dot{\psi}_0 \right\} \equiv \left\{ A_0^1, \ A_0^2, \ A_0^3, \ \dot{\psi}_0, \ \right\} \in \mathbf{R}^4 , \tag{4.3}$$

which contains only the unknown quantities $\mathbf{A}_0$ and $\dot{\psi}_0$. We simplify the expressions for the operators defined in (3.34), (3.35), and (3.36) for linear-isotropic materials as follows:

$$^{(l)}\mathcal{G}_{m_0}(\mathbf{W}, \Upsilon_0) \quad := \quad \int_{\Omega \backslash \Omega_{cond}} \epsilon(\mathbf{x})(\operatorname{grad} W_\psi) \cdot \left(\operatorname{grad} \dot{\psi}_0\right) \, d\Omega \, , \qquad (4.4)$$

$$^{(l)}\mathcal{G}_{k_0}(\mathbf{W}, \Upsilon_0) \quad := \quad \int_{\Omega} \frac{1}{\mu(\mathbf{x})} (\operatorname{curl} \mathbf{W}_A) \cdot (\operatorname{curl} \mathbf{A}_0) \, d\Omega \, , \quad \text{and} \qquad (4.5)$$

$$^{(l)}\mathcal{G}_{f_0}(\mathbf{W}) \quad := \quad \int_{\Gamma_{h_{A_0}}} \mathbf{W}_A \cdot (\mathbf{H}_0 \times \hat{\mathbf{n}}) \, d(\Omega) + \int_{\Omega} \mathbf{W}_A \cdot \mathbf{J}_{a_0} \, d\Omega$$

$$- \int_{\Gamma_{h\dot{\psi}_0}} W_\psi (\mathbf{D} \cdot \hat{\mathbf{n}}) \, d(\partial\Omega) \, . \qquad (4.6)$$

Recall that the weighting function has the form

$$\mathbf{W} := \left\{ \mathbf{W}_A \,\middle|\, W_\psi \right\} \in \mathbf{R}^4 \, .$$

The weak form (3.30) now becomes

$$\boxed{\begin{array}{l} \text{Find } \Upsilon_0 \in \, {}^{(l)}\mathcal{S}_0 \text{ such that} \\[2mm] {}^{(l)}\mathcal{G}_{m_0}(\mathbf{W}, \Upsilon_0) + {}^{(l)}\mathcal{G}_{k_0}(\mathbf{W}, \Upsilon_0) = {}^{(l)}\mathcal{G}_{f_0}(\mathbf{W}) \, , \qquad \forall \, \mathbf{W} \in \mathcal{V}_0 \, . \end{array}} \qquad (4.7)$$

The space of trial functions $^{(l)}\mathcal{S}_0$ is defined to be

$$^{(l)}\mathcal{S}_0 := \left\{ \begin{array}{l} \mathbf{W} = \left\{ W^1, \, W^2, \, W^3, \, W^4 \right\} \\[3mm] \left| \, \left\{ W^1, \, W^2, \, W^3 \right\} \in \mathcal{S}_{A_0} \quad \text{and} \quad W^4 \in \mathcal{S}_{\psi_0} \right. \end{array} \right\} \, . \qquad (4.8)$$

To account for the non-homogeneous essential boundary condition, let us split the solution Υ_0 into a known function $\overset{[k]}{\Upsilon_0} \in \, {}^{(l)}\mathcal{S}_0$ that satisfies the essential boundary condition and an unknown function $\overset{[u]}{\Upsilon_0} \in \mathcal{V}_0$ that satisfies the homogeneous essential boundary condition, i.e., $\Upsilon_0 = \overset{[k]}{\Upsilon_0} + \overset{[u]}{\Upsilon_0}$. As all operators involved are linear, we

can rewrite the above weak form as follows

$$
\begin{aligned}
&\text{Given } \overset{[k]}{\Upsilon}_0 \in {}^{(l)}\mathcal{S}_0, \text{ find } \overset{[u]}{\Upsilon}_0 \in \mathcal{V}_0 \text{ such that} \\[2mm]
&{}^{(l)}\mathcal{G}_{m_0}(\mathbf{W}, \overset{[u]}{\Upsilon}_0) + {}^{(l)}\mathcal{G}_{k_0}(\mathbf{W}, \overset{[u]}{\Upsilon}_0) = {}^{(l)}\mathcal{G}_{f_0}(\mathbf{W}) \\[2mm]
&\quad - {}^{(l)}\mathcal{G}_{m_0}(\mathbf{W}, \overset{[k]}{\Upsilon}_0) - {}^{(l)}\mathcal{G}_{k_0}(\mathbf{W}, \overset{[k]}{\Upsilon}_0), \qquad \forall\, \mathbf{W} \in \mathcal{V}_0 .
\end{aligned}
$$

(4.9)

4.1.2. Discrete Weak Form

The conforming FE method for solving (4.9) consists of finding an *approximate* solution $\overset{[u]}{\Upsilon}_{0h}(\mathbf{x})$ in a finite-dimensional subspace $\mathcal{V}_{0h} \subset \mathcal{V}_0$, where $\overset{[u]}{\Upsilon}_{0h}(\mathbf{x})$ is a solution to the following problem

$$
\begin{aligned}
&\text{Given } \overset{[k]}{\Upsilon}_{0h} \in {}^{(l)}\mathcal{S}_{0h}, \text{ find } \overset{[u]}{\Upsilon}_{0h} \in \mathcal{V}_{0h} \text{ such that} \\[2mm]
&{}^{(l)}\mathcal{G}_{m_0}(\mathbf{W}_h, \overset{[u]}{\Upsilon}_{0h}) + {}^{(l)}\mathcal{G}_{k_0}(\mathbf{W}_h, \overset{[u]}{\Upsilon}_{0h}) = {}^{(l)}\mathcal{G}_{f_0}(\mathbf{W}_h) \\[2mm]
&\quad - {}^{(l)}\mathcal{G}_{m_0}(\overset{[k]}{\Upsilon}_{0h}, \mathbf{W}_h) - {}^{(l)}\mathcal{G}_{k_0}(\overset{[k]}{\Upsilon}_{0h}, \mathbf{W}_h), \qquad \forall\, \mathbf{W}_h \in \mathcal{V}_{0h} .
\end{aligned}
$$

(4.10)

The space $\mathcal{V}_0$ requires that the functions satisfy the homogeneous essential boundary condition on part of the boundary of $\partial\Omega$. However, in practice, it is more convenient to construct a finite element space $\mathcal{W}_h$ that has no such requirement at the boundary. These requirements are later imposed on $\mathcal{W}_h$ to obtain the finite element space $\mathcal{V}_{0h}$. From definitions (3.3), (3.8), and (3.31) it is clear that if $\mathbf{v} := \{v^1, \cdots, v^4\} \in \mathcal{V}_0$, then if v^i are chosen as polynomials, we have the equivalence

$$
v^i \in \mathcal{H}^1(\Omega) \qquad \Longleftrightarrow \qquad v^i \in \mathcal{C}^0\left(\bar{\Omega}\right)
$$

for $i = 1, \cdots, 4$, where $\bar{\Omega} := \Omega \cup \partial\Omega$ is the closure of Ω, and

$$
\mathcal{C}^0\left(\bar{\Omega}\right) := \left\{ v : \bar{\Omega} \to \mathbf{R} \quad \text{and } v \text{ is continuous} \right\} .
$$

To define a finite element space $\mathcal{W}_h$, we must specify the following (Johnson [1987, p.79]): (1) A compact subset T of $\bar{\Omega}$ with a non-empty interior and Lipschitz-continuous boundary, (2) a finite-dimensional space P_T of polynomials defined on T of finite dimension, and (3) a set Σ of parameters called *degrees of freedom*, to describe the functions in $\mathcal{V}_{0h}$. To recapitulate, a *finite element* discretization is a triplet $(T,\ P_T,\ \Sigma)$, such that a function in P_T is uniquely determined by the degrees of freedom Σ. An example of a choice of the triplet $(T,\ P_T,\ \Sigma)$ is the case of nodal FE described below. Let

$$\left\{ N_k : \bar{\Omega} \to \mathbf{R} \text{ for } k = 1, \cdots, \aleph \right\}$$

be a set of basis functions in $\mathcal{V}_0$, such that N_k's are not required to satisfy the homogeneous essential boundary conditions, and $N_k \in P_T$ (i.e., when restricted to element T, the basis function N_k belongs to the set of polynomials P_T). Let

$$\mathcal{W}_h := span\left\{ N_1, \cdots, N_\aleph \right\}\ , \tag{4.11}$$

$\forall\ \mathbf{v}(\mathbf{x}) = \{v^1, \cdots, v^4\} \in \mathcal{W}_h,$

$$v^i(\mathbf{x}) = \sum_{k=1}^{\aleph} d_k^i N_k\ , \tag{4.12}$$

where $d_k^i = d_k\left(v^i(\mathbf{x})\right)$ and

$$d_k(N_j) = \delta_{kj}\ .$$

A good summary of the various requirements that space $\mathcal{W}_h$ should satisfy in order to be a finite element discretization is listed in Ciarlet [1987, pp.1.126–1.127].

Finite element method in its simplest form consists of *triangulation*[15] (or discretization) of the domain $\bar{\Omega}$ into a finite elements of (Ciarlet [1987, p.1.125]). The

---

[15] The word traingulation is used to designate general discretization of $\bar{\Omega}$ into finite elements, which are not necessarily triangles in two-dimensions.

triangulation $\mathcal{T}_h$ over the domain $\overline{\Omega}$ is expressed as a union of triangles T, in such a way that whenever triangles T_1 and T_2 are distinct triangles of $\mathcal{T}_h$, their intersection is (i) either empty, or a (ii) vertex common to T_1 and T_2, or (iii) an edge common to T_1 and T_2, (iv) or a facet common to T_1 and T_2. The case of "unresolved nodes", such as in Figure 4.1 is not allowed. In most finite elements, the space of functions P_T are chosen to be polynomial functions. The coefficients of the polynomial $v \in P_T$ constitute the set of the degrees of freedom Σ.

In electromagnetics, the most common elements used for triangulation of three dimensional domains are the tetrahedral elements and the hexahedral elements (Sabonnadiere [1987]). The tetrahedral elements are especially useful for irregular domains and automatic meshing. The 20-noded hexahedral brick element is a common choice for regular domains with curved boundaries. However, here, we will confine ourselves to regular domains with straight boundaries, making the 8-noded hexahedral brick element the perfect choice. The advantage of using the 8-noded first-order hexahedral brick element is the ease in meshing and eventually coding. Next, we review the 8-noded first-order Lagrange isoparametric brick element for a simple case for the finite-dimensional space $\vartheta_h \subset \vartheta$, with $\vartheta_h \equiv C^0\left(\overline{\Omega}\right)$. We will later use the same principles to construct the space $\mathcal{V}_{0h}$.

4.1.2.1. First-order Lagrange isoparametric 8-noded brick element

The finite element $(T,\ P_T,\ \Sigma)$ corresponding to the first-order hexahedral 8-noded brick element used to construct the space ϑ_h is defined as follows: (1) The geometric object T is a hexahedral brick; (2) the space $P_T := Q_1(T)$ is chosen to be
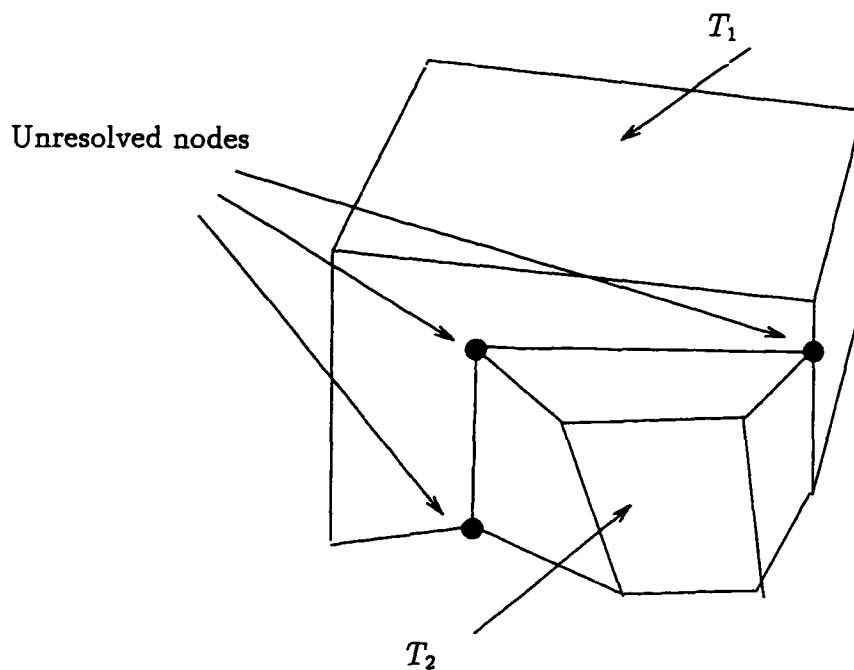
Figure 4.1. An example of a forbidden triangulation

the space of tri-linear functions

$$Q_1(T) := \left\{ v \mid v \text{ is trilinear on T, i.e., } v(\mathbf{x}) = \sum_{i,j,k=0}^{1} a_{ijk} (x^1)^i (x^2)^j (x^3)^k , \right.$$
$$\left. \mathbf{x} \in T \text{ , where } a_{ijk} \in \mathbf{R} \right\} ;$$

and (3) the set of degrees of freedom Σ consists of the values of the unknown function $\mathbf{v} \in \vartheta_h$ at the nodes of the triangulation $\mathcal{T}_h$. Such finite element space implies that the basis functions N_i's are the "hat" function, i.e., trilinear function that has a value one at one node and a value zero at the remaining nodes. These trilinear hat functions are constructed using isoparametric mapping.

In isoparametric mapping (Hughes [1987, pp.118–120]), the unknown function to be determined in the element T is mapped from a parent element Ω^e using the same basis functions that are used to construct ϑ_h. For a hexahedral brick element, if $\boldsymbol{\xi} := \{\xi^1, \xi^2, \xi^3\} \in \mathbf{R}^3$ is the coordinates of a point in the parent element Ω^e, then the coordinates of a point $\mathbf{x} \in T$ is

$$\mathbf{x}(\boldsymbol{\xi}) := \sum_{a=1}^{8} N_{T_a}(\boldsymbol{\xi}) \, \mathbf{x}_{T_a} \, ,$$

and the unknown function $\mathbf{v}(\mathbf{x}) \in \mathcal{V}_{0h}$ for $\mathbf{x} \in T$ is

$$\mathbf{v}(\mathbf{x}) := \sum_{a=1}^{8} N_{T_a}(\boldsymbol{\xi}) \, \mathbf{v}_{T_a} \, .$$

The co-ordinates of the vertex a of the brick T is $\mathbf{x}_{T_a}$, and the value of the function $\mathbf{v}$ is $\mathbf{v}_{T_a}$. The parent element Ω^e is a biunit cube $[-1, 1] \times [-1, 1] \times [-1, 1]$ centered at the origin $\boldsymbol{\xi} := \{0, 0, 0\}$. The parent element Ω^e is mapped to the brick T via the map $\chi : \Omega^e \mapsto T$. The element basis functions are

$$\boxed{N_{T_a}(\boldsymbol{\xi}) := \frac{1}{8} \left(1 + \xi^1 \xi^1_{\ a}\right) \left(1 + \xi^2 \xi^2_{\ a}\right) \left(1 + \xi^3 \xi^3_{\ a}\right) \, ,} \tag{4.13}$$

where $\boldsymbol{\xi}_a = \left\{\xi^1_{\ a}, \xi^2_{\ a}, \xi^3_{\ a}\right\}$, for $a = 1, \cdots, 8$, are the co-ordinates of the vertices of the cube Ω^e in the $\boldsymbol{\xi}$ co-ordinate system; these co-ordinates are given in Table 4.1. The entire transformation is illustrated in Figures 4.2.

Consider a domain $\bar{\Omega}$ with a triangulation $\mathcal{T}_h$ using hexahedral bricks, and having a total of $\aleph$ nodes. Then the set of degrees of freedom Σ consists of the

Table 4.1. Local co-ordinates of the vertices of the 8-noded brick element.

a	ξ^1_a	ξ^2_a	ξ^3_a
1	-1	-1	-1
2	1	-1	-1
3	1	1	-1
4	-1	1	-1
5	-1	-1	1
6	1	-1	1
7	1	1	1
8	-1	1	1

values of the unknown function $v \in \vartheta_h$ at the nodes of the FE mesh. The function v can be described by using the basis functions $N_j(\mathbf{x})$, $i = 1, \ldots, \aleph$, or alternately, using the local basis functions for each element $T \in \mathcal{T}_h$ as follows.

$$
\begin{aligned}
v(\mathbf{x}) \; &= \sum_{k=1}^{\aleph} d_k \left(v(\mathbf{x}) \right) N_k \\
&= \sum_{T \in \mathcal{T}_h} \left\{ \sum_{k=1}^{8} d_{T_k} \left(v(\mathbf{x}) \right) N_{T_k}(\boldsymbol{\xi}) \right\} .
\end{aligned}
\tag{4.14}
$$

The description of the function using the basis N_k is called the global viewpoint, and that using basis N_{T_k} is called the local or element viewpoint. The global viewpoint is useful in establishing the mathematical properties of the finite element method, whereas the element viewpoint is useful for computer implementation. Note that at a node shared by two elements T_1 and T_2 that belong to $\mathcal{T}_h$, the value of the function v due to the basis functions associated with element T_1 is the same as that associated with element T_2. Hence, if i is the local node number of the common node in element T_1, and j local node number of that common node in element T_2, then the degrees of freedom $d_{T_{1i}}$ and $d_{T_{2j}}$ are the same.

Parent element Ω^e
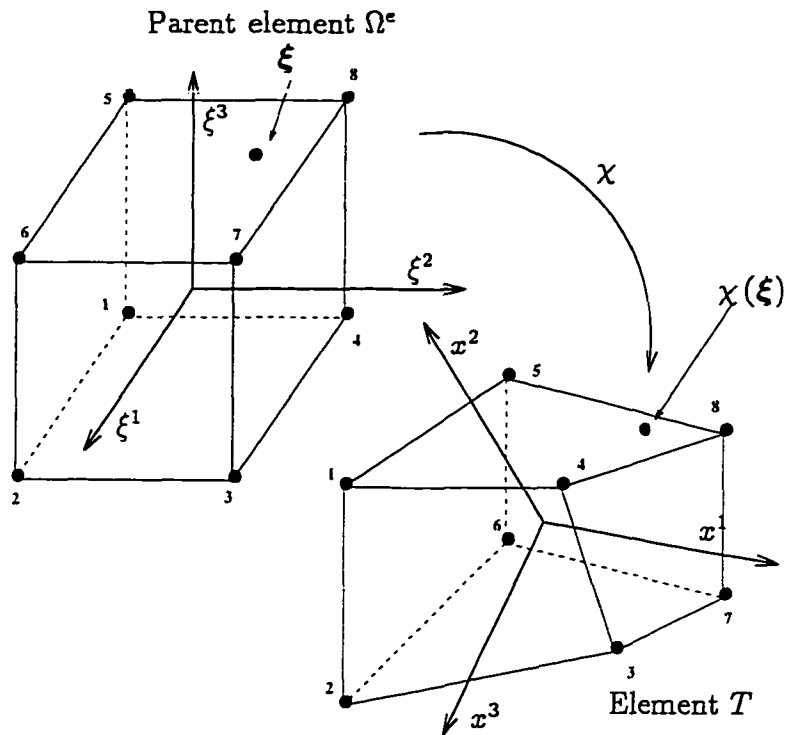
Figure 4.2. First-order Lagrange 8-noded isoparametric brick element

4.1.2.2. Matrix equation

In this section we develop the matrix equations with the global viewpoint for a static problem. The space $\mathcal{W}_h$ is constructed using the first-order Lagrange isoparametric 8-noded brick elements as done for space ϑ_h in the previous subsection, i.e., a function $\mathbf{v} := \{v^1, \cdots, v^4\} \in \mathcal{W}_h$ is represented by a set of basis functions $N_k(\mathbf{x})$, $k = 1, \ldots, \aleph$, as in (4.12)

$$v^i(\mathbf{x}) = \sum_{k=1}^{\aleph} d_k^i \left(v(\mathbf{x}) \right) N_k \, ,$$

for $i = 1, \cdots, 4$. The degrees of freedom d_k^i are the values of the function v^i at node k of the triangulation $\mathcal{T}_h$. However, functions in space $\mathcal{V}_0$ must satisfy the essential

homogeneous boundary condition. Therefore, we define the space $\mathcal{V}_{0h} \subset \mathcal{V}_0$ to be

$$
\mathcal{V}_{0h} := \left\{ \mathbf{v} \in \mathcal{W}_h \,\middle|\, \begin{array}{l} \mathbf{v} \text{ satisfies the homogeneous essential boundary} \\[2ex] \text{condition specified in } \mathcal{V}_0 \end{array} \right\} . \tag{4.15}
$$

Similarly, we define the space $^{(l)}\mathcal{S}_{0h} \subset {}^{(l)}\mathcal{S}_0$ to be

$$
^{(l)}\mathcal{S}_{0h} := \left\{ \mathbf{v} \in \mathcal{W}_h \,\middle|\, \begin{array}{l} \mathbf{v} \text{ satisfies the essential boundary} \\[2ex] \text{condition specified in } ^{(l)}\mathcal{S}_0 \end{array} \right\} , \tag{4.16}
$$

where the left superscript "l" denotes space of trial functions for problems with linear-isotropic materials, and the right subscript "h" denotes a finite-dimensional space of trial functions. The known function $\overset{[k]}{\Upsilon}_{0h}(\mathbf{x}) := \left\{ \overset{[k]}{\Upsilon^i_{0_h}}, \cdots, \overset{[k]}{\Upsilon^i_{0_h}} \right\} \in {}^{(l)}\mathcal{S}_{0h}$, the unknown function $\overset{[u]}{\Upsilon}_{0h}(\mathbf{x}) := \left\{ \overset{[u]}{\Upsilon^1_{0_h}}, \cdots, \overset{[u]}{\Upsilon^4_{0_h}} \right\} \in \mathcal{V}_{0h}$, and the weighting function $\mathbf{W}(\mathbf{x}) \in \mathcal{V}_{0h}$, are represented in terms of the basis functions as in (4.12). However, note that the appropriate degrees of freedom related to the essential boundary conditions have to be constrained to account for the essential boundary conditions. These representations are used to express the operators $^{(l)}\mathcal{G}_{m_0}$, $^{(l)}\mathcal{G}_{k_0}$, and $^{(l)}\mathcal{G}_{f_0}$ in terms of the basis functions and the degrees of freedom. In the setup of the matrix equation, we reduce the mathematical rigor to improve readability.

To set up the final matrix equation, we arrange the degrees of freedom as follows. First, we arrange the degrees of freedom that correspond to $\mathbf{A}_0$ beginning with node 1 and ending with node $\aleph$ as follows.

$$
\left\{ \overbrace{d^1_1(\mathbf{A}_0), d^2_1(\mathbf{A}_0), d^3_1(\mathbf{A}_0)}^{node\ 1} \middle| \cdots \middle| \underbrace{d^1_\aleph(\mathbf{A}_0), d^2_\aleph(\mathbf{A}_0), d^3_\aleph(\mathbf{A}_0)}_{node\ \aleph} \right\} \in \mathbf{R}^{(1 \times 3\aleph)} . \tag{4.17}
$$

Similarly, we arrange all the degrees of freedom that correspond to $\dot{\psi}_0$ as follows.

$$\left\{ d_1^{i4}\left(\dot{\psi}_0\right) \middle| \cdots \middle| d_{\aleph}^{i4}\left(\dot{\psi}_0\right) \right\} \quad \in \bar{\mathsf{R}}^{(1\times\aleph)} . \tag{4.18}$$

Using the above arrangement, we define the following matrices for the operators $^{(l)}\mathcal{G}_{k_0}$, $^{(l)}\mathcal{G}_{m_0}$, and $^{(l)}\mathcal{G}_{f_0}$ defined in (4.5), (4.4), and (4.6). For operator $^{(l)}\mathcal{G}_{k_0}$ we define the matrix[16] $\mathcal{K}^{AA} := \left[\mathcal{K}_{IJ}^{AA} \right] \in \mathsf{R}^{(3\aleph\times3\aleph)}$, with

$$K_{IJ}^{AA} := \int_\Omega \frac{1}{\mu(\mathbf{x})} \frac{\partial N_k}{\partial x^m} \frac{\partial N_l}{\partial x^p} \varepsilon_{mni} \varepsilon_{pqj} \delta_{ij} \, d\Omega , \tag{4.19}$$

where k is the node number corresponding to the position I, and l is the node number corresponding to the position J in the arrangement defined in (4.17). For example, if $I = 4$, then the degree of freedom is $d_2^1(\mathbf{A}_0)$ in (4.17), the node number (the right subscript) is 2, and hence $k = 2$. Summation convention is implied on the repeated indices, except for those indices in parentheses or indicated otherwise. The permutation symbol ε_{mni} is defined to have the value 0, +1, or −1 as follows:

$$\varepsilon_{mni} := \begin{cases} 0 & \text{when any two indices are equal} \\ +1 & \text{when } m, n, i \text{ are a even permutation of } 1, 2, 3 \\ -1 & \text{when } m, n, i \text{ are a odd permutation of } 1, 2, 3 \end{cases} .$$

For operator $^{(l)}\mathcal{G}_{f_0}$ we define the column matrix $\mathcal{F}^{A_0} := \left\{ F_J^{A_0} \right\} \in \mathsf{R}^{(3\aleph\times1)}$, with

$$\mathcal{F}_J^{A_0} := \int_{\Gamma_{h_{A_0}}} (\mathbf{H}_0\times\hat{\mathbf{n}})^i N_l \delta_{ij} \, d(\Omega) + \int_\Omega J_{a_0}^i N_l \delta_{ij} \, d\Omega , \tag{4.20}$$

where l is the node number corresponding to the position J in the arrangement defined in (4.17). For operator $^{(l)}\mathcal{G}_{m_0}$ we define the matrix $\mathcal{M}^{\psi\psi} := \left[\mathcal{M}_{IJ}^{\psi\psi} \right] \in \mathsf{R}^{(\aleph\times\aleph)}$, with

$$\mathcal{M}_{IJ}^{\psi\psi} := \int_{\Omega\setminus\Omega_{cond}} \epsilon(\mathbf{x}) \frac{\partial N_k}{\partial x^i} \frac{\partial N_l}{\partial x^j} \delta_{ij} \, d\Omega , \tag{4.21}$$

---

[16] Each of the entries in these matrices are calculated using Gauss integration. For the problems solved in this report, numerical experiments have shown that a two-point Gauss integration in each direction is sufficient, i.e., a total of $2^3 \equiv 8$ Gauss points, to obtain an accurate integration.

where k is the node number corresponding to the position I, and l is the node number corresponding to the position J in the arrangement defined in (4.18). For operator $^{(l)}\mathcal{G}_{f_0}$ we define the column matrix $\mathcal{F}^{\psi_0} := \left\{ \mathcal{F}_J^{\psi_0} \right\} \in \mathbf{R}^{(\aleph \times 1)}$,

$$\mathcal{F}_J^{\psi_0} := -\int_{\Gamma_{h\psi_0}} (\mathbf{D} \cdot \hat{\mathbf{n}}) \, N_l \, d(\partial \Omega) \ , \tag{4.22}$$

where l is the node number corresponding to the position J in the arrangement defined in (4.18).

The matrix equation for the static case is stated as follows

Find $\widetilde{\mathcal{A}_0} \in \mathbf{R}^{(3n_{A_0} \times 1)}$ and $\widetilde{\dot{\psi}_0} \in \mathbf{R}^{(n_{\psi_0} \times 1)}$ such that

$$\begin{bmatrix} K^{AA} & 0 \\ 0 & M^{\psi\psi} \end{bmatrix} \left\{ \begin{matrix} \widetilde{\mathcal{A}_0} \\ \widetilde{\dot{\psi}_0} \end{matrix} \right\} = \left\{ \begin{matrix} F^{A_0} \\ F^{\psi_0} \end{matrix} \right\} \ , \tag{4.23}$$

where $\widetilde{\mathcal{A}_0}$ contains the unknown degrees of freedom corresponding to the vector potential $\mathbf{A}_0$, and $\widetilde{\dot{\psi}_0}$ contains the unknown degrees of freedom corresponding to the scalar potential $\dot{\psi}_0$. Their arrangement of components in $\widetilde{\mathcal{A}_0}$ and $\widetilde{\dot{\psi}_0}$ has been discussed earlier. The number n_{A_0} corresponds to the number of nodes at which the vector potential $\mathbf{A}_0$ is to be determined, and the number n_{ψ_0} corresponds to the number nodes at which the scalar potential $\dot{\psi}_0$ is to be determined. The matrix $K^{AA} \in \mathbf{R}^{(3n_{A_0} \times 3n_{A_0})}$ and $M^{\psi\psi} \in \mathbf{R}^{(n_{\psi_0} \times n_{\psi_0})}$ are symmetric and positive semi-definite.[17] The matrices K^{AA} and $M^{\psi\psi}$, and the column vectors F^{A_0} and F^{ψ_0} are derived by deleting the appropriate rows and columns in the matrices defined above so as to impose the essential boundary condition.

---

[17] For piece-wise constant material properties, two-point Gauss integration is used to calculated the entries in the matrix K^{AA} and $M^{\psi\psi}$. Numerical experiments show that no significant improvement in accuracy is achieved with more number of Gauss points.

4.1.3. Coulomb Gauge

To implement Coulomb gauge (3.11) we define a matrix ${}^{(p)}\mathcal{K}^{AA} := \left[{}^{(p)}\mathcal{K}^{AA}_{IJ} \right] \in$ $\mathbf{R}^{(3\aleph \times 3\aleph)}$, with

$$
{}^{(p)}\mathcal{K}^{AA}_{IJ} := \int_\Omega \flat(\mathbf{x}) \frac{\partial N_k}{\partial x^i} \frac{\partial N_l}{\partial x^j} \, d\Omega \, , \tag{4.24}
$$

where k is the node number corresponding to the index I, and l is the node number corresponding to the index J. The indices i and j are the directions corresponding to the indices I and J. The matrix ${}^{(p)}\mathcal{K}^{AA}$ is added to matrix $\mathcal{K}^{AA}$ to enforce the Coulomb gauge. Note that reduced integration[18] is used to calculate the entries of the matrix ${}^{(p)}\mathcal{K}^{AA}$. The matrix ${}^{(p)}K^{AA}$ is constructed by deleting the appropriate row and columns in the ${}^{(p)}\mathcal{K}^{AA}$.

4.1.3.1. Quadrature points and the choice of $\flat$

The number of quadrature points used to integrate the entries of the matrix ${}^{(p)}K^{AA}$ decides the number of constraints imposed on the linear system of equations. From numerical experiments, we observe that $2 \times 2 \times 2$ gauss integration points is sufficient to integrate exactly the FE matrices for the l.i.h. materials. An integration scheme with $2 \times 2 \times 2$ gauss integration points to integrate the matrix is termed as *full* integration. On the contrary, an integration scheme with $1 \times 1 \times 1$ gauss integration points is termed as *reduced* integration, and consequently, the matrix is *under*-integrated. The consequence of *reduced* integration is a singular matrix. Each integration point used to evaluate the penalty matrix ${}^{(p)}K^{AA}$ imposes a constraint. Hence, if we use *full* integration for ${}^{(p)}K^{AA}$ and K^{AA}, then the number of constraints would equal the number of degrees of freedom, and in some cases, it is conceivable that the number of constraints will exceed the number of d.o.f.. Hence, if we increase the value of the penalty $\flat$, then constraints will force the solution to be *locked* close

---

[18] For piece-wise constant material properties, one-point Gauss integration is used to calculated the entries in the matrix ${}^{(p)}\mathcal{K}^{AA}$.

to zero.

To avoid the *locking* we implement *selective reduced* integration, where we use *reduced* integration for matrix $^{(p)}K^{AA}$ and *full* integration for matrix K^{AA}. To avoid numerical difficulties associated with imposing the penalty, we must choose the penalty $þ$ carefully. A guideline used in the selection of the penalty $þ$ is that we must ensure that $þ \leq 10^{p/2}$, where p is the number of decimal digits stored in each computer "word." For the DEC system, with single precision we choose $þ \leq 10^4$, and with double precision we choose $þ \leq 10^7$.

An alternate method to implement the penalty, is to use *consistent* penalty method (Cook, Malkus and Plesha [1989]). Here, the "constraint points," i.e., the gauss integration points used for the integration of the entries in $^{(p)}K^{AA}$, are separated from the gauss integration points used to integrate the entries in K^{AA}. An 8-noded brick element with one "constraint point" in the middle is an example of a 3-D element used in the *consistent* penalty method. See Cook et al. [1989] for a more detailed overview.

4.2. Transient Problem

As a consequence of the linear-isotropic constitutive relationships (4.1) the potentials $\mathbf{A}$ and ψ used in the transient problems are related to the field quantities $\mathbf{D}$, $\mathbf{H}$, and $\mathbf{J}_f$ as follows:

$$\mathbf{D} = -\epsilon(\mathbf{x})\left(\operatorname{grad}\dot{\psi} + \frac{\partial \mathbf{A}}{\partial t}\right), \quad \mathbf{H} = \frac{1}{\mu(\mathbf{x})}\operatorname{curl}\mathbf{A}, \quad \mathbf{J}_f = -\sigma(\mathbf{x})\left(\operatorname{grad}\dot{\psi} + \frac{\partial \mathbf{A}}{\partial t}\right).$$
$$(4.25)$$

4.2.1. Weak Form

Our goal is to transform (3.25) to a matrix equation. Given the combined potential $\Pi_0 \in S_0$ and $\dot{\Pi}_0 \in \dot{S}_0$, we need to find the combined potential $\Pi \in S$ for

all $t > 0$, and for all $\mathbf{x} \in \Omega$. Using the expressions in (4.25) we obtain simplified expressions for the operators defined in (3.26), (3.27), and (3.28) for linear-isotropic materials to be as follows.

$$^{(l)}\mathcal{G}_m(\mathbf{W}, \ddot{\Pi}) \quad := \int_\Omega \mathbf{W}_A \cdot \epsilon(\mathbf{x}) \frac{\partial}{\partial t} \left(\operatorname{grad} \dot{\psi} + \frac{\partial \mathbf{A}}{\partial t} \right) \, d\Omega$$

$$+ \int_\Omega \operatorname{grad} W_\psi \cdot \epsilon(\mathbf{x}) \frac{\partial}{\partial t} \left(\operatorname{grad} \dot{\psi} + \frac{\partial \mathbf{A}}{\partial t} \right) \, d\Omega , \quad (4.26)$$

$$^{(l)}\mathcal{G}_b(\mathbf{W}, \dot{\Pi}) \quad := \int_\Omega \mathbf{W}_A \cdot \sigma(\mathbf{x}) \left(\operatorname{grad} \dot{\psi} + \frac{\partial \mathbf{A}}{\partial t} \right) \, d\Omega$$

$$+ \int_\Omega \operatorname{grad} W_\psi \cdot \sigma(\mathbf{x}) \left(\operatorname{grad} \dot{\psi} + \frac{\partial \mathbf{A}}{\partial t} \right) \, d\Omega , \quad (4.27)$$

$$^{(l)}\mathcal{G}_k(\mathbf{W}, \Pi) \quad := \int_\Omega (\operatorname{curl} \mathbf{W}_A) \cdot \frac{1}{\mu(\mathbf{x})} (\operatorname{curl} \mathbf{A}) \, d\Omega . \quad (4.28)$$

Note that the arguments for $^{(l)}\mathcal{G}_m$, $^{(l)}\mathcal{G}_b$, and $^{(l)}\mathcal{G}_k$ are not the same. The linearized expression for $\mathcal{G}_f(\mathbf{W})$ is the same as in (3.29), hence, $^{(l)}\mathcal{G}_f(\mathbf{W}) := \mathcal{G}_f(\mathbf{W})$.

As the above expressions for operators $^{(l)}\mathcal{G}_m$, $^{(l)}\mathcal{G}_b$, and $^{(l)}\mathcal{G}_k$ are functions of not only Π, but also also its time derivatives $\dot{\Pi}$ and $\ddot{\Pi}$, it is more convenient to construct a new operator

$$^{(l)}\mathcal{G}_{dyn}(\mathbf{W}, \Pi, \dot{\Pi}, \ddot{\Pi}) := {}^{(l)}\mathcal{G}_m(\mathbf{W}, \ddot{\Pi}) + {}^{(l)}\mathcal{G}_b(\mathbf{W}, \dot{\Pi}) + {}^{(l)}\mathcal{G}_k(\mathbf{W}, \Pi) , \quad (4.29)$$

where the arguments of $^{(l)}\mathcal{G}_{dyn}$ explicitly indicates its dependence on Π, $\dot{\Pi}$, $\ddot{\Pi}$, and $\mathbf{W}$.

Using the above expressions we transform the weak form (3.25) to the following.

Given $\Pi_0(\mathbf{x})$ and $\dot{\Pi}_0(\mathbf{x})$, find $\Pi \in \mathcal{S} \ \forall \ \mathbf{x} \in \Omega$ and $t > 0$ such that

$$^{(l)}\mathcal{G}_{dyn}(\mathbf{W}, \Pi, \dot{\Pi}, \ddot{\Pi}) = {}^{(l)}\mathcal{G}_f(\mathbf{W}) \qquad \forall \ \mathbf{W} \in \mathcal{V} , \quad (4.30)$$

4.2.2. Discrete Weak Form

4.2.2.1. Time discretization: Newmark method

In order to solve the above weak form, we first discretize in time using the Newmark method (Hughes [1987, p. 491]). The Newmark method includes the trapezoidal rule as a special case. Let the unknown potential Π at at time step $t = t_n$ be designated by

$$\Pi_n(\mathbf{x}) := \Pi(\mathbf{x}, t_n) \, .$$

Also let

$$\dot{\Pi}_n(\mathbf{x}) := \dot{\Pi}(\mathbf{x}, t_n) \quad \text{and} \quad \ddot{\Pi}_n(\mathbf{x}) := \ddot{\Pi}(\mathbf{x}, t_n) \, .$$

Assuming that $\left(\Pi_n, \dot{\Pi}_n, \ddot{\Pi}_n\right)$ satisfy the weak form (4.30) at time t_n, i.e.,

$$^{(l)}\mathcal{G}_{dyn}\left(\mathbf{W}, \Pi_n, \dot{\Pi}_n, \ddot{\Pi}_n\right) = \, ^{(l)}\mathcal{G}_f(\mathbf{W}) \qquad \forall \, \mathbf{W} \in \mathcal{V} \, , \qquad (4.31)$$

we want to obtain the solution $\left(\Pi_{n+1}, \dot{\Pi}_{n+1}, \ddot{\Pi}_{n+1}\right)$ at time t_{n+1} such that

$$^{(l)}\mathcal{G}_{dyn}\left(\mathbf{W}, \Pi_{n+1}, \dot{\Pi}_{n+1}, \ddot{\Pi}_{n+1}\right) = \, ^{(l)}\mathcal{G}_f(\mathbf{W}) \qquad \forall \, \mathbf{W} \in \mathcal{V} \, . \qquad (4.32)$$

Let

$$\Delta\Pi_{n+1}(\mathbf{x}) := \Pi_{n+1}(\mathbf{x}) - \Pi_n(\mathbf{x}) \, .$$

Then, Newmark time-stepping algorithm defines the relationship between the two solutions $\left(\Pi_n, \dot{\Pi}_n, \ddot{\Pi}_n\right)$ and $\left(\Pi_{n+1}, \dot{\Pi}_{n+1}, \ddot{\Pi}_{n+1}\right)$ to be

$$
\begin{aligned}
\ddot{\Pi}_{n+1} &= \tilde{\ddot{\Pi}}_{n+1} + \frac{1}{(\Delta t_{n+1})^2 \, \beta} \Delta\Pi_{n+1} \, , \\
\dot{\Pi}_{n+1} &= \tilde{\dot{\Pi}}_{n+1} + \frac{\gamma}{(\Delta t_{n+1}) \, \beta} \Delta\Pi_{n+1} \, , \\
\Pi_{n+1} &= \Pi_n + \Delta\Pi_{n+1} \, ,
\end{aligned}
\qquad (4.33)
$$

where

$$\ddot{\tilde{\Pi}}_{n+1} := -\frac{1}{\Delta t_{n+1}\,\beta}\dot{\Pi}_n - \frac{1-2\beta}{2\beta}\ddot{\Pi}_n ,$$

$$\dot{\tilde{\Pi}}_{n+1} = -\left(1-\frac{\gamma}{\beta}\right)\dot{\Pi}_n - \frac{\Delta t_{n+1}}{2\beta}(2\beta-\gamma)\ddot{\Pi}_n ,$$

$$(4.34)$$

the time step is $\Delta t_{n+1} := t_{n+1} - t_n$, and (β,γ) are parameters for the Newmark algorithm. Note that $\beta = 0.25$ and $\gamma = 0.5$ corresponds to the trapezoidal rule which guarantee the unconditional stability and also maintain second order accuracy.

The general case, when operator $^{(l)}\mathcal{G}_{dyn}$ is a nonlinear function of $\Delta\Pi_{n+1}$, when (4.33) is substituted for $\left(\Pi_{n+1},\dot{\Pi}_{n+1},\ddot{\Pi}_{n+1}\right)$ requires further linearization of operator $^{(l)}\mathcal{G}_{dyn}$. However, in our case, for linear-isotropic materials, the $^{(l)}\mathcal{G}_{dyn}$ is a linear function of $\Delta\Pi_{n+1}$. The expression for $^{(l)}\mathcal{G}_{dyn}$ in terms of $\Delta\Pi_{n+1}$ is obtained by substituting (4.33) in (4.26)–(4.28). The weak form (4.30) to find the unknown $\Delta\Pi_{n+1}$ at time step t_{n+1} can now be written as

Given $\left(\Pi_n, \dot{\Pi}_n, \ddot{\Pi}_n\right)$ find $\Delta\Pi_{n+1} \in \mathcal{V}$ such that

$$\frac{1}{\left(\Delta t_{n+1}\right)^2\beta}{}^{(l)}\mathcal{G}_m(\mathbf{W},\Delta\Pi_{n+1}) + \frac{\gamma}{\Delta t_{n+1}\,\beta}{}^{(l)}\mathcal{G}_b(\mathbf{W},\Delta\Pi_{n+1})$$

$$+\,{}^{(l)}\mathcal{G}_k(\mathbf{W},\Delta\Pi_{n+1}) = {}^{(l)}\mathcal{G}_f(\mathbf{W}) - {}^{(l)}\mathcal{G}_m(\mathbf{W},\ddot{\tilde{\Pi}}_{n+1}) - {}^{(l)}\mathcal{G}_m(\mathbf{W},\dot{\tilde{\Pi}}_{n+1})$$

$$\forall\,\mathbf{W} \in \mathcal{V} .$$

$$(4.35)$$

An important assumption is that the essential boundary conditions must be satisfied by the initial values, i.e., $\Pi_0 \in \mathcal{S}$. In such a case, the above weak form is valid for every step n, in the time-stepping algorithm. Note that the solution space $\mathcal{S}$, and hence, space $\mathcal{V}$, is invariant with respect to time t.

4.2.2.2. Matrix equation: Spatial discretization

In this section we develop the matrix equations with a global viewpoint for the time step $n + 1$, i.e., we discretize problem (4.35). The space $\mathcal{W}_h$ is constructed as before using the 8-noded first-order Lagrange isoparametric brick elements as done for space ϑ_h in the previous section, i.e., a function $\mathbf{v} := \{v^1, \cdots, v^4\} \in \mathcal{W}_h$ is represented by a set of basis functions $N_k(\mathbf{x})$, $k = 1, \ldots, \aleph$, as in (4.12). The degrees of freedom d_k^i are the values of the function v^i at node k of the triangulation $\mathcal{T}_h$. However, functions in space $\mathcal{V}$ must satisfy the essential homogeneous boundary condition. Therefore, we define the space $\mathcal{V}_h \subset \mathcal{V}$ to be

$$\mathcal{V}_h := \left\{ \mathbf{v} \in \mathcal{W}_h \,\middle|\, \begin{array}{l} \mathbf{v} \text{ satisfies the homogeneous essential boundary} \\ \\ \text{condition specified in } \mathcal{V} \end{array} \right\} . \tag{4.36}$$

The unknown function $\Delta\Pi_{n+1}(\mathbf{x})$, the known function $\Pi_n(\mathbf{x})$, and the weighting function $\mathbf{W}_h(\mathbf{x})$ are represented in terms of the basis functions as in (4.12). The appropriate degrees of freedom must be constrained to account for the essential boundary conditions. These representations are used to express the operators $^{(l)}\mathcal{G}_m$, $^{(l)}\mathcal{G}_k$, and $^{(l)}\mathcal{G}_f$ in terms of the basis functions and the degrees of freedom. In the set up of the matrix equations we reduce the mathematical rigor to improve readability.

To set up the final matrix equation we arrange the degrees of freedom as follows. First, we arrange the degrees of freedom that correspond to $\mathbf{A}$ beginning with node 1 and ending with node $\aleph$ as follows.

$$\left\{ \overbrace{d_1^1(\mathbf{A}), d_1^2(\mathbf{A}), d_1^3(\mathbf{A})}^{node\ 1} \,\middle|\, \cdots \,\middle|\, \underbrace{d_\aleph^1(\mathbf{A}), d_\aleph^2(\mathbf{A}), d_\aleph^3(\mathbf{A})}_{node\ \aleph} \right\} \quad \in \mathbf{R}^{(1\times 3\aleph)} . \tag{4.37}$$

Similarly, we arrange all the degrees of freedom that correspond to ψ as follows.

$$\left\{ d_1^4(\psi) \;\middle|\; \cdots \;\middle|\; d_{\aleph}^4(\psi) \right\} \quad \in \mathsf{R}^{(1 \times \aleph)} . \tag{4.38}$$

Using the above arrangement, we define the following matrices for the operators ${}^{(l)}\mathcal{G}_m$, ${}^{(l)}\mathcal{G}_b$, ${}^{(l)}\mathcal{G}_k$, and ${}^{(l)}\mathcal{G}_f$ defined in (4.26), (4.27), (4.28), and (3.29). Matrix $\mathcal{M}^{AA} := \left[\mathcal{M}_{IJ}^{AA} \right] \in \mathsf{R}^{(3\aleph \times 3\aleph)}$ where

$$\mathcal{M}_{IJ}^{AA} := \int_\Omega \epsilon(\mathbf{x}) N_k N_l \delta_{ij} \, d\Omega , \tag{4.39}$$

matrix $\mathcal{B}^{AA} := \left[\mathcal{B}_{IJ}^{AA} \right] \in \mathsf{R}^{(3\aleph \times 3\aleph)}$ where

$$\mathcal{B}_{IJ}^{AA} := \int_\Omega \sigma(\mathbf{x}) N_k N_l \delta_{ij} \, d\Omega , \tag{4.40}$$

matrix $\mathcal{K}^{AA} := \left[\mathcal{K}_{IJ}^{AA} \right] \in \mathsf{R}^{(3\aleph \times 3\aleph)}$ where

$$\mathcal{K}_{IJ}^{AA} := \int_\Omega \mu(\mathbf{x}) \frac{\partial N_k}{\partial x^m} \frac{\partial N_l}{\partial x^p} \varepsilon_{mn(i)} \varepsilon_{pq(j)} \delta_{(i)(j)} \, d\Omega , \tag{4.41}$$

column matrix $\mathcal{F}^{An+1} := \left[\mathcal{F}_J^{An+1} \right] \in \mathsf{R}^{(3\aleph \times 1)}$ where

$$\mathcal{F}_J^{An+1} := \int_{\Gamma_{h_A}} (\mathbf{H} \times \hat{\mathbf{n}})^i N_l \delta_{i(j)} \, d(\Omega) + \int_\Omega J_a^i N_l \delta_{i(j)} \, d\Omega , \tag{4.42}$$

where k is the node number corresponding to the position I, and l is the node number corresponding to the position J in the arrangement defined in (4.37).

Matrix $\mathcal{M}^{\psi\psi} := \left[\mathcal{M}_{IJ}^{\psi\psi} \right] \in \mathsf{R}^{(\aleph \times \aleph)}$ where

$$\mathcal{M}_{IJ}^{\psi\psi} := \int_\Omega \epsilon(\mathbf{x}) \frac{\partial N_k}{\partial x^i} \frac{\partial N_l}{\partial x^j} \delta_{ij} \, d\Omega , \tag{4.43}$$

matrix $\mathcal{B}^{\psi\psi} := \left[\mathcal{B}_{IJ}^{\psi\psi} \right] \in \mathsf{R}^{(\aleph \times \aleph)}$ where

$$\mathcal{B}_{IJ}^{\psi\psi} := \int_\Omega \sigma(\mathbf{x}) \frac{\partial N_k}{\partial x^i} \frac{\partial N_l}{\partial x^j} \delta_{ij} \, d\Omega , \tag{4.44}$$

matrix $\mathcal{K}^{\psi\psi} := \left[\mathcal{K}_{IJ}^{\psi\psi} \right] \in \mathsf{R}^{(\aleph \times \aleph)}$ where

$$\mathcal{K}_{IJ}^{\psi\psi} := 0 , \tag{4.45}$$

column matrix $\mathcal{F}^{\psi_{n+1}} := \left[\mathcal{F}_J^{\psi_{n+1}}\right] \in \mathsf{R}^{(\mathbf{N} \times 1)}$ where

$$\mathcal{F}_J^{\psi_{n+1}} := -\int_{\Gamma_{h\psi}} \left(\frac{\partial \mathbf{D}}{\partial t} \cdot \hat{\mathbf{n}}\right) N_l \, d(\partial\Omega) - \int_{\Gamma_{h\psi}} (\mathbf{J}_f \cdot \hat{\mathbf{n}}) \, N_l \, d(\partial\Omega)$$
$$- \int_\Omega (\operatorname{div} \mathbf{D} \cdot \hat{\mathbf{n}}) \, N_l \, d(\Omega) , \tag{4.46}$$

where k is the node number corresponding to the position I, and l is the node number corresponding to the position J in the arrangement defined in (4.38).

Matrix $\mathcal{M}^{A\psi} := \left[\mathcal{M}_{IJ}^{A\psi}\right] \in \mathsf{R}^{(3\mathbf{N} \times \mathbf{N})}$ where

$$\mathcal{M}_{IJ}^{A\psi} := \int_\Omega \epsilon(\mathbf{x}) N_k \frac{\partial N_l}{\partial x^i} \, d\Omega , \tag{4.47}$$

matrix $\mathcal{B}^{A\psi} := \left[\mathcal{B}_{IJ}^{A\psi}\right] \in \mathsf{R}^{(3\mathbf{N} \times \mathbf{N})}$ where

$$\mathcal{B}_{IJ}^{A\psi} := \int_\Omega \sigma(\mathbf{x}) N_k \frac{\partial N_l}{\partial x^i} \, d\Omega , \tag{4.48}$$

matrix $\mathcal{K}^{A\psi} := \left[\mathcal{K}_{IJ}^{A\psi}\right] \in \mathsf{R}^{(3\mathbf{N} \times \mathbf{N})}$ where

$$\mathcal{K}_{IJ}^{A\psi} := 0 , \tag{4.49}$$

where k is the node number corresponding to the position I in the arrangement defined in (4.37), and l is the node number corresponding to the position J in the arrangement defined in (4.38). The index i is the direction corresponding to the position I. For example, if $I = 4$, then the degree of freedom is $d_2^1(\mathbf{A})$ in (4.17), which corresponds to A^1 (i.e., the right superscript is 1), and hence $i = 1$.

Matrix $\mathcal{M}^{\psi A} := \left[\mathcal{M}_{IJ}^{\psi A}\right] \in \mathsf{R}^{(\mathbf{N} \times 3\mathbf{N})}$ where

$$\mathcal{M}_{IJ}^{\psi A} := \int_\Omega \epsilon(\mathbf{x}) \frac{\partial N_k}{\partial x^j} N_l \, d\Omega , \tag{4.50}$$

matrix $\mathcal{B}^{\psi A} := \left[\mathcal{B}_{IJ}^{\psi A}\right] \in \mathsf{R}^{(\mathbf{N} \times 3\mathbf{N})}$ where

$$\mathcal{B}_{IJ}^{\psi A} := \int_{\Omega} \sigma(\mathbf{x}) \frac{\partial N_k}{\partial x^j} N_l \, d\Omega \, , \tag{4.51}$$

matrix $\mathcal{K}^{\psi A} := \left[\mathcal{K}_{IJ}^{\psi A} \right] \in \mathbf{R}^{(\aleph \times 3\aleph)}$ where

$$\mathcal{K}_{IJ}^{\psi A} := 0 \, , \tag{4.52}$$

where k is the node number corresponding to the position I in the arrangement defined in (4.38), and l is the node number corresponding to the position J in the arrangement defined in (4.37). The index j is the direction corresponding to the position J in the arrangement defined in (4.37).

Using the above defined matrices, we can transform the discrete weak form (4.35) at each time step to the following matrix equation.

Given $\dot{\tilde{\mathcal{A}}}_n, \ddot{\tilde{\mathcal{A}}}_n \in \mathbf{R}^{(3\aleph \times 1)}$ and $\dot{\tilde{\psi}}_n, \ddot{\tilde{\psi}}_n \in \mathbf{R}^{(\aleph \times 1)}$, find $\Delta \tilde{\mathcal{A}}_{n+1} \in \mathbf{R}^{(3n_A \times 1)}$ and $\Delta \tilde{\psi}_{n+1} \in \mathbf{R}^{(n_\psi \times 1)}$, such that

$$\left(\frac{1}{(\Delta t_{n+1})^2 \beta} \begin{bmatrix} M^{AA} & M^{A\psi} \\ M^{\psi A} & M^{\psi\psi} \end{bmatrix} + \frac{\gamma}{\Delta t_{n+1} \beta} \begin{bmatrix} B^{AA} & B^{A\psi} \\ B^{\psi A} & B^{\psi\psi} \end{bmatrix} + \begin{bmatrix} K^{AA} & 0 \\ 0 & 0 \end{bmatrix} \right) \begin{Bmatrix} \Delta \tilde{\mathcal{A}}_{n+1} \\ \Delta \tilde{\psi}_{n+1} \end{Bmatrix}$$

$$= \begin{Bmatrix} F^{A}{}_{n+1} \\ F^{\psi}{}_{n+1} \end{Bmatrix} - \begin{bmatrix} \mathcal{M}^{AA} & \mathcal{M}^{A\psi} \\ \mathcal{M}^{\psi A} & \mathcal{M}^{\psi\psi} \end{bmatrix} \begin{Bmatrix} \ddot{\tilde{\mathcal{A}}}_n \\ \ddot{\tilde{\psi}}_n \end{Bmatrix} - \begin{bmatrix} \mathcal{B}^{AA} & \mathcal{B}^{A\psi} \\ \mathcal{B}^{\psi A} & \mathcal{B}^{\psi\psi} \end{bmatrix} \begin{Bmatrix} \dot{\tilde{\mathcal{A}}}_n \\ \dot{\tilde{\psi}}_n \end{Bmatrix} \, .$$

$$\tag{4.53}$$

The column matrices $\dot{\tilde{\mathcal{A}}}_n, \ddot{\tilde{\mathcal{A}}}_n$ and $\dot{\tilde{\psi}}_n, \ddot{\tilde{\psi}}_n$ contain the respective degrees of freedom at time t_n. The column matrices $\Delta \tilde{\mathcal{A}}_{n+1}$ and $\Delta \tilde{\psi}_{n+1}$, contain the increments to the vector potential and the scalar potential, respectively. The mass matrix

$$M := \begin{bmatrix} M^{AA} & M^{A\psi} \\ M^{\psi A} & M^{\psi\psi} \end{bmatrix} \in \mathbf{R}^{((3n_A + n_\psi) \times (3n_A + n_\psi))} \, , \tag{4.54}$$

is positive definite, however, the damping matrix

$$
B := \begin{bmatrix} B^{AA} & B^{A\psi} \\ B^{\psi A} & B^{\psi\psi} \end{bmatrix} \in \mathsf{R}^{\left((3n_A+n_\psi)\times(3n_A+n_\psi)\right)} , \tag{4.55}
$$

and the stiffness matrix

$$
K := \begin{bmatrix} K^{AA} & 0 \\ 0 & 0 \end{bmatrix} \in \mathsf{R}^{\left((3n_A+n_\psi)\times(3n_A+n_\psi)\right)} , \tag{4.56}
$$

are positive semi-definite. These matrices are obtained from their counterparts defined above by deleting the appropriate rows and columns so as to impose the essential boundary conditions. The number n_A corresponds to the number of nodes at which the vector potential $\mathbf{A}$ is to be determined, and the number n_ψ corresponds to the number nodes at which the scalar potential ψ is to be determined. The Coulomb gauge is enforced similar to the magnetostatic case in Section 4.1.3 on page 67. The matrix $^{(p)}K^{AA}$ is added to the stiffness matrix K^{AA}.

4.3. Time-Harmonic Problem

As a consequence of the linear-isotropic constitutive relationships (4.1) the potentials $\bar{\mathbf{A}}_0$ and $\bar{\psi}_0$ used in the time-harmonic problems are related to the field quantities $\bar{\mathbf{D}}_0$, $\bar{\mathbf{H}}_0$, and $\bar{\mathbf{J}}_{f_0}$ as follows:

$$
\begin{aligned}
\mathbf{D}_{0_r} &= \omega\epsilon(\mathbf{x})\,(\operatorname{grad}\psi_i + \mathbf{A}_i) , & \mathbf{D}_{0_i} &= -\omega\epsilon(\mathbf{x})\,(\operatorname{grad}\psi_r + \mathbf{A}_r) , \\
\mathbf{H}_r &= \frac{1}{\mu(\mathbf{x})}\operatorname{curl}\mathbf{A}_r , & \mathbf{H}_i &= \frac{1}{\mu(\mathbf{x})}\operatorname{curl}\mathbf{A}_i , \\
\mathbf{J}_{f_{0_r}} &= \omega\sigma(\mathbf{x})\,(\operatorname{grad}\psi_i + \mathbf{A}_i) , & \mathbf{J}_{f_{0_i}} &= -\omega\sigma(\mathbf{x})\,(\operatorname{grad}\psi_r + \mathbf{A}_r) .
\end{aligned} \tag{4.57}
$$

4.3.1. Weak Form

Our goal is to transform (3.51) to a matrix equation. Using the expressions in (4.57) we obtain simplified expressions for the operators defined in (3.52)–(3.57)

for linear-isotropic materials as follows:

$$
^{(l)}\mathcal{G}_{mr}(\bar{\mathbf{W}},\bar{\Pi}_0) \quad := \omega^2 \int_\Omega \mathbf{W}_{A_r} \cdot \epsilon(\mathbf{x})\,(\operatorname{grad}\psi_{0_r} + \mathbf{A}_{0_r})\ d\Omega
$$

$$
+ \omega^2 \int_\Omega \operatorname{grad} W_{\psi_r} \cdot \epsilon(\mathbf{x})\,(\operatorname{grad}\psi_{0_r} + \mathbf{A}_{0_r})\ d\Omega\ , \quad (4.58)
$$

$$
^{(l)}\mathcal{G}_{mi}(\bar{\mathbf{W}},\bar{\Pi}_0) \quad := \omega^2 \int_\Omega \mathbf{W}_{A_i} \cdot \epsilon(\mathbf{x})\,(\operatorname{grad}\psi_{0_i} + \mathbf{A}_{0_i})\ d\Omega
$$

$$
+ \omega^2 \int_\Omega \operatorname{grad} W_{\psi_i} \cdot \epsilon(\mathbf{x})\,(\operatorname{grad}\psi_{0_i} + \mathbf{A}_{0_i})\ d\Omega\ , \quad (4.59)
$$

$$
^{(l)}\mathcal{G}_{br}(\bar{\mathbf{W}},\bar{\Pi}_0) \quad := -\omega \int_\Omega \mathbf{W}_{A_r} \cdot \sigma(\mathbf{x})\,(\operatorname{grad}\psi_{0_i} + \mathbf{A}_{0_i})\ d\Omega
$$

$$
- \omega \int_\Omega \operatorname{grad} W_{\psi_r} \cdot \sigma(\mathbf{x})\,(\operatorname{grad}\psi_{0_i} + \mathbf{A}_{0_i})\ d\Omega\ , \quad (4.60)
$$

$$
^{(l)}\mathcal{G}_{bi}(\bar{\mathbf{W}},\bar{\Pi}_0) \quad := \omega \int_\Omega \mathbf{W}_{A_i} \cdot \sigma(\mathbf{x})\,(\operatorname{grad}\psi_{0_r} + \mathbf{A}_{0_r})\ d\Omega
$$

$$
+ \omega \int_\Omega \operatorname{grad} W_{\psi_i} \cdot \sigma(\mathbf{x})\,(\operatorname{grad}\psi_{0_r} + \mathbf{A}_{0_r})\ d\Omega\ , \quad (4.61)
$$

$$
^{(l)}\mathcal{G}_{kr}(\bar{\mathbf{W}},\bar{\Pi}_0) \quad := \quad \int_\Omega (\operatorname{curl}\mathbf{W}_{A_r}) \cdot \frac{1}{\mu(\mathbf{x})}\,(\operatorname{curl}\mathbf{A}_r)\ d\Omega\ , \quad (4.62)
$$

$$
^{(l)}\mathcal{G}_{ki}(\bar{\mathbf{W}},\bar{\Pi}_0) \quad := \quad \int_\Omega (\operatorname{curl}\mathbf{W}_{A_i}) \cdot \frac{1}{\mu(\mathbf{x})}\,(\operatorname{curl}\mathbf{A}_i)\ d\Omega\ . \quad (4.63)
$$

The weak form (3.51) is simplified to the following.

Find $\bar{\Pi}_0 \in {}^{(l)}\bar{\mathcal{S}}$ such that

$$
{}^{(l)}\bar{\mathcal{G}}_m(\bar{\mathbf{W}},\bar{\Pi}_0) + {}^{(l)}\bar{\mathcal{G}}_b(\bar{\mathbf{W}},\bar{\Pi}_0) + {}^{(l)}\bar{\mathcal{G}}_k(\bar{\mathbf{W}},\bar{\Pi}_0) = {}^{(l)}\bar{\mathcal{G}}_f(\bar{\mathbf{W}})\ , \qquad \forall\,\bar{\mathbf{W}} \in \bar{\mathcal{V}}\ ,
$$

$$(4.64)$$

where the operators ${}^{(l)}\bar{\mathcal{G}}_m := {}^{(l)}\mathcal{G}_{mr} + i\,{}^{(l)}\mathcal{G}_{mi}$, ${}^{(l)}\bar{\mathcal{G}}_b := {}^{(l)}\mathcal{G}_{br} + i\,{}^{(l)}\mathcal{G}_{bi}$, ${}^{(l)}\bar{\mathcal{G}}_k :=$
${}^{(l)}\mathcal{G}_{kr} + i\,{}^{(l)}\mathcal{G}_{ki}$, and ${}^{(l)}\bar{\mathcal{G}}_f := {}^{(l)}\mathcal{G}_{f_r} + i\,{}^{(l)}\mathcal{G}_{f_i} \equiv \mathcal{G}_{f_r} + i\mathcal{G}_{f_i}$. The space of trial functions
${}^{(l)}\bar{\mathcal{S}} := \bar{\mathcal{S}}$.

To account for the non-homogeneous essential boundary condition, let us split
the solution $\bar{\Pi}_0$ into a known function $\overset{[k]}{\bar{\Pi}_0} \in {}^{(l)}\bar{\mathcal{S}}$ that satisfies the essential boundary

condition and an unknown function $\overset{[u]}{\bar{\Pi}_0} \in \bar{\mathcal{V}}$ that satisfies the homogeneous essential boundary condition, i.e., $\bar{\Pi}_0 = \overset{[k]}{\bar{\Pi}_0} + \overset{[u]}{\bar{\Pi}_0}$. As all the operators are linear, we can rewrite the above weak form as follows.

$$
\begin{array}{l}
\text{Given } \overset{[k]}{\bar{\Pi}_0} \in {}^{(l)}\bar{\mathcal{S}}, \text{ find } \overset{[u]}{\bar{\Pi}_0} \in \bar{\mathcal{V}} \text{ such that} \\[2ex]
{}^{(l)}\bar{\mathcal{G}}_m(\bar{\mathbf{W}}, \overset{[u]}{\bar{\Pi}_0}) + {}^{(l)}\bar{\mathcal{G}}_b(\bar{\mathbf{W}}, \overset{[u]}{\bar{\Pi}_0}) + {}^{(l)}\bar{\mathcal{G}}_k(\bar{\mathbf{W}}, \overset{[u]}{\bar{\Pi}_0}) \\[2ex]
\quad = {}^{(l)}\bar{\mathcal{G}}_f(\bar{\mathbf{W}}) - {}^{(l)}\bar{\mathcal{G}}_m(\bar{\mathbf{W}}, \overset{[k]}{\bar{\Pi}_0}) - {}^{(l)}\bar{\mathcal{G}}_b(\bar{\mathbf{W}}, \overset{[k]}{\bar{\Pi}_0}) - {}^{(l)}\bar{\mathcal{G}}_k(\bar{\mathbf{W}}, \overset{[k]}{\bar{\Pi}_0}), \quad \forall \bar{\mathbf{W}} \in \bar{\mathcal{V}}.
\end{array}
$$

$$(4.65)$$

4.3.2. Discrete Weak Form

Following the procedure used in the previous section, we approximate the $\overset{[u]}{\bar{\Pi}_0}$ by $\overset{[u]}{\bar{\Pi}_{0_h}} \in \bar{\mathcal{V}}_h$, and thereby we limit the solution to the following discrete problem.

$$
\begin{array}{l}
\text{Given } \overset{[k]}{\bar{\Pi}_{0_h}} \in {}^{(l)}\bar{\mathcal{S}}_h, \text{ find } \overset{[u]}{\bar{\Pi}_{0_h}} \in \bar{\mathcal{V}}_h \text{ such that} \\[2ex]
{}^{(l)}\bar{\mathcal{G}}_m(\bar{\mathbf{W}}, \overset{[u]}{\bar{\Pi}_{0_h}}) + {}^{(l)}\bar{\mathcal{G}}_b(\bar{\mathbf{W}}, \overset{[u]}{\bar{\Pi}_{0_h}}) + {}^{(l)}\bar{\mathcal{G}}_k(\bar{\mathbf{W}}, \overset{[u]}{\bar{\Pi}_{0_h}}) \\[2ex]
\quad = {}^{(l)}\bar{\mathcal{G}}_f(\bar{\mathbf{W}}) - {}^{(l)}\bar{\mathcal{G}}_m(\bar{\mathbf{W}}, \overset{[k]}{\bar{\Pi}_{0_h}}) - {}^{(l)}\bar{\mathcal{G}}_b(\bar{\mathbf{W}}, \overset{[k]}{\bar{\Pi}_{0_h}}) - {}^{(l)}\bar{\mathcal{G}}_k(\bar{\mathbf{W}}, \overset{[k]}{\bar{\Pi}_{0_h}}), \quad \forall \bar{\mathbf{W}} \in \bar{\mathcal{V}}_h.
\end{array}
$$

$$(4.66)$$

4.3.2.1. Matrix equation

Using the arrangement for matrices and the column vectors in the transient problem, we transform the discrete weak form (4.66) into the following matrix equa-

tion.

Given $\tilde{\mathcal{A}}_r^k \in \bar{R}^{(3\aleph \times 1)}$, $\tilde{\mathcal{A}}_i^k \in R^{(3\aleph \times 1)}$, $\tilde{\psi}_r^k \in R^{(\aleph \times 1)}$, and $\tilde{\psi}_i^k \in R^{(\aleph \times 1)}$,

find $\tilde{\mathcal{A}}_r \in R^{(3n_{A_r} \times 1)}$, $\tilde{\mathcal{A}}_i \in R^{(3n_{A_i} \times 1)}$, $\tilde{\psi}_r \in R^{(n_{\psi_r} \times 1)}$, and $\tilde{\psi}_i \in R^{(n_{\psi_i} \times 1)}$,

such that

$$
\begin{bmatrix} {}^rK - \omega^2\,({}^rM) & \omega\,({}^iB) \\[2ex] -\omega\,({}^rB) & {}^iK - \omega^2\,({}^iM) \end{bmatrix} \begin{Bmatrix} \tilde{\mathcal{A}}_r \\[1ex] \tilde{\psi}_r \\[1ex] \tilde{\mathcal{A}}_i \\[1ex] \tilde{\psi}_i \end{Bmatrix}
$$

$$
= \begin{Bmatrix} {}^rF^A \\[1ex] {}^rF^\psi \\[1ex] {}^iF^A \\[1ex] {}^iF^\psi \end{Bmatrix} - \begin{bmatrix} {}^r\mathcal{K} - \omega^2\,({}^r\mathcal{M}) & \omega\,({}^i\mathcal{B}) \\[2ex] -\omega\,({}^r\mathcal{B}) & {}^i\mathcal{K} - \omega^2\,({}^i\mathcal{M}) \end{bmatrix} \begin{Bmatrix} \tilde{\mathcal{A}}_r^k \\[1ex] \tilde{\psi}_r^k \\[1ex] \tilde{\mathcal{A}}_i^k \\[1ex] \tilde{\psi}_i^k \end{Bmatrix} .
$$

$$(4.67)$$

The "mass" matrices

$$
{}^rM := \begin{bmatrix} {}^rM^{AA} & {}^rM^{A\psi} \\[1ex] {}^rM^{\psi A} & {}^rM^{\psi\psi} \end{bmatrix} \in R^{((3n_{A_r}+n_{\psi_r})\times(3n_{A_r}+n_{\psi_r}))} , \tag{4.68}
$$

and

$$
{}^iM := \begin{bmatrix} {}^iM^{AA} & {}^iM^{A\psi} \\[1ex] {}^iM^{\psi A} & {}^iM^{\psi\psi} \end{bmatrix} \in R^{((3n_{A_i}+n_{\psi_i})\times(3n_{A_i}+n_{\psi_i}))} , \tag{4.69}
$$

are positive definite. The "damping" matrices

$$
{}^rB := \begin{bmatrix} {}^rB^{AA} & {}^rB^{A\psi} \\[1ex] {}^rB^{\psi A} & {}^rB^{\psi\psi} \end{bmatrix} \in R^{((3n_{A_i}+n_{\psi_i})\times(3n_{A_r}+n_{\psi_r}))} , \tag{4.70}
$$

and

$$
{}^iB := \begin{bmatrix} {}^iB^{AA} & {}^iB^{A\psi} \\ {}^iB^{\psi A} & {}^iB^{\psi\psi} \end{bmatrix} \in \mathbf{R}^{((3n_{A_r}+n_{\psi_r})\times(3n_{A_i}+n_{\psi_i}))} , \tag{4.71}
$$

and the "stiffness" matrices

$$
{}^rK := \begin{bmatrix} {}^rK^{AA} & {}^rK^{A\psi} \\ {}^rK^{\psi A} & {}^rK^{\psi\psi} \end{bmatrix} \in \mathbf{R}^{((3n_{A_r}+n_{\psi_r})\times(3n_{A_r}+n_{\psi_r}))} , \tag{4.72}
$$

and

$$
{}^iK := \begin{bmatrix} {}^iK^{AA} & {}^iK^{A\psi} \\ {}^iK^{\psi A} & {}^iK^{\psi\psi} \end{bmatrix} \in \mathbf{R}^{((3n_{A_i}+n_{\psi_i})\times(3n_{A_i}+n_{\psi_i}))} , \tag{4.73}
$$

are positive semi-definite. The above matrices are obtained by deleting the appropriate rows and columns from the respective matrices below.

Similarly, The "mass" matrices

$$
{}^r\mathcal{M} := \begin{bmatrix} {}^r\mathcal{M}^{AA} & {}^r\mathcal{M}^{A\psi} \\ {}^r\mathcal{M}^{\psi A} & {}^r\mathcal{M}^{\psi\psi} \end{bmatrix} \in \mathbf{R}^{((3\aleph+\aleph)\times(3\aleph+\aleph))} , \tag{4.74}
$$

and

$$
{}^i\mathcal{M} := \begin{bmatrix} {}^i\mathcal{M}^{AA} & {}^i\mathcal{M}^{A\psi} \\ {}^i\mathcal{M}^{\psi A} & {}^i\mathcal{M}^{\psi\psi} \end{bmatrix} \in \mathbf{R}^{((3\aleph+\aleph)\times(3\aleph+\aleph))} , \tag{4.75}
$$

are positive definite. The "damping" matrices

$$
{}^r\mathcal{B} := \begin{bmatrix} {}^r\mathcal{B}^{AA} & {}^r\mathcal{B}^{A\psi} \\ {}^r\mathcal{B}^{\psi A} & {}^r\mathcal{B}^{\psi\psi} \end{bmatrix} \in \mathbf{R}^{((3\aleph+\aleph)\times(3\aleph+\aleph))} , \tag{4.76}
$$

and

$$
{}^i\mathcal{B} := \begin{bmatrix} {}^i\mathcal{B}^{AA} & {}^i\mathcal{B}^{A\psi} \\ {}^i\mathcal{B}^{\psi A} & {}^i\mathcal{B}^{\psi\psi} \end{bmatrix} \in \mathbf{R}^{((3\aleph+\aleph)\times(3\aleph+\aleph))} , \tag{4.77}
$$

and the "stiffness" matrices

$$
{}^r\mathcal{K} := \begin{bmatrix} {}^r\mathcal{K}^{AA} & {}^r\mathcal{K}^{A\psi} \\ {}^r\mathcal{K}^{\psi A} & {}^r\mathcal{K}^{\psi\psi} \end{bmatrix} \in \mathbf{R}^{((3\aleph+\aleph)\times(3\aleph+\aleph))} , \tag{4.78}
$$

and

$$
{}^{i}\mathcal{K} := \begin{bmatrix} {}^{i}\mathcal{K}^{AA} & {}^{i}\mathcal{K}^{A\psi} \\ {}^{i}\mathcal{K}^{\psi A} & {}^{i}\mathcal{K}^{\psi\psi} \end{bmatrix} \in \mathbf{R}^{((3\aleph+\aleph)\times(3\aleph+\aleph))} , \tag{4.79}
$$

are positive semi-definite. The prefix "r" indicates that the matrix is associated with the real part of the potentials. The prefix "i" indicates that the matrix is associated with imaginary part of the the potentials. The respective expressions for the coefficients of the matrices were defined earlier in the discussion on the matrix equations for the transient problem. The numbers n_{A_r} and n_{A_i} correspond to the number of nodes at which the real and imaginary parts of the vector potential $\bar{A}$ are to be determined. The numbers n_{ψ_r} and n_{ψ_i} correspond to the number nodes at which the real and imaginary parts scalar potential ψ are to be determined. The Coulomb gauge is enforced similar to the magnetostatic case in Section 4.1.3 on page 67. The matrix ${}^{(p)}K^{AA}$ is added to the stiffness matrices ${}^{r}K^{AA}$ and ${}^{i}K^{AA}$.

CHAPTER 5
POST PROCESSING: THE LUMPED PARAMETER MODEL

To establish a lumped parameter model for an electromagnetic device such as a capacitor, it is necessary to relate the electromagnetic field quantities $\mathbf{E}$ and $\mathbf{B}$, to the circuit quantities (lumped parameters) such as voltage V, current I, capacitance C, inductance L, and resistance R. Moreover, it is necessary to relate the vector potential $\mathbf{A}$ and the scalar ψ, to the lumped parameters. The focus of this chapter is to outline the necessary relations between the continuum FE solution and the discrete lumped parameters. We begin with an explanation of the lumped parameter model for the capacitor. We present the relations between the lumped parameters and the field quantities. We conclude this chapter with the expressions relating the lumped parameters to the FE matrices and solution vectors that were defined in Chapter 4.

In this chapter, we include discussions and expressions relating solutions for problems with transient excitations to its equivalent circuit parameters. For example, the expressions (5.16), (5.17), and (5.18), express resistance R, inductance L, and capacitance C, as a function of time t. The reader is forewarned that a more comprehensive study is required to explain the validity of such expressions for general transient excitations (i.e., for time-dependent excitations that cannot be expressed as a linear combination of sine and cosine functions of time).

Problems with electromagnetic devices can be, predominantly, classified into two categories. The first category of problems is with an input current. The voltage measured between the terminals of the device is used to compute the impedance of the device, and subsequently, the R, L, and C. The second category of problems is

<center>82</center>

with an input voltage. The current flowing through the device is measured so as to compute the impedance, and subsequently, the R, L, and C. The focus of this work is solution to problems that belong to the second category, i.e., where a voltage is prescribed at the terminations of the capacitor and the current is calculated from the FE solution. The current flowing through the system is calculated using the power stored by the electric current density $\mathbf{J}_f$, the displacement current density $\frac{\partial \mathbf{D}}{\partial t}$, and the magnetic induction $\mathbf{B}$. The total power divided by the input voltage is the current flowing through the device.

A simple circuit model for the capacitor, connects the resistance R, the inductance L, and the capacitance C in series as done in Figure 5.1. One of the important assumptions in the simple circuit model is that the disturbance is propagated around the circuit instantaneously. This assumption is only valid if the wavelength is much greater than the dimension (circuit length) of the device. A rule of thumb in electromagnetics is that the model is applicable to those devices whose circuit length and transverse cross-sections are smaller than 1/8th of the wavelength. In order to extend the applicability of the simple RLC circuit model to larger devices, we assume that the lumped parameters R, L, and C are frequency dependent. A FE analysis computes the potentials at any given excitation frequency. From the potentials we calculate the R, L, and C at that frequency. Another approach is to use the concept of distributed capacitance, inductance and resistance. One such attempt is the transmission line[19] model; see e.g., Kraus [1984]. Post processing, i.e., obtaining the lumped parameters from a FE solution, for the transmission line model is beyond the scope of the present work.

---

[19] A transmission line may be defined as a device for transmitting or guiding energy. Transmission line models are necessary to model waveguides, radio links, etc.

All Frequencies
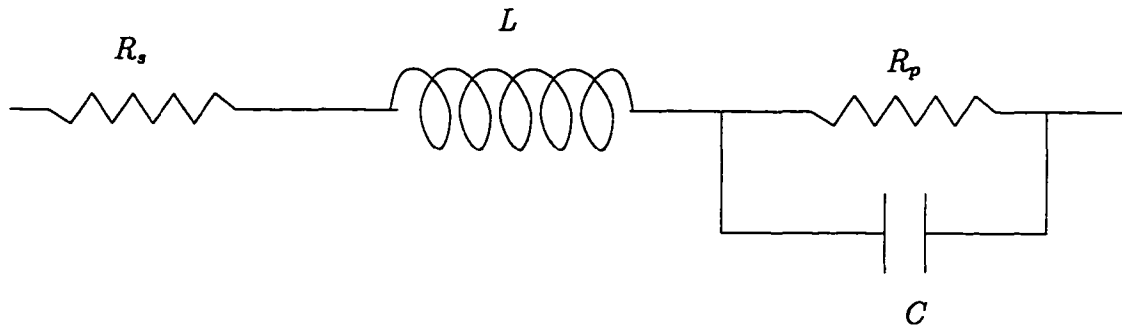
High Frequency
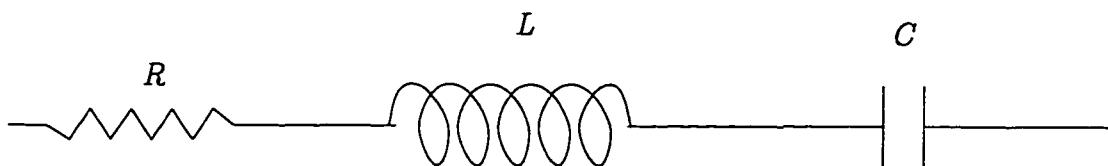
Figure 5.1. Equivalent Circuit Model for MLCC

5.1. Equivalent Circuit Model for a Capacitor

A capacitor can be represented by a series combination of an ideal capacitance C, a resistance R, and an inductance L, as in Sarjeant [1990] and Anand [1993]. In the equivalent circuit model the resistance R_s is due to the conductors, i.e., the electrodes, end terminations, etc. The leakage resistance R_p is due to the resistivity of the lossy dielectric material. In general $R_s >> R_p$.

However, as shown in Figure 5.1 we could alternately dispense with R_p and R_s and construct a model that has a single R. This resistance R is frequency dependent.

The impedance of the upper circuit at frequency $f = \omega/2/\pi$ in Figure 5.1 is

$$\bar{Z} = R_s + i\omega L + \left\{ \frac{\frac{-i}{\omega C} R_p}{R_p - \frac{i}{\omega C}} \right\} .$$

However, at high frequencies we can approximate the impedance to be

$$\bar{Z} = R_s + i\omega L + \frac{-i}{\omega C} . \tag{5.1}$$

This is same as that shown by the lower circuit in Figure 5.1. The magnitude of the impedance is given by

$$|\bar{Z}| = \left[R^2 + \left(\omega L - \frac{1}{\omega C} \right)^2 \right]^{1/2} ,$$

where the resistance R is frequency dependent; at high frequencies $R \approx R_s$.

At low frequencies the capacitive reactance $\dfrac{i}{\omega C}$ dominates, however, at high frequencies the inductive term $i\omega L$ dominates. At a certain frequency called the self resonant frequency (srf), the capacitive reactance cancels the inductive term, and hence, the capacitor acts like a pure resistor. If the inductance L and the capacitance C are not dependent on frequency, then the self resonant frequency srf is

$$srf = \frac{1}{2\pi\sqrt{LC}} . \tag{5.2}$$

The resistance at the self resonant frequency is defined as the equivalent series resistance esr. In general, it is best to stay below the srf so as to avoid large power loss in the capacitor. Caution must be employed when using the capacitor above the srf where the capacitor behaves like an inductor, and therefore a very little current flow could result in large voltage drop across the terminals.

The esr, esl and srf are measured using an AC source. The capacitor is excited by an AC voltage V at a certain frequency f. The current is then measured. The impedance

$$\bar{Z} = \frac{\bar{V}}{\bar{I}} = Z_r + iZ_i ,$$

where Z_r and Z_i are the real and imaginary parts of $\bar{Z}$. The *esr* is given by $R = Z_r$ at any frequency f. The *esl* is calculated at a high frequency $\hat{f}$ by

$$L = esl = \frac{Z_i}{\omega} = \frac{Z_i}{2\pi \hat{f}} \ .$$

The typical behavior of the impedance as a function of frequency is shown in Figure 5.2. A sudden drop in the impedance is observed close to the self resonant frequency.

However, the behavior of the MLCC is more complex. The distribution of current inside the capacitor depends on the frequency. Hence, the *srf* is determined by examining the behavior of $\bar{Z}$ over a range on frequencies. The frequency where $|\bar{Z}|$ achieves the minimum is the *srf*, and $esr = |\bar{Z}|$. The *esl* is measured as before by selecting a frequency $\hat{f}$ much higher than the *srf*, where $esl = Z_i/(2\pi \hat{f})$. To reiterate, equation (5.2) cannot be used to compute the *srf* for a MLCC.

5.2. Circuit Quantities in Terms of Electromagnetic Fields

The lumped parameters R, L, and C for the simple RLC circuit model for a capacitor are obtained at a particular frequency. To calculate the *esr*, *esl* and *srf* we have to follow the procedure outlined in the end of the previous section, i.e., we have to "sweep" through a range of frequencies to calculate the curve in Figure 5.2. Unlike Figure 5.2, for a MLCC, we expect many local minima. The expressions for the lumped parameters in this section can be found in the current literature, e.g., see Kraus [1984, p. 376].

5.2.1. Voltage

The voltage V between two points is defined as follows.

$$V := -\int_{\mathcal{L}} \mathbf{E} \cdot \hat{\mathbf{t}} \, d\mathcal{L} \ , \tag{5.3}$$
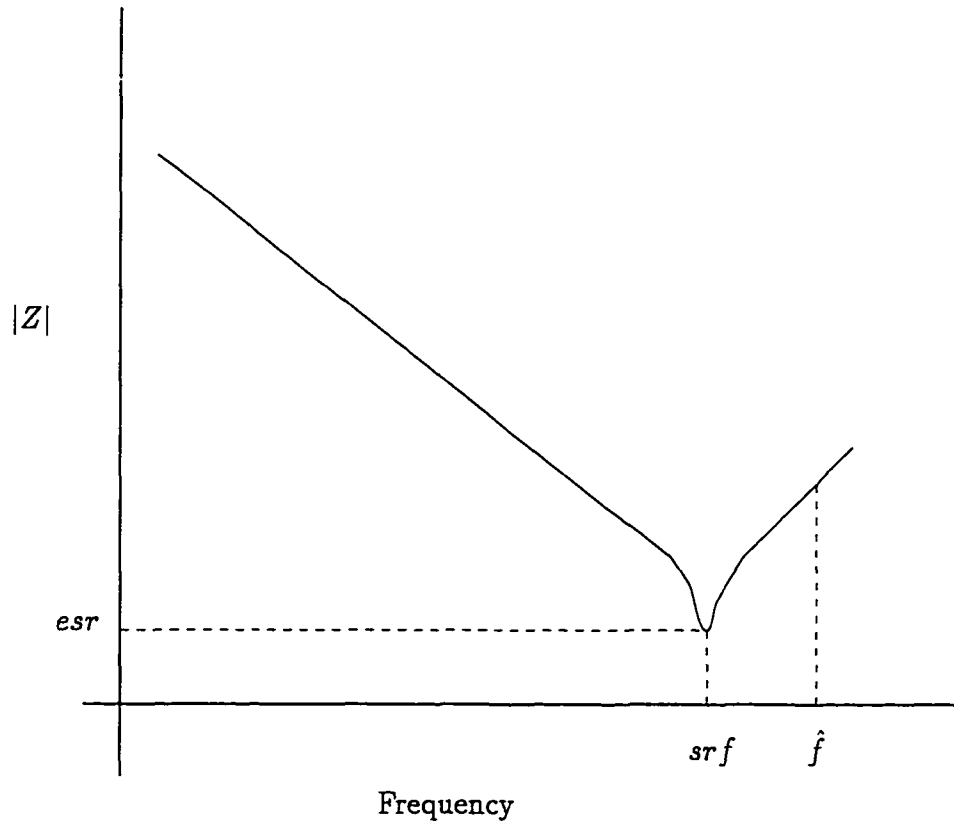
Figure 5.2. Impedance $|\bar{Z}|$ vs frequency f for a simple capacitor. Both the quantities are plotted using a logarithmic scale.

where $\mathcal{L}$ is any arbitrary path that connects the two points, and $\hat{t}$ is the tangent to the path at any point x on the path $\mathcal{L}$. If the path $\mathcal{L}$ is curved, then the tangent $\hat{t}$ changes as we move along the path; see Figure 5.3 for details.

In the presence of a battery or a generator, the electric field $\mathbf{E}$ is non-conservative. This non-conservative field drives the current through the electromagnetic device. This driving force is termed as the electro motive force (e.m.f.) $\mathcal{E}$. The e.m.f. is the integral of $\mathbf{E}$ around the circuit. However, if we split the device and the generator, then the e.m.f. supplied to the device is the line integral of the electric field between

the terminations of the device that connect to the generator, i.e,

$$\mathcal{E} := \int_{\mathcal{L}} \mathbf{E} \cdot \hat{\mathbf{t}} \, d\mathcal{L} = \int_{\mathcal{L}} \operatorname{grad} \dot{\psi} \cdot \hat{\mathbf{t}} \, d\mathcal{L} + \int_{\mathcal{L}} \dot{\mathbf{A}} \cdot \hat{\mathbf{t}} \, d\mathcal{L} , \qquad (5.4)$$

where $\hat{\mathbf{t}}$ is the tangent to the path at any point $\mathbf{x}$ on the path $\mathcal{L}$. Using circuit theory we can show that

$$\mathcal{E} = IR + \frac{1}{C} \int I \, dt + L \frac{dI}{dt} , \qquad (5.5)$$

and for time harmonic fields

$$\bar{\mathcal{E}} = \bar{I}R + \frac{\bar{I}}{i\omega C} + i\omega \bar{I} L ; \qquad (5.6)$$

see e.g., Kraus [1984].

Voltage is measured by a voltmeter. The "voltmeter reading"

$$V_{reading} := - \int_{Leads} \mathbf{E} \cdot \hat{\mathbf{t}} \, d\mathcal{L} , \qquad (5.7)$$

depends of the path of the leads connecting the voltmeter to an electromagnetic device. The path of integration inside the electromagnetic device is represented by $\mathcal{L}$, and the voltmeter is connected between Points 1 and Point 2 via the path *Leads*. In Figure 5.3 a dotted line represents the path *Leads*.

In an electrostatic problem, $\mathbf{E} = -\operatorname{grad} \dot{\psi}$. Hence, the field $\mathbf{E}$ is conservative, and

$$\oint \mathbf{E} \cdot \hat{\mathbf{t}} \, d\mathcal{L} , = 0$$

Hence, the voltmeter reading is simply the potential difference, i.e.,

$$V_{reading} := - \int_{Leads} \mathbf{E} \cdot \hat{\mathbf{t}} \, d\mathcal{L} , = - \int_{\mathcal{L}} \mathbf{E} \cdot \hat{\mathbf{t}} \, d\mathcal{L} = \dot{\psi}^{(2)} - \dot{\psi}^{(1)} , \qquad (5.8)$$

where $\dot{\psi}^{(i)}$ represents the value of the time derivative of the scalar potential at Point i. However, for time varying fields the voltmeter reading is path dependent: $V_{reading}$
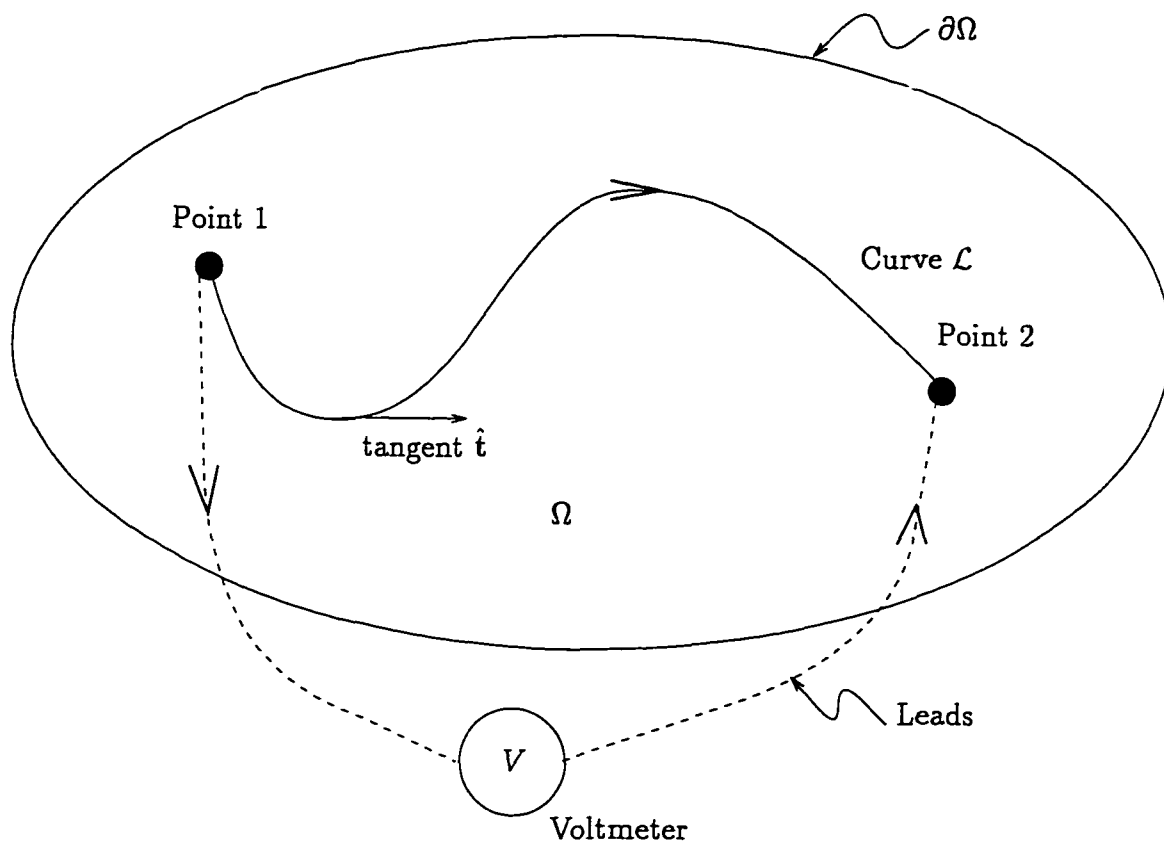
Figure 5.3. Voltage

depends on the path *Leads*. This is similar to the concept of "current return path" used to define the inductance of the device. For time varying fields

$$\mathbf{E} = -\text{grad}\,\dot{\psi} - \dot{\mathbf{A}} \qquad \Rightarrow \qquad \oint \mathbf{E} \cdot \hat{t}\, d\mathcal{L} = - \oint \dot{\mathbf{A}} \cdot \hat{t}\, d\mathcal{L} \,,$$

which, in general, is not equal to zero. Hence, the voltmeter reading becomes

$$V_{reading} := - \int_{Leads} \mathbf{E} \cdot \hat{t}\, d\mathcal{L} \,, = - \int_{\mathcal{L}} \mathbf{E} \cdot \hat{t}\, d\mathcal{L} - \oint \dot{\mathbf{A}} \cdot \hat{t}\, d\mathcal{L} \,. \qquad (5.9)$$

If we can configure the leads such that

$$\int_{Leads} \dot{\mathbf{A}} \cdot \hat{t}\, d\mathcal{L} = 0 \,,$$

then

$$V_{reading} := -\int_{Leads} \mathbf{E} \cdot \hat{t} \; d\mathcal{L} \; , = -\int_{\mathcal{L}} \left(\mathbf{E} + \dot{\mathbf{A}}\right) \cdot \hat{t} \; d\mathcal{L} \; .$$

But $\mathbf{E} = -\text{grad} \dot{\psi} - \dot{\mathbf{A}}$, and hence,

$$V_{reading} := \dot{\psi}^{(2)} - \dot{\psi}^{(1)} \; .$$

Mayergoyz [1993] uses different paths for the voltmeter leads to determine the electromagnetic potentials $\mathbf{A}$ and ψ.

For the MLCC problem at low frequencies, the magnetic field and consequently the magnetic vector potential $\mathbf{A}$ are much smaller than the electric field. It is observed from numerical experiments that at low frequencies the voltage measured between the electrodes is, for all practical purposes, not path dependent. However, at higher frequencies (above $10^6 \; Hz$), the voltage measured between the electrodes is path dependent. But the focus of the present formulation is to solve problems with a prescribed input voltage $V_{applied}$. By choice we define the voltage to be the difference in the scalar potential, i.e.,

$$V_{applied} := -\int_{\mathcal{L}} \mathbf{E} \cdot \hat{t} \; d\mathcal{L} = \dot{\psi}^{(2)} - \dot{\psi}^{(1)} \; . \tag{5.10}$$

The consequence of such a choice is that the path *Leads* that connect the capacitor (or any other passive electromagnetic device) to the e.m.f. generator is such that

$$\int_{Leads} \dot{\mathbf{A}} \cdot \hat{t} \; d\mathcal{L} = 0 \; .$$

To reiterate, the above choice (to specify the voltage by using only ψ) constrains the "current return path," i.e., the path *Leads* is arbitrarily fixed.

5.2.2. Current

The total current I at a surface $\partial\Omega_I$ is defined as the surface integral of the normal component of the current density $\mathbf{J}_f$, i.e.,

$$I := \int_{\partial\Omega_I} \mathbf{J}_f \cdot \hat{n} \; d(\partial\Omega) \; . \tag{5.11}$$

However, if the surface $\partial\Omega_I$ is enclosed within a conductor, then we can neglect the term $\dfrac{\partial \mathbf{D}}{\partial t}$ in the Ampere's law

$$\operatorname{curl} \mathbf{H} = \mathbf{J}_f + \frac{\partial \mathbf{D}}{\partial t} \ ,$$

and hence derive an alternate expression

$$I := \int_{\mathcal{L}_I} \mathbf{H} \cdot \hat{\mathbf{t}} \ d\mathcal{L} \ , \tag{5.12}$$

where curve $\mathcal{L}_I$ encloses surface $\partial\Omega_I$ as shown in Figure 5.4, and $\hat{\mathbf{t}}$ is the tangent to the curve $\mathcal{L}_I$. In practice, the surface $\partial\Omega_I$ is chosen to be the cross-section of the conductor entering the device. A more complete definition of current is obtained from electromagnetic power. The induced current is defined as the electromagnetic power divided by the applied voltage.

5.2.2.1. Lumped Parameters for the RLC Circuit Model

For a time-harmonic problem, the lumped parameters can be directly calculated from the voltage and current. From the earlier discussions it is evident that the impedance of the circuit is given by $\bar{Z} = \dfrac{\bar{V}}{\bar{I}}$, where the $\bar{V}$ is the complex voltage and $\bar{I}$ is the complex current. From (5.1) we can equate the real part of $\bar{Z}$ to the resistance R and the imaginary part to $\left(\omega L - \dfrac{1}{\omega C}\right)$.

5.2.3. Power in Terms of Fields

The Maxwell equations can be derived based on the principle of virtual power. The principle of virtual power is the main tool in continuum thermodynamics, especially when dealing with coupled fields. The pioneering work by Maugin [1980][20]

---

[20] Maugin [1980] uses the basic laws of electromagnetics (the Gauss's laws, Ampere's law and Faraday's law) to derive the equations for discrete charges and particles. It is followed by the principle of statistical averaging and virtual power to derive the equations for the continuum. It is here that the concept of electromagnetic stress tensor, the electromagnetic momentum, and Poynting vector are useful. Such an approach accounts for finite deformations of the volume. Discussion along these lines is beyond the scope of the present work. The reader is referred to Eringen and Maugin [1990] for details.
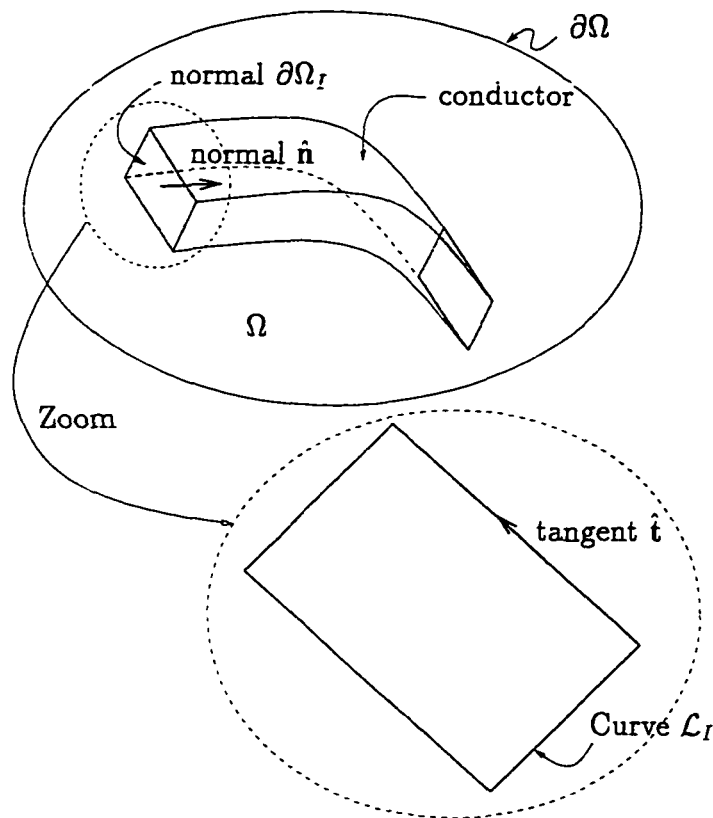
Figure 5.4. Current

explains the use of this principle to derive equations that model the coupling between electrical, mechanical and thermal systems. The approach followed in this work derives the weak form for the FE solution from Maxwell equations. An alternate approach is to derive the weak from the expression of electromagnetic power. In the approach presented here, the definition of power is useful to relate the field quantities and the potentials to the lumped parameters. The different parts of electromagnetic power stored in a volume Ω are defined below. The electric power

$$\mathcal{P}_E := \int_{\mathbf{R}^3} \int_0^{\mathbf{E}} \frac{d\mathbf{D}}{dt} \cdot \delta \mathbf{E} \; d\Omega \; ,$$

and for linear isotropic material we have

$$\mathcal{P}_E := \frac{1}{2} \int_{\mathbf{R}^3} \frac{d\mathbf{D}}{dt} \cdot \mathbf{E} \, d\Omega \ . \tag{5.13}$$

The magnetic power

$$\mathcal{P}_H := \int_{\mathbf{R}^3} \int_0^{\mathbf{H}} \frac{d\mathbf{B}}{dt} \cdot \delta\mathbf{H} \, d\Omega \ ,$$

and for linear isotropic material we have

$$\mathcal{P}_H := \frac{1}{2} \int_{\mathbf{R}^3} \frac{d\mathbf{B}}{dt} \cdot \mathbf{H} \, d\Omega \ . \tag{5.14}$$

The resistive power

$$\mathcal{P}_J := \int_{\mathbf{R}^3} \int_0^{\mathbf{E}} \mathbf{J}_f \cdot \delta\mathbf{E} \, d\Omega \ ,$$

and for linear isotropic material we have

$$\mathcal{P}_J := \frac{1}{2} \int_{\mathbf{R}^3} \mathbf{J}_f \cdot \mathbf{E} \, d\Omega \ . \tag{5.15}$$

In an electromagnetic system with no thermal and mechanical interactions, the total power in the volume Ω is conserved in accordance with Poynting's theorem (Wangsness [1986, p. 357]) where

$$-\int_\Omega \frac{d\mathbf{D}}{dt} \cdot \mathbf{E} \, d\Omega - \int_\Omega \frac{d\mathbf{B}}{dt} \cdot \mathbf{H} \, d\Omega = \int_\Omega \mathbf{J}_f \cdot \mathbf{E} \, d\Omega + \int_{\partial\Omega} \mathbf{E} \times \mathbf{H} \, d(\partial\Omega) \ ,$$

$\mathbf{S} := \mathbf{E} \times \mathbf{H}$ is the *Poynting vector*. The Poynting vector represents the power flux, i.e., the instantaneous flow of energy, and points in the direction of energy flow. The surface $(\partial\Omega)$ encloses the volume Ω. For the capacitor problem we neglect any loss due to radiation. Hence, the driving power from the generator is split into the power loss due to a resistance, power stored due to the displacement current, and the power stored due to the magnetic induction.

5.2.3.1. Lumped parameters

To obtain the lumped parameters from the above definitions of power, it is necessary to obtain the equivalent expressions for power in the circuit model. Consider a RLC circuit model for high frequencies in Figure 5.1, where the resistance R, the inductance L and the capacitance C are connected in series. Let V be the voltage applied and I be the current. From circuit analysis we know that the resistive power is $\frac{1}{2}RI^2$, the inductive power is $\frac{1}{2}LI\frac{dI}{dt}$, and the capacitive power is $\frac{1}{2}CV\frac{dV}{dt}$. The applied voltage V depends on the configuration of the path *Leads* (see Section 5.2.1 on page 86). Relating the powers stored in the circuit to the powers in terms of the field quantities in (5.13), (5.14), and (5.15), we obtain the following. The resistance R is

$$R = \frac{2\mathcal{P}_J}{I^2} \approx \frac{\int_\Omega \mathbf{J}_f \cdot \mathbf{E} \, \partial\Omega}{I^2} \,, \qquad (5.16)$$

capacitance C is

$$C = \frac{2\mathcal{P}_E}{\frac{dV}{dt}V} \approx \frac{\int_\Omega \frac{d\mathbf{D}}{dt} \cdot \mathbf{E} \, \partial\Omega}{\frac{dV}{dt}V} \,, \qquad (5.17)$$

and inductance L is

$$L = \frac{2\mathcal{P}_H}{\frac{dI}{dt}I} \approx \frac{\int_\Omega \frac{d\mathbf{B}}{dt} \cdot \mathbf{H} \, \partial\Omega}{\frac{dI}{dt}I} \,. \qquad (5.18)$$

In the above expressions we neglect the contribution to the powers outside the volume Ω.

5.2.4. Power and the Lumped Parameters in Terms of Potentials

The different powers in the electromagnetic device can be represented in terms of potentials. To do so we limit our discussions to time harmonic problems. Consider a device represented by the volume Ω in Figure 5.5. If the applied voltage between surface $(\partial\Omega)^{(1)}$ and $(\partial\Omega)^{(2)}$ is represented by the complex quantity $\bar{V}$, and

the induced current is represented by $\bar{I}$, the net power in the system is given by

$$\bar{\mathcal{P}} := \bar{V}\bar{I}^* = \bar{Z}I^2 = I^2\left(R + i\omega L + \frac{1}{i\omega C}\right) , \tag{5.19}$$

where $\bar{I}^*$ is the complex conjugate of $\bar{I}$, and $I^2 := \bar{I}\,\bar{I}^*$. The equivalent resistance, inductance and capacitance are represented by R, L, and C, respectively. As explained earlier, we define the voltage $\bar{V} := -i\omega\mathrm{grad}\,\bar{\psi}$. The induced current is measured to be

$$\bar{I}^* = \int_{(\partial\Omega)^{(1)}} \mathbf{J}_f \cdot \hat{\mathbf{n}} \; d(\partial\Omega) = \int_{(\partial\Omega)^{(2)}} \mathbf{J}_f \cdot \hat{\mathbf{n}} \; d(\partial\Omega) . \tag{5.20}$$

Hence, the power in the volume Ω in Figure 5.5 is given by

$$\bar{\mathcal{P}} = \bar{V}\bar{I}^* = \int_\Omega \left(-i\omega\mathrm{grad}\,\bar{\psi}\right) \cdot \bar{\mathbf{J}}^* \; d\Omega , \tag{5.21}$$

where $\bar{\mathbf{J}} := \bar{\mathbf{J}}_f + i\omega\bar{\mathbf{D}}$; see Morweiser and Meunier [1994] for details.

Relating (5.20) to (5.21) and using $\bar{\mathbf{E}} = -i\omega\mathrm{grad}\,\bar{\psi} - i\omega\bar{\mathbf{A}}$ Morweiser and Meunier [1994] derives the following expressions for the lumped parameters:

$$RI^2 = Re\left\{\int_\Omega \bar{\mathbf{E}}\cdot\bar{\mathbf{J}}^* \; d\Omega\right\} + Im\left\{\int_\Omega \omega\bar{\mathbf{A}}\cdot\bar{\mathbf{J}}^* \; d\Omega\right\} , \tag{5.22}$$

$$\frac{1}{\omega C}I^2 = -Im\left\{\int_\Omega \bar{\mathbf{E}}\cdot\bar{\mathbf{J}}^* \; d\Omega\right\} , \tag{5.23}$$

$$LI^2 = Re\left\{\int_\Omega \bar{\mathbf{A}}\cdot\bar{\mathbf{J}}^* \; d\Omega\right\} , \tag{5.24}$$

where the current

$$I^2 = \frac{\mathcal{P}^2}{V^2} .$$

The symbols $Re\ \{\cdot\}$ and $Im\ \{\cdot\}$ indicate the real and imaginary parts of the quantity in the brackets, e.g., $Re\ \{\bar{I}\} = I_r$ and $Im\ \{\bar{I}\} = I_i$

The expression for power in (5.22), (5.23), and (5.24) can be obtained from (5.16), (5.17), and (5.18) using Maxwell equations. For example, the integral

$$Re\left\{\int_\Omega \bar{\mathbf{B}}\cdot\bar{H}^* \; d\Omega\right\} = Re\left\{\int_\Omega \bar{\mathbf{A}}\cdot\bar{J}^* \; d\Omega\right\} + Re\left\{\int_{(\partial\Omega)} \bar{\mathbf{A}} \times \bar{H}^* \; d(\partial\Omega)\right\} ,$$
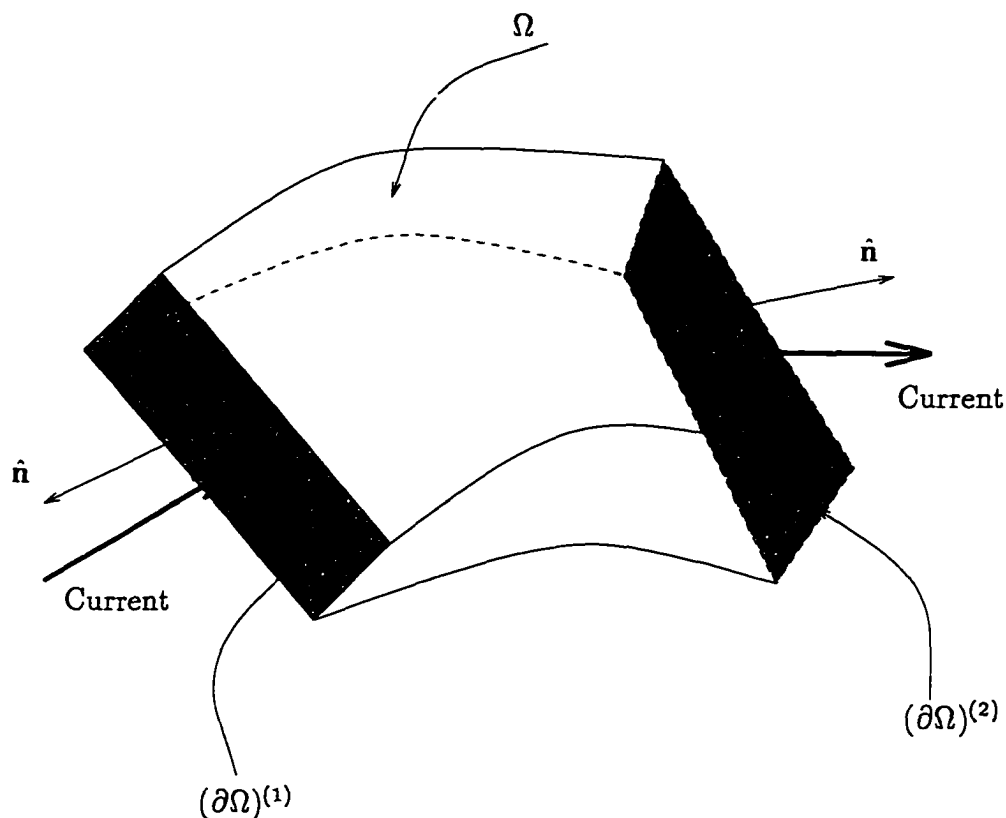
Figure 5.5. Flow of current through a volume Ω. A voltage is imposed at surfaces $(\partial\Omega)^{(1)}$ and $(\partial\Omega)^{(2)}$. There is no current flowing out of the other four sides, i.e., $\bar{\mathbf{J}}\cdot\hat{\mathbf{n}} = 0$ on the other four surfaces.

and hence, if the surface $(\partial\Omega)$ is sufficiently far away from the center of the problem, then

$$\int_\Omega \bar{\mathbf{B}}\cdot\bar{H}^* \, d\Omega \quad \approx \quad \int_\Omega \bar{\mathbf{A}}\cdot\bar{J}^* \, d\Omega \, .$$

The expressions in terms of the potentials have an advantage depending upon the type of the problem and the excitation frequency. For example, in a circuit with the electric current much larger than the displacement current, the integral

$$Re\left\{\int_\Omega \bar{\mathbf{A}}\cdot\bar{\mathbf{J}}^* \, d\Omega\right\}$$

only needs to be computed in the conductor.

5.3. Circuit Quantities from the FE Solution

In this section, the circuit quantities are expressed in terms of the finite element solution for the potentials $\mathbf{A}$ and ψ. Recall that the lumped parameters R, L, and C were defined in (5.16), (5.17), and (5.18). For time-harmonic problems simplified expressions were obtained for the lumped parameters in (5.22), (5.23), and (5.24).

5.3.1. Static Problem

For an electrostatic problem ($\mathbf{A} \equiv 0$), the voltage V between Node i and Node j in the finite element mesh is defined to be

$$V := \overset{\bullet}{\psi_0^j} - \overset{\bullet}{\psi_0^i} .$$

There is no current inside the confines of the boundary Ω for an electrostatic problem. In the static problem, the power is zero, and hence, we calculate the lumped parameters in terms of energies. The electric energy is

$$\frac{1}{2} \int_\Omega \mathbf{D} \cdot \mathbf{E} \, d\Omega = \frac{1}{2} \left\{ \widetilde{\overset{\bullet}{\psi_0}} \right\}^T \left[M^{\psi\psi} \right] \left\{ \widetilde{\overset{\bullet}{\psi_0}} \right\} ,$$

where the solution vector $\left\{ \widetilde{\overset{\bullet}{\psi_0}} \right\}$ and the "mass" matrix $\left[M^{\psi\psi} \right]$ are as defined in (4.23). The capacitive energy in the circuit is equal to $\frac{1}{2}CV^2$. The capacitance C is defined to be

$$\boxed{C := \frac{\left\{ \widetilde{\overset{\bullet}{\psi_0}} \right\}^T \left[M^{\psi\psi} \right] \left\{ \widetilde{\overset{\bullet}{\psi_0}} \right\}}{V^2} .} \qquad (5.25)$$

For a magnetostatic problem, a current $\mathbf{J}_{a_0}$ is specified on the domain Ω. The current is calculated as in (5.11), by replacing $\mathbf{J}_f$ by $\mathbf{J}_{a_0}$. The magnetic energy is

$$\frac{1}{2} \int_\Omega \mathbf{B} \cdot \mathbf{H} \, d\Omega = \left\{ \widetilde{\mathcal{A}_0} \right\}^T \left[K^{AA} \right] \left\{ \widetilde{\mathcal{A}_0} \right\} .$$

The inductive energy in the circuit is equal to $\frac{1}{2}LI^2$. The inductance L is defined to be

$$L := \frac{\left\{\widetilde{\mathcal{A}_0}\right\}^T \left[K^{AA}\right] \left\{\widetilde{\mathcal{A}_0}\right\}}{I^2} .$$

(5.26)

5.3.2. Transient Problem

In the transient problem we calculate the lumped parameters at each time step. Hence, e.g., the resistance can change with time.

At time $t = t_n$, the electric field $\mathbf{E}$ is given by

$$\mathbf{E}(\mathbf{x}, t_n) = -[\nabla \cdot N] \left\{ \begin{array}{c} \dot{\widetilde{\mathcal{A}}}_n \\ \dot{\widetilde{\psi}}_n \end{array} \right\} - [N] \left\{ \begin{array}{c} \dot{\widetilde{\mathcal{A}}}_n \\ 0 \end{array} \right\} ,$$

(5.27)

and the magnetic field $\mathbf{B}$ is given by

$$\mathbf{B}(\mathbf{x}, t_n) = [\nabla \times N] \left\{ \begin{array}{c} \dot{\widetilde{\mathcal{A}}}_n \\ \dot{\widetilde{\psi}}_n \end{array} \right\} .$$

(5.28)

The finite element solution vectors $\dot{\widetilde{\mathcal{A}}}_n$ and $\dot{\widetilde{\psi}}_n$ are as defined in (4.53). The matrices $[\nabla \cdot N]$, $[N]$, and $[\nabla \times N]$ are defined in Remark 5.1.

Remark 5.1. Recall that in (4.37) the value of the vector potential $\mathbf{A}$ at time $t = t_n$ is arranged in a column vector. Similarly, in (4.38) the value of the scalar potential ψ at time $t = t_n$ is arranged in a column vector. Corresponding to such an arrangement we define the matrix $[N] \in \mathbf{R}^{4 \times 4\aleph}$ as follows ($\aleph$ represents the number of nodes in the finite element mesh).

$$[N] :=$$

$$\begin{bmatrix} N_1 & 0 & 0 & | & N_2 & 0 & 0 & | & \cdots & | & N_\aleph & 0 & 0 & | & \cdots \\ 0 & N_1 & 0 & | & 0 & N_2 & 0 & | & \cdots & | & 0 & N_\aleph & 0 & | & \cdots \\ 0 & 0 & N_1 & | & 0 & 0 & N_2 & | & \cdots & | & 0 & 0 & N_\aleph & | & \cdots \\ 0 & 0 & 0 & | & 0 & 0 & 0 & | & \cdots & | & 0 & 0 & 0 & | & \cdots \end{bmatrix}$$

$$
\begin{bmatrix}
\cdots & | & 0 & 0 & 0 & \cdots & 0 \\
\cdots & | & 0 & 0 & 0 & \cdots & 0 \\
\cdots & | & 0 & 0 & 0 & \cdots & 0 \\
\cdots & | & N_1 & N_2 & N_3 & \cdots & N_{\aleph}
\end{bmatrix} ,
$$

$$(5.29)$$

where N_1 to $N_{\aleph}$ are the basis functions corresponding to the $\aleph$ nodes in the mesh. The three components of the vector potential and one component of the scalar potential at a point $\mathbf{x}$ and time $t = t_n$ are given by

$$
\left\{
\begin{array}{c}
A^1(\mathbf{x}, t_n) \\
A^2(\mathbf{x}, t_n) \\
A^3(\mathbf{x}, t_n) \\
\psi(\mathbf{x}, t_n)
\end{array}
\right\}
= [N]
\left\{
\begin{array}{c}
\tilde{\dot{\mathcal{A}}}_n \\
\dot{\tilde{\psi}}_n
\end{array}
\right\}
\qquad \in \mathbf{R}^{4 \times 1} ,
$$

$$(5.30)$$

where

$$
\left\{
\begin{array}{c}
\tilde{\dot{\mathcal{A}}}_n \\
\dot{\tilde{\psi}}_n
\end{array}
\right\}
\qquad \in \mathbf{R}^{4\aleph \times 1} ,
$$

is the solution to the finite element problem; there are four degrees of freedom per node, and $\aleph$ nodes.

Corresponding to the curl $\mathbf{A}$ we define a matrix $[\nabla \times N] \in \mathbf{R}^{3 \times 4\aleph}$ as follows.

$$[\nabla \times N] :=$$

$$
\begin{bmatrix}
0 & -\dfrac{\partial N_1}{\partial x^3} & \dfrac{\partial N_1}{\partial x^2} & | & \cdots & | & 0 & -\dfrac{\partial N_{\aleph}}{\partial x^3} & \dfrac{\partial N_{\aleph}}{\partial x^2} & | & \cdots \\
& & & | & & | & & & & | & \cdots \\
\dfrac{\partial N_1}{\partial x^3} & 0 & -\dfrac{\partial N_1}{\partial x^1} & | & \cdots & | & \dfrac{\partial N_{\aleph}}{\partial x^3} & 0 & -\dfrac{\partial N_{\aleph}}{\partial x^1} & | & \cdots \\
& & & | & & | & & & & | & \cdots \\
-\dfrac{\partial N_1}{\partial x^2} & \dfrac{\partial N_1}{\partial x^1} & 0 & | & \cdots & | & -\dfrac{\partial N_{\aleph}}{\partial x^2} & \dfrac{\partial N_{\aleph}}{\partial x^1} & 0 & | & \cdots
\end{bmatrix}
$$

$$
\begin{bmatrix}
\cdots & | & 0 & 0 & 0 & \cdots & 0 \\
\cdots & | & & & & & \\
\cdots & | & 0 & 0 & 0 & \cdots & 0 \\
\cdots & | & & & & & \\
\cdots & | & 0 & 0 & 0 & \cdots & 0
\end{bmatrix} ,
$$

$$(5.31)$$

so that

$$\text{curl } \mathbf{A}(\mathbf{x}, t_n) \equiv \nabla \times \left\{ \begin{array}{c} A^1(\mathbf{x}, t_n) \\ A^2(\mathbf{x}, t_n) \\ A^3(\mathbf{x}, t_n) \end{array} \right\} = [\nabla \times N] \left\{ \begin{array}{c} \dot{\tilde{A}}_n \\ \dot{\tilde{\psi}}_n \end{array} \right\} \qquad \in \bar{\mathbf{R}}^{3 \times 1} . \qquad (5.32)$$

Corresponding to the div $\mathbf{A}$ we define a matrix $[\nabla \bullet N] \in \mathbf{R}^{1 \times 4\aleph}$ as follows.

$$[\nabla \times N] :=$$

$$\left[\begin{array}{ccccccccccc} \dfrac{\partial N_1}{\partial x^1} & \dfrac{\partial N_1}{\partial x^2} & \dfrac{\partial N_1}{\partial x^3} & | & \cdots & | & \dfrac{\partial N_\aleph}{\partial x^1} & \dfrac{\partial N_\aleph}{\partial x^2} & \dfrac{\partial N_\aleph}{\partial x^3} & | & 0 \quad 0 \quad \cdots \quad 0 \end{array} \right] ,$$

$$(5.33)$$

so that

$$\text{div } \mathbf{A}(\mathbf{x}, t_n) \equiv \nabla \bullet \left\{ \begin{array}{c} A^1(\mathbf{x}, t_n) \\ A^2(\mathbf{x}, t_n) \\ A^3(\mathbf{x}, t_n) \end{array} \right\} = [\nabla \bullet N] \left\{ \begin{array}{c} \dot{\tilde{A}}_n \\ \dot{\tilde{\psi}}_n \end{array} \right\} \qquad \in \mathbf{R} . \qquad (5.34)$$

Corresponding to the grad ψ we define a matrix $[\nabla N] \in \mathbf{R}^{3 \times 4\aleph}$ as follows.

$$[\nabla N] := \left[\begin{array}{ccccccc} 0 & 0 & \cdots & 0 & | & \dfrac{\partial N_1}{\partial x^1} & \cdots & \dfrac{\partial N_\aleph}{\partial x^1} \\ & & & & | & & \\ 0 & 0 & \cdots & 0 & | & \dfrac{\partial N_1}{\partial x^2} & \cdots & \dfrac{\partial N_\aleph}{\partial x^2} \\ & & & & | & & \\ 0 & 0 & \cdots & 0 & | & \dfrac{\partial N_1}{\partial x^2} & \cdots & \dfrac{\partial N_\aleph}{\partial x^2} \end{array} \right] ,$$

$$(5.35)$$

so that

$$\text{grad } \psi(\mathbf{x}, t_n) = [\nabla N] \left\{ \begin{array}{c} \dot{\tilde{A}}_n \\ \dot{\tilde{\psi}}_n \end{array} \right\} \qquad \in \mathbf{R}^{3 \times 1} . \qquad (5.36)$$

We extend the above matrix representation as follows. We express the matrix $[N] \in \mathbf{R}^{4 \times 4\aleph}$ in terms of two matrices $[N_A] \in \mathbf{R}^{3 \times 3\aleph}$ and $[N_\psi] \in \mathbf{R}^{1 \times \aleph}$,

$$[N] =: \left[\begin{array}{cc} N_A & 0 \\ 0 & N_\psi \end{array} \right] \qquad \in \mathbf{R}^{4\aleph \times 4\aleph} ,$$

where

$$[N_A] := \begin{bmatrix} N_1 & 0 & 0 & | & N_2 & 0 & 0 & | & \cdots & | & N_{\aleph} & 0 & 0 \\ 0 & N_1 & 0 & | & 0 & N_2 & 0 & | & \cdots & | & 0 & N_{\aleph} & 0 \\ 0 & 0 & N_1 & | & 0 & 0 & N_2 & | & \cdots & | & 0 & 0 & N_{\aleph} \end{bmatrix},$$

and

$$[N_\psi] := \begin{bmatrix} N_1 & N_2 & N_3 & \cdots & N_{\aleph} \end{bmatrix}.$$

The spatial derivatives of the potentials $\mathbf{A}$ and ψ can be expressed in terms of matrices $[N_A] \in \mathbf{R}^{3 \times 3\aleph}$ and $[N_\psi] \in \mathbf{R}^{1 \times \aleph}$ as follows.

Corresponding to the curl $\mathbf{A}$ we define a matrix $[\nabla \times N_A] \in \mathbf{R}^{3 \times 3\aleph}$ to be

$$[\nabla \times N_A] :=$$

$$\begin{bmatrix} 0 & -\dfrac{\partial N_1}{\partial x^3} & \dfrac{\partial N_1}{\partial x^2} & | & \cdots & | & 0 & -\dfrac{\partial N_{\aleph}}{\partial x^3} & \dfrac{\partial N_{\aleph}}{\partial x^2} \\[2mm] \dfrac{\partial N_1}{\partial x^3} & 0 & -\dfrac{\partial N_1}{\partial x^1} & | & \cdots & | & \dfrac{\partial N_{\aleph}}{\partial x^3} & 0 & -\dfrac{\partial N_{\aleph}}{\partial x^1} \\[2mm] -\dfrac{\partial N_1}{\partial x^2} & \dfrac{\partial N_1}{\partial x^1} & 0 & | & \cdots & | & -\dfrac{\partial N_{\aleph}}{\partial x^2} & \dfrac{\partial N_{\aleph}}{\partial x^1} & 0 \end{bmatrix},$$

(5.37)

so that

$$\operatorname{curl}\mathbf{A}(\mathbf{x}, t_n) \equiv \nabla \times \left\{ \begin{array}{c} A^1(\mathbf{x}, t_n) \\ A^2(\mathbf{x}, t_n) \\ A^3(\mathbf{x}, t_n) \end{array} \right\} = [\nabla \times N_A] \left\{ \tilde{\mathcal{A}}_n \right\} \qquad \in \mathbf{R}^{3 \times 1}. \qquad (5.38)$$

Corresponding to the div $\mathbf{A}$ we define a matrix $[\nabla \cdot N_A] \in \mathbf{R}^{1 \times 3\aleph}$ to be

$$[\nabla \cdot N_A] :=$$

$$\begin{bmatrix} \dfrac{\partial N_1}{\partial x^1} & \dfrac{\partial N_1}{\partial x^2} & \dfrac{\partial N_1}{\partial x^3} & | & \cdots & | & \dfrac{\partial N_{\aleph}}{\partial x^1} & \dfrac{\partial N_{\aleph}}{\partial x^2} & \dfrac{\partial N_{\aleph}}{\partial x^3} \end{bmatrix},$$

(5.39)

so that

$$\operatorname{div} \mathbf{A}(\mathbf{x}, t_n) \equiv \nabla \bullet \left\{ \begin{array}{c} A^1(\mathbf{x}, t_n) \\ A^2(\mathbf{x}, t_n) \\ A^3(\mathbf{x}, t_n) \end{array} \right\} = [\nabla \bullet N_A] \left\{ \dot{\tilde{\mathcal{A}}}_n \right\} \qquad \in \mathbf{R} \ . \qquad (5.40)$$

Corresponding to the grad ψ we define a matrix $[\nabla N_\psi] \in \mathbf{R}^{3 \times 3 \aleph}$ to be

$$[\nabla N_\psi] := \begin{bmatrix} \dfrac{\partial N_1}{\partial x^1} & \cdots & \dfrac{\partial N_\aleph}{\partial x^1} \\[2mm] \dfrac{\partial N_1}{\partial x^2} & \cdots & \dfrac{\partial N_\aleph}{\partial x^2} \\[2mm] \dfrac{\partial N_1}{\partial x^2} & \cdots & \dfrac{\partial N_\aleph}{\partial x^2} \end{bmatrix} \ ,$$

$$(5.41)$$

so that

$$\operatorname{grad} \psi(\mathbf{x}, t_n) = [\nabla N_\psi] \left\{ \dot{\tilde{\psi}}_n \right\} \qquad \in \mathbf{R}^{3 \times 1} \ . \qquad (5.42)$$

The matrix representation that uses $[N_A] \in \mathbf{R}^{3 \times 3 \aleph}$ and $[N_\psi] \in \mathbf{R}^{1 \times \aleph}$ is convenient to represent portions of the mass, damping, and stiffness matrices. See Chapter 6 for details. ∎

To calculate the voltage between two nodes in the finite element mesh, we must first establish a path between the 2 nodes. In the present formulation we choose to construct a path by using piecewise straight lines. Moreover, we choose to integrate the voltage element by element. Hence, we choose a straight line from a node to its adjoining node, and repeat this process till we reach the desired node. An example is shown in Figure 5.6, where we draw a line between the node i and node l via node j and node k. To calculate the voltage drop between node i and node l, we integrate the electric field $\mathbf{E}$ as in (5.3) in the 3 segments separately and then sum it up; the expression for $\mathbf{E}$ at any position $\mathbf{x}$ is given by (5.27). The present implementation does not allow a single straight line connecting node i to node l. Hence, voltage V_{il}

between node i and node l is given by

$$V_{il} := - \int_{node\ i}^{node\ j} \mathbf{E} \cdot \hat{\mathbf{t}}\ d\mathcal{L} - \int_{node\ j}^{node\ k} \mathbf{E} \cdot \hat{\mathbf{t}}\ d\mathcal{L} - \int_{node\ k}^{node\ l} \mathbf{E} \cdot \hat{\mathbf{t}}\ d\mathcal{L} , \qquad (5.43)$$

i.e., a sum of integrals over three straight line segments. For the above integral, we propose to construct the leads of the voltmeter that reads the voltage such that the voltage is only the integral of the scalar potential, i.e., electric field $\mathbf{E}$ in the above expression can be given by

$$- [\nabla \cdot N] \left\{ \begin{array}{c} \dot{\tilde{\mathcal{A}}}_n \\ \dot{\psi}_n \end{array} \right\} .$$

Note that for a voltage driven problem, the voltage is "known" quantity specified by the user as boundary conditions to the FE problem.

The current I at time $t = t_n$ is calculated as in (5.11), where the current density $\mathbf{J}_f$ is

$$\mathbf{J}_f((\mathbf{x}, t_n) = \sigma(\mathbf{x})\mathbf{E}(\mathbf{x}, t_n) = -\sigma(\mathbf{x})\,[\nabla \cdot N] \left\{ \begin{array}{c} \dot{\tilde{\mathcal{A}}}_n \\ \dot{\psi}_n \end{array} \right\} - \sigma(\mathbf{x})\,[N] \left\{ \begin{array}{c} \dot{\tilde{\mathcal{A}}}_n \\ 0 \end{array} \right\} . \qquad (5.44)$$

The electric power $\mathcal{P}_E$ at time $t = t_n$ is

$$\mathcal{P}_E(t_n) := \frac{1}{2} \left\{ \begin{array}{c} \ddot{\tilde{\mathcal{A}}}_n \\ \ddot{\psi}_n \end{array} \right\}^T \left[\begin{array}{cc} \mathcal{M}^{AA} & \mathcal{M}^{A\psi} \\ \mathcal{M}^{\psi A} & \mathcal{M}^{\psi\psi} \end{array} \right] \left\{ \begin{array}{c} \dot{\tilde{\mathcal{A}}}_n \\ \dot{\psi}_n \end{array} \right\} ,$$

where the solution vector and the "mass" matrix $\left[\mathcal{M} \right]$ are as defined in (4.53). The capacitance C is defined to be

$$C := \frac{\left\{ \begin{array}{c} \ddot{\tilde{\mathcal{A}}}_n \\ \ddot{\psi}_n \end{array} \right\}^T \left[\begin{array}{cc} \mathcal{M}^{AA} & \mathcal{M}^{A\psi} \\ \mathcal{M}^{\psi A} & \mathcal{M}^{\psi\psi} \end{array} \right] \left\{ \begin{array}{c} \dot{\tilde{\mathcal{A}}}_n \\ \dot{\psi}_n \end{array} \right\}}{\dfrac{dV}{dt} V} . \qquad (5.45)$$

node i

node j

node k

node l
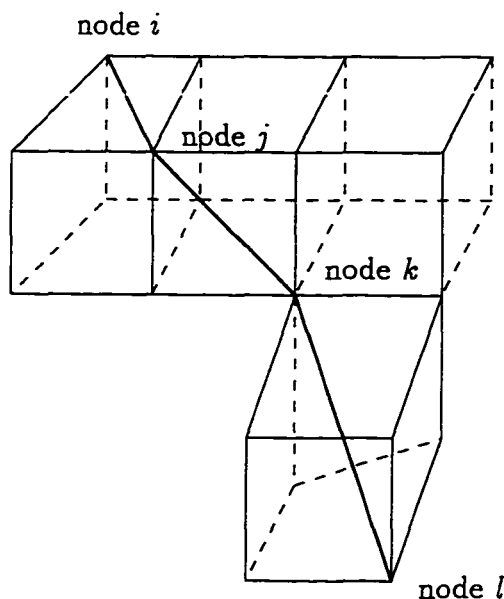
Figure 5.6. Path to calculate the voltage

The resistive power $\mathcal{P}_J$ at time $t = t_n$ is

$$\mathcal{P}_J(t_n) := \frac{1}{2} \left\{ \begin{array}{c} \dot{\tilde{A}}_n \\ \dot{\tilde{\psi}}_n \end{array} \right\}^T \left[\begin{array}{cc} \mathcal{B}^{AA} & \mathcal{B}^{A\psi} \\ \mathcal{B}^{\psi A} & \mathcal{B}^{\psi\psi} \end{array} \right] \left\{ \begin{array}{c} \dot{\tilde{A}}_n \\ \dot{\tilde{\psi}}_n \end{array} \right\} ,$$

where the solution vector and the "damping" matrix $\left[\mathcal{B} \right]$ are as defined in (4.53).
The resistance R is defined to be

$$R := \frac{\left\{ \begin{array}{c} \dot{\tilde{A}}_n \\ \dot{\tilde{\psi}}_n \end{array} \right\}^T \left[\begin{array}{cc} \mathcal{B}^{AA} & \mathcal{B}^{A\psi} \\ \mathcal{B}^{\psi A} & \mathcal{B}^{\psi\psi} \end{array} \right] \left\{ \begin{array}{c} \dot{\tilde{A}}_n \\ \dot{\tilde{\psi}}_n \end{array} \right\}}{I^2} . \qquad (5.46)$$

The magnetic power $\mathcal{P}_H$ at time $t = t_n$ is

$$\mathcal{P}_H(t_n) := \frac{1}{2} \left\{ \begin{array}{c} \ddot{\tilde{A}}_n \\ \ddot{\tilde{\psi}}_n \end{array} \right\}^T \left[\begin{array}{cc} \mathcal{K}^{AA} & 0 \\ 0 & 0 \end{array} \right] \left\{ \begin{array}{c} \dot{\tilde{A}}_n \\ \dot{\tilde{\psi}}_n \end{array} \right\} ,$$

where the solution vector and the "stiffness" matrix $\left[\mathcal{K}\right]$ are as defined in (4.53). The inductance L is defined to be

$$
L := \frac{\left\{ \begin{array}{c} \ddot{\tilde{A}}_n \\ \ddot{\tilde{\psi}}_n \end{array} \right\}^T \left[\begin{array}{cc} \mathcal{K}^{AA} & 0 \\ 0 & 0 \end{array} \right] \left\{ \begin{array}{c} \dot{\tilde{A}}_n \\ \dot{\tilde{\psi}}_n \end{array} \right\}}{\dfrac{dI}{dt} I} .
$$

(5.47)

5.3.3. Time Harmonic Problem

The lumped parameters involve both the real and imaginary parts of the solution. The electric field $\mathbf{E}$ is given by

$$
\bar{\mathbf{E}}(\mathbf{x}) = \mathbf{E}_r + i\mathbf{E}_i
$$

(5.48)

$$
= \omega \left[\nabla \cdot N\right] \left\{ \begin{array}{c} \tilde{A}_i \\ \tilde{\psi}_i \end{array} \right\} + \omega \left[N\right] \left\{ \begin{array}{c} \tilde{A}_i \\ 0 \end{array} \right\} - i\omega \left[\nabla \cdot N\right] \left\{ \begin{array}{c} \tilde{A}_r \\ \tilde{\psi}_r \end{array} \right\} - i\omega \left[N\right] \left\{ \begin{array}{c} \tilde{A}_r \\ 0 \end{array} \right\} ,
$$

and the magnetic field $\mathbf{B}$ is given by

$$
\bar{\mathbf{B}}(\mathbf{x}) = \mathbf{B}_r + i\mathbf{B}_i = \left[\nabla \times N\right] \left\{ \begin{array}{c} \tilde{A}_r \\ \tilde{\psi}_r \end{array} \right\} + i \left[\nabla \times N\right] \left\{ \begin{array}{c} \tilde{A}_i \\ \tilde{\psi}_i \end{array} \right\}
$$

(5.49)

The finite element solution vectors $\tilde{A}_r$, $\tilde{A}_i$, $\tilde{\psi}_r$, and $\tilde{\psi}_i$ are as defined in (4.67).

The voltage for the time harmonic problem is calculated similar to the transient problem presented in the previous section with expression (5.48) for the electric field. Hence, the voltage $\bar{V}$ has a real component V_r and an imaginary component V_i, i.e., $\bar{V} = V_r + iV_i$. The magnitude of the voltage is $|\bar{V}| = \sqrt{V_r^2 + V_i^2}$. The current $\bar{I}$ is calculated as in (5.11), where the current density $\bar{\mathbf{J}}_f$ is

$$
\mathbf{J}_f(\mathbf{x}) = \mathbf{J}_{f_r} + i\mathbf{J}_{f_i}
$$

(5.50)

$$
= \sigma(\mathbf{x})\omega \left[\nabla \cdot N\right] \left\{ \begin{array}{c} \tilde{A}_i \\ \tilde{\psi}_i \end{array} \right\} + \sigma(\mathbf{x})\omega \left[N\right] \left\{ \begin{array}{c} \tilde{A}_i \\ 0 \end{array} \right\}
$$

$$-\sigma(\mathbf{x})i\omega\left[\nabla\cdot N\right]\left\{\begin{array}{c}\tilde{\mathcal{A}}_r\\ \tilde{\psi}_r\end{array}\right\}-\sigma(\mathbf{x})i\omega\left[N\right]\left\{\begin{array}{c}\tilde{\mathcal{A}}_r\\ 0\end{array}\right\}\ .$$

The current $\bar{I}$ has a real component I_r and an imaginary component I_i, i.e., $\bar{I} = I_r + iI_i$. The magnitude of the current is $|\bar{I}| = \sqrt{I_r^2 + I_i^2}$.

The electric power $\mathcal{P}_E$ is

$$\mathcal{P}_E := \frac{1}{2}\omega^3\left\{\begin{array}{c}\tilde{\mathcal{A}}_r\\ \tilde{\psi}_r\end{array}\right\}^T\left[\begin{array}{cc}{}^r\mathcal{M}^{AA} & {}^r\mathcal{M}^{A\psi}\\ {}^r\mathcal{M}^{\psi A} & {}^r\mathcal{M}^{\psi\psi}\end{array}\right]\left\{\begin{array}{c}\tilde{\mathcal{A}}_r\\ \tilde{\psi}_r\end{array}\right\}+\frac{1}{2}\omega^3\left\{\begin{array}{c}\tilde{\mathcal{A}}_i\\ \tilde{\psi}_i\end{array}\right\}^T\left[\begin{array}{cc}{}^i\mathcal{M}^{AA} & {}^i\mathcal{M}^{A\psi}\\ {}^i\mathcal{M}^{\psi A} & {}^i\mathcal{M}^{\psi\psi}\end{array}\right]\left\{\begin{array}{c}\tilde{\mathcal{A}}_i\\ \tilde{\psi}_i\end{array}\right\}\ ,$$

where the solution vector and the "mass" matrix $\left[\mathcal{M}\right]$ are as defined in (4.67). The capacitance C is defined to be

$$\boxed{C := \frac{2\mathcal{P}_E}{\omega|\bar{V}|^2}}\ . \tag{5.51}$$

The resistive power $\mathcal{P}_J$ is

$$\mathcal{P}_J := \frac{1}{2}\omega^2\left\{\begin{array}{c}\tilde{\mathcal{A}}_r\\ \tilde{\psi}_r\end{array}\right\}^T\left[\begin{array}{cc}{}^r\mathcal{B}^{AA} & {}^r\mathcal{B}^{A\psi}\\ {}^r\mathcal{B}^{\psi A} & {}^r\mathcal{B}^{\psi\psi}\end{array}\right]\left\{\begin{array}{c}\tilde{\mathcal{A}}_r\\ \tilde{\psi}_r\end{array}\right\}+\frac{1}{2}\omega^2\left\{\begin{array}{c}\tilde{\mathcal{A}}_i\\ \tilde{\psi}_i\end{array}\right\}^T\left[\begin{array}{cc}{}^i\mathcal{B}^{AA} & {}^i\mathcal{B}^{A\psi}\\ {}^i\mathcal{B}^{\psi A} & {}^i\mathcal{B}^{\psi\psi}\end{array}\right]\left\{\begin{array}{c}\tilde{\mathcal{A}}_i\\ \tilde{\psi}_i\end{array}\right\}\ ,$$

where the solution vector and the "damping" matrix $\left[\mathcal{B}\right]$ are as defined in (4.67). The resistance R is defined to be

$$\boxed{R := \frac{2\mathcal{P}_J}{|\bar{I}|^2}}\ . \tag{5.52}$$

The magnetic power $\mathcal{P}_H$ is

$$\mathcal{P}_H := \frac{1}{2}\omega\left\{\begin{array}{c}\tilde{\mathcal{A}}_r\\ \tilde{\psi}_r\end{array}\right\}^T\left[\begin{array}{cc}{}^r\mathcal{K}^{AA} & 0\\ 0 & 0\end{array}\right]\left\{\begin{array}{c}\tilde{\mathcal{A}}_r\\ \tilde{\psi}_r\end{array}\right\}+\frac{1}{2}\omega\left\{\begin{array}{c}\tilde{\mathcal{A}}_i\\ \tilde{\psi}_i\end{array}\right\}^T\left[\begin{array}{cc}{}^i\mathcal{K}^{AA} & 0\\ 0 & 0\end{array}\right]\left\{\begin{array}{c}\tilde{\mathcal{A}}_i\\ \tilde{\psi}_i\end{array}\right\}\ ,$$

where the solution vector and the "stiffness" matrix $\left[\mathcal{B}\right]$ are as defined in (4.67). The inductance L is defined to be

$$\boxed{L := \frac{2\mathcal{P}_H}{\omega|\bar{I}|^2}}\ . \tag{5.53}$$

Note that similar expressions for the lumped parameters in (5.22), (5.23), and (5.24) can be be obtained in terms of the FE matrices and the solution vectors.

CHAPTER 6
SCALING: CHANGING THE UNIT SYSTEM

Maxwell equations (2.1) to (2.4) can be expressed in many unit systems. Maxwell equations in some of the commonly used unit systems are presented in Table 6.1. The choice of the unit system depends on the type of application. Our choice until now has been the SI system of units. In this chapter, we propose a new *generalized* unit system based on a multiple-scale technique.

In the past, much of the FE analysis was done by solving uncoupled electromagnetic problems, where the problems to determine the electric and the magnetic fields were solved separately. The decoupled formulation neglects the effects of eddy currents. The reader is forewarned that the multiple scale technique has little or no effect on the solution to decoupled electromagnetic problems. However, the increased operating frequencies (10^9 Hz and higher) demand a coupled solution. The coupled electromagnetic solution is an interaction between the electric current and the electric and the magnetic fields. For miniature devices at the frequency of interest, in the SI unit system, the numerical values of the terms related to the electric current dominates those that are related to the other physical processes. As the electric current is only present inside the conductor, the terms of the FE matrix inside the conductor are much larger than those outside the conductor. Hence, a large condition number[21] of the matrix in the ensuing FE solution. This leads to numerical ill-conditioning, and often makes analysis impossible (see e.g., Morweiser et al. [1994]). In the past, researchers have suggested the use of scaling. MacNeal

---

[21] Condition number is defined using the 2-norm, i.e., the ratio of the largest to the smallest singular (eigen) value.

[1989] suggest the use of a VOMS (Voltage Ohm Meters Second) unit system. However, unlike the proposed *generalized* unit system, the VOMS unit system cannot be modified to account for a change in the excitation frequency and the material properties. The use of the *generalized* unit system leads to an "optimal" condition number of the ensuing matrices.

The new multiple scale technique allows the flexibility to choose an effective interaction between the different physical processes. An appropriate choice of the scaling parameter reduces the condition number and allows an accurate numerical solution. The technique is based on the physics of the electromagnetic problem. We begin by transforming Maxwell equations to a *generalized* unit system where the electromagnetic quantities are non-dimensionalized: The quantities c, ϵ_0, and μ_0 in the constitutive laws and Maxwell equations are eliminated. The physical meaning and the numerical values of the electric and magnetic field quantities in the *generalized* unit system depends on two scaling parameters. A suitable choice of the scaling parameters shifts the focus of the problem away from the dominating effect of the conductors, and as a consequence, reduces the condition number and significantly improves the accuracy. The scaled Maxwell equations are more convenient for problem formulation and subsequent mathematical analysis.

The transformation between the rationalized CGS unit system to the *generalized* system for the electromagnetic quantities are represented as follows.

$$
\begin{aligned}
{}^{\text{GEN}}\mathbf{D} &= \beta_D\, {}^{\text{RCGS}}\mathbf{D}\;, & {}^{\text{GEN}}\mathbf{E} &= \beta_E\, {}^{\text{RCGS}}\mathbf{E}\;, & {}^{\text{GEN}}\mathbf{P} &= \beta_P\, {}^{\text{RCGS}}\mathbf{P}\;, \\
{}^{\text{GEN}}\mathbf{H} &= \beta_H\, {}^{\text{RCGS}}\mathbf{H}\;, & {}^{\text{GEN}}\mathbf{B} &= \beta_B\, {}^{\text{RCGS}}\mathbf{B}\;, & {}^{\text{GEN}}\mathbf{M} &= \beta_M\, {}^{\text{RCGS}}\mathbf{M}\;, \quad (6.1) \\
{}^{\text{GEN}}\mathbf{J}_f &= \beta_{J_f}\, {}^{\text{RCGS}}\mathbf{J}_f\;, & {}^{\text{GEN}}\rho_f &= \beta_\rho\, {}^{\text{RCGS}}\rho_f\;,
\end{aligned}
$$

and

$$
\begin{aligned}
{}^{\text{GEN}}x &= \beta_x\, {}^{\text{RCGS}}x\;, & {}^{\text{GEN}}t &= \beta_t\, {}^{\text{RCGS}}t\;, & {}^{\text{GEN}}mass &= \beta_m\, {}^{\text{RCGS}}mass\;, \\
& & {}^{\text{GEN}}\mathbf{F} &= \beta_F\, {}^{\text{RCGS}}\mathbf{F}\;,
\end{aligned}
$$

$$(6.2)$$

where the quantities with left superscript $RCGS$ are in the rationalized CGS system and the quantities with left superscript GEN are in the *generalized* system. The multiplicative factors $\beta_D, \cdots, \beta_P$ are arbitrary dimensional constants that are to be determined using dimensional analysis. However, the *twelve* multiplicative factors listed above are not independent; they are related to each other via Maxwell equations (gives four relations), constitutive laws (gives four relations), the force equation (gives two relations), and Newton's law (gives one relation). There are total of $4+4+2+1 = 11$ relations, and *twelve* unknowns. Hence, if we fix values for *two* out of the twelve multiplicative factors, the remaining *ten* multiplicative factors can be determined. The equations in the rationalized CGS units are as follows: The four Maxwell equations

$$\frac{1}{c}\frac{\partial \mathbf{B}}{\partial t} + \operatorname{curl} \mathbf{E} = \mathbf{0} \,,$$

$$\operatorname{div} \mathbf{D} - \rho_f = 0 \,,$$

$$-\frac{\partial \mathbf{D}}{\partial t} + \frac{1}{c}\operatorname{curl} \mathbf{H} - \frac{1}{c}\mathbf{J}_f = \mathbf{J}_a \,,$$

$$\operatorname{div} \mathbf{B} = 0 \,,$$

the two constitutive laws

$$\mathbf{D} = \mathbf{E} + \mathbf{P} \,,$$

$$\mathbf{H} = \mathbf{B} - \mathbf{M} \,,$$

the force equation

$$\mathbf{f} = \rho_f \mathbf{E} + \frac{1}{c}\mathbf{J}_f \times \mathbf{B} \,,$$

and the Newton's law

$$\mathbf{F} = m\ddot{\mathbf{x}} \,,$$

where all the quantities in the above equations are in the rationalized *CGS* unit system. The symbols $\mathbf{f}$, $\mathbf{F}$, m, and $\ddot{\mathbf{x}}$ represent the force per unit volume, force, mass and acceleration, respectively. The equations in the *generalized* unit system are similar, except the factor $\dfrac{1}{c}$ is omitted; see Table 6.1. The above equations are compared in terms of dimensions to the equivalent equations in the *generalized* unit system to obtain the following: Four relations from Maxwell equations, i.e.,

$$\frac{\beta_J}{\beta_H}\beta_z = \frac{1}{c} , \qquad \frac{\beta_D}{\beta_H}\frac{\beta_z}{\beta_t} = \frac{1}{c} ,$$
$$\frac{\beta_B}{\beta_B}\frac{\beta_z}{\beta_t} = \frac{1}{c} , \qquad \frac{\beta_P}{\beta_D}\beta_z = 1 , \tag{6.3}$$

four relations from the constitutive laws, i.e.,

$$\frac{\beta_B}{\beta_D} = 1 , \qquad \frac{\beta_P}{\beta_D} = 1 ,$$
$$\frac{\beta_B}{\beta_H} = 1 , \qquad \frac{\beta_M}{\beta_H} = 1 , \tag{6.4}$$

two relations from the force equation, i.e.,

$$\beta_\rho\beta_E = \frac{\beta_P}{\beta_x^3} , \qquad \beta_J\beta_B = \frac{1}{c}\frac{\beta_P}{\beta_x^3} , \tag{6.5}$$

and one relation from Newton's law, i.e.,

$$\beta_F = \frac{\beta_m\beta_x}{\beta_t^2} . \tag{6.6}$$

As mentioned above, there are twelve multiplicative factors and eleven relations. Hence, we can write the ten multiplicative factors in terms of the remaining two. The choice is arbitrary. However, the structure of Maxwell equations do not permit the choice of β_t independent of β_x. In this work we choose β_F and β_x to be independent, and express the remaining ten multiplicative factors in terms of β_F and β_x. The motivation for the choice is as follows. To preserve the physical meaning of force during the transformation, the choice of β_F to be independent proves to

be convenient. As the geometric dimensions of the device can be easily observed, the choice of β_z to be independent proves to be convenient when deciding the value of the scaling parameter. The *ten* remaining multiplicative factors are expressed in terms of two multiplicative factors β_P and β_z as follows:

$$
\beta_E \equiv \beta_D \equiv \beta_P \equiv \beta_B \equiv \beta_H \equiv \beta_M = \frac{\sqrt{\beta_P}}{\beta_z} ,
$$

$$
\beta_\rho = \frac{\sqrt{\beta_P}}{\beta_z^2} , \qquad \beta_J = \frac{1}{c} \frac{\sqrt{\beta_P}}{\beta_z^2} ,
$$

$$
\beta_t = c\, \beta_z , \qquad \beta_m = c^2\, \beta_P\, \beta_z .
$$

$$\tag{6.7}$$

The relations between the quantities in each of the unit systems are given in Table 6.2. The multiplicative factors for the material properties ϵ, μ and σ are obtained from the relations

$$
\mathbf{E} = \epsilon\, \mathbf{D} , \qquad \mathbf{H} = 1/\mu\, \mathbf{B} , \qquad \mathbf{J}_f = \sigma\, \mathbf{E} .
$$

Factors for the current I and the voltage V are obtained from the relations

$$
I = \int_{(\partial\Omega)_I} \mathbf{J}_f \cdot \hat{\mathbf{n}}\, d(\partial\Omega) , \qquad \text{and} \qquad V = \int_{\mathcal{L}} \mathbf{E} \cdot \hat{\mathbf{t}}\, d\mathcal{L} .
$$

The relations for the lumped parameters, i.e., the resistance R, the inductance L, and the capacitance C are obtained from

$$
R = \frac{V}{I} , \qquad L = \frac{V}{\frac{dI}{dt}} , \qquad C = \frac{\frac{dV}{dt}}{I} .
$$

These relations remain unchanged in the rationalized CGS and the *generalized* unit system.

To relate the numerical values of the quantities in the *generalized* system to that in the other systems we define the numerical (dimensionless) multiplicative

factor α_D to be

$$\beta_D =: \alpha_D \frac{Generalized\ units}{RCGS\ units} \ .$$

and similarly the remaining *eleven* multiplicative factors $\alpha_B, \cdots, \alpha_P$. We obtain the values for the remaining numerical multiplicative factors in terms of α_P and α_z, where

$$\beta_P =: \alpha_P \frac{Generalized\ dyne}{dyne} \ ,$$

and

$$\beta_z =: \alpha_z \frac{Generalized\ meter}{centimeter} \ .$$

Using α_P and α_z in (6.7), we obtain a conversion of the numerical values between the unit systems; the conversion between the most useful quantities are listed in Table 6.3 and Table 6.4. The conversion between the other unit systems has been previously discussed in Srinivas [1992]. The universal constants are the speed of light in vacuum $c = 2.99792458 \times 10^{10}\ cm/s$, the permittivity of free space $\epsilon_0 = 1/(36\pi) \times 10^{-9}\ SI\ units$, and the permeability of free space $\mu_0 = 4\pi \times 10^{-7}\ SI\ units$.

Remark 6.1. The scaling factor α_P does not scale the matrices in the FE solution. This is because the factor α_P appears with equal powers on all the terms involved in the Maxwell equations. The scaling factor α_P simply cancels out in the ensuing FE formulation. Hence, a simplification used in the formulation for capacitors is to fix

$$\boxed{\beta_P := 1 \ ,} \tag{6.8}$$

and obtain all the multiplicative factors in terms of β_z. Such a transformation preserves the physical meaning of the force in the *generalized* unit system to be same as in other systems. The relations between the quantities in each of the unit systems is given in Table 6.2 with $\beta_P = 1$.

The consequence of (6.8) is

$$\boxed{\alpha_{_F} = 1 \; ,}$$

(6.9)

i.e., 1 *dyne* := 1 ^{GBN}*dyne*. To obtain the numerical scaling factors for the other quantities in terms of $\alpha_{_z}$, set $\alpha_{_F} = 1$ in Table 6.3 and Table 6.4. ∎

6.1. Scaling the Matrix Equations

In the preceding sections, the final matrix equations obtained via the finite element formulation are linear equations of the form

$$A\,d = b \, ,$$

(6.10)

where $A \in \mathbf{R}^{n \times n}$ is a non-singular matrix, $b \in \mathbf{R}^{n \times 1}$ is the right-hand side, and $d \in \mathbf{R}^{n \times 1}$ is the solution. The condition number of the matrix A decides the numerical accuracy of the solution b. In this section we examine the effects of the condition number on the solution for the method of "Gauss Elimination." We also present a method of "scaling" or "pre-conditioning" to alleviate the effects of poor condition numbers. Though we choose the method of "Gauss Elimination" to demonstrate the effects of scaling, similar comments are applicable to other solution methods.

To begin with, we describe, in brief, the effects of scaling on the solution to a system of linear equations. We present a procedure to scale the matrix equations from a numerical standpoint. Lack of a method to choose the scaling coefficients is its major shortcoming. We then present a procedure to scale the matrix equations by changing the unit system used in Maxwell equations, i.e., by changing $\beta_{_z}$. Such an approach is motivated by the "physics" of the problem, and hence, proves to be convenient.

Table 6.1. Maxwell equations in the different unit systems. The symbol **f** represents the electromagnetic force per unit volume, i.e., the electromagnetic force density

Unit System	**D, H**	Maxwell equations
CGS esu	$\mathbf{D} = \mathbf{E} + 4\pi\mathbf{P}$ $\mathbf{H} = c^2\mathbf{B} - 4\pi\mathbf{M}$	$\operatorname{div}\mathbf{D} = 4\pi\rho_f,\quad \operatorname{curl}\mathbf{H} = 4\pi\mathbf{J}_f + \dfrac{\partial\mathbf{D}}{\partial t}$ $\operatorname{div}\mathbf{B} = 0,\qquad \operatorname{curl}\mathbf{E} + \dfrac{\partial\mathbf{B}}{\partial t} = 0$
CGS emu	$\mathbf{D} = \dfrac{1}{c^2}\mathbf{E} + 4\pi\mathbf{P}$ $\mathbf{H} = \mathbf{B} - 4\pi\mathbf{M}$	$\operatorname{div}\mathbf{D} = 4\pi\rho_f,\quad \operatorname{curl}\mathbf{H} = 4\pi\mathbf{J}_f + \dfrac{\partial\mathbf{D}}{\partial t}$ $\operatorname{div}\mathbf{B} = 0,\qquad \operatorname{curl}\mathbf{E} + \dfrac{\partial\mathbf{B}}{\partial t} = 0$
CGS Gaussian (unrationalized)	$\mathbf{D} = \mathbf{E} + 4\pi\mathbf{P}$ $\mathbf{H} = \mathbf{B} - 4\pi\mathbf{M}$	$\operatorname{div}\mathbf{D} = 4\pi\rho_f,\quad \operatorname{curl}\mathbf{H} = \dfrac{4\pi}{c}\mathbf{J}_f + \dfrac{1}{c}\dfrac{\partial\mathbf{D}}{\partial t}$ $\operatorname{div}\mathbf{B} = 0,\qquad \operatorname{curl}\mathbf{E} + \dfrac{1}{c}\dfrac{\partial\mathbf{B}}{\partial t} = 0$ $\mathbf{f} = \rho_f\mathbf{E} + \dfrac{1}{c}\mathbf{J}_f \times \mathbf{B}$
CGS Heaviside-Lorentz (rationalized)	$\mathbf{D} = \mathbf{E} + \mathbf{P}$ $\mathbf{H} = \mathbf{B} - \mathbf{M}$	$\operatorname{div}\mathbf{D} = \rho_f,\quad \operatorname{curl}\mathbf{H} = \dfrac{1}{c}\mathbf{J}_f + \dfrac{1}{c}\dfrac{\partial\mathbf{D}}{\partial t}$ $\operatorname{div}\mathbf{B} = 0,\qquad \operatorname{curl}\mathbf{E} + \dfrac{1}{c}\dfrac{\partial\mathbf{B}}{\partial t} = 0$ $\mathbf{f} = \rho_f\mathbf{E} + \dfrac{1}{c}\mathbf{J}_f \times \mathbf{B}$
SI system	$\mathbf{D} = \epsilon_0\mathbf{E} + \mathbf{P}$ $\mathbf{H} = \dfrac{1}{\mu_0}\mathbf{B} - \mathbf{M}$	$\operatorname{div}\mathbf{D} = \rho_f,\quad \operatorname{curl}\mathbf{H} = \mathbf{J}_f + \dfrac{\partial\mathbf{D}}{\partial t}$ $\operatorname{div}\mathbf{B} = 0,\qquad \operatorname{curl}\mathbf{E} + \dfrac{\partial\mathbf{B}}{\partial t} = 0$ $\mathbf{f} = \rho_f\mathbf{E} + \mathbf{J}_f \times \mathbf{B}$
Generalized system	$\mathbf{D} = \mathbf{E} + \mathbf{P}$ $\mathbf{H} = \mathbf{B} - \mathbf{M}$	$\operatorname{div}\mathbf{D} = \rho_f,\quad \operatorname{curl}\mathbf{H} = \mathbf{J}_f + \dfrac{\partial\mathbf{D}}{\partial t}$ $\operatorname{div}\mathbf{B} = 0,\qquad \operatorname{curl}\mathbf{E} + \dfrac{\partial\mathbf{B}}{\partial t} = 0$ $\mathbf{f} = \rho_f\mathbf{E} + \mathbf{J}_f \times \mathbf{B}$

Table 6.2. Conversion of symbols in equations.

Rationalized *CGS*	Gaussian *CGS*	*SI*	*Generalized*
$^{\text{RCGS}}q$	$^{\text{CGS}}q\sqrt{4\pi}$	$^{\text{SI}}q/\sqrt{\epsilon_0}$	$1/(\beta_z\sqrt{\beta_F})\ ^{\text{GEN}}q$
$^{\text{RCGS}}\mathbf{D}$	$^{\text{CGS}}\mathbf{D}/\sqrt{4\pi}$	$\sqrt{1/\epsilon_0}\,^{\text{SI}}\mathbf{D}$	$\beta_z/\sqrt{\beta_F}\ ^{\text{GEN}}\mathbf{D}$
$^{\text{RCGS}}\mathbf{E}$	$^{\text{CGS}}\mathbf{E}/\sqrt{4\pi}$	$\sqrt{\epsilon_0}\,^{\text{SI}}\mathbf{E}$	$\beta_z/\sqrt{\beta_F}\ ^{\text{GEN}}\mathbf{E}$
$^{\text{RCGS}}\mathbf{J}_f$	$^{\text{CGS}}\mathbf{J}_f\sqrt{4\pi}$	$^{\text{SI}}\mathbf{J}_f/\sqrt{\epsilon_0}$	$c\,\beta_z^2/\sqrt{\beta_F}\ ^{\text{GEN}}\mathbf{J}_f$
$^{\text{RCGS}}\rho_f$	$^{\text{CGS}}\rho_f\sqrt{4\pi}$	$^{\text{SI}}\rho_f/\sqrt{\epsilon_0}$	$\beta_z^2/\sqrt{\beta_F}\ ^{\text{GEN}}\rho_f$
$^{\text{RCGS}}\mathbf{H}$	$^{\text{CGS}}\mathbf{H}/\sqrt{4\pi}$	$\sqrt{\mu_0}\,^{\text{SI}}\mathbf{H}$	$\beta_z/\sqrt{\beta_F}\ ^{\text{GEN}}\mathbf{H}$
$^{\text{RCGS}}\mathbf{B}$	$^{\text{CGS}}\mathbf{B}/\sqrt{4\pi}$	$\sqrt{1/\mu_0}\,^{\text{SI}}\mathbf{B}$	$\beta_z/\sqrt{\beta_F}\ ^{\text{GEN}}\mathbf{B}$
$^{\text{RCGS}}\mathbf{M}$	$^{\text{CGS}}\mathbf{M}\sqrt{4\pi}$	$\sqrt{\mu_0}\,^{\text{SI}}\mathbf{M}$	$\beta_z/\sqrt{\beta_F}\ ^{\text{GEN}}\mathbf{M}$
$^{\text{RCGS}}\mathbf{P}$	$^{\text{CGS}}\mathbf{P}\sqrt{4\pi}$	$^{\text{SI}}\mathbf{P}/\sqrt{\epsilon_0}$	$\beta_z/\sqrt{\beta_F}\ ^{\text{GEN}}\mathbf{P}$
$^{\text{RCGS}}x$	$^{\text{CGS}}x$	$^{\text{SI}}x$	$^{\text{GEN}}x/\beta_z$
$^{\text{RCGS}}t$	$^{\text{CGS}}t$	$^{\text{SI}}t$	$^{\text{GEN}}t/(c\beta_z)$
$^{\text{RCGS}}mass$	$^{\text{CGS}}mass$	$^{\text{SI}}mass$	$^{\text{GEN}}mass/(c^2\beta_z\beta_F)$
$^{\text{RCGS}}F$	$^{\text{CGS}}F$	$^{\text{SI}}F$	$^{\text{GEN}}F/\sqrt{\beta_F}$
$^{\text{RCGS}}\epsilon$	$^{\text{CGS}}\epsilon$	$^{\text{SI}}\epsilon/\epsilon_0$	$^{\text{GEN}}\epsilon$
$^{\text{RCGS}}\mu$	$^{\text{CGS}}\mu$	$^{\text{SI}}\mu/\mu_0$	$^{\text{GEN}}\mu$
$^{\text{RCGS}}\sigma$	$4\pi\ ^{\text{CGS}}\sigma$	$^{\text{SI}}\sigma/\epsilon_0$	$c\,\beta_z\ ^{\text{GEN}}\sigma$
$^{\text{RCGS}}I$	$\sqrt{4\pi}\ ^{\text{CGS}}I$	$^{\text{SI}}I/\sqrt{\epsilon_0}$	$c/\sqrt{\beta_F}\ ^{\text{GEN}}I$
$^{\text{RCGS}}V$	$^{\text{CGS}}V/\sqrt{4\pi}$	$\sqrt{\epsilon_0}\,^{\text{SI}}V$	$1/\sqrt{\beta_F}\,^{\text{GEN}}V$
$^{\text{RCGS}}C$	$4\pi\ ^{\text{CGS}}C$	$^{\text{SI}}C/\epsilon_0$	$^{\text{GEN}}C/\beta_z$
$^{\text{RCGS}}L$	$^{\text{CGS}}L/(4\pi)$	$\epsilon_0\ ^{\text{SI}}L$	$^{\text{GEN}}L/(c^2\beta_z)$
$^{\text{RCGS}}R$	$^{\text{CGS}}R/(4\pi)$	$\epsilon_0\ ^{\text{SI}}R$	$^{\text{GEN}}R/c$

Table 6.3. Conversion of numerical values.

	Rationalized CGS	Gaussian CGS	SI	Generalized
q	1 $statcoulomb$	$\dfrac{1}{\sqrt{4\pi}}$ $statcoulomb$	$\dfrac{10^{-9}}{3\sqrt{4\pi}}$ $coulomb$	$\alpha_z\sqrt{\alpha_F}$ $^{\text{GEN}}coulomb$
$\mathbf{D}$	1 $\dfrac{statvolt}{cm}$	$\sqrt{4\pi}$ $\dfrac{statvolt}{cm}$	$\dfrac{10^{-5}}{(3\sqrt{4\pi})}$ $\dfrac{coulombs}{m^2}$	$\dfrac{\sqrt{\alpha_F}}{\alpha_z}$ $\dfrac{^{\text{GEN}}volt}{^{\text{GEN}}m}$
$\mathbf{E}$	1 $\dfrac{statvolt}{cm}$	$\sqrt{4\pi}$ $\dfrac{statvolt}{cm}$	$3\times10^4\sqrt{4\pi}$ $\dfrac{volts}{m}$	$\dfrac{\sqrt{\alpha_F}}{\alpha_z}$ $\dfrac{^{\text{GEN}}volt}{^{\text{GEN}}m}$
$\mathbf{J}_f$	1 $\dfrac{statampere}{(cm)^2}$	$\dfrac{1}{\sqrt{4\pi}}$ $\dfrac{statampere}{(cm)^2}$	$\dfrac{1}{3\sqrt{4\pi}}\times10^{-5}$ $\dfrac{ampere}{m^2}$	$\dfrac{\sqrt{\alpha_F}}{3\alpha_z^2\times10^{10}}$ $\dfrac{^{\text{GEN}}ampere}{(^{\text{GEN}}m)^2}$
ρ_f	1 $\dfrac{statcoulomb}{(cm)^3}$	$\dfrac{\sqrt{\alpha_F}}{\sqrt{4\pi}}$ $\dfrac{statcoulomb}{(cm)^3}$	$\dfrac{1}{3\sqrt{4\pi}}\times10^{-3}$ $\dfrac{coulomb}{m^3}$	$\dfrac{\sqrt{\alpha_F}}{\alpha_z^2}$ $\dfrac{^{\text{GEN}}coulomb}{(^{\text{GEN}}m)^3}$
$\mathbf{H}$	1 $oersted$	$\sqrt{4\pi}$ $oersted$	$\dfrac{10^3}{\sqrt{4\pi}}$ $\dfrac{ampere-turns}{m}$	$\dfrac{\sqrt{\alpha_F}}{\alpha_z}$ $^{\text{GEN}}oersted$
$\mathbf{B}$	1 $gauss$	$\sqrt{4\pi}$ $gauss$	$\sqrt{4\pi}10^{-4}$ $tesla$	$\dfrac{\sqrt{\alpha_F}}{\alpha_z}$ $^{\text{GEN}}gauss$
$\mathbf{M}$	1 $gauss$	$\dfrac{1}{\sqrt{4\pi}}$ $gauss$	$\dfrac{10^3}{\sqrt{4\pi}}$ $\dfrac{amperes}{m}$	$\dfrac{\sqrt{\alpha_F}}{\alpha_z}$ $^{\text{GEN}}gauss$
$\mathbf{P}$	1 $\dfrac{statcoulomb}{(cm)^2}$	$\dfrac{1}{\sqrt{4\pi}}$ $\dfrac{statcoulomb}{(cm)^2}$	$\dfrac{10^{-5}}{3\sqrt{4\pi}}$ $\dfrac{coulomb}{m^2}$	$\dfrac{\sqrt{\alpha_F}}{\alpha_z}$ $\dfrac{^{\text{GEN}}coulomb}{(^{\text{GEN}}m)^2}$
x	1 cm	1 cm	10^{-2} m	α_z $^{\text{GEN}}m$
t	1 s	1 s	1 s	$3\alpha_z\times10^{10}$ $^{\text{GEN}}s$
$mass$	1 gm	1 gm	10^{-3} kg	$9\alpha_z\alpha_F\times10^{20}$ $^{\text{GEN}}gm$
F	1 $dyne$	1 $dyne$	10^{-5} $newton$	α_F $^{\text{GEN}}dyne$
ϵ	1 $RCGS\ units$	1 $CGS\ units$	$\dfrac{1}{4\pi\times9\times10^9}$ $SI\ units$	1 $^{\text{GEN}}units$
μ	1 $RCGS\ units$	1 $CGS\ units$	$4\pi\times10^{-7}$ $SI\ units$	1 $^{\text{GEN}}units$
σ	1 $RCGS\ units$	$\dfrac{1}{4\pi}$ $CGS\ units$	$\dfrac{1}{4\pi\times9\times10^9}$ $SI\ units$	$\dfrac{1}{3\alpha_z\times10^{10}}$ $^{\text{GEN}}units$

Table 6.4. Conversion of numerical values (continued).

	Rationalized CGS	Gaussian CGS	SI	$Generalized$
I	$1 \quad statampere$	$\dfrac{1}{\sqrt{4\pi}}\ statampere$	$\dfrac{10^{-9}}{3\sqrt{4\pi}}\ ampere$	$\dfrac{\sqrt{\alpha_F}}{3\times 10^{10}}\ {}^{\text{GEN}}ampere$
V	$1 \quad statvolt$	$\sqrt{4\pi}\quad statvolt$	$3\sqrt{4\pi}\times 10^2 \quad volt$	$\sqrt{\alpha_F}\qquad {}^{\text{GEN}}volt$
C	$1 \quad statfarad$	$\dfrac{1}{4\pi}\quad statfarad$	$\dfrac{10^{-11}}{9(4\pi)}\quad farad$	$\alpha_z \qquad {}^{\text{GEN}}farad$
L	$1 \quad stathenry$	$4\pi \quad stathenry$	$9(4\pi)\times 10^{11} henry$	$9\alpha_z \times 10^{20}\ {}^{\text{GEN}}henry$
R	$1 \quad statohm$	$4\pi \quad statohm$	$9(4\pi)\times 10^{11}\quad ohm$	$3\times 10^{10} \qquad {}^{\text{GEN}}ohm$

6.1.1. Ill-conditioned Matrices in Electromagnetics

The condition number of the finite element matrices are related to the following:

1. **Geometric dimensions** of the elements that comprise the finite element model is critical to the condition number of the matrices. The main reasons for *geometric* ill-conditioning is poor aspect ratio,[22] e.g., extremely thin electrodes.

2. Large change in **material properties**, in particular conductivity, contributes more towards ill-conditioning than geometric ill-conditioning. For example, in passive electromagnetic devices a mix between conductors and non-conductors leads to a jump in conductivity, and hence, ill-conditioning.

---

[22] Aspect ratio is defined as ratio between the largest edge and the smallest edge of an element.

A conventional method to alleviate ill-conditioning is to use a Coulomb gauge, i.e., impose a constraint $\operatorname{div} \mathbf{A} = 0$ in the volume Ω. However, the penalty term due to the Coulomb gauge could over constrain the shape functions, and thereby result in a less accurate solution. Our approach of changing the unit system, and thereby scaling the matrices, try to improve the condition number of the matrices even in the ungauged problem. However, this method of scaling is also applicable to a solution with Coulomb or algebraic gauge.

6.1.2. Accuracy and Error Estimation

To assess the roundoff errors that occur in the solution to the matrix equation $A\, d = b$, we consider an "ideal" situation. We neglect the roundoff errors in the entire solution process, except while storing the matrices.[23] Let $fl(A) := A + E$ be the non-singular matrix that is stored in the computer. The matrix $E \in \mathbf{R}^{n \times n}$ is the roundoff error. The solution to the matrix equation

$$(A + E)\, \hat{d} = b\,,$$

is given by $\hat{d} \in \mathbf{R}^{n \times n}$. The relative error (accuracy) of the solution is related to the difference between the computed solution $\hat{d}$ and the exact solution d, and is given by

$$\frac{\|\, \hat{d} - d\, \|}{\|\, d\, \|}\,.$$

See Remark 6.2 for the definition of the vector norms used in this document.

Remark 6.2. The most popular norms used in numerical analysis are *Holder* or *p-norms* and are defined by

$$\|\, d\, \|_p := \left(|d^1|^p + |d^2|^p + \cdots + |d^n|^p \right)^{1/p}\,,$$

---

[23] The error $e \in \mathbf{R}^{n \times 1}$ in storing the vector b is neglected in the arguments presented below. This simplifies the explanation.

where vector $d := \{d^1, d^2, \cdots, d^n\} \in \mathbf{R}^{n \times 1}$. Some of the typical *p-norms* are as follows.

$$\| d \|_1 := \left(|d^1| + |d^2| + \cdots + |d^n| \right) ,$$

$$\| d \|_2 := \left(|d^1|^2 + |d^2|^2 + \cdots + |d^n|^2 \right)^{1/2} = (d^T d)^{1/2} ,$$

$$\| d \|_\infty := \max_i |d^i| .$$

∎

Remark 6.3. Similar to the vector norms defined in Remark 6.2, we define the *p-norms* for a matrix $A \in \mathbf{R}^{m \times n}$ to be

$$\| A \|_p := \sup_{d \neq 0} \frac{\| A d \|_p}{\| d \|_p} ,$$

where $d \in \mathbf{R}^{n \times 1}$. Some of the typical *p-norms* are as follows.

$$\| A \|_1 := \max_j \sum_{i=1}^m |A_{ij}| ,$$

$$\| A \|_\infty := \max_i \sum_{j=1}^n |A_{ij}| ,$$

where $A := [A_{ij}]$, i.e., A_{ij} are is coefficient of the matrix A at row i and column j. The condition number $\kappa_p(A)$ of the matrix A is defined to be

$$\kappa_p(A) := \| A \|_p \| A^{-1} \|_p ,$$

where $\| A^{-1} \|_p$ is the p-norm of A^{-1}. For the 2-norm it can be shown that

$$\kappa_2(A) := \| A \|_2 \| A^{-1} \|_2 = \frac{\sigma_{max}}{\sigma_{min}} ,$$

where σ_{max} and σ_{min} are the maximum and the minimum singular values of the matrix A, respectively. ∎

The error in the Gauss elimination procedure is related to the condition number of the matrix A as follows.

$$\frac{\parallel \hat{d} - d \parallel_p}{\parallel d \parallel_p} \leq \frac{\parallel E \parallel_p}{\parallel A \parallel_p} \kappa_p(A) \, ,$$

where matrix E is the roundoff error. However, if we use the ∞-norm we have the error to be

$$\frac{\parallel \hat{d} - d \parallel_\infty}{\parallel d \parallel_\infty} \leq \tau^{-\iota} \kappa_\infty(A) \, ,$$

where τ is the machine base used by the computer, and ι is the number of digits of floating point precision;[24] see Golub and van Loan [1987] for details. Such an approximation is possible because we assume the roundoff error in storing the matrix A is given by

$$\frac{\parallel E \parallel_\infty}{\parallel A \parallel_\infty} \leq \tau^{-\iota} \, .$$

Infinity norm is used in this section because of the relative ease in calculating it.

Suppose the condition number $\kappa_\infty(A) \approx \tau^\varpi$ then the roundoff error can be approximated to be

$$\boxed{\frac{\parallel \hat{d} - d \parallel_\infty}{\parallel d \parallel_\infty} \leq \tau^{\varpi - \iota} \, .} \tag{6.11}$$

One of the methods to decrease the roundoff error is to "pre-process" matrix A before solution. The idea is to scale the matrix A by pre and post multiplying it by two other matrices, and thereby reduce the condition number. One of the simple methods to scale is to use two diagonal matrices D_1 and D_2 as follows.

$$D_1 := diag(\tau^{l_1}, \cdots, \tau^{l_n}) \in \mathbf{R}^{n \times n}$$

$$D_1 := diag(\tau^{r_1}, \cdots, \tau^{r_n}) \in \mathbf{R}^{n \times n}$$

---

[24] For example, a DEC 5000 computer has a 16 digit accuracy in the decimal system when calculating using double precision; i.e., $\tau = 10$ and $\iota = 16$.

It is hoped that by choosing values of the integers $l_1, \cdots, l_n$ and $r_1, \cdots, r_n$ we can obtain a better conditioned matrix $D_1^{-1} A D_2$. The solution to the linear system of equations $Ad = b$ can be found by solving the scaled system $D_1^{-1} A D_2 y = b$. We do the following

$$
\begin{aligned}
D_1^{-1} A D_2 &= LU && \text{(LU factorization)} \\
Lw &= D_1^{-1} b && \text{(forward elimination)} \\
Uy &= w && \text{(back elimination)} \\
d &= D_2 y \ .
\end{aligned}
$$

Matrix D_1 scales the equations in matrix A, the matrix D_2 the unknowns d. Hence, if $\kappa_\infty(D_1^{-1} A D_2)$ can be made considerably smaller than $\kappa_\infty(A)$, then we expect the computed solution $\hat{d}$ to be closer to the "exact" solution d. However, there is no convenient method to construct the matrices D_1 and D_2. The absence of a convenient procedure to construct D_1 and D_2 motivates changing the unit system, which is described in the next section.

6.1.3. Changing Unit Systems

Changing the unit system effects the condition number of the matrix in the resulting linear system of equations, thereby changing the accuracy of the solution. We change the unit system used to formulate the electromagnetic problem from the *SI* units to the *generalized* units using Table 6.2. The *generalized* unit system allows us to choose a value for β_z (or α_z) thereby changing the condition number of the matrices. Note that the scaling factor α_F does not scale the matrices in the FE solution, hence, it has been set to one, i.e., $\alpha_F = 1$. We study this effect on static, transient and time harmonic problems. Numerical experiments in Chapter 8 demonstrates the efficacy of scaling.

6.1.3.1. Static problem

Change in the unit system does not significantly improve the condition number of the matrices in equation (4.23)

$$\begin{bmatrix} K^{AA} & 0 \\ 0 & M^{\psi\psi} \end{bmatrix} \begin{Bmatrix} \widetilde{A}_0 \\ \widetilde{\dot{\psi}}_0 \end{Bmatrix} = \begin{Bmatrix} F^{A_0} \\ F^{\psi_0} \end{Bmatrix} ,$$

of the static problem. This is because the matrix equation

$$\begin{bmatrix} M^{\psi\psi} \end{bmatrix} \begin{Bmatrix} \widetilde{\dot{\psi}}_0 \end{Bmatrix} = \begin{Bmatrix} F^{\psi_0} \end{Bmatrix} , \tag{6.12}$$

for the electrostatic problem is not coupled to the matrix equation

$$\begin{bmatrix} K^{AA} \end{bmatrix} \begin{Bmatrix} \widetilde{A}_0 \end{Bmatrix} = \begin{Bmatrix} F^{A_0} \end{Bmatrix} , \tag{6.13}$$

for the magnetostatic problem.

To explain the effects of the change in the unit system on the matrices we define the mass and stiffness matrices in terms of the notation introduced in Remark 5.1. The "mass" matrix $\begin{bmatrix} M^{\psi\psi} \end{bmatrix} \in R^{(n_{\psi_0} \times n_{\psi_0})}$ has n_{ψ_0} rows and n_{ψ_0} columns. However, before imposing the essential boundary condition, i.e., before removing the appropriate rows and columns, the size of the matrix is $\aleph$ rows and $\aleph$ columns ($\aleph$ is the number of nodes in the finite element mesh). In the explanation presented below, we work with the matrix $\begin{bmatrix} \mathcal{M}^{\psi\psi} \end{bmatrix} \in R^{(\aleph \times \aleph)}$. If we remove the appropriate rows and columns in $\begin{bmatrix} \mathcal{M}^{\psi\psi} \end{bmatrix}$ then we obtain the matrix $\begin{bmatrix} M^{\psi\psi} \end{bmatrix}$. Using the notations used in Remark 5.1 we express $\begin{bmatrix} \mathcal{M}^{\psi\psi} \end{bmatrix} \in$ as follows.

$$\begin{bmatrix} \mathcal{M}^{\psi\psi} \end{bmatrix} = \int_{\Omega \backslash \Omega_{cond}} \epsilon(\mathbf{x}) \left[\nabla \cdot N_\psi \right]^T \left[\nabla \cdot N_\psi \right] d\Omega ,$$

where each element in $\begin{bmatrix} \mathcal{M}^{\psi\psi} \end{bmatrix}$ is an integral of the corresponding element in the matrix $\left[\nabla \cdot N_\psi \right]^T \left[\nabla \cdot N_\psi \right]$.

Similarly, to explain the effects on the "stiffness" matrix, consider the matrix $\left[\mathcal{K}^{AA} \right] \in R^{(3\aleph \times 3\aleph)}$; if we remove the appropriate rows and columns in $\left[\mathcal{K}^{AA} \right]$ then we obtain the matrix $\left[K^{AA} \right] \in R^{(3n_{A_0} \times 3n_{A_0})}$. Using the notations used in Remark 5.1 we express $\left[\mathcal{K}^{AA} \right] \in$ as follows.

$$\left[\mathcal{K}^{AA} \right] = \int_{\Omega} \frac{1}{\mu(\mathbf{x})} \left[\nabla \times N_A \right]^T \left[\nabla \times N_A \right] \, d\Omega \, ,$$

where each element in $\left[\mathcal{K}^{AA} \right]$ is an integral of the corresponding element in the matrix $\left[\nabla \times N_A \right]^T \left[\nabla \times N_A \right]$.

Following the methodology presented in the previous sections we can derive the expression for the matrices using the *generalized* unit system. Here, we only present the final expression for the matrix; the details are left to the reader.[25] Using the notations used in Remark 5.1 we express $\left[{}^{\text{GEN}}\mathcal{M}^{\psi\psi} \right]$ as follows.

$$\left[{}^{\text{GEN}}\mathcal{M}^{\psi\psi} \right] = \int_{{}^{\text{GEN}}\Omega \backslash \Omega_{cond}} {}^{\text{GEN}}\epsilon(\mathbf{x}) \left[{}^{\text{GEN}}\nabla \cdot N_\psi \right]^T \left[{}^{\text{GEN}}\nabla \cdot N_\psi \right] \, d\Omega \, ,$$

where each element in $\left[\mathcal{M}^{\psi\psi} \right]$ is an integral of the corresponding element in the matrix $\left[{}^{\text{GEN}}\nabla \cdot N_\psi \right]^T \left[{}^{\text{GEN}}\nabla \cdot N_\psi \right]$. The spatial dimensions and the spatial derivatives are now in terms of the *generalized* unit system. Similarly, we express $\left[{}^{\text{GEN}}\mathcal{K}^{AA} \right]$ as follows.

$$\left[{}^{\text{GEN}}\mathcal{K}^{AA} \right] = \int_{{}^{\text{GEN}}\Omega} \frac{1}{{}^{\text{GEN}}\mu(\mathbf{x})} \left[{}^{\text{GEN}}\nabla \times N_A \right]^T \left[{}^{\text{GEN}}\nabla \times N_A \right] \, d\Omega \, ,$$

Changing the unit system changes the numerical values of the elements of the above matrices. The numerical values of the mass and stiffness matrices in the *SI* and the *generalized* unit system are related as follows.

$$\left[{}^{\text{SI}}\mathcal{M}^{\psi\psi} \right] = \left(\epsilon_0 \alpha_x \times 10^2 \right) \left[{}^{\text{GEN}}\mathcal{M}^{\psi\psi} \right] \quad \text{and} \quad \left[{}^{\text{SI}}\mathcal{K}^{AA} \right] = \left(\frac{\alpha_x}{\mu_0} \times 10^2 \right) \left[{}^{\text{GEN}}\mathcal{K}^{AA} \right] \, .$$

---

[25] The quantities in the *generalized* system of units are indicated by the left superscript ${}^{\text{GEN}}$, i.e., ${}^{\text{GEN}}\mathbf{D}$ is the quantity $\mathbf{D}$ expressed in *generalized* units. A missing left superscript indicates a quantity in the *SI* system.

The above relations also holds for the matrices $\left[M^{\psi\psi} \right]$ and $\left[K^{AA} \right]$ i.e.,

$$\left[{}^{\text{SI}} M^{\psi\psi} \right] = \left(\epsilon_0 \alpha_z \times 10^2 \right) \left[{}^{\text{GEN}} M^{\psi\psi} \right] \quad \text{and} \quad \left[{}^{\text{SI}} K^{AA} \right] = \left(\frac{\alpha_z \times 10^2}{\mu_0} \right) \left[{}^{\text{GEN}} K^{AA} \right] \quad .$$

The condition number (in 2-norm) of the above matrices is the ratio of their largest and smallest eigenvalues. All the elements of the mass matrix change by a numerical scaling factor $(\epsilon_0 \alpha_z \times 10^2)$. Hence, the ratio of the largest to the smallest eigenvalue, i.e., the condition number, remains the same for the mass matrix in the SI and the *generalized* unit system. Similar argument is applicable to the stiffness matrix. As the numerical scaling factor for the mass matrix is $(\epsilon_0 \alpha_z \times 10^2)$, and the stiffness matrix is $(\mu_0 \alpha_z \times 10^2)$, the overall condition number of the matrix

$$\begin{bmatrix} K^{AA} & 0 \\ 0 & M^{\psi\psi} \end{bmatrix}$$

changes. However, linear equations in (4.23) can be uncoupled into a set of two equations (6.12) and (6.13). Hence, as the condition number of $\left[M^{\psi\psi} \right]$ and $\left[K^{AA} \right]$ are not effected, the scaling factors $(\epsilon_0 \alpha_z \times 10^2)$ and $(\mu_0 \alpha_z \times 10^2)$ have no effect on the solution.

6.1.3.2. Transient problem

The set of linear equations to be solved for each time step in the transient problem is stated in (4.53). The matrix on the left-hand side is

$$\left(\frac{1}{(\Delta t_{n+1})^2 \beta} \begin{bmatrix} M^{AA} & M^{A\psi} \\ M^{\psi A} & M^{\psi\psi} \end{bmatrix} + \frac{\gamma}{\Delta t_{n+1} \beta} \begin{bmatrix} B^{AA} & B^{A\psi} \\ B^{\psi A} & B^{\psi\psi} \end{bmatrix} + \begin{bmatrix} K^{AA} & 0 \\ 0 & 0 \end{bmatrix} \right) \quad , \quad (6.14)$$

where β and γ are parameters in the Newmark algorithm, and the time step size $\Delta t_{n+1} = t_{n+1} - t_n$. The condition number of the above matrix determines the accuracy of the solution.

As explained in the static problem, we can express the mass, damping and the stiffness matrices in (6.14) in terms of the matrices in Remark 5.1. Once again we shall use matrices of the size $(4\aleph \times 4\aleph)$, i.e., the matrices before the appropriate rows and columns are removed. The mass matrix

$$\begin{bmatrix} \mathcal{M}^{AA} & \mathcal{M}^{A\psi} \\ \mathcal{M}^{\psi A} & \mathcal{M}^{\psi\psi} \end{bmatrix} = \int_\Omega \epsilon(\mathbf{x}) \begin{bmatrix} [N_A]^T [N_A] & [N_A]^T [\nabla N_\psi] \\ [\nabla N_\psi]^T [N_A] & [\nabla N_\psi]^T [\nabla N_\psi] \end{bmatrix} d\Omega , \quad (6.15)$$

the damping matrix

$$\begin{bmatrix} \mathcal{B}^{AA} & \mathcal{B}^{A\psi} \\ \mathcal{B}^{\psi A} & \mathcal{B}^{\psi\psi} \end{bmatrix} = \int_\Omega \sigma(\mathbf{x}) \begin{bmatrix} [N_A]^T [N_A] & [N_A]^T [\nabla N_\psi] \\ [\nabla N_\psi]^T [N_A] & [\nabla N_\psi]^T [\nabla N_\psi] \end{bmatrix} d\Omega , \quad (6.16)$$

and the stiffness matrix

$$\begin{bmatrix} \mathcal{K}^{AA} & 0 \\ 0 & 0 \end{bmatrix} = \int_\Omega \frac{1}{\mu(\mathbf{x})} \begin{bmatrix} [\nabla \times N_A]^T [\nabla \times N_A] & 0 \\ 0 & 0 \end{bmatrix} d\Omega , \quad (6.17)$$

are of the size $(4\aleph \times 4\aleph)$.

For the *generalized* system of units, the quantities used to define the three matrices above will be in the *generalized* system of units. For example, the mass matrix becomes

$$\begin{bmatrix} {}^{\text{GEN}}\mathcal{M}^{AA} & {}^{\text{GEN}}\mathcal{M}^{A\psi} \\ {}^{\text{GEN}}\mathcal{M}^{\psi A} & {}^{\text{GEN}}\mathcal{M}^{\psi\psi} \end{bmatrix} = \int_{{}^{\text{GEN}}\Omega} {}^{\text{GEN}}\epsilon({}^{\text{GEN}}\mathbf{x}) {}^{\text{GEN}} \begin{bmatrix} [N_A]^T [N_A] & [N_A]^T [\nabla N_\psi] \\ [\nabla N_\psi]^T [N_A] & [\nabla N_\psi]^T [\nabla N_\psi] \end{bmatrix} d\Omega .$$

$$(6.18)$$

Changing the unit system changes the numerical values of the elements in the matrix. Using Table 6.3 and 6.4 we obtain the following relation between the matrices in the *SI* and *generalized* unit system. The mass matrices

$$\begin{bmatrix} {}^{\text{SI}}\mathcal{M}^{AA} & {}^{\text{SI}}\mathcal{M}^{A\psi} \\ {}^{\text{SI}}\mathcal{M}^{\psi A} & {}^{\text{SI}}\mathcal{M}^{\psi\psi} \end{bmatrix} = \epsilon_0 \begin{bmatrix} \left(\alpha_z^3 \times 10^6\right) {}^{\text{GEN}} M^{AA} & \left(\alpha_z^2 \times 10^4\right) {}^{\text{GEN}} M^{A\psi} \\ \left(\alpha_z^2 \times 10^4\right) {}^{\text{GEN}} M^{\psi A} & \left(\alpha_z \times 10^2\right) {}^{\text{GEN}} M^{\psi\psi} \end{bmatrix} , \quad (6.19)$$

the damping matrices

$$\begin{bmatrix} {}^{\text{SI}}B^{AA} & {}^{\text{SI}}B^{A\psi} \\ {}^{\text{SI}}B^{\psi A} & {}^{\text{SI}}B^{\psi\psi} \end{bmatrix} = c\epsilon_0 \begin{bmatrix} \left(\alpha_z^4 \times 10^6\right) {}^{\text{GEN}}B^{AA} & \left(\alpha_z^3 \times 10^4\right) {}^{\text{GEN}}B^{A\psi} \\ \left(\alpha_z^3 \times 10^4\right) {}^{\text{GEN}}B^{\psi A} & \left(\alpha_z^2 \times 10^2\right) {}^{\text{GEN}}B^{\psi\psi} \end{bmatrix}, \quad (6.20)$$

and the stiffness matrices

$$\begin{bmatrix} {}^{\text{SI}}\mathcal{K}^{AA} & 0 \\ 0 & \end{bmatrix} = \begin{bmatrix} \left(\frac{\alpha_z \times 10^2}{\mu_0}\right) {}^{\text{GEN}}M^{AA} & 0 \\ 0 & 0 \end{bmatrix}, \quad (6.21)$$

are related by the numerical multiplicative factor α_z. Different values of α_z results in different *generalized* unit systems. The condition number of the matrices for a particular problem is determined by the choice of α_z. Using the above relations, the matrix (6.14) in the *generalized* system of units is related to that in the SI units as follows.

$$\begin{aligned} \left[{}^{\text{GEN}}\mathbb{K}\right] := & \left(\frac{1}{\left({}^{\text{GEN}}\Delta t_{n+1}\right)^2 \beta} \begin{bmatrix} {}^{\text{GEN}}M^{AA} & {}^{\text{GEN}}M^{A\psi} \\ {}^{\text{GEN}}M^{\psi A} & {}^{\text{GEN}}M^{\psi\psi} \end{bmatrix} \right. \\ & \left. + \frac{\gamma}{{}^{\text{GEN}}\Delta t_{n+1} \beta} \begin{bmatrix} {}^{\text{GEN}}B^{AA} & {}^{\text{GEN}}B^{A\psi} \\ {}^{\text{GEN}}B^{\psi A} & {}^{\text{GEN}}B^{\psi\psi} \end{bmatrix} + \begin{bmatrix} {}^{\text{GEN}}K^{AA} & 0 \\ 0 & 0 \end{bmatrix}\right) \\ = & \frac{1}{\left({}^{\text{SI}}\Delta t_{n+1}\right)^2 \beta} \begin{bmatrix} \frac{c^2}{\epsilon_0 \alpha_z \times 10^6} {}^{\text{SI}}M^{AA} & \frac{c^2}{\epsilon_0 \times 10^4} {}^{\text{SI}}M^{A\psi} \\ \frac{c^2}{\epsilon_0 \times 10^4} {}^{\text{SI}}M^{\psi A} & \frac{c^2 \alpha_z}{\epsilon_0 \times 10^2} {}^{\text{SI}}M^{\psi\psi} \end{bmatrix} \quad (6.22) \\ & + \frac{\gamma}{{}^{\text{SI}}\Delta t_{n+1} \beta} \begin{bmatrix} \frac{1}{\epsilon_0 \alpha_z^3 \times 10^6} {}^{\text{SI}}B^{AA} & \frac{1}{\epsilon_0 \alpha_z^2 \times 10^4} {}^{\text{SI}}B^{A\psi} \\ \frac{1}{\epsilon_0 \alpha_z^2 \times 10^4} {}^{\text{SI}}B^{\psi A} & \frac{1}{\epsilon_0 \alpha_z \times 10^2} {}^{\text{SI}}B^{\psi\psi} \end{bmatrix} \\ & + \begin{bmatrix} \frac{1}{\mu_0 \alpha_z \times 10^2} {}^{\text{SI}}K^{AA} & 0 \\ 0 & 0 \end{bmatrix}. \end{aligned}$$

For the problem at hand the material properties and the geometry are fixed, and hence, the matrices in the SI system of units are fixed. However, changing the value

for α_z can improve the condition number of the matrix $\mathbb{K}$ in the *generalized* system of units. In theory, we could find an optimal value for α_z to minimize the condition number of the matrix $^{\text{GEN}}\mathbb{K}$, i.e.,

$$\alpha_z^{opt} := \min_{\alpha_z \neq 0} \left(\text{Condition number of } ^{\text{GEN}}\mathbb{K} \right) ,$$

(6.23)

where α_z^{opt} is the optimal multiplicative factor. Numerically, we could construct a coarse mesh for the problem at hand, and vary α_z to find an approximate optimal value.

6.1.3.3. Time harmonic problem

The set of linear equations to be solved for the time-harmonic problem (4.67) involves the matrix

$$\begin{bmatrix} ^r K - (\omega^2)\,^r M & (\omega)\,^i B \\ \\ -(\omega)\,^r B & ^i K - (\omega^2)\,^i M \end{bmatrix} ,$$

(6.24)

where ω is the frequency of the driving force. The condition number of the above matrix determines the accuracy of the solution. As the above matrix is unsymmetric, its condition number plays a more crucial role in the solution.

The relationships (6.19) to (6.21) for the mass, damping and stiffness matrices are the same for the time harmonic problem. This implies that the condition number of the matrix

$$\left[\overline{^{\text{GEN}}\mathbb{K}} \right] := \begin{bmatrix} ^{\text{GEN}}\,^r K - \left(^{\text{GEN}}\omega^2\right)\,^{\text{GEN}}\,^r M & \left(^{\text{GEN}}\omega\right)\,^{\text{GEN}}\,^i B \\ \\ -\left(^{\text{GEN}}\omega\right)\,^{\text{GEN}}\,^r B & ^{\text{GEN}}\,^i K - \left(^{\text{GEN}}\omega^2\right)\,^{\text{GEN}}\,^i M \end{bmatrix} ,$$

(6.25)

can be changed by varying the numerical multiplicative factor α_z. Note that the frequency ${}^{SI}\omega = \dfrac{1}{c\alpha_z}{}^{GEN}\omega$. Similar to the transient problem, we can find an optimal value for α_z to minimize the condition number of the matrix $\overline{{}^{GEN}\mathbb{K}}$, i.e.,

$$\alpha_z^{opt} := \min_{\alpha_z \neq 0} \left(\text{Condition number of } \overline{{}^{GEN}\mathbb{K}} \right) , \qquad (6.26)$$

where α_z^{opt} is the optimal multiplicative factor.

The effects of scaling depends on the excitation frequency. At very low frequencies, Maxwell equations require a solution to only an uncoupled problem. For an uncoupled problem, where the vector potential $\mathbf{A}$ and the scalar potential ψ are solved separately, scaling has little or no effect. Hence, scaling is most effective for problems at high frequencies; for the MLCC, scaling is recommended for excitations above $10^6\ Hz$.

CHAPTER 7
ADVANCED MLCC: MESH GENERATION AND
ELECTROSTATIC SOLUTION

The advanced multilayer capacitor introduced by Ngo [1990] achieves the desired decrease in equivalent series resistance esr and equivalent series inductance esl, and an increase in capacitance. One of the reasons for its improved performance is due to the fact that the positive terminations are immediately surrounded by negative terminations. The reduced current path between the negative and positive conductors decreases the esr. A smaller esl is because the electrodes come in parallel to each other. Moreover, the ceramics used in the capacitor have high permittivity, and hence, high capacitance. The esr and esl degrade the performance of the capacitor beyond the self-resonant frequency. However, low values of esr and esl, combined with high capacitance, increases the self-resonant frequency and improves the performance of the advanced MLCCs. From experiments it is determined that a $10\mu Farad$ capacitor with the geometry proposed by Ngo [1990] has $esr = 6.7 \times 10^{-4} ohm$, $esl = 14.8 \times 10^{-12} Henry$, and the self resonant frequency $srf = 13.0 MHz$. The conducting material used for the electrodes and the vias is silver palladium, and the dielectric material is a ceramic such as barium titanate. Their material properties are listed in Table 7.1. The leakage resistance of the conductors are neglected.

As a first step to model the advanced MLCC, in this chapter, we construct a mesh for the complex geometry and calculate an electrostatic solution. The matrix equation (4.23) is solved, where the degrees of freedom corresponding to the vector potential **A** is equal to zero, i.e., $\widetilde{\mathcal{A}}_0 = 0$. Hence, only the scalar potential needs

<center>130</center>

Table 7.1. Material properties for the MLCC in SI unit system.

Material	Permittivity ϵ ($Farad/m$)	Permeability μ ($Henry/m$)	Conductivity σ ($1/(ohm - m)$)
Dielectric	$1500\epsilon_0$	μ_0	0.0
Electrodes & Vias	ϵ_0	$1.0008\ \mu_0$	2.9412×10^6
Bus	ϵ_0	$0.999991\ \mu_0$	5.8×10^7
Air	ϵ_0	$1.0000004\ \mu_0$	0.0

to be calculated outside the conductors. The mesh generation and the subsequent FE solution are implemented using MODULEF (Bernadou et al. [1986]). The electrostatic solution only provides a value for capacitance, which is determined to be $11.8 \mu Farad$. The effects of the surrounding air on the value of capacitance is minimal, indicating there is very little fringing of the electric field. We explore the use of symmetry in the solution of the electrostatic problem, where the one-half, one-quater, and one-eighth of the capacitor are modelled with the appropriate boundary conditions. Capacitance obtained from the models using symmetry agree very well with the results for the complete capacitor.

7.1. Mesh Generation

The geometry proposed for the MLCC by Ngo [1990] consists of stacked electrode sheets with dielectric ceramics in between them. For the purpose of our discussion, the alternate electrodes are referred to as positive electrodes and the remaining are negative electrodes. The positive electrodes are connected by a group of positive vias running perpendicular to the electrodes. These positive vias pass insulatingly through a hole in the negative electrodes. Similarly, the negative vias connect the negative electrodes. A cross section of the geometry is shown in Figure 7.1. The

terminations (which is connected to the external circuit) for a conventional capacitor is at opposite ends of the electrodes. However, such terminations leads to higher *esl* and lower *srf*. Hence, the MLCC provides multiple terminations for *each* electrode. The positive-electrode terminations run parallel to one side of the capacitor and the negative-electrode electrode terminations run parallel to other side. The topmost electrode is referred to as the positive (top) bus, and the bottom electrode is the negative bus; see Figure 7.2.

The capacitor can be divided into stacks of cells. Figure 7.1 shows that the MLCC has $4 \times 4 = 16$ stacks of cells. An exploded view through the thickness of a single stack is presented in Figure 7.2. A single stack consists of number of groups of positive and negative electrodes with the dielectric in between. There is a positive bus on the top and a negative bus at the bottom. The positive vias only contact the positive electrodes. A cell is defined as a pair of negative and positive electrodes with the dielectric in between. A typical cell is shown in Figure 7.3. A stack is constructed by "stacking" the cells in Figure 7.3 one on top of the other. Some modifications are made for the cells on the top and the bottom of the stack. The entire MLCC is constructed by appropriately connecting a set of stacks. These logical divisions in cells and stacks form the basis of the bottom-up construction of the mesh.

For the 4×4 stack, $10 \mu Farad$ MLCC, each cell has a cross-section of $0.635cm \times 0.635cm$. The thickness of the electrodes are $1.5 \mu m$, and the dielectric is $15 \mu m$. The width of the electrode (to allow holes for the vias) is $0.508cm$. There are 27 dielectric layers and 14 pairs of electrodes in the entire MLCC. Hence, with $4 \times 4 = 16$ stacks, that equals $16 \times 27 = 432$ cells connected in a novel architecture. A simple estimate of the capacitance of each cell is $10/432 \approx 0.0231 \mu Farad$. See Anand [1993] for a more comprehensive description of the geometry proposed by Ngo [1990].

A model for the MLCC consists of a mesh with the MLCC in the middle surrounded by air. This surrounding air, henceforth, shall be referred to as the airbox. During mesh construction we divide the domain in to the airbox and the capacitor. These are meshed separately and glued together. The division and the assembly is carefully planned to avoid any "unresolved nodes" as in Figure 4.1. The geometry of the airbox is an hexahedron with the capacitor in the center as in Figure 7.4. The airbox is further divided into six hexahedra as in Figure 7.5. In our construction, we choose to only mesh the three of hexahedra's shown in Figure 7.6. The remaining three are generated using mirror images. Finally the mesh for the capacitor is generated. This is accomplished by dividing each layer (a group of positive and negative electrodes with the dielectric in between) into smaller hexahedra as shown in Figure 7.7. Note that four distinct hexahedra are required to completely describe the capacitor since the edges terminate with *vias*. Next, each of the four distinct hexahedral regions can be broken into layers of seven simpler hexahedral regions. This is illustrated in Figure 7.8. For such a complicated geometry a new mesh generator had to be created using the existing modules in MODULEF. The code presently is limited to generating hexahedral brick elements with straight edges. All aspects of mesh generation, including coding using MODULEF, is discussed in Langford, Srinivas and Vu-Quoc [1995]. George [1991] explains in detail some of the popular mesh generation techniques.

7.2. Solution without symmetry

The MLCC has an architecture of interconnected electrodes and vias. This makes an accurate analytical estimate of the capacitance impossible. In order to establish bounds on the value of capacitance we employ the analytical formula for

an ideal parallel plate capacitor, i.e., the capacitance

$$C = \frac{\epsilon_0 A}{d},$$

where A is the area and d is distance between the electrodes. The capacitor has 14 pairs of electrodes, 27 layers of the dielectric, and 40 vias (20 positive and 20 negative). Each pair of electrodes is divided into $4 \times 4 = 16$ cells. The capacitance of each cell is estimated by the above formula. The upper bound on the area is $(6.35 \times 10^{-3}) \times (6.35 \times 10^{-3}) = 4.03225 \times 10^{-5}\ m^2$, and the lower bound is $(5.08 \times 10^{-3}) \times (5.08 \times 10^{-3}) = 2.58064 \times 10^{-5}\ m^2$. The bounds are estimated from the area of the electrode in each cell: The upper bound corresponds to the case when the holes in the electrode (for the vias) are covered with conducting material, and the lower bound corresponds to the case when the holes in the electrode (for the vias) and its immediate surroundings are covered with the dielectric. From the above arguments we estimate that the capacitance of the entire capacitor lies in between the upper bound

$$16 \times 27 \times \frac{1500\epsilon_0\,(4.03225 \times 10^{-5})}{15.0 \times 10^{-6}} = 15.416\ \mu F,$$

and the lower bound

$$16 \times 27 \times \frac{1500\epsilon_0\,(2.58064 \times 10^{-5})}{15.0 \times 10^{-6}} = 9.8663\ \mu F.$$

The effect of the vias and the bus/terminations has not considered.

The electrostatic solution using the FE method has been discussed in detail in the previous sections. To recapitulate, we solve the problem (2.23) with some simplifications. We define a new scalar potential ϕ as follows

$$\mathbf{E}_0 =: -\operatorname{grad}\phi.$$

The difference in the potential ϕ gives the voltage between two points. For electrostatic problems we only need to solve for the potential $\dot{\psi}_0 \equiv \phi$ in the non-conductive region $\Omega \setminus \Omega_{cond}$. Hence, the problem is defined as follows.

$$
\boxed{
\begin{aligned}
&\text{Find } \phi \in \mathbf{R} \text{ such that}\\
&\qquad \operatorname{div}(\epsilon \operatorname{grad}\phi) = 0 \qquad \text{in } (\Omega \setminus \Omega_{cond}) ,\\
&\qquad\qquad\qquad\; \phi = \phi_a \qquad\;\; \text{on } \Gamma_{g\dot{\psi}_0}\\
&\qquad\qquad \mathbf{D}_0 \cdot \hat{n} = (\mathbf{D}_0 \cdot \hat{n})_a \quad \text{on } \Gamma_{h\dot{\psi}_0} .
\end{aligned}
}
$$

We use linear-isotropic materials with $\mathbf{D}_0 = \epsilon(\mathbf{x})\mathbf{E}_0 = -\epsilon(\mathbf{x})\operatorname{grad}\dot{\psi}_0$. The permittivity is piece-wise constant and its values are listed in Table 7.1. The boundary $\partial\Omega =: \overline{\Gamma_{h\dot{\psi}_0} \cup \Gamma_{g\dot{\psi}_0}}$, where $\Gamma_{g\dot{\psi}_0}$ corresponds to the surface of the conductors with the voltage ϕ_a specified. The remaining part of the boundary is $\Gamma_{h\dot{\psi}_0}$ where $\mathbf{D}_0 \cdot \hat{n} = 0$ is specified. The capacitance is obtained from the electric energy stored in the material, i.e.,

$$
C := \frac{\int_{(\Omega \setminus \Omega_{cond})} (\epsilon \operatorname{grad}\phi) \cdot (\operatorname{grad}\phi)\, d\Omega}{V^2} . \tag{7.1}
$$

where V is the potential difference between the positive and the negative electrodes. The potential difference is specified in the problem in terms of appropriate values to ϕ_a at the surface of the conductors. Using the matrix representation in Chapter 4 we can write the capacitance to be

$$
\boxed{
C = \frac{\{\widetilde{\dot{\psi}_0}\}^T [M^{\psi\psi}] \{\widetilde{\dot{\psi}_0}\}}{V^2} \equiv \frac{\{\widetilde{\phi}\}^T [M^{\psi\psi}] \{\widetilde{\phi}\}}{V^2} ;
}
\tag{7.2}
$$

see Chapter 5 for details. The column vector $\{\widetilde{\phi}\} \equiv \{\widetilde{\dot{\psi}_0}\}$ is the solution for the potential ϕ at the nodes in the mesh.

7.2.1. FE Results Without an Airbox

This model does not include the surrounding air. The value of the capacitance is computed to be 11.88 μ $Farad$. The effect of the mesh size is studied. Figure 7.9

Table 7.2. Capacitance with increasing number of elements in the thickness direction.

Number of elements in thickness dir. for each layer	Degrees required	Memory for solution	CPU time	Capacitance in $\mu\,Farad$
3	35640	50 MB	3 minutes	11.8811395
5	53181	80 MB	4 minutes	11.8811258
7	70677	106 MB	5 minutes	11.8810694
9	88173	133 MB	6 minutes	11.8810603
11	105669	158 MB	8 minutes	11.8810576

and Table 7.2 show the convergence of the capacitance with increasing the number of elements in the thickness direction.

The accuracy of the FE solution depends on the data available for the component. The physical properties of the materials and the geometry are changed during the manufacturing process. Moreover the material properties of the capacitors change with temperature. For example, Table 7.3 (from Moulson and Herbert [1990]) is a list of typical change in capacitance with temperature and corresponding codes for different types of capacitors. Hence, for a better estimate of the capacitance, a good measurement of the properties of the materials and the geometry is required.

7.2.2. FE Results with an Airbox

The non-conducting domain, for which the solution is determined, extends to infinity. However, the mesh is truncated at a finite distance from the capacitor. The present formulation specifies a zero flux (a zero Neumann boundary condition) at the truncated boundary. This introduces errors. The thickness of the MLCC is much smaller than the cross-section, and hence, we expect very little fringing. This

Table 7.3. Typical capacitance variation for Class II capacitors (only a small part is listed below).

EIA code	Temperature range ($^\circ C$)	EIA code	Capacitance change/%
X7	-55 to +125	D	±3.3
X5	-55 to +85	E	±4.7
Y5	-30 to +85	F	±7.5
Z5	+10 to +85	P	±10

implies that the value of the capacitance should be, to a large extent, unaffected by the size of the airbox.

The code developed for mesh generation allows a exponential change in the size of the elements in the airbox. The thickness of the elements next to the capacitor is much smaller than the elements close to the exterior of the airbox. This allows a smaller number elements, and hence, a smaller number of degrees of freedom, to model a large airbox. Addition of a three element thick airbox to the capacitor increases the number of nodes from 35640 to 59616: The number of degrees of freedom and solution time have increased significantly; the complexity of the mesh is clearly evident from Figure 7.10. Adding a six element thick airbox increases the number of nodes to 83637. Figure 7.11 shows the change in the capacitance with the overall size of the airbox. Lack of convergence is attributed to the inability to further refine the airbox due to limitations of the computer resources. The change in capacitance due to the inclusion of the airbox is very small, and hence, may be omitted for an electrostatic solution.

To better understand the behavior of the electric field inside the MLCC, we construct a smaller model with 3 cells in each stack (i.e., 2 pairs of electrodes), and $2 \times 2 = 4$ stacks placed beside each other. The mesh in Figure 7.12 shows a scaled

mesh. The iso-contours of the potentials at different cross-sections are shown in Figures 7.13, 7.14, 7.15, and 7.16. These are scaled plots, hence the fringing (closely packed iso-contours) can be seen in the airbox. However, the model with the exact dimensions shows negligible fringing.

7.3. Solution with Symmetry

The architecture of the MLCC allows us to exploit the symmetry in the solution, and hence, model only a small part of the capacitor. Figures 7.13, 7.14, 7.15, and 7.16 shows that we can exploit the symmetry of the geometry: For example, the solution on the either sides of the horizontal plane in Figure 7.13 are mirror images of each other with opposite signs for the potentials. Also, the solution on either sides of the vertical plane in Figure 7.14 are mirror images of each other. Normal electric flux can be set zero on the plane of symmetry, i.e., $\epsilon(\text{grad }\phi) \cdot \hat{n}$ is zero on the symmetry plane, where $\hat{n}$ represents the normal to the plane.

For one-half and one-quarter models we set the normal flux equal to zero at the plane of symmetry. For the one-eighth model we use following engineering approximation for boundary condition at the nodes in the dielectric that do not lie on the symmetry plane:

$$\epsilon(\text{grad }\phi) = \epsilon\frac{\Delta V}{\Delta z} ,$$

where ΔV is the potential difference between electrodes, and Δz is the distance between electrodes. The results for the $2 \times 2 \times 3$ stack of cells are presented in Table 7.4. The mesh[26] and the iso-contours for the potentials are shown in Figures 7.17, 7.18, 7.19, 7.20, 7.21, 7.22, 7.23, 7.24, 7.25, 7.26, 7.27, and 7.28, using a

---

[26] The mesh for the symmetry-based models is generated using Version 2.0 of the mesh generator. This substantially revised version eliminates the option to include an airbox, and includes options to model a one-half, one-quarter or one-eighth of a capacitor.

Table 7.4. Capacitance using symmetry for a $2 \times 2 \times 3$ stack of cells.

Symmetry	capacitance ($\mu\, Farad$)	Degrees of freedom
Whole	0.27784285	2448
Quarter	0.27889800	833
Eighth	0.27946214	441

visually-appealing aspect ratio (the dimensions are not representative of a real capacitor). The capacitance listed in Table 7.4 must be multiplied by $\dfrac{(4 \times 4 \times 27)}{(2 \times 2 \times 3)}$ to estimate the capacitance of the whole capacitor to be approximately $11.9\mu\ Farad$.
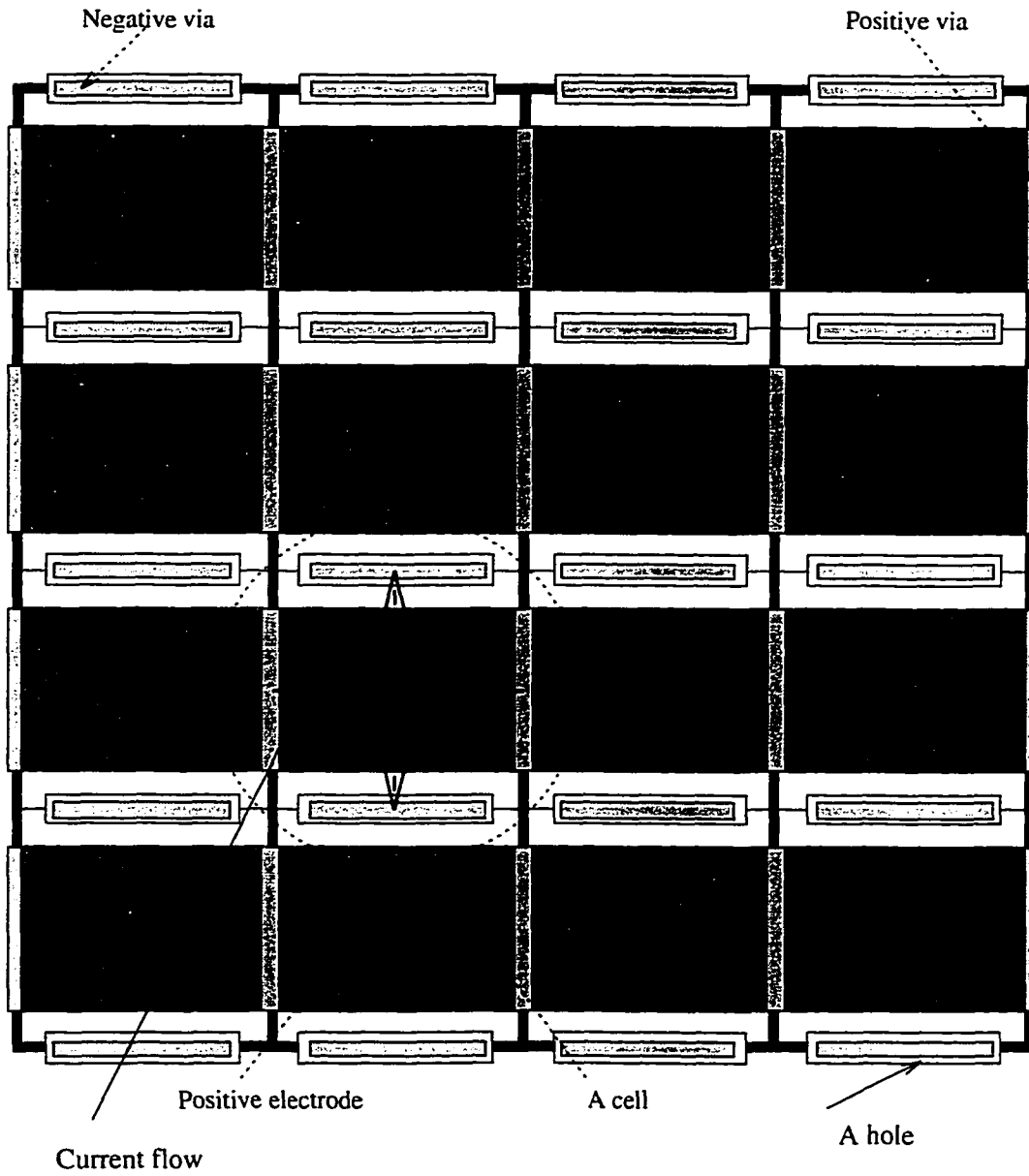
Figure 7.1. Advanced multilayer ceramic capacitor.
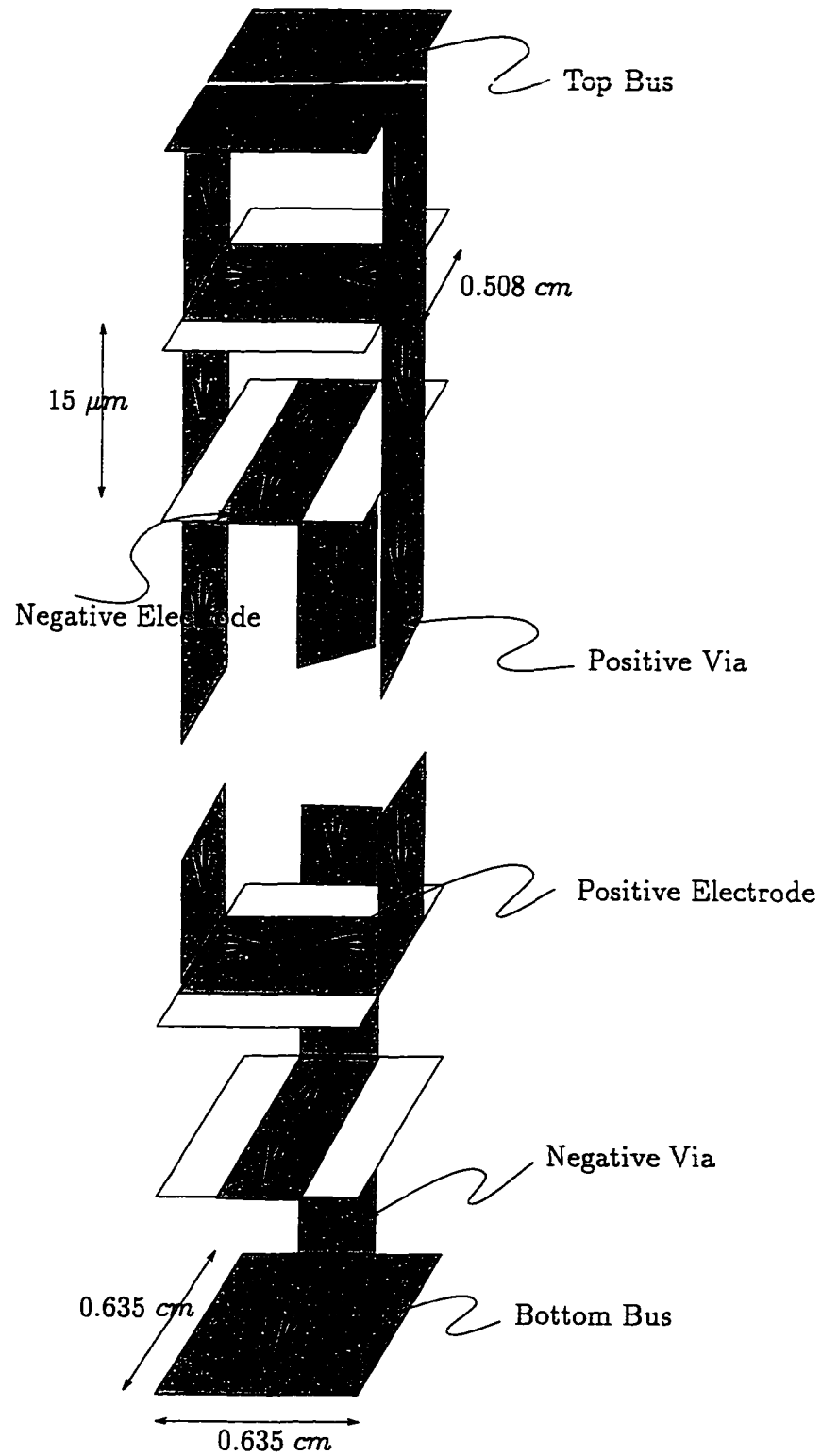
Figure 7.2. A single stack of an MLCC. There are two positive and two negative vias (only one is shown). Current flows along the arrows.

Dielectric

0.508 cm

Positive Electrode

0.635 cm

0.75 μm

15 μm

Negative Via

0.75 μm

Positive Via

Negative Electrode

0.635 cm
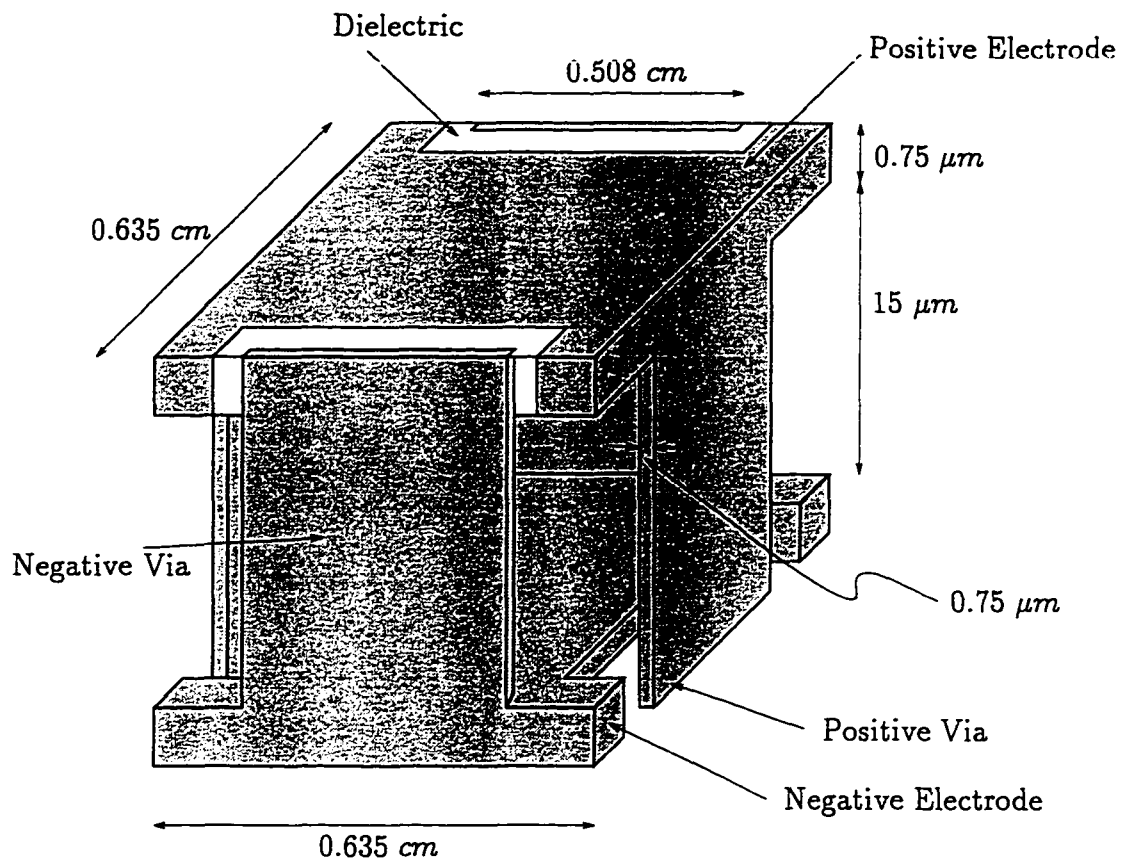
Figure 7.3. A typical single cell in the interior of a stack. The cells on the exterior required to be modified so as to attach to the bus and the terminations.
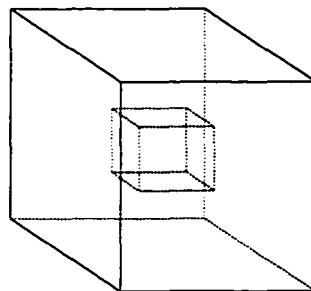
Figure 7.4. The geometry of the airbox.
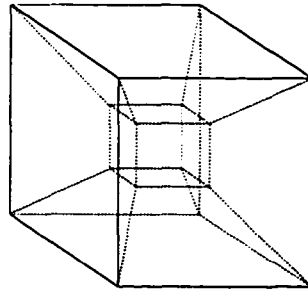
Figure 7.5. The airbox domain can be logically divided into six hexahedra.
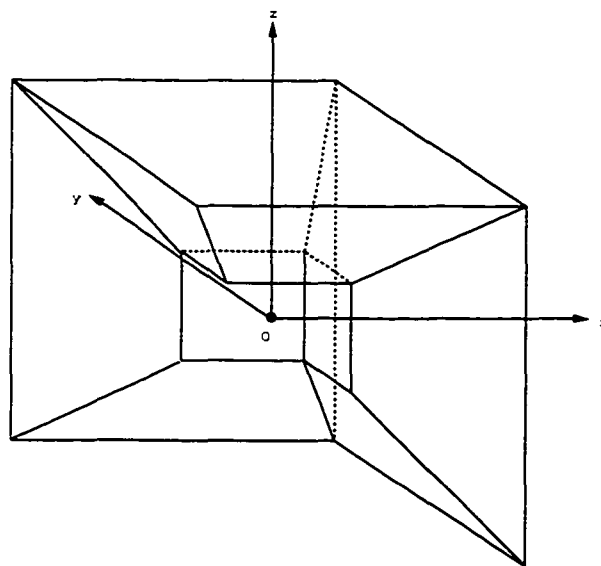
Figure 7.6. Once the three unique hexahedra have been glued together, the completing piece can be obtained by three mirroring operations about orthogonal planes through O.
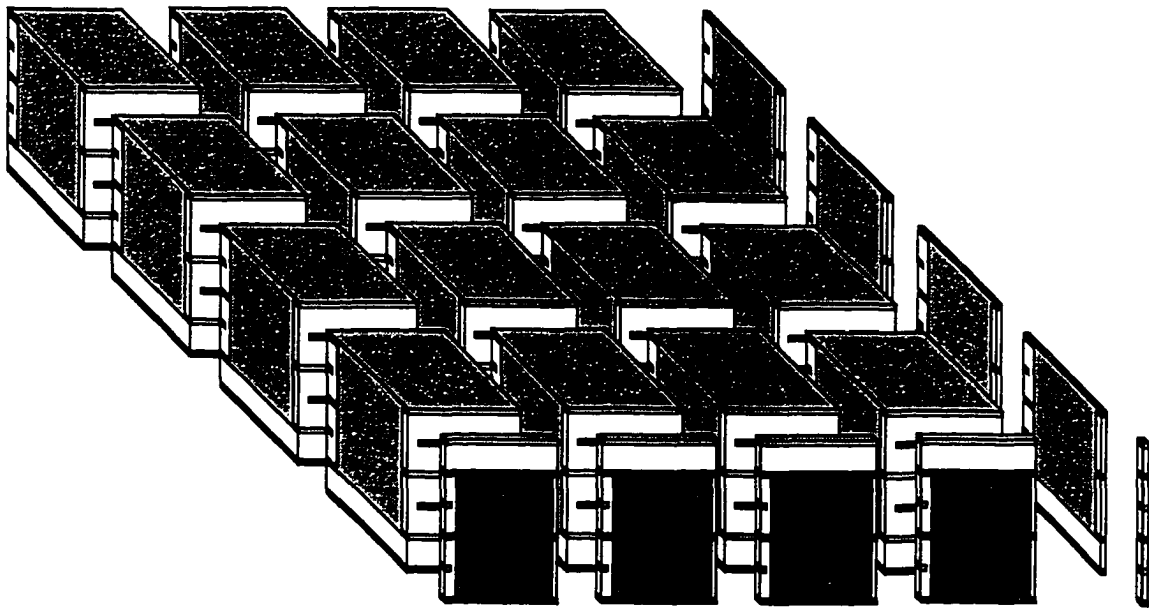
Figure 7.7. The domain of the advanced multilayer ceramic capacitor can be logically divided into a repetitive array of four distinct hexahedral regions.
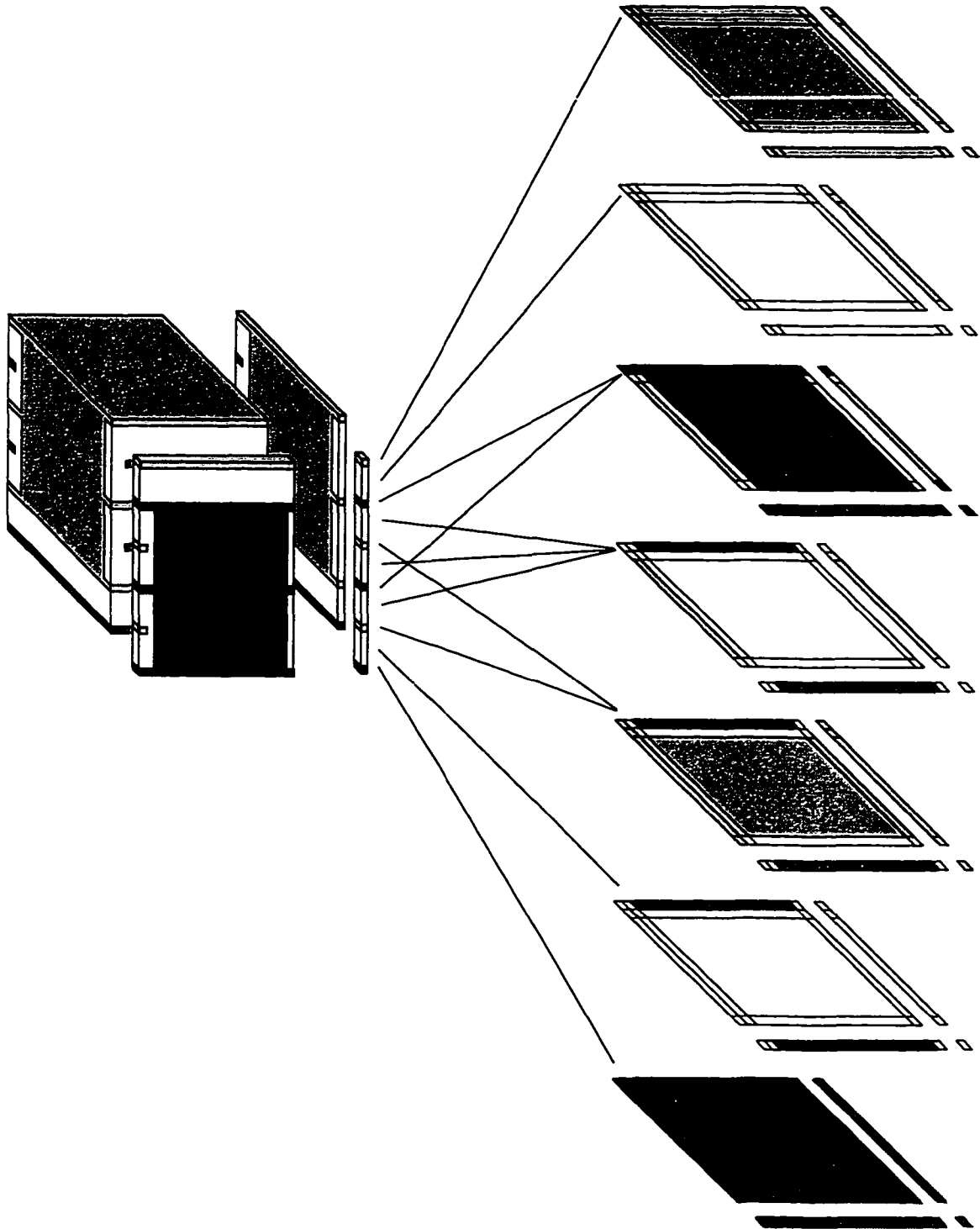
Figure 7.8. The four distinct hexahedral regions illustrated in the previous figure can be further reduced to layers of seven distinct hexahedral regions.
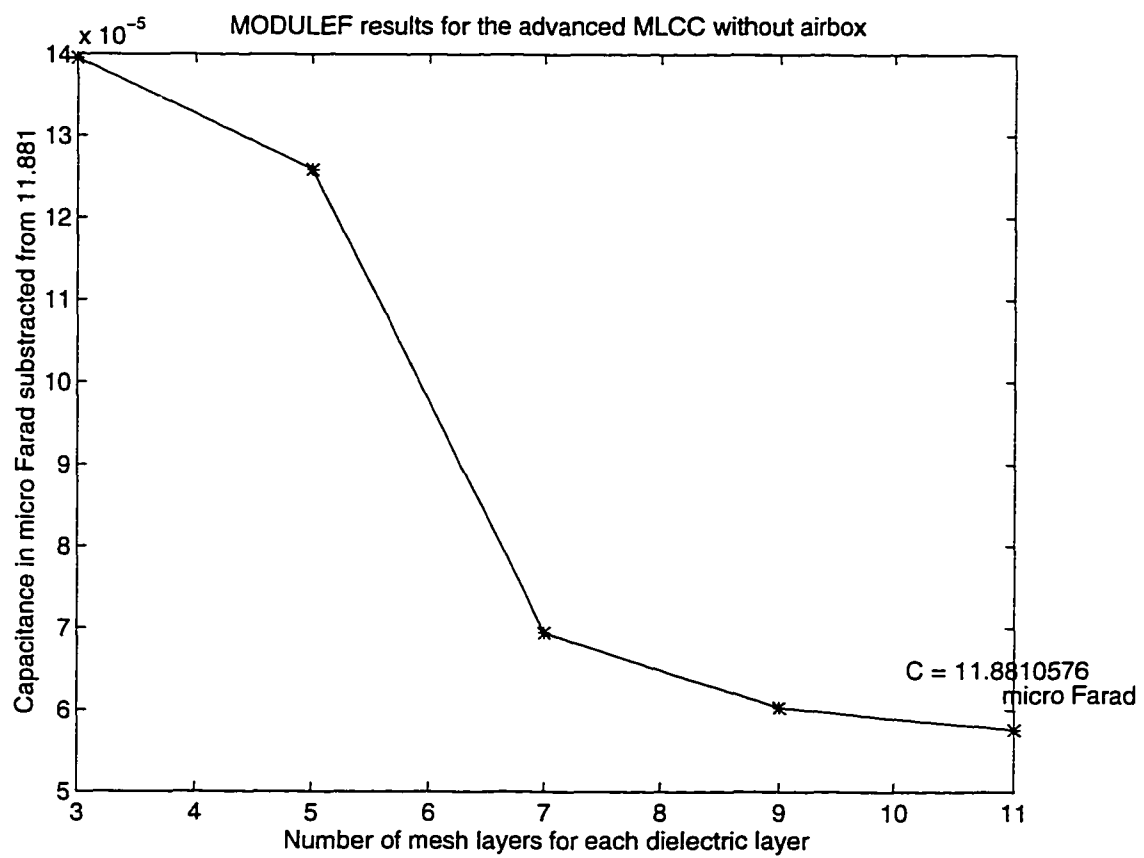
Figure 7.9. The capacitance converges with better refinement of the dielectric.
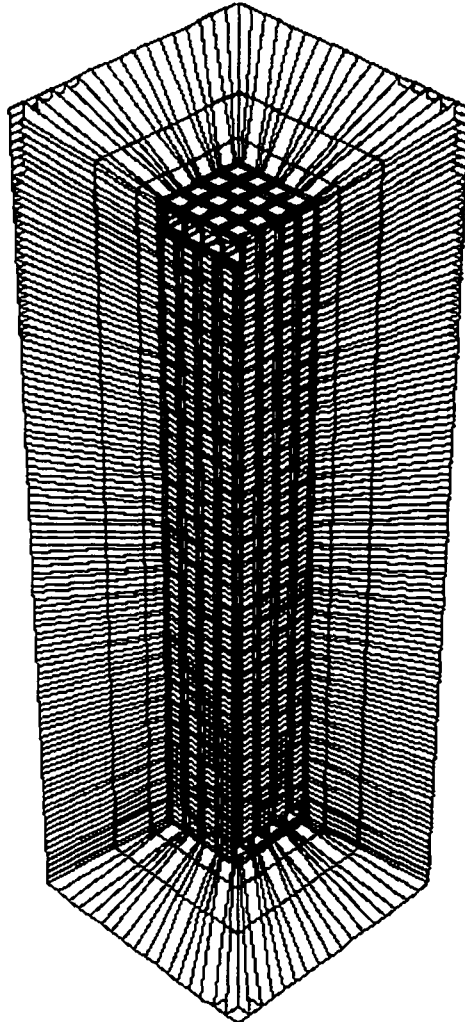
Figure 7.10. The entire MLCC with an airbox.
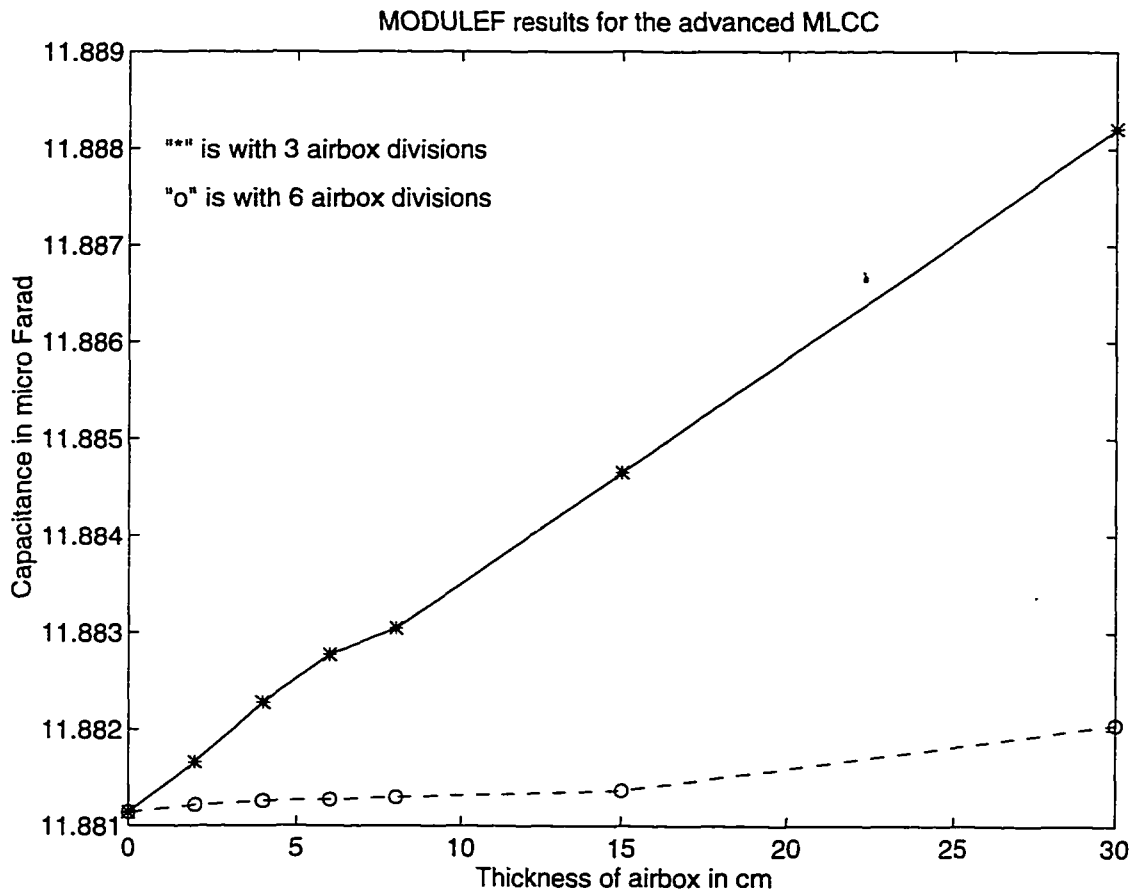
Figure 7.11. Capacitance with increasing airbox thicknesses. Poor mesh refinement in the airbox prevents us from seeing such convergence.
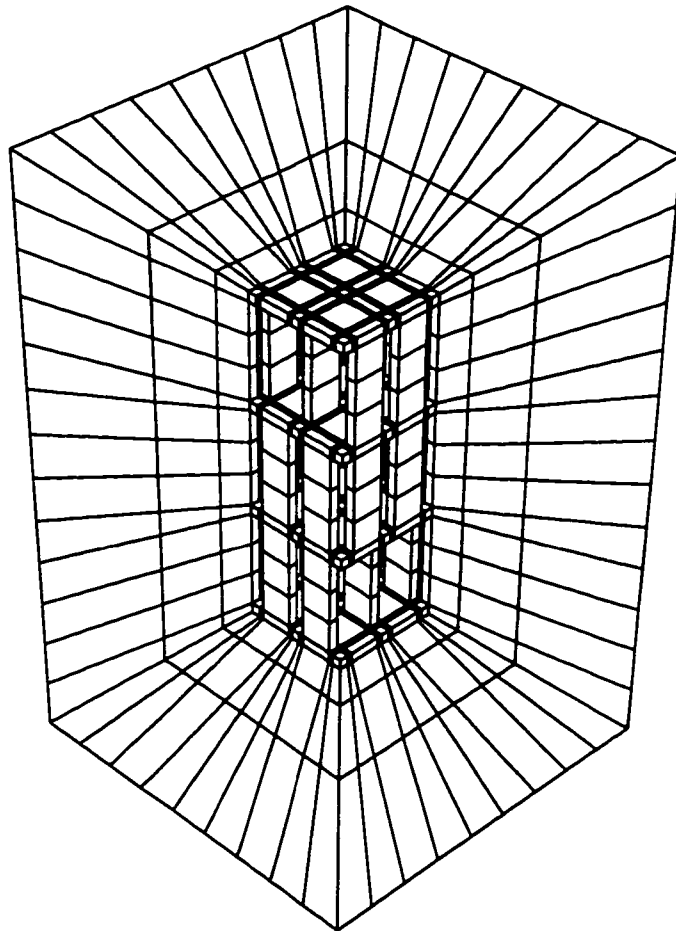
Figure 7.12. The mesh for a $2 \times 2 \times 3$ stack of cells. Dielectric and frontal airbox sections are removed for clarity.
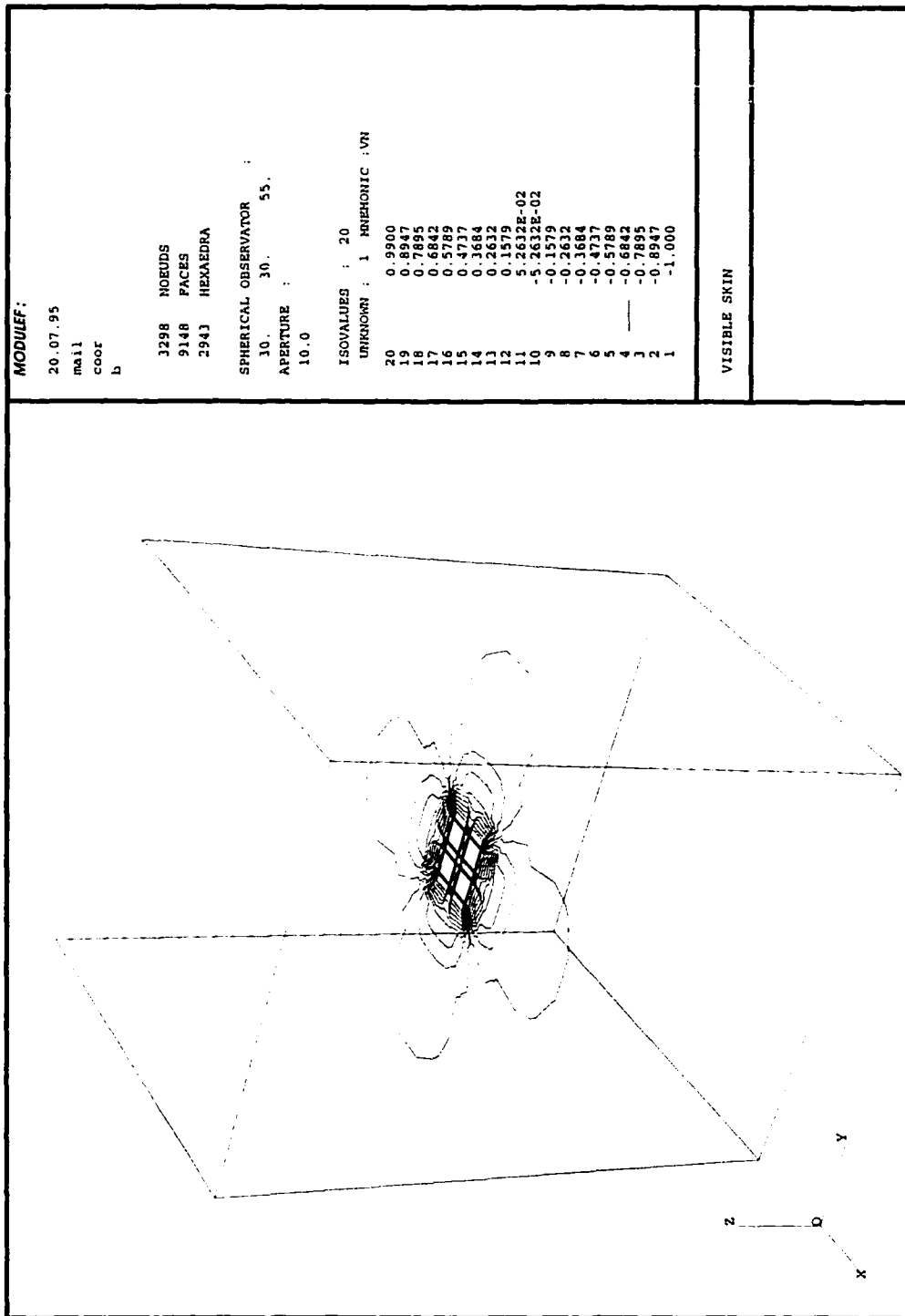
Figure 7.13. Isocontours of the potential ϕ at a horizontal plane at the center of the dielectric of a $2 \times 2 \times 3$ stack of cells.
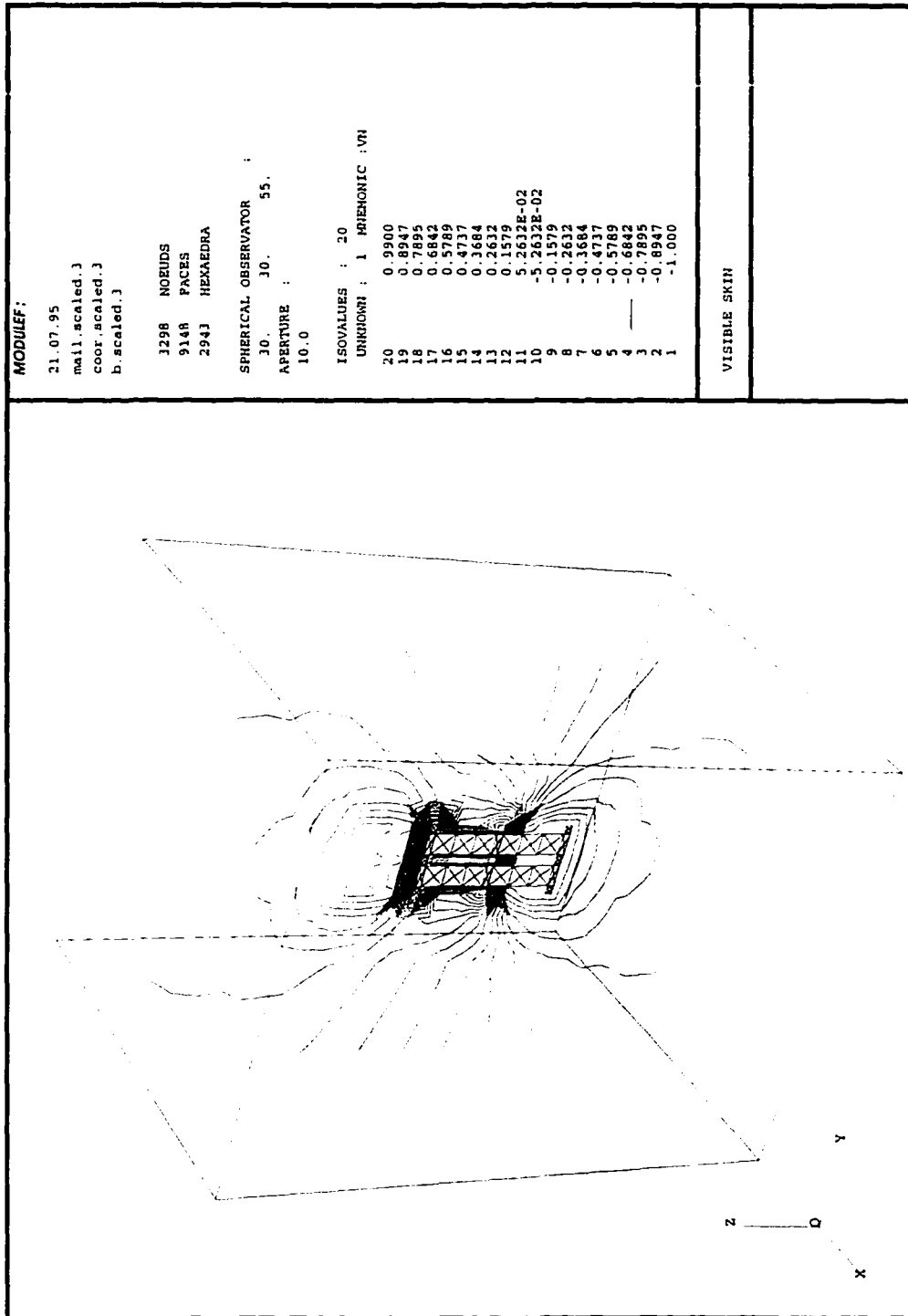
Figure 7.14. Isocontours of the potential ϕ at a vertical plane cutting through the center of the vias for a $2 \times 2 \times 3$ stack of cells.
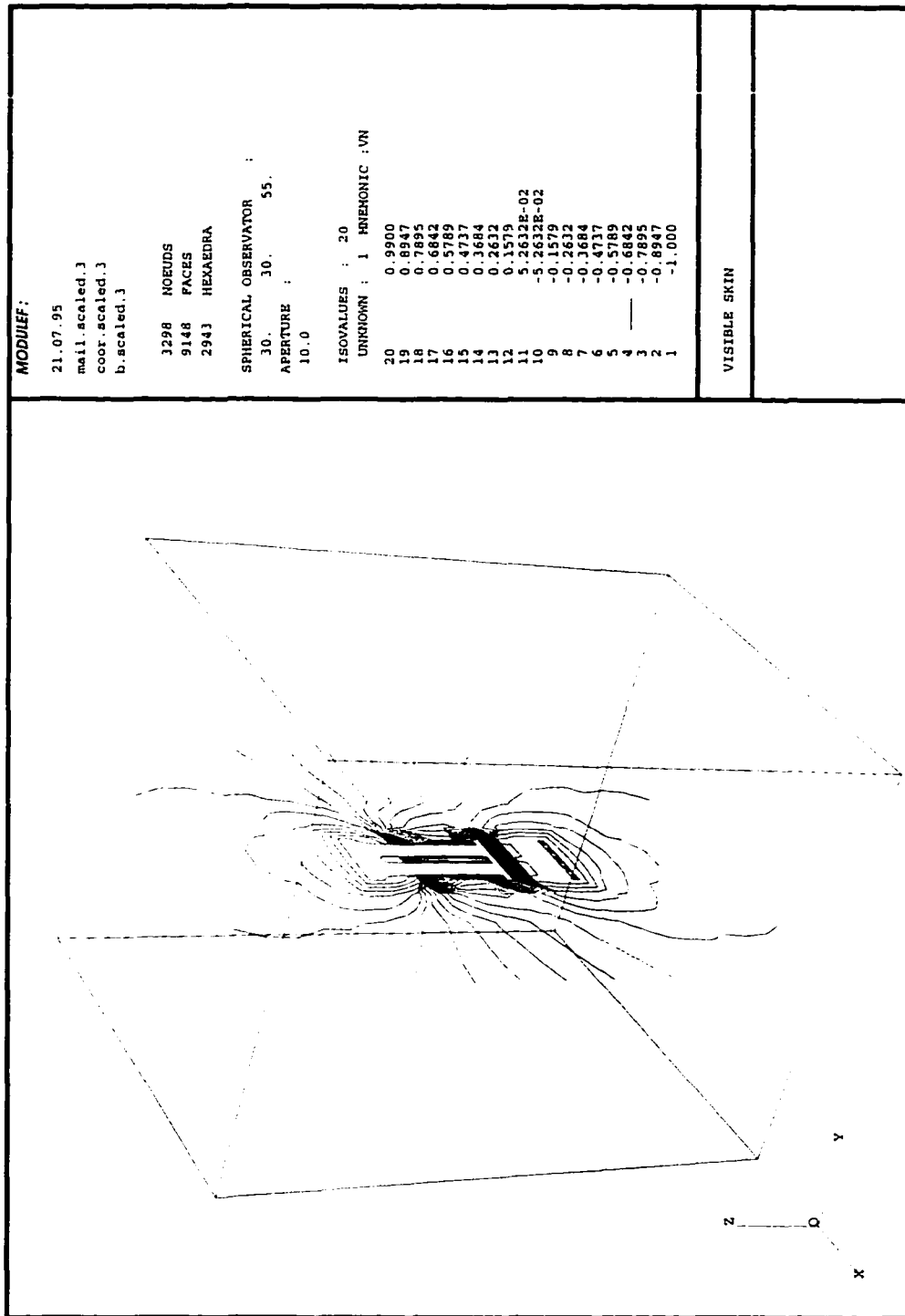
Figure 7.15. Isocontours of the potential ϕ at a vertical plane cutting through the dielectric for a $2 \times 2 \times 3$ stack of cells.

MODULEF:

21.07.95

mail.scaled.3
coor.scaled.3
b.scaled.3

1298 NOEUDS
9148 FACES
2943 HEXAEDRA

SPHERICAL OBSERVATOR :
30.   30.   55.

APERTURE :
10.0

ISOVALUES : 20
UNKNOWN : 1 MNEMONIC :VN

20	0.9900
19	0.8947
18	0.7895
17	0.6842
16	0.5789
15	0.4737
14	0.3684
13	0.2632
12	0.1579
11	5.2632E-02
10	-5.2632E-02
9	-0.1579
8	-0.2632
7	-0.3684
6	-0.4737
5	-0.5789
4	-0.6842
3	-0.7895
2	-0.8947
1	-1.000

SKIN + ELIMINATION
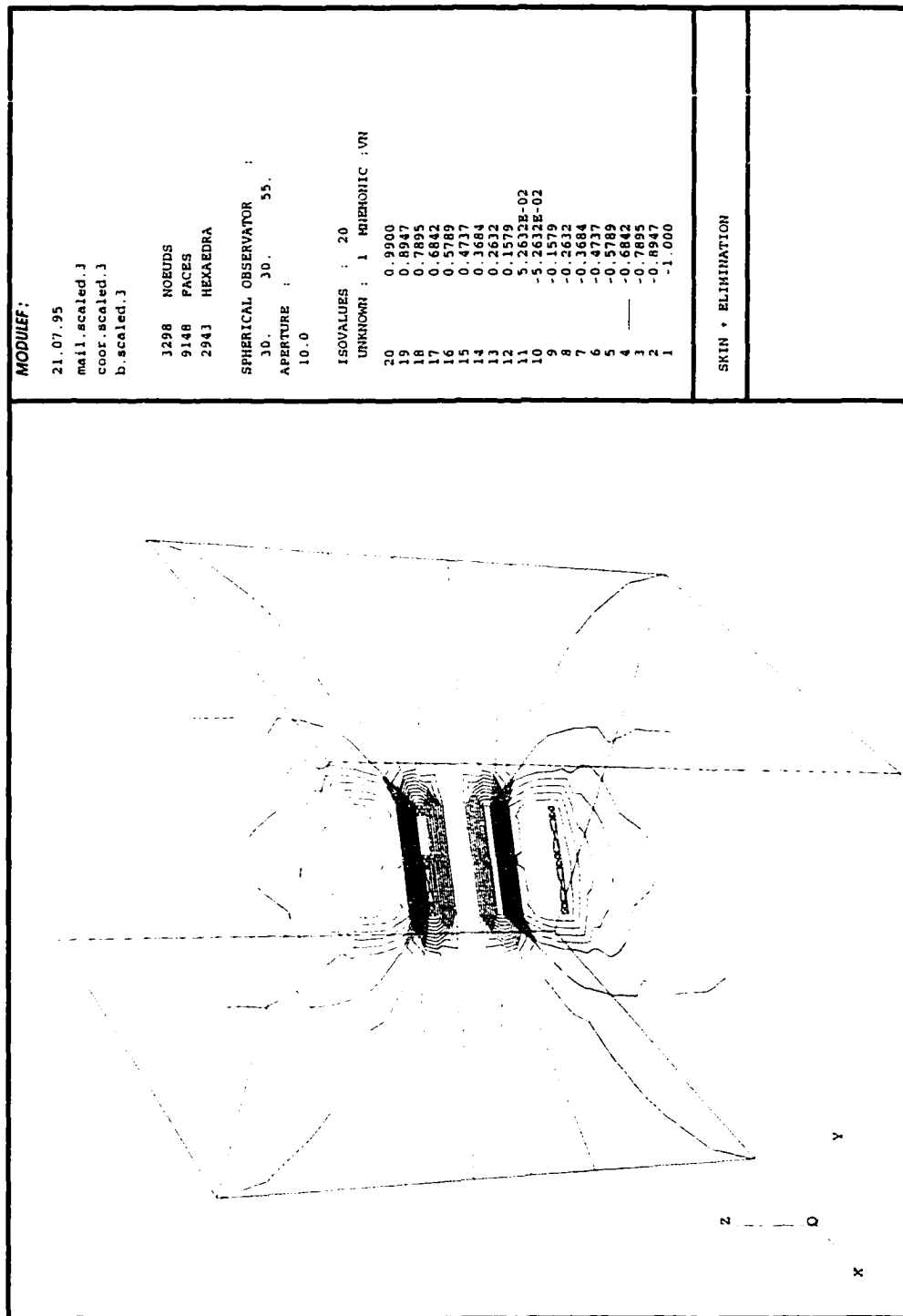
Figure 7.16. Isocontours of the potential ϕ at a vertical plane at an angle with the vias for a 2 × 2 × 3 stack of cells.
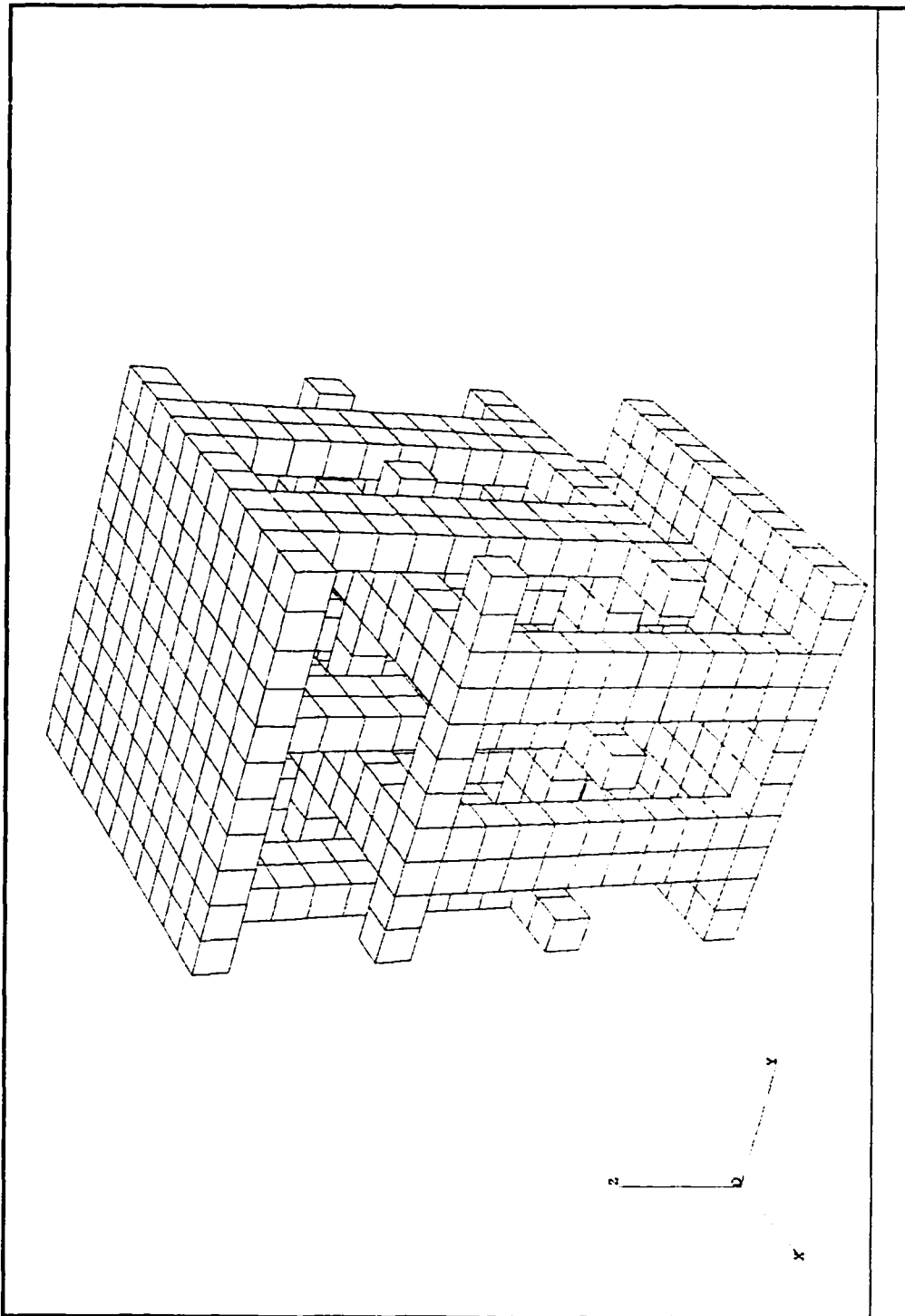
Figure 7.17. This multilayer capacitor is used to demonstrate that a a capacitor can be accurately modeled with a smaller mesh by using symmetry. This configuration is the reference for future comparisons.
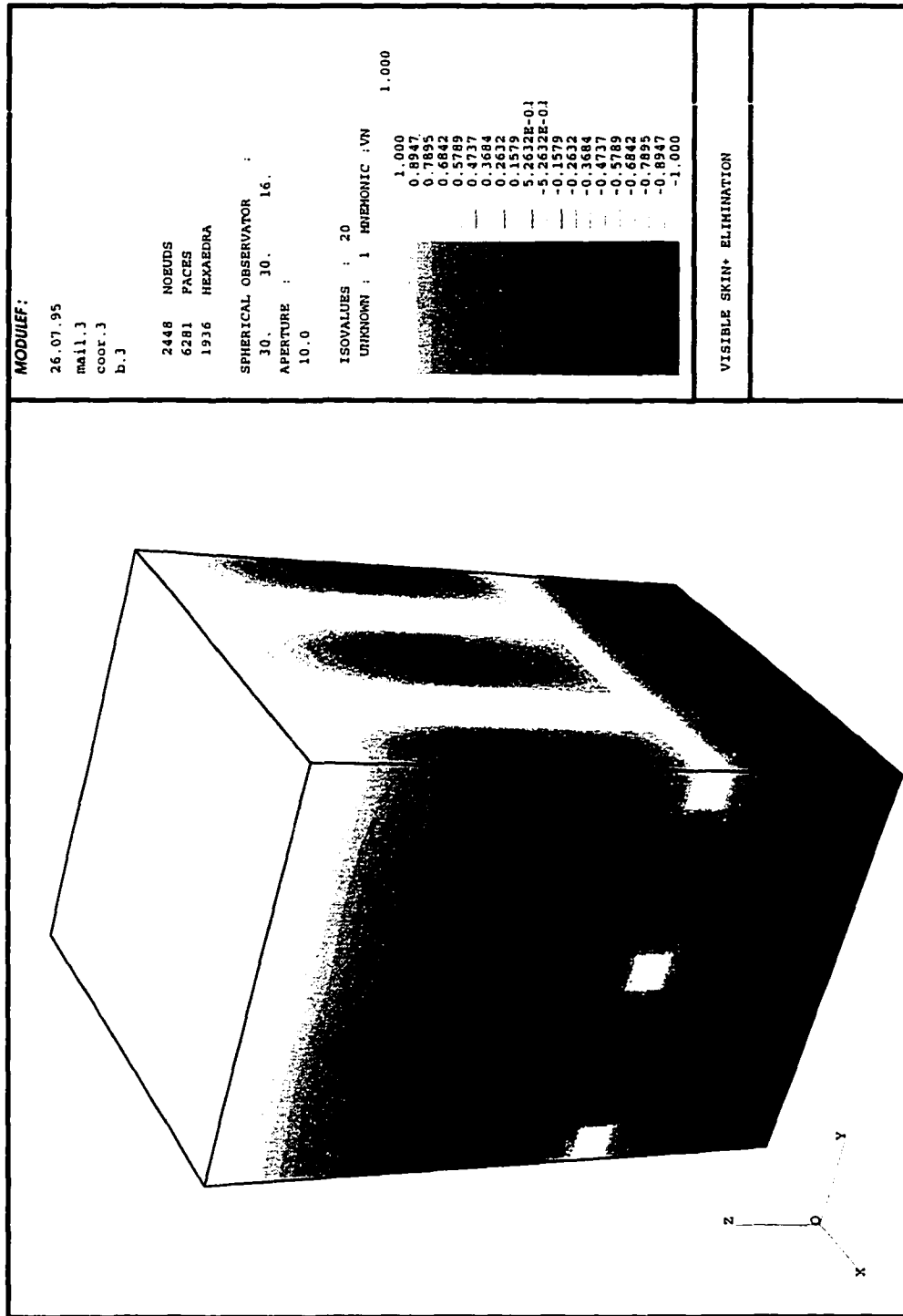
Figure 7.18. The voltage on the outer surface of the full-capacitor model provides a reference to check the accuracy of partial-capacitor models.
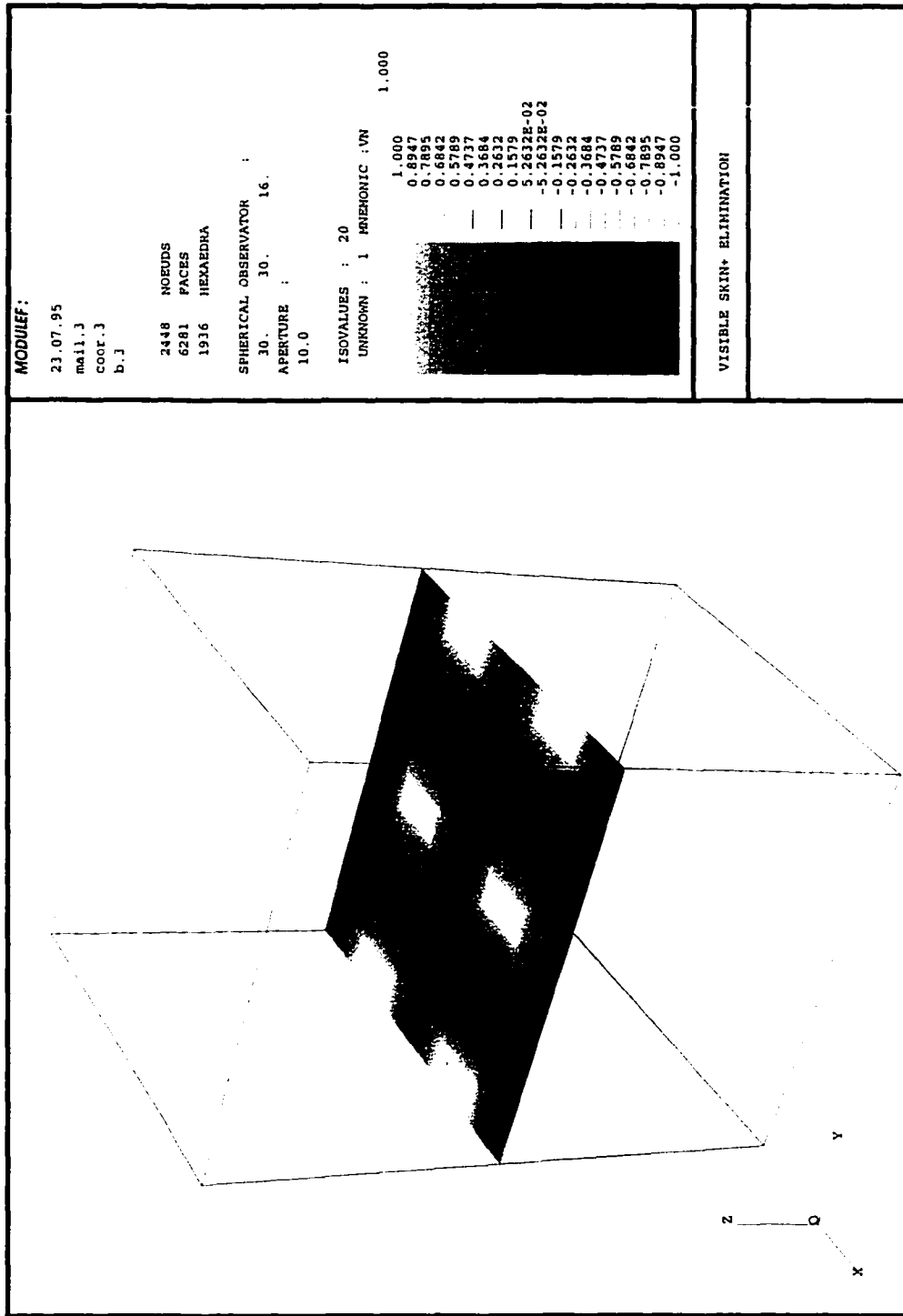
Figure 7.19. An x-y slice through the center of the capacitor is not a plane of symmetry. It provides a reference to check the accuracy of smaller symmetry-based models.
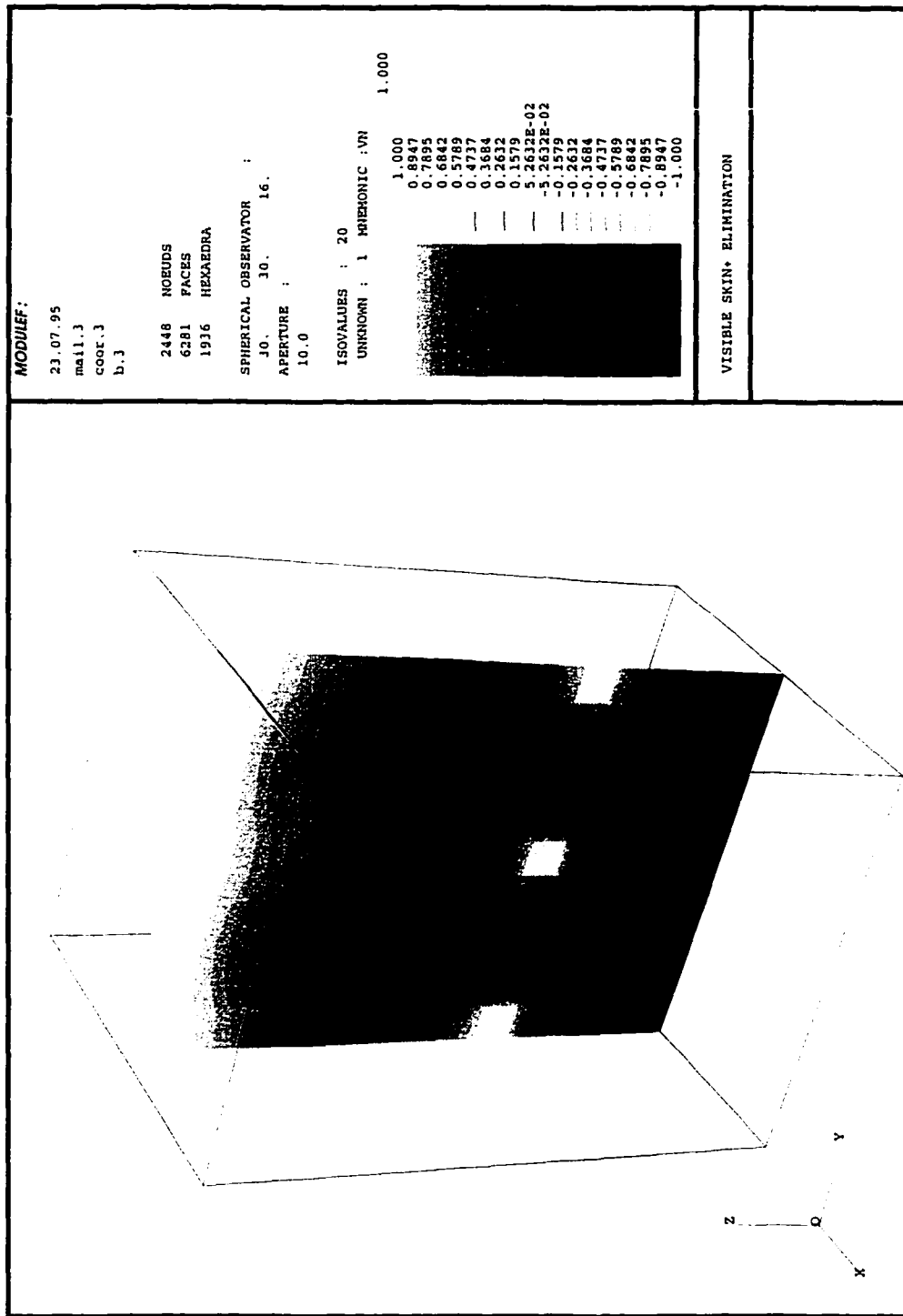
Figure 7.20. A y-z slice through the center of the capacitor marks a plane of symmetry. It also provides a reference to check the accuracy of smaller partial-capacitor models.

MODULEF:

26.07.95

mail.3
coor.3
b.3

2448   NOEUDS
6281   FACES
1936   HEXAEDRA

SPHERICAL OBSERVATOR
    30.   30.   16.
APERTURE :
10.0

ISOVALUES : 20
UNKNOWN : 1   MNEMONIC :VN

1.000
0.8947
0.7895
0.6842
0.5789
0.4737
0.3684
0.2632
0.1579
5.2632E-0%
-5.2632E-0%
-0.1579
-0.2632
-0.3684
-0.4737
-0.5789
-0.6842
-0.7895
-0.8947
-1.000

1.000

VISIBLE SKIN+ ELIMINATION
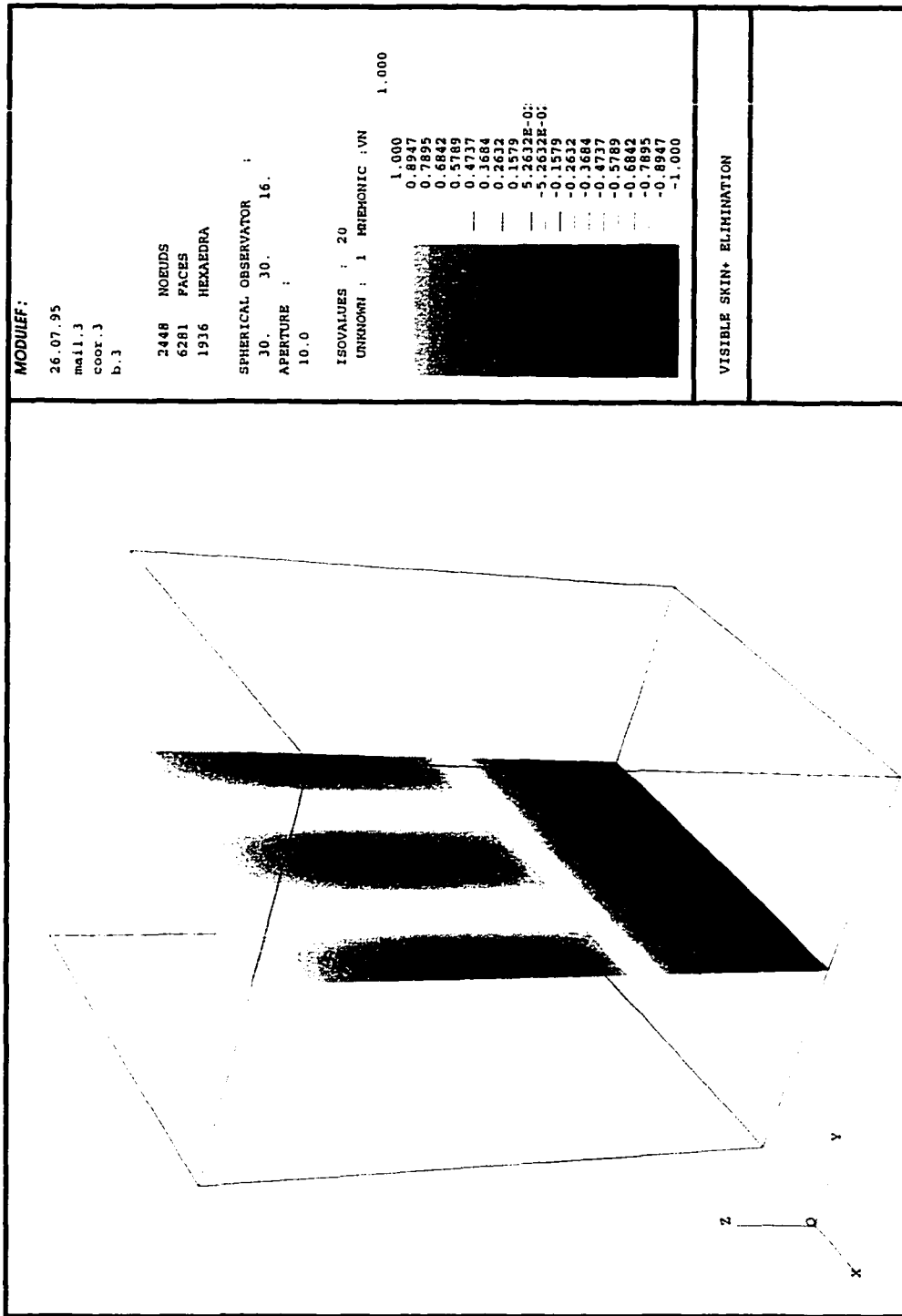
Figure 7.21. An x-z slice through the center of the capacitor marks a plane of symmetry. It also provides a reference to check the accuracy of smaller symmetry-based models.
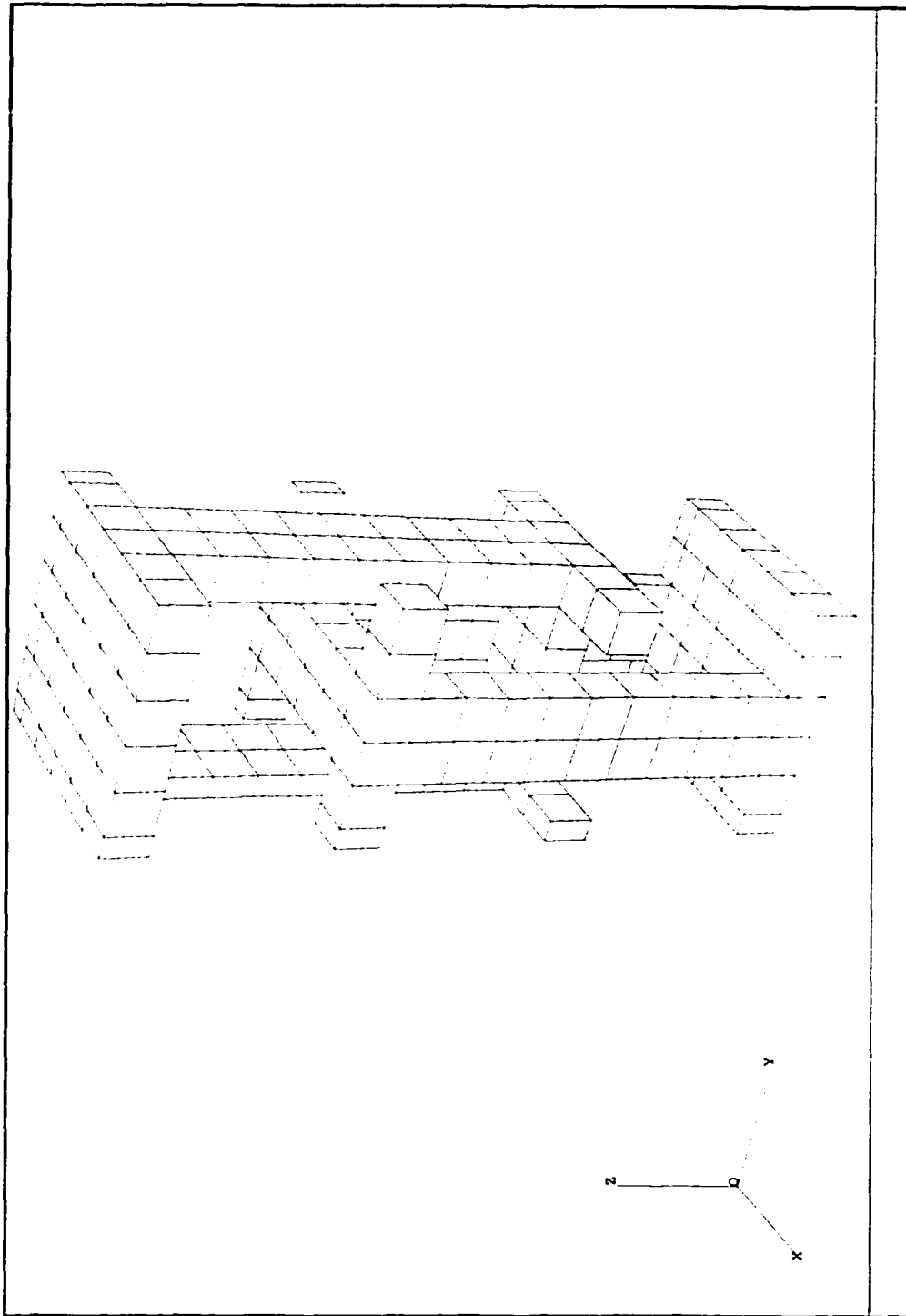
Figure 7.22. Symmetry allows the entire capacitor to be accurately represented by this quarter-capacitor. A zero-flux boundary condition is imposed on all external dielectric surfaces.
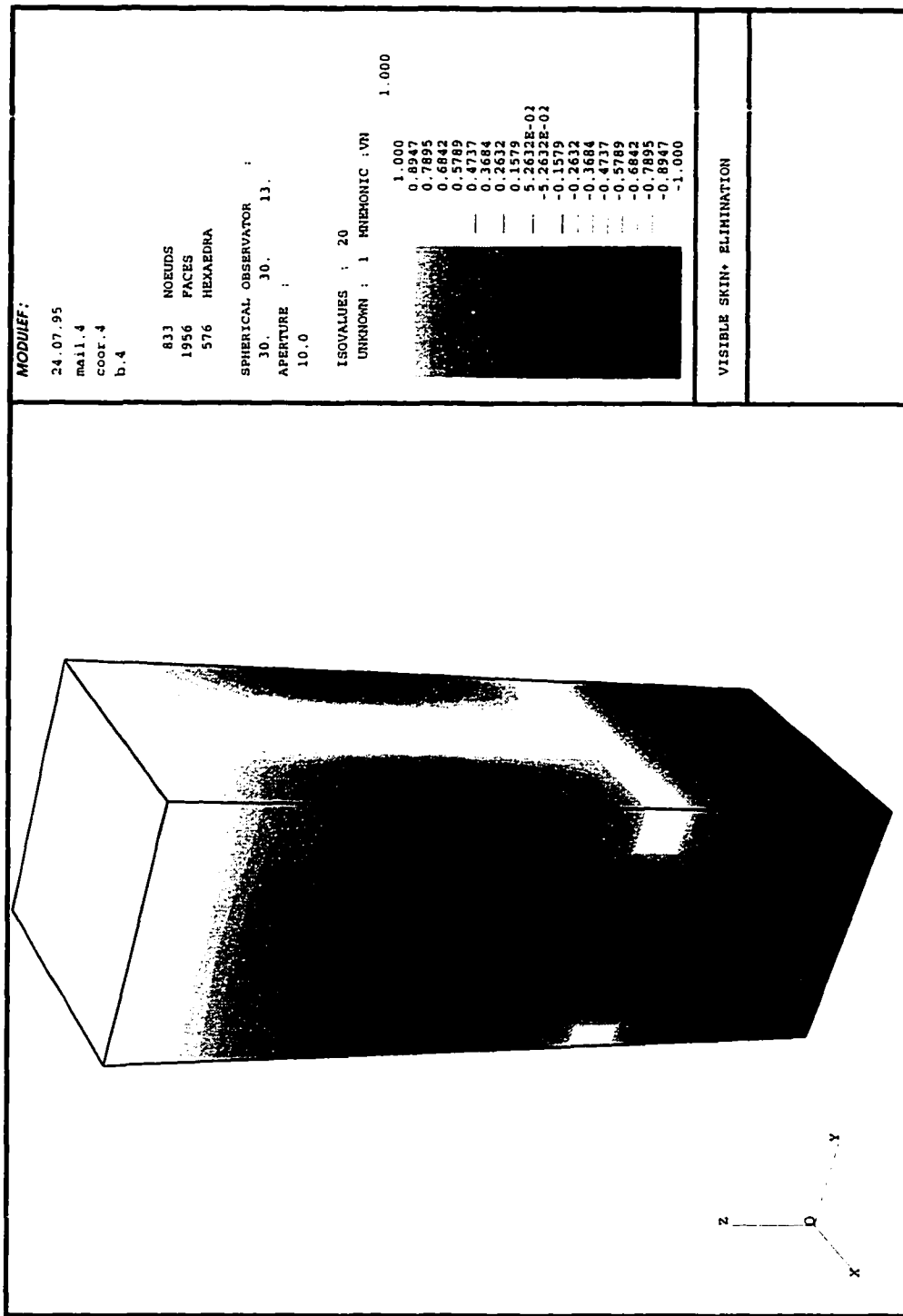
Figure 7.23. The voltages on the external surface of the quarter-capacitor can be compared to those on the surface of the whole capacitor.
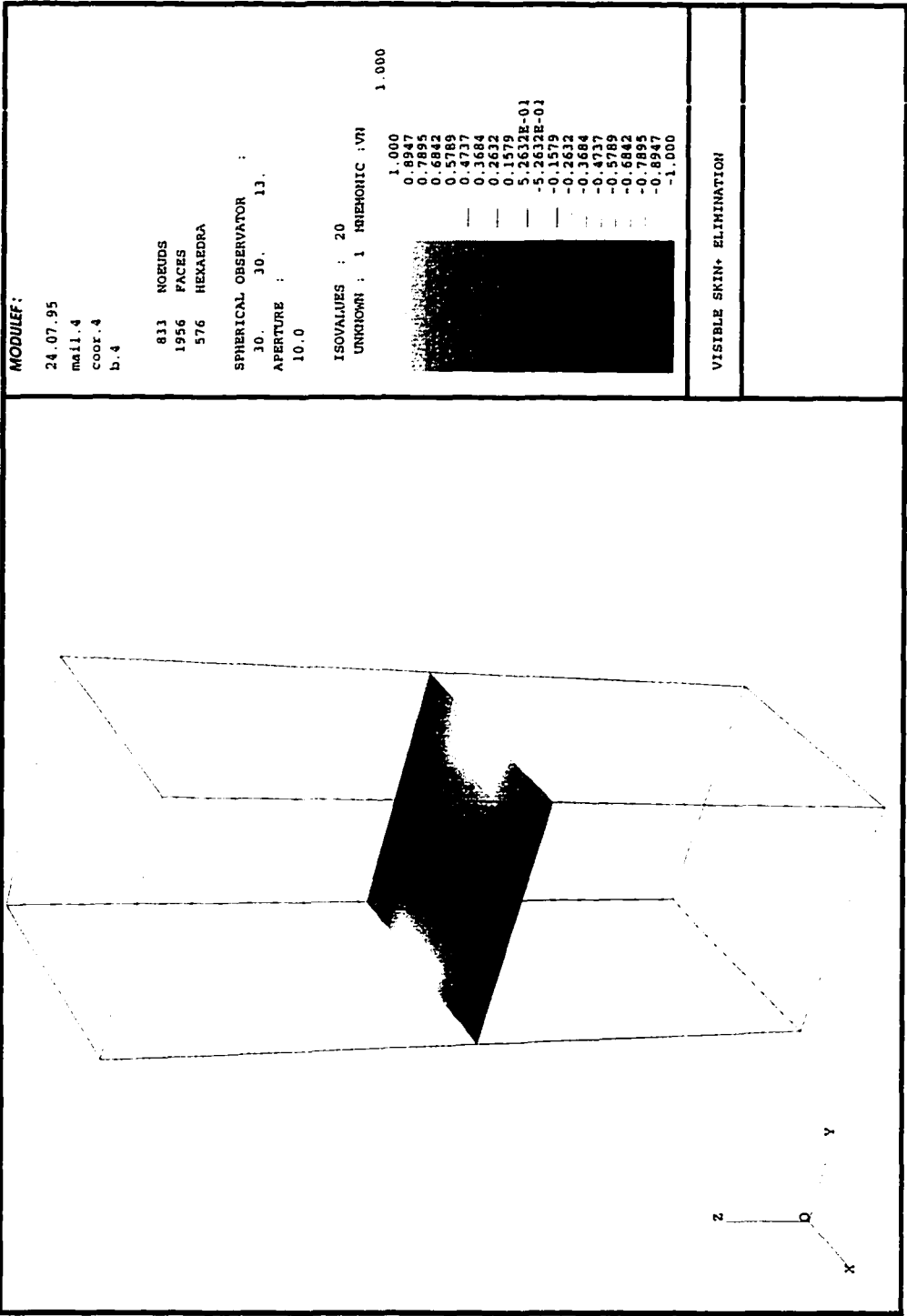
Figure 7.24. The voltages on this x-y slice through the center of the quarter-capacitor can be compared to those on the x-y slice through the center of the whole capacitor.
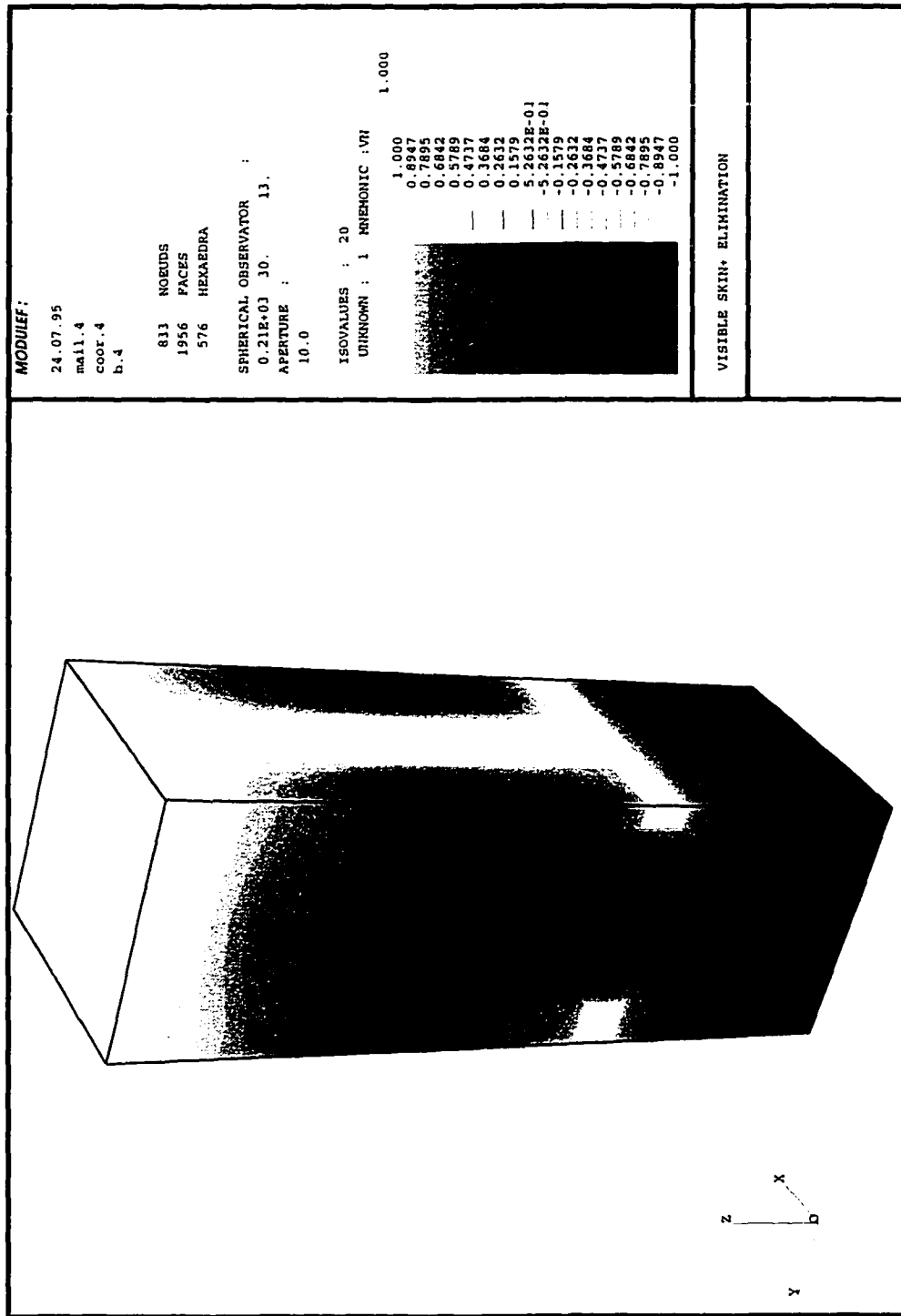
Figure 7.25. A rotation of the quarter-capacitor reveals x-z and y-z surfaces that correspond to the x-z and y-z slices through the center of the whole capacitor.
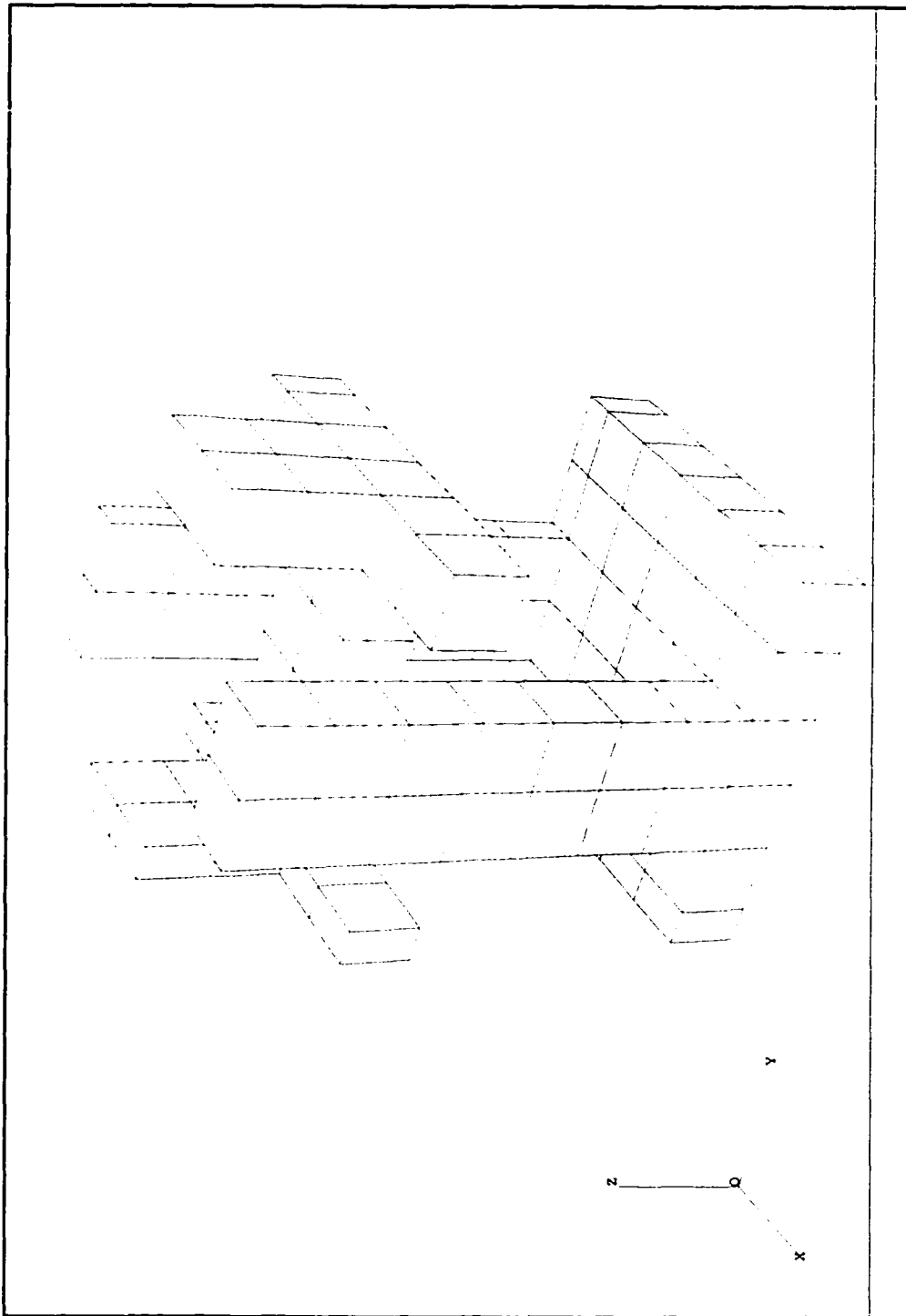
Figure 7.26. Since an x-y slice passing through the center of the whole capacitor is not a plane of symmetry, this eighth-capacitor model is mathematically invalid. We thus consider this an engineering approximation of the capacitor, impose a no-flux boundary condition on the vertical dielectric surfaces, and impose a flux of $\varepsilon \frac{\Delta V}{\Delta z}$ on the top dielectric surface, where Δz is the distance between electrodes.
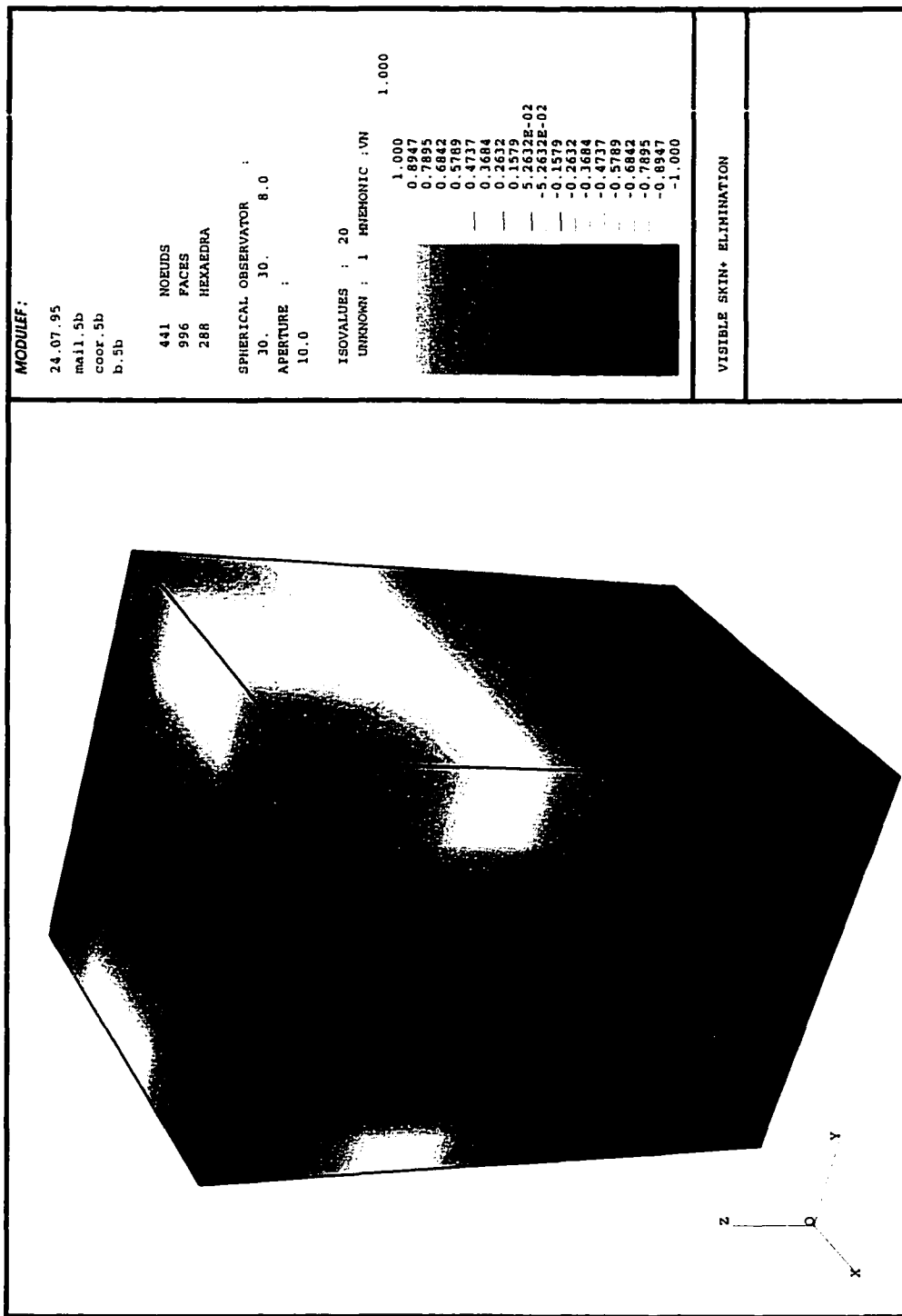
Figure 7.27. The voltages on the external surface of the eighth-capacitor can be compared to those on the surface of the whole capacitor.
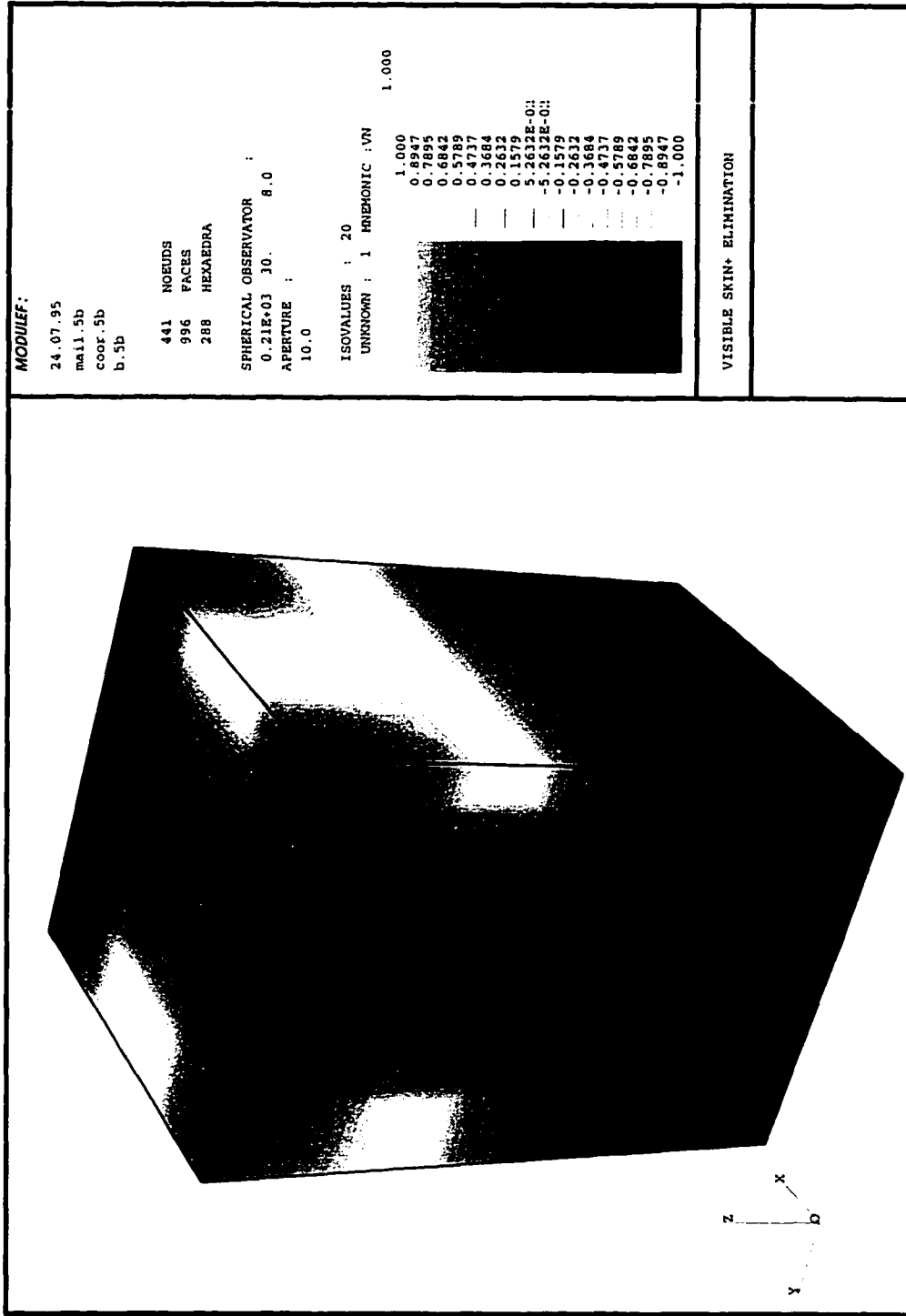
Figure 7.28. A rotation of the eighth-capacitor reveals x-y, x-z and y-z surfaces that correspond to the x-y, x-z and y-z slices through the center of the whole capacitor.

CHAPTER 8
BENCHMARK ELECTROMAGNETIC PROBLEMS

Coupled time-varying Finite Element (FE) solutions for three-dimensional geometries is implemented on the computer using FEAP (Zienkiewicz and Taylor [1989]) and MODULEF (Bernadou et al. [1986]). The solutions are computationally expensive: A transient solution requires four degrees of freedom (d.o.f.) per node, and a time-harmonic solution requires eight d.o.f. per node. Although the final banded matrix is stored using skyline (or profile) storage, the memory requirements for complex problems could exceed the computational resources available today. In this chapter, we explore solutions to benchmark electromagnetic problems listed in Table 8.1. The FE and analytical results are compared. We also study the effects of scaling Maxwell equations from the *SI* unit system to the *generalized* unit system.

In Section 8.1, we examine the electric field inside a lossy dielectric material. The transient and time-harmonic FE solutions are identical to the analytical solution. The lumped parameters, i.e., the resistance R and capacitance C are derived from the FE solution. In Section 8.2, we study the wave propagation inside a cube. Here, we use the magnetic vector potential $\mathbf{A}$. The Coulomb gauge is imposed via the penalty method. The choice of the penalty parameter is crucial to the accuracy of the solution.

As discussed in Chapter 6, effective solutions to coupled electromagnetic problems require the use of a multiple-scale technique. However, scaling does not improve the solution of uncoupled problems. To explain the effects of scaling, in Section 8.3, we study the solution to the electric and magnetic fields inside a simple parallel plate capacitor, where a dielectric material is sandwiched between two metal plates.

166

The dielectric material has zero conductivity and the metal electrodes have finite conductivity. The dimensions of the dielectric and metal plates are equal to that of a single cell in a MLCC proposed by Ngo [1990]. We conclude that scaling improves the condition number of the FE matrix in both transient and time-harmonic problems. However, only solutions to time-harmonic problems show a significant improvement in accuracy. We study the effects of mesh refinement on the choice of an optimal scaling factor α_z^{opt}. We conclude that α_z^{opt} is not significantly effected by mesh refinement. However, the scaling factor α_z^{opt} depends on the excitation frequency and the material properties.

The domain of influence of the electromagnetic fields extends to infinity. The capacitive power is primarily stored inside the dielectric material. The resistive power is stored inside the conductors. However, depending on the direction of the current inside the conductors, the inductive power could be stored, either, in between the electrodes, or in the air surrounding the capacitor. In Section 8.4, we compare the inductance obtained from the FE solution to the values from the simple formulae proposed by Grover [1973]. We conclude that a sufficiently large box of air surrounding the capacitor must be included in the FE model to obtain an accurate value for the inductance.

Note that most applications for a MLCC are in circuits that are excited by voltages, currents, or fields at a certain fixed frequency. Hence, we focus our attention on time-harmonic solutions.[27]

8.1. Lossy Dielectric Materials

The problem in Figure 8.1 consists of two lossy dielectric materials joined together. The first $1.0\,m \times 2.0\,m \times 2.0\,m$ (length $\times$ breadth $\times$ height) block has

---

[27] Non-linear material properties may demand a full transient solution.

Table 8.1. A synopsis of the numerical examples presented in this section.

Problem description	Potentials used	Type of solution	Remarks
The lossy dielectric material in a parallel plate capacitor. The electrodes are ignored. (Mac-Neal [1992])	ψ	Transient & time-harmonic.	Effects of a jump in material properties for both the transient & the time-harmonic problems. Compared with an analytical solution.
Wave propagation in a homogeneous non-conducting cube. Fields $\mathbf{E}$ and $\mathbf{B}$ are specified on the surface of the cube. (Monk [1993])	$\mathbf{A}$	Time-harmonic.	Effects of coupling between different components of $\mathbf{A}$. Effects of mesh size and the choice of Dirichlet or Neumann boundary condition. Both gauged and ungauged solution. Scaling not an issue. Compared with an analytical solution.
Parallel plate capacitor.	$\mathbf{A}$, ψ	Transient & time-harmonic.	Problem small enough to clearly understand the effects of scaling.
Two parallel electrodes with constant current. (Anand [1993])	$\mathbf{A}$, ψ	Time-harmonic.	Calculate R and L. Study the effects of mesh size and scaling. Compared with an analytical solution.

the material properties $\epsilon^{(1)} = \epsilon_0$, $\mu^{(1)} = \mu_0$, and $\sigma^{(1)} = 3.3333 \times 10^{-6}$ $1/(ohm-m)$,

and the second $1.0\ m \times 2.0\ m \times 2.0\ m$ block has the material properties $\epsilon^{(2)} = \epsilon_0$,

$\mu^{(2)} = \mu_0$, and $\sigma^{(2)} = 6.6666 \times 10^{-6}$ $1/(ohm-m)$.

8.1.1. FE Model

We limit the scope of the solution to only electric fields, and hence, we set the vector potential $\mathbf{A}$ to be zero. The transient electrodynamic problem can be stated

as follows.

> Given $\dot{\psi}_0 \equiv 0$, $\ddot{\psi}_0 \equiv 0$, $\dot{\psi}_0$ that satisfies initial conditions, find $\psi(\mathbf{x}, t)$ forall $\mathbf{x} \in \Omega$ and $t > 0$, such that
> $$\text{div}\,(\sigma\,\text{grad}\,\dot{\psi}) + \text{div}\,(\epsilon\,\text{grad}\,\ddot{\psi}) = 0 \quad \text{in } \Omega\,,$$
> $$\dot{\psi} = \dot{\psi}_a \quad \text{at Surfaces A \& C}$$
> $$\left(\sigma\,\text{grad}\,\dot{\psi} + \epsilon\,\text{grad}\,\ddot{\psi}\right) \cdot \hat{\mathbf{n}} = 0 \quad \text{on other exterior surfaces}\,.$$

The initial conditions $\dot{\psi}_0 := \dot{\psi}(\mathbf{x}, t = 0)$ is obtained by solving the following problem.

> Find $\dot{\psi}_0 \in \mathbf{R}$ such that
> $$\text{div}\,\left(\epsilon\,\text{grad}\,\dot{\psi}_0\right) = 0 \quad \text{in } \Omega\,,$$
> $$\dot{\psi}_0 = \dot{\psi}_{0_a} \quad \text{at Surfaces A \& C}$$
> $$\left(\epsilon\,\text{grad}\,\dot{\psi}_0\right) \cdot \hat{\mathbf{n}} = 0 \quad \text{on other exterior surfaces}\,.$$

Material properties ϵ and σ are piece-wise constant. The voltages $\dot{\psi}_a$ and $\dot{\psi}_{0_a}$ are specified at Surfaces A and C. The voltage V, the current I, the capacitance C and the R for the lumped parameter model is obtained from expressions in Chapter 5.

8.1.2. Equivalent Circuit Model: Transient Excitation

An equivalent circuit for the sandwich lossy dielectric is shown in Figure 8.2. The capacitance $C^{(1)}$ and the resistance $R^{(1)}$ that model the first block (the lossy dielectric material between Surfaces A and B) are given by

$$R^{(1)} = \frac{\text{(length)}}{\text{(area)(conductivity)}} = \frac{1}{4 \times 3.3333 \times 10^{-6}} = 7.5008 \times 10^4 \; ohm\,,$$

and

$$C^{(1)} = \frac{\text{(area)(permittivity)}}{\text{(length)}} = \frac{4 \times 8.85 \times 10^{-12}}{1} = 3.5400 \times 10^{-11} \; Farad\,.$$

Similarly, $C^{(2)}$ and $R^{(2)}$ that model the second block and are given by

$$R^{(2)} = \frac{1}{4 \times 6.6666 \times 10^{-6}} = 3.7498 \times 10^4 \; ohm\,,$$
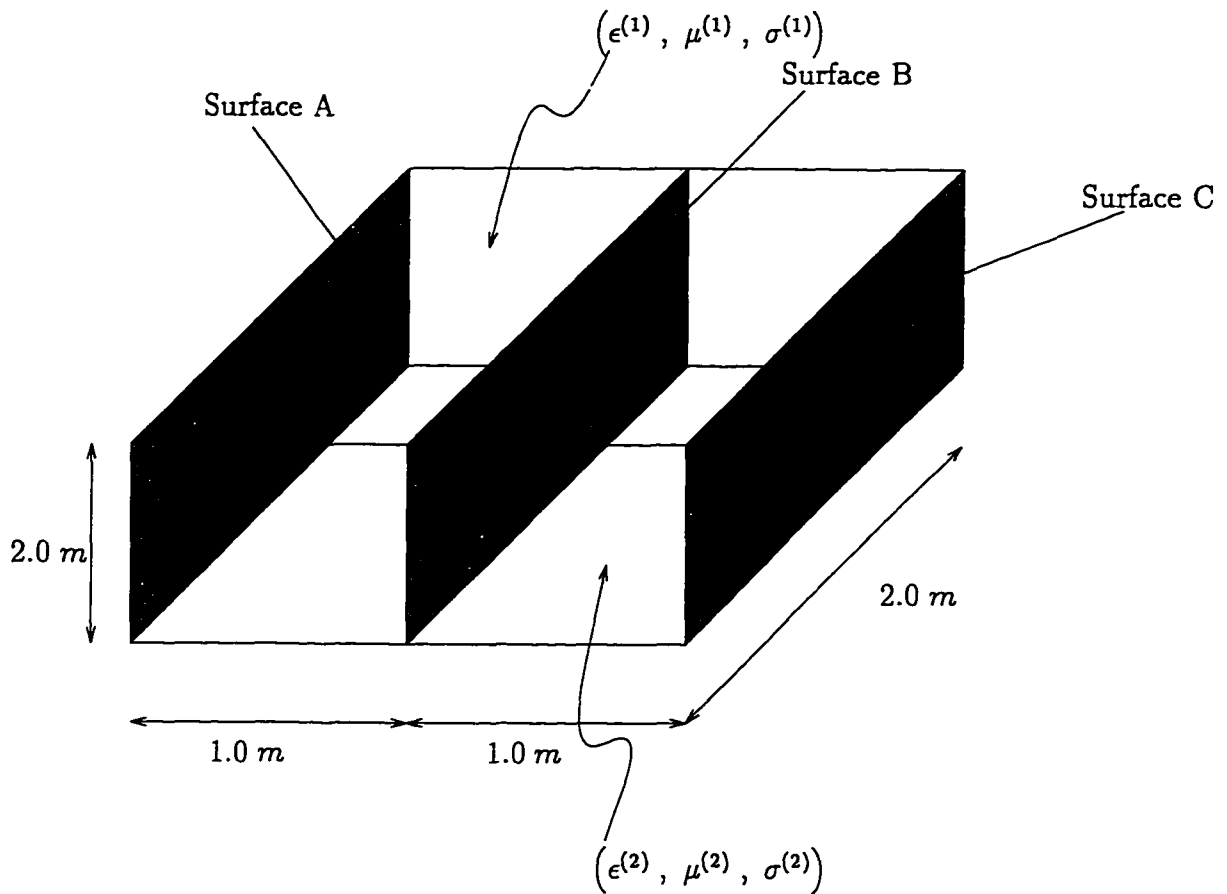
Figure 8.1. Lossy dielectric inside a capacitor. This is a sandwich of two lossy dielectric materials with different material properties. The plane at Surface B, divides the two materials.
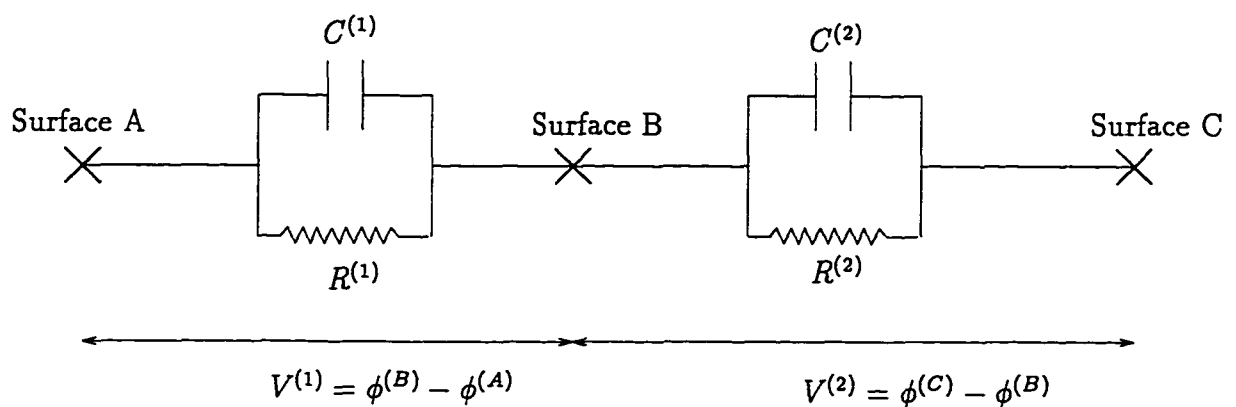
Figure 8.2. An equivalent circuit model for a lossy dielectric.

and

$$C^{(2)} = \frac{4 \times 8.85 \times 10^{-12}}{1} = 3.5400 \times 10^{-11} \ Farad \ .$$

The total voltage drop V between Surfaces A and C is split into two parts $V^{(1)}$ and $V^{(2)}$, where $V = V^{(1)} + V^{(2)}$. For a problem with a specified voltage V, we can express the current I flowing through the circuit and the voltages $V^{(1)}$ and $V^{(2)}$ as follows.

$$V^{(1)} \ = \ \frac{1}{f_1} \int_{t_0}^{t} f_1 f_2 \ dt \ , \tag{8.1}$$

$$V^{(2)} \ = \ V \ - \ V^{(1)} \ , \tag{8.2}$$

where

$$f_1 \ := \ \frac{C^{(2)}}{C^{(1)} + C^{(2)}} \frac{dV}{dt} \ + \ \frac{1}{R^{(2)} \left(C^{(1)} + C^{(2)} \right)} \ , \tag{8.3}$$

$$f_2 \ := \ e^{\left(f_3 \ t \right)} \ , \tag{8.4}$$

$$f_3 \ := \ \frac{\left(R^{(1)} + R^{(2)} \right)}{R^{(1)} R^{(2)} \left(C^{(1)} + C^{(2)} \right)} \ , \tag{8.5}$$

and the total current I is given by

$$I = C^{(1)} \frac{d \ V^{(1)}}{dt} + \frac{1}{R^{(1)}} V^{(1)} = C^{(2)} \frac{d \ V^{(2)}}{dt} + \frac{1}{R^{(2)}} V^{(2)} \ . \tag{8.6}$$

In the ensuing example we specify a voltage of

$$V = V_0 \ \cos \omega \ t \ , \tag{8.7}$$

between Surfaces A and C. From the above expressions we obtain the voltage between Surfaces A and B to be

$$V^{(1)} \ = \ \frac{C^{(1)} V_0 \omega}{\left(C^{(1)} + C^{(2)} \right)} \frac{\left(f_3 \sin \omega \ t - \omega \cos \omega \ t \right)}{f_3^2 + \omega^2}$$

$$+ \frac{V_0}{R^{(2)} \left(C^{(1)} + C^{(2)} \right)} \frac{\left(f_3 \cos \omega \ t + \omega \sin \omega \ t \right)}{f_3^2 + \omega^2}$$

$$-V_0 \frac{\left(\frac{C^{(1)}}{(C^{(1)}+C^{(2)})}\omega^2 + \frac{1}{R^{(2)}(C^{(1)}+C^{(2)})}f_3^2\right)}{f_3^2 + \omega^2}e(-f_3\,t)\,, \qquad (8.8)$$

and the current I is given by substituting the expression for $V^{(1)}$ in (8.6).

8.1.3. Equivalent Circuit Model: Time Harmonic Excitation

For the time harmonic problem, we can express the complex current $\bar{I}$ and voltages $\bar{V}^{(1)}$ and $\bar{V}^{(2)}$ in terms of the complex voltage $\bar{V}$. The impedance due to the first block is

$$\bar{Z}^{(1)} = \frac{R^{(1)}}{i\omega R^{(1)}C^{(1)} + 1}$$

and the impedance due to the second block is

$$\bar{Z}^{(2)} = \frac{R^{(2)}}{i\omega R^{(2)}C^{(2)} + 1}\,.$$

The total impedance $\bar{Z} = \bar{Z}^{(1)} + \bar{Z}^{(2)}$ is related to the current $\bar{I}$ as follows

$$\bar{I} = \frac{\bar{V}}{\bar{Z}} = \frac{\bar{V}}{\bar{Z}^{(1)} + \bar{Z}^{(2)}}\,.$$

The voltage is each block is given by

$$\bar{V}^{(1)} = \bar{I}\,\bar{Z}^{(1)} = \bar{I}\,\frac{R^{(1)}}{i\omega R^{(1)}C^{(1)} + 1}\,,$$

and

$$\bar{V}^{(2)} = \bar{I}\,\bar{Z}^{(2)} = \bar{I}\,\frac{R^{(2)}}{i\omega R^{(2)}C^{(2)} + 1}\,.$$

8.1.4. Numerical Results

The domain in Figure 8.1 is divided into eight elements: The first four elements correspond to the first block and the next four elements correspond to the second block. There are 27 nodes. The transient behavior of the voltages and the current obtained from the finite element model is compared to the analytical solution in Figure 8.3. The mesh and the electric field $\mathbf{E}$ at time $t = 1.0 \times 10^{-4}$ are given in Figure 8.4. The time-harmonic FE solution is compared to the circuit model below.

Quantity	FE model	Circuit model
Voltage $\bar{V}^{(1)}$	$6.64854 \times 10^{-1} - 1.75064 \times 10^{-2}i$	$6.64850 \times 10^{-1} - 1.75060 \times 10^{-2}i$
Current $\bar{I}$	$8.90075 \times 10^{-6} + 1.17878 \times 10^{-6}i$	$8.9008 \times 10^{-6} + 1.1787 \times 10^{-6}i$

The variation in the scalar potential ψ is piece-wise linear and so are the FE basis functions (interpolation), and hence, a near perfect model for the lossy dielectric.

8.2. Wave Propagation in a Cube

The problem of determining the propagation of a wave inside a cube tests the applicability of the present finite element formulation to time-harmonic problems. We solve for the potentials $\bar{A}$ and $\bar{\psi}$. The fields are computed from numerical derivatives of the potentials. As the interpolation functions for the potentials are piece-wise linear, we have the derivatives to be constant inside an element. The errors in the field quantities decrease with mesh refinement. The Coulomb gauge does not effect the accuracy when the potentials (Dirichlet boundary condition) $\bar{A}$ and $\bar{\psi}$ are specified on the exterior boundary, however, Coulomb gauge is required to model the cube when the fields (Neumann boundary condition) $\bar{E}$ and $\bar{B}$ are specified at the exterior boundary.

The accuracy of the results are comparable to the solutions using special elements such as the edge elements (Monk [1992]). However, as the focus of the present work is to model the global properties (the lumped parameters) of the device, we choose not to employ any special elements to treat material interfaces.

Consider a cube $\Omega := [0,1]^3$ that is subjected to a time harmonic electric and magnetic field at the boundary. The material inside is a dielectric with zero conductivity, with the material properties $\epsilon = 1$, $\mu = 1$, $\sigma = 0$. We choose a

plane wave solution for the cube to be

$$
\begin{aligned}
\bar{\mathbf{E}} &= \mathbf{a}\, \exp\left(-i\omega\mathbf{k}\cdot\mathbf{x}\right) &&\in \mathbf{C}^3\,, \\
\bar{\mathbf{B}} &= \left(\mathbf{k}\times\mathbf{a}\right)\exp\left(-i\omega\mathbf{k}\cdot\mathbf{x}\right) &&\in \mathbf{C}^3\,,
\end{aligned}
\tag{8.9}
$$

where the vectors $\mathbf{a}\in\mathbf{R}^3$ and $\mathbf{k}\in\mathbf{R}^3$ are defined to be such that $|\mathbf{a}|=1$ and $|\mathbf{k}|=1$, with $\mathbf{a}\cdot\mathbf{k}=0$. The angular frequency of the wave is ω and the wave number is given by $|\mathbf{k}|$. A set of potentials that corresponds to the fields in (8.9) are

$$
\begin{aligned}
\bar{\mathbf{A}} &= -\frac{\mathbf{a}}{i\omega}\,\exp\left(-i\omega\mathbf{k}\cdot\mathbf{x}\right) &&\in \mathbf{C}^3\,, \\
\bar{\psi} &= 0 &&\in \mathbf{C}\,.
\end{aligned}
\tag{8.10}
$$

Note that this above set of potentials is one of the infinite choices possible. The above choice satisfies the Coulomb gauge $\operatorname{div}\bar{\mathbf{A}}=\bar{0}$.

In our test example we choose

$$
\begin{aligned}
\mathbf{a} &= \frac{2}{\sqrt{14}}\left(1.0\,\hat{\mathbf{e}}_1 + 1.5\,\hat{\mathbf{e}}_1 + 0.5\,\hat{\mathbf{e}}_1\right)\,, \\[2mm]
\mathbf{k} &= \frac{2}{\sqrt{13}}\left(-1.5\,\hat{\mathbf{e}}_1 + 1.0\,\hat{\mathbf{e}}_1 + 0.0\,\hat{\mathbf{e}}_1\right)\,.
\end{aligned}
\tag{8.11}
$$

We obtain the potentials and the field quantities inside the dielectric material by the following two methods.

Using Dirichlet boundary condition: The potentials $\bar{\mathbf{A}}$ and $\bar{\psi}$ in (8.10) are imposed on the exterior surface $(\partial\Omega)$.

Using Neumann boundary condition: The fields $\bar{\mathbf{E}}$ and $\bar{\mathbf{B}}$ in (8.9) are imposed on the exterior surface $(\partial\Omega)$.

The fields are obtained inside the dielectric via postprocessing. The fields are then compared to the exact solution in (8.9). The L^2 norm is used to measure the

error in the approximation. The L^2 norm of the real part of the electric field $\mathbf{E}_r$ over the volume Ω is defined to be

$$\| \mathbf{E}_r \|_{L^2} := \int_\Omega (\mathbf{E}_r \cdot \mathbf{E}_r) \ d\Omega \ . \qquad (8.12)$$

If $\Delta\mathbf{E}_r$ is the error between the FE solution and the exact solution, then the L^2 norm of the error in the real part of the electric field is

$$\| \Delta\mathbf{E}_r \|_{L^2} := \int_\Omega (\Delta\mathbf{E}_r \cdot \Delta\mathbf{E}_r) \ d\Omega \ . \qquad (8.13)$$

Similarly we define the errors in the remaining field quantities.

The cube in Figure 8.5 is meshed using 8-noded brick elements with three different meshes that are shown in Figure 8.6. The coarse mesh has 8 elements and 27 nodes, the second mesh has 16 elements and 125 nodes, and the most refined mesh has 512 elements and 729 nodes. The number of degrees of freedom increase with the number of nodes in the mesh. The final size of the matrix in the FE solution for the three different meshes is given in Table 8.2. For the FE solution obtained using a Dirichlet boundary condition, the contour and vector plots on a slice for the real and imaginary parts of the electric field are given in Figures 8.7, 8.8, 8.9, and 8.10. The variations of the electric field on a horizontal line in the slice plane are given in Figures 8.11 and 8.12. Figure 8.13 plots the magnitude of the errors in the field quantities along the line. The global errors in the field quantities decrease as the mesh is refined; see Figure 8.14. The errors are comparable to the solutions obtained by Monk [1992]. The solution is not sensitive to the Coulomb gauge.

For the FE solution obtained using a Neumann boundary condition, the solution is very sensitive to the Coulomb gauge. Figure 8.15 shows the decrease in the L^2-norm of the error in the real part of the electric field with increasing values for

Table 8.2. The size of the matrix, i.e., number of simultaneous linear equations to be solved in the FE problem. The meshes are given in Figure 8.6.

Mesh	Number of Nodes	Number of equations	
		Dirichlet b.c.	Neumann b.c.
1	27	8	208
2	125	216	992
3	729	2744	5824

the penalty parameter. The penalty term is imposed using reduced integration. The $\operatorname{div}\bar{A}$ also decreases with increasing values for the penalty parameter. Figure 8.16 shows that the values of the electric field along a line parallel to the $\hat{e}_1$-axis passing through the center of the cube $(0.5, 0.5, 0.5)$. The FE solution approaches the exact solution as the penalty parameter is increased. However, a penalty parameter greater than 1×10^2 does not significantly improve the solution. Note that very high penalty parameters will over constrain the solution, and force it to be zero everywhere. Moreover, with the use of reduced integration, large penalty parameters lead to ill-conditioned matrices.

8.3. Effects of Scaling: Study a Parallel Plate Capacitor

We apply the multiple-scale technique discussed in Chapter 6 to a simple parallel plate capacitor shown in Figure 8.18. The dimensions of the parallel plate capacitor are equal to the single cell in a MLCC. The parallel plate capacitor considered here does not have the positive and negative vias of the single cell; the top and bottom electrodes are flat rectangular plates unlike the single cell that was shown in Figure 7.3. The electrodes have a footprint of $0.635cm \times 0.635cm$, and are

$1.5\mu m$ thick. The dielectric in between is $15\mu m$ thick. The material properties for the electrode and the dielectric are listed in Table 7.1.

A voltage is applied at the top plane of the top electrode and the bottom plane of the bottom electrode. The electric and magnetic fields are determined by solving the coupled electromagnetic problem, i.e., the vector potential **A** and the scalar potential ψ are solved simultaneously. The matrix equation (4.53) is solved for each time step in the transient solution. The entries in the matrices are functions of the time step size Δt_{n+1}. Similarly, the matrix equation (4.67) is solved for each frequency to determine the time-harmonic solution. The entries in the matrices are functions of the angular frequency ω.

As explained in Chapter 6, the use of the multiple-scale technique reduces the condition number of the FE matrices thereby increasing the accuracy of the solution. We examine the effect on the condition number with the changing mesh size. The capacitor shown in Figure 8.18 is discretized using four different meshes: The number of nodes for the four meshes shown in Figure 8.18 range from 20 nodes for mesh (a) to 245 nodes for mesh (d). Table 8.3 lists the number of nodes, the number of elements, and the unconstrained degrees of freedom in the FE solution. Figure 8.19 shows the effect of changing the mesh size[28] and varying the scaling factor α_z for the transient and the time-harmonic solutions, respectively. We observe that the mesh size does not significantly effect the choice of the optimal scaling factor α_z^{opt}. We conclude for this particular example that $\alpha_z^{opt} \approx 10^3$ for the transient and time-harmonic solutions. Hence, in practice, we could choose the optimal scaling factor α_z^{opt} from a coarse mesh and use it for a refined mesh. We also observe that the

---

[28] The mesh size is determined by the size of the smallest element in the mesh. Here, the radius of the smallest sphere that encloses completely an element is used to measure the size of an element. In general, more the number of nodes, smaller the size of the element, and smaller the mesh size.

condition number increases with an increase in the number of degrees of freedom in the solution. The condition number shows a significant improvement from the *SI* system of units to the *generalized* system of units for both the transient and the time-harmonic solutions; see Table 8.4 for details. The relative error improves significantly for the time-harmonic solution: For mesh (d) we observe in Table 8.4 that the relative error improves from $\mathcal{O}(10^{-2})\%$ in the *SI* unit system to $\mathcal{O}(10^{-8})\%$ in the optimal *generalized* unit system. However, the relative error does not significantly improve for the transient solutions. The reason being that the time-harmonic problem demands a solution to an unsymmetric matrix, as opposed to a symmetric matrix for a transient problem.

In Figure 8.20, we examine the effect of change in the time step size for transient solutions, and the change in frequency for the time harmonic solutions. It is evident that the optimal scaling factor α_x^{opt} depends on the time step size and the frequency. For transient solutions, at smaller time step size, numerical difference between the the coefficients $(1/\mu)$, $\sigma/\Delta t_{n+1}$, and $\epsilon/\Delta t_{n+1}^2$ of the FE matrices (6.22) are smaller, and we obtain smaller condition numbers. Similarly, for time-harmonic solutions, at higher frequencies, the numerical difference between the the coefficients $(1/\mu)$, $\sigma\omega$, and $\epsilon\omega^2$ of the FE matrices (6.25) are smaller, and we obtain smaller condition numbers. Moreover, the optimal scaling factor α_x^{opt} changes with frequency. For example, in a time-harmonic solution, $\alpha_x^{opt} \approx 10^1$ for $\omega = 10^5$, and $\alpha_x^{opt} \approx 10^3$ for $\omega = 10^9$. The effect of frequency on the numerical conditioning of a solution to Maxwell equations is discussed in Chapter 9.

The properties of the material, i.e., the conductivity σ, permittivity ϵ, and the permeability μ effects the choice of an optimal scaling factor. Figure 8.21 shows the effect of changing the conductivity with the *SI* unit system and the *generalized* unit system. It is evident, that a higher conductivity and lower frequency, degrade the

Table 8.3.   The specifications of the different meshes used to solve the parallel plate capacitor problem.   The different meshes are shown in Figure 8.18.

Mesh	Number of nodes	Number of elements	Degrees of freedom	
			Transient	Time-harmonic
(a)	20	4	64	128
(b)	45	16	144	288
(c)	125	64	400	800
(d)	245	144	784	1568

Table 8.4.   The condition number and relative error for the parallel plate capacitor problem.   The different meshes are shown in Figure 8.18.

Mesh	SI unit system		$Generalized$ unit system $(\alpha_z = 10^3)$	
	Condition number	Relative error	Condition number	Relative error
Transient solutions				
(a)	8.75×10^{18}	2.40×10^{-17}	9.10×10^8	1.05×10^{-17}
(b)	1.15×10^{19}	1.95×10^{-17}	1.22×10^9	1.95×10^{-17}
(c)	1.70×10^{19}	1.43×10^{-17}	1.27×10^9	1.02×10^{-17}
(d)	1.80×10^{19}	1.53×10^{-17}	1.34×10^9	1.41×10^{-17}
Time-harmonic solutions				
(a)	5.21×10^{20}	2.17×10^{-5}	3.27×10^{12}	1.05×10^{-11}
(b)	2.74×10^{21}	6.26×10^{-5}	4.39×10^{12}	9.48×10^{-11}
(c)	2.40×10^{20}	7.08×10^{-5}	4.58×10^{12}	1.96×10^{-10}
(d)	2.55×10^{20}	8.04×10^{-5}	4.52×10^{12}	2.06×10^{-10}

condition of the solution in the SI unit system and the use of the multiple-scaling technique is imperative to avoid numerical ill-conditioning.

8.4. Inductance of Two Metal Electrodes

The computation of the inductance of two parallel conducting plates provides a comparison between the simple formula for inductance developed by Grover [1973] and the FE results. The formula for inductance developed by Grover [1973] is used by Anand [1993] to compute the inductance of the entire MLCC. The geometry of the two parallel conducting plates is shown in Figure 8.23. The length l of each plate is 0.635×10^{-2} m, and the breadth b is 0.635×10^{-2} m. The thickness t is 1.5×10^{-6} m. The plates are separated a distance $h = 15 \times 10^{-6}$ m.

Remark 8.1. The behavior of the magnetic field $\mathbf{B}$ around an infinitely long straight wire carrying current provides an insight into the behavior of the magnetic field around the electrodes of a capacitor. Wangsness [1986, pp. 242–243] shows that the magnetic field decays as an inverse function of distance from the conductor. This suggests that bigger the size of the surrounding box of air, better the approximation for the magnetic field, and hence a more accurate value for the inductance. As computational resources limit the size of the box of air. The inverse relationship between the magnetic field and the distance from the conductor suggests that much of the magnetic field is concentrated near the capacitor, and hence, we expect only small errors in the value of the inductance. ∎

The formula for the self-inductance L of each plate for a uniform distribution of current is given by

$$L = 2l \left[\log_e \left(\frac{l}{d} + \sqrt{1 + \frac{l^2}{d^2}} \right) + \frac{d}{l} \right] \quad n\,Henry \;, \qquad (8.14)$$

where the Geometric Mean Distance (GMD) d is

$$d = 0.22313\,b \quad cm\;. \qquad (8.15)$$

The mutual-inductance $\mathfrak{M}$ between the two plates is given by the formula (8.14), where L is replaced by $\mathfrak{M}$ and the GMD d is calculated as follows.

$$\log_e (d) = \frac{h^2}{b^2} \log_e(h) + \frac{1}{2} \left(1 - \frac{h^2}{b^2}\right) \log_e \left(h^2 + b^2\right) + 2\frac{h}{b} \tan^{-1} \left(\frac{h}{b}\right) - \frac{3}{2}, \quad (8.16)$$

where h is the distance separating the two plates. Note that the units for distances used in the above inductance formulas must be in $centi-meter$, and the inductance is obtained in $nano - Henry$.

The total inductance of the two conducting plates is a combination of the self-inductance of each plate and the mutual-inductance between the two plates. The total inductance is calculated as follows. The matrix equation

$$\begin{bmatrix} \bar{Z}_{1,1} & \bar{Z}_{1,2} \\ \bar{Z}_{2,1} & \bar{Z}_{2,2} \end{bmatrix} \left\{ \begin{matrix} \bar{I}_1 \\ \bar{I}_2 \end{matrix} \right\} = \left\{ \begin{matrix} V \\ V \end{matrix} \right\}, \quad (8.17)$$

is solved to determine the currents $\bar{I}_1$ and $\bar{I}_2$ in each plate, where V is the voltage applied to the ends of the plates. The entries in the impedance matrix are as follows.

$$\bar{Z}_{i,i} = R + iwL \quad \text{for } i = \{1,2\} ,$$

$$\bar{Z}_{i,j} = iw\mathfrak{M} \qquad \text{for } i, j = \{1,2\} \text{ and } i \neq j , \quad (8.18)$$

where the resistance of each plate is given by

$$R = \frac{l}{\sigma\, t\, b} . \quad (8.19)$$

The total impedance of the two conducting plates is

$$\bar{Z} = \frac{V}{(I_1 + I_2)} , \quad (8.20)$$

and the total inductance is

$$L_{total} = \frac{Z_i}{\omega} , \quad (8.21)$$

and the total resistance is

$$R_{total} = Z_r , \quad (8.22)$$

where $\bar{Z} = Z_r + iZ_i$. The numerical values for the total resistance and inductance in the second column of Table 8.5, are computed using the above formulas.

The FE solution is calculated using a two step procedure discussed in Algorithm 9.2. In the first step, the scalar potential $\bar{\psi}$ is computed from the imposed voltage V at the ends of the plates. Figure 8.24 shows the boundary conditions. We impose $\psi_r = -1/\omega$ on the left end and $\psi_r = +1/\omega$ on the right end of the plates. The voltage $V = i\omega\bar{\psi}$, and hence, the boundary conditions for $\bar{\psi}$ in Figure 8.24 is equal to a voltage of $2i$ between the ends of the plates. The current obtained from this step is used in the second step of Algorithm 9.2 to calculate the vector potential $\bar{A}$, and subsequently, the magnetic field $\bar{B}$. The resistance and the inductance are calculated using the expressions derived in Chapter 5. The results are listed in the third column of Table 8.5. The domain in Figure 8.24 is discretized using a mesh of 972 nodes and 704 elements; the mesh is shown in Figure 8.25. Form the results we observe that the inductance obtained from the FE analysis is smaller (by approximately 14%) than the inductance predicted by the formula from Grover [1973]. One of the reasons for the difference could be the effects of the size of the surrounding air. However, the computational resources limit the size of the airbox. We observe, as expected, an increase in the inductance with the increase in the size of the airbox. These results were computed using the *generalized* units system with a scaling factor of 10^3.

Table 8.5. The the total resistance and inductance for the two conducting plates shown in Figure 8.23, with uniform current. The FE solution is calculated using Algorithm 9.2 in conjunction with the multiple-scale technique. Four different meshes are used with increasing size of the surrounding box of air. The results are in the SI unit system.

Method	Size of the airbox (in *meters*)	Resistance R_{total} (in *ohm*)	Inductance L_{total} (in *Henry*)
Formula by Grover [1973]	—	0.1137 *ohm*	1.7792 *nH*
FE solution	0.01 *m*	0.1137 *ohm*	1.3406 *nH*
	0.1 *m*	0.1135 *ohm*	1.5219 *nH*
	1.0 *m*	0.1130 *ohm*	1.5334 *nH*
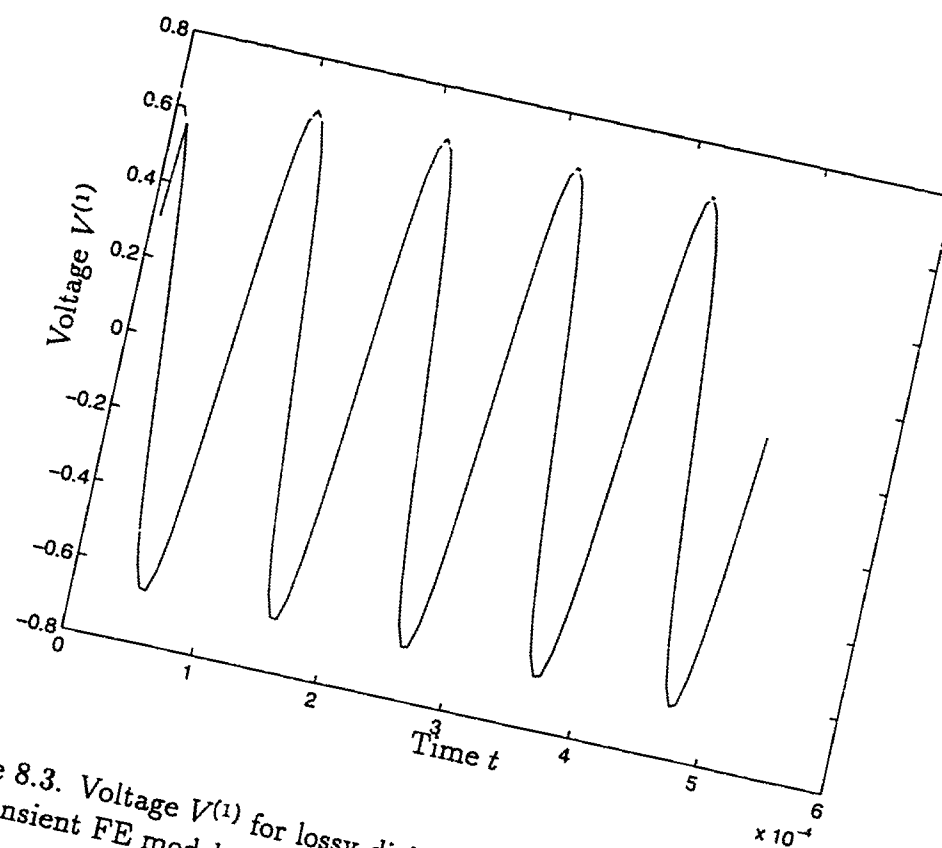
Figure 8.3. Voltage $V^{(1)}$ for lossy dielectric. The solid line represents the transient FE model and the dashed line is from the circuit model.
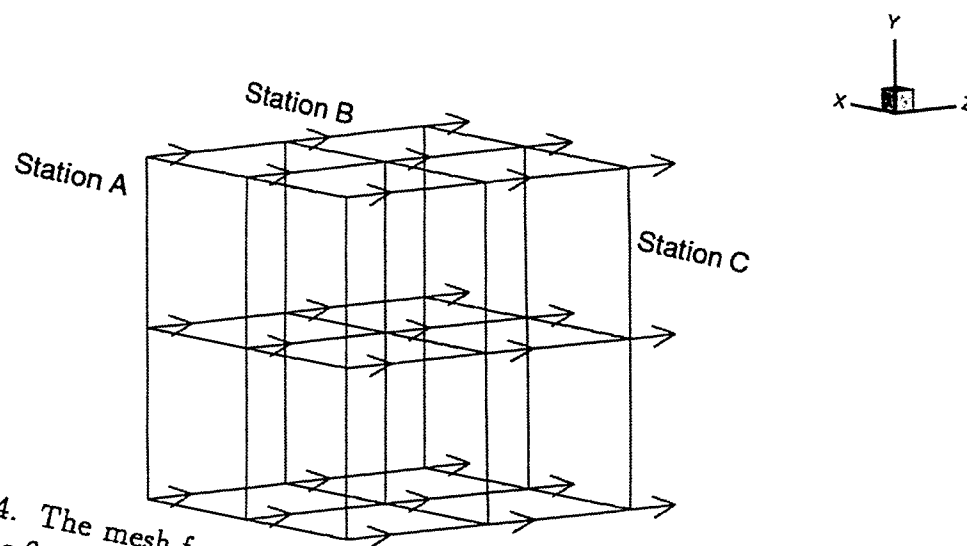
Figure 8.4. The mesh for the lossy dielectric. The arrows represent the electric field $\mathbf{E}$ at time $t = 1.0 \times 10^{-4}$ obtained from the transient FE model.

$$\Omega := [0,1]^3$$

$$\epsilon = 1 \, , \, \mu = 1 \, , \, \sigma = 0$$

1.0 m

1.0 m

$\hat{\mathbf{e}}_3$

$\hat{\mathbf{e}}_2$

$\hat{\mathbf{e}}_1$

1.0 m
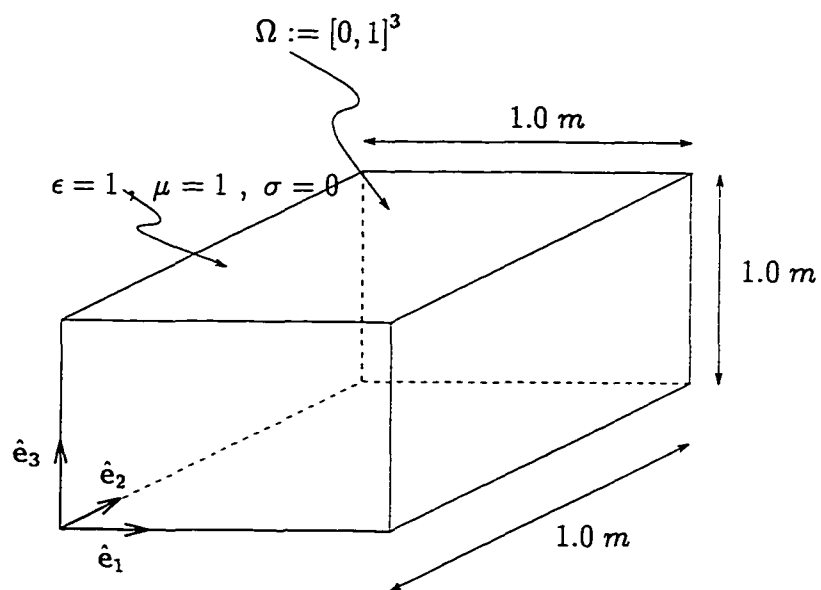
Figure 8.5. The cube for the wave propagation problem.
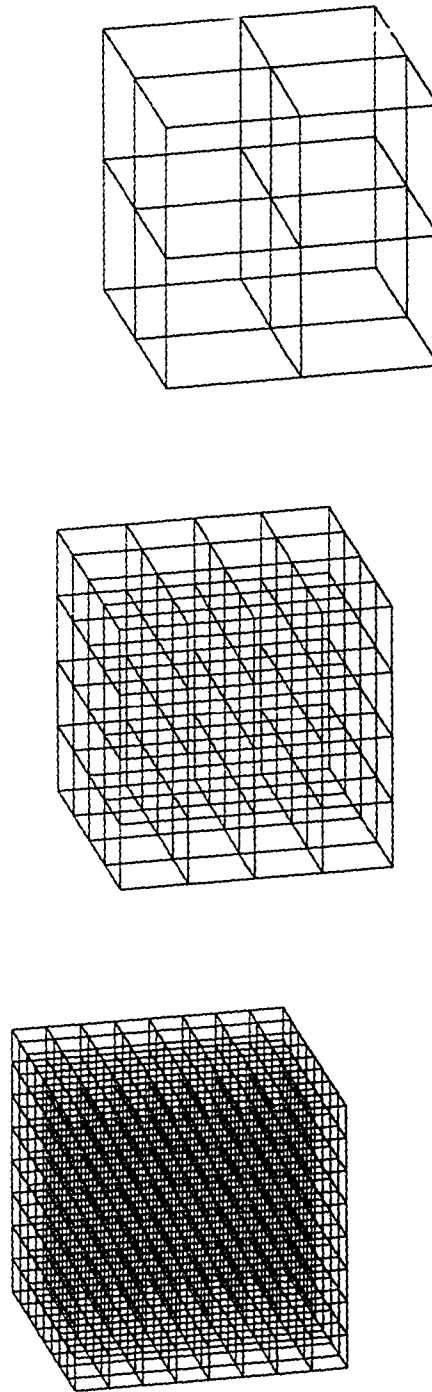
Figure 8.6. Three meshes for the cube. The topmost mesh has 4 elements, the mesh in between has 64 elements, and the mesh at the bottom has 512 elements.
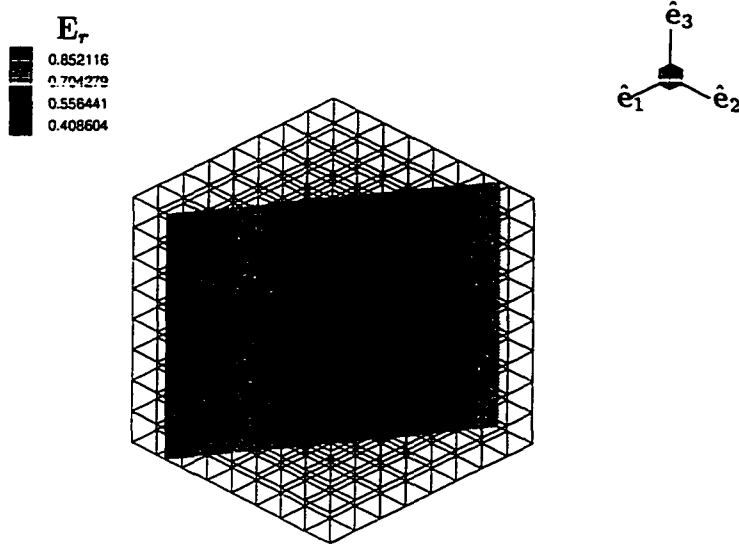
Figure 8.7. Contour plot for the magnitude of the real part of the electric field. The slice plane has a normal $1.0\hat{e}_1 + 1.5\hat{e}_2$.
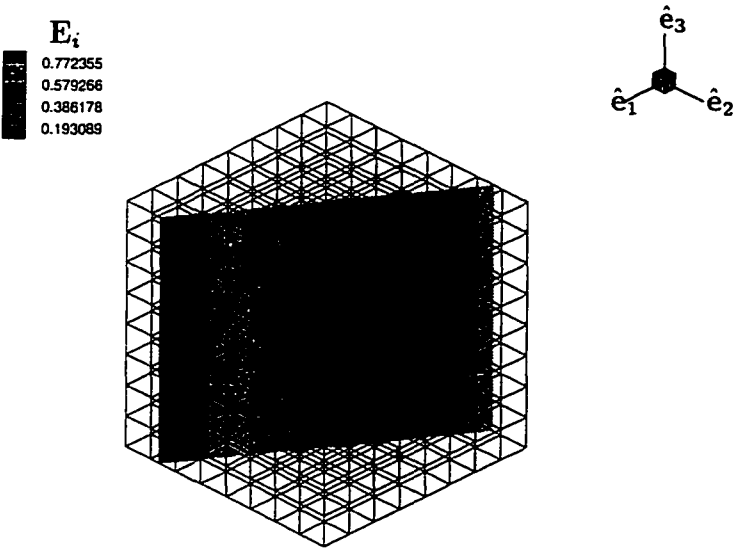
Figure 8.8. Contour plot for the magnitude of the imaginary part of the electric field. The slice plane has a normal $1.0\hat{e}_1 + 1.5\hat{e}_2$.
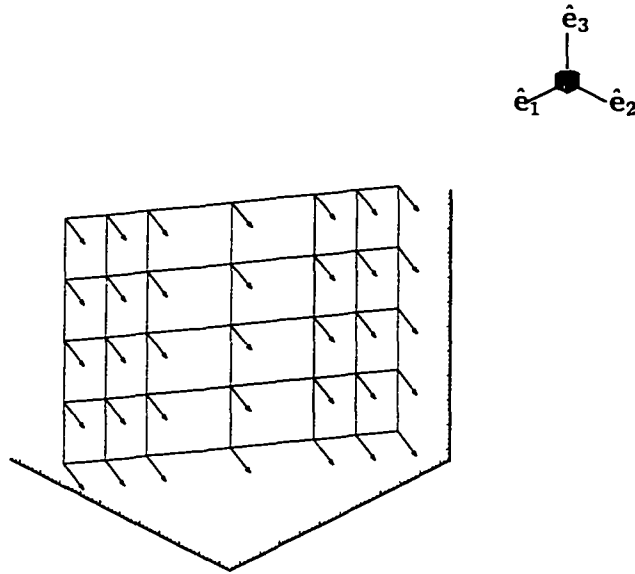
Figure 8.9. A vector plot for E_r. The slice plane has a normal $1.0\hat{e}_1 + 1.5\hat{e}_2$.
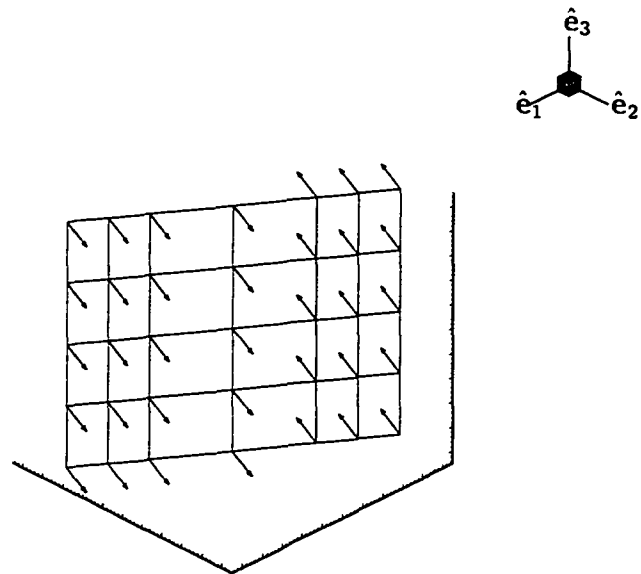
Figure 8.10. A vector plot for E_i. The slice plane has a normal $1.0\hat{e}_1 + 1.5\hat{e}_2$.
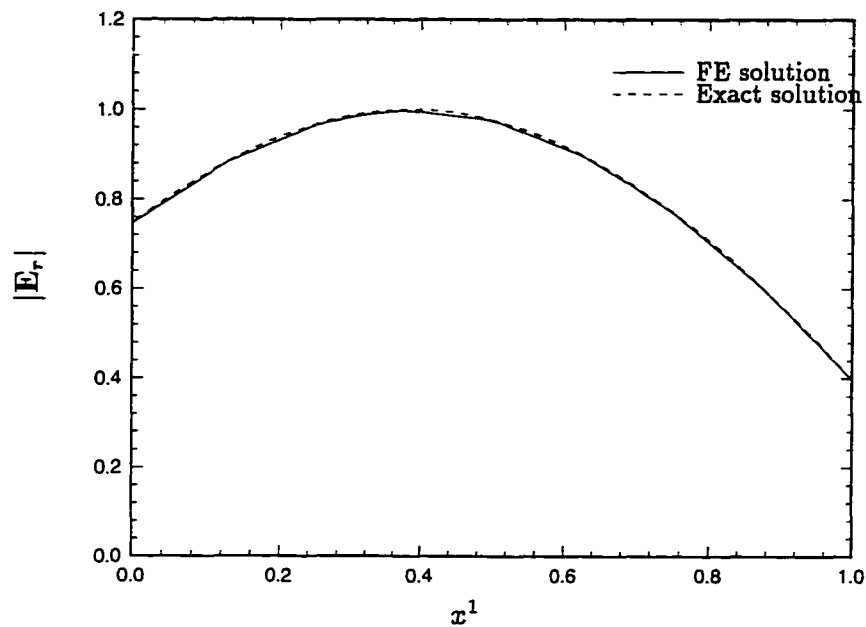
Figure 8.11. The magnitude of the real part of the electric field along a straight line. The line is formed by the intersection of the slice plane that has a normal $1.0\hat{e}_1 + 1.5\hat{e}_2$ and the horizontal plane (i.e., $x^3 = 0$).
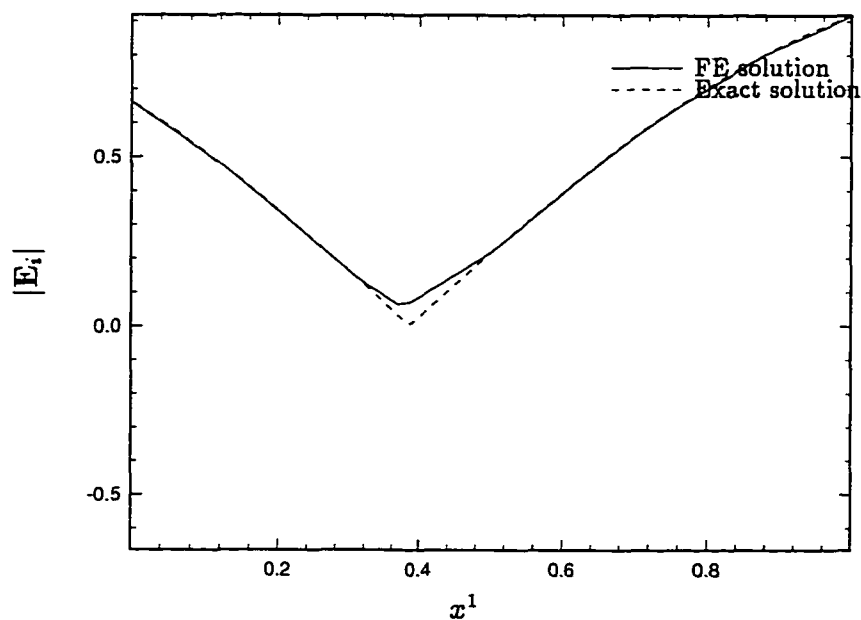
Figure 8.12. The magnitude of the imaginary part of the electric field along a straight line. The line is formed by the intersection of the slice plane that has a normal $1.0\hat{e}_1 + 1.5\hat{e}_2$ and the horizontal plane (i.e., $x^3 = 0$).
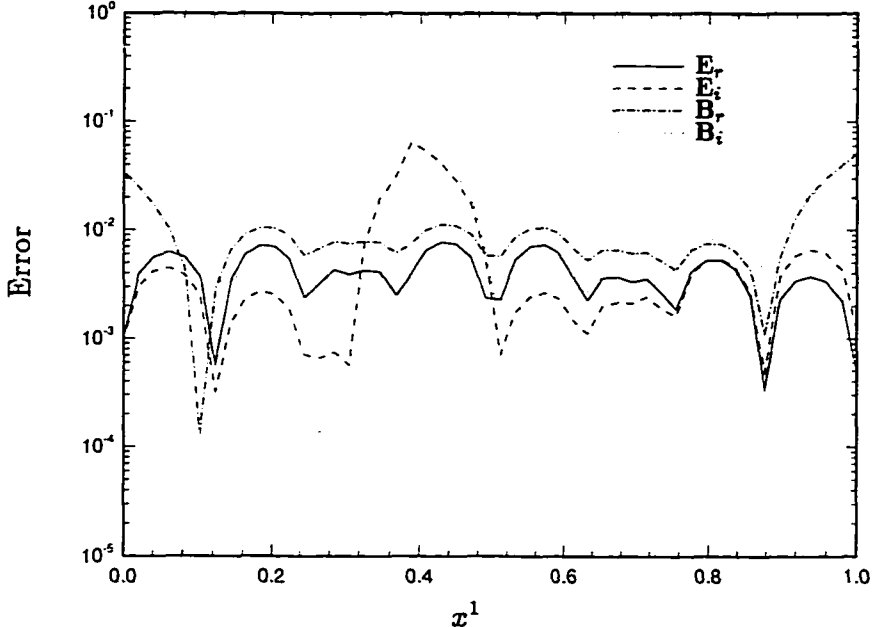
Figure 8.13. The magnitude of the errors in the field quantities along a straight line. The line is formed by the intersection of the slice plane that has a normal $1.0\hat{e}_1 + 1.5\hat{e}_2$ and the horizontal plane (i.e., $x^3 = 0$). The FE solution is compared with the exact solution.
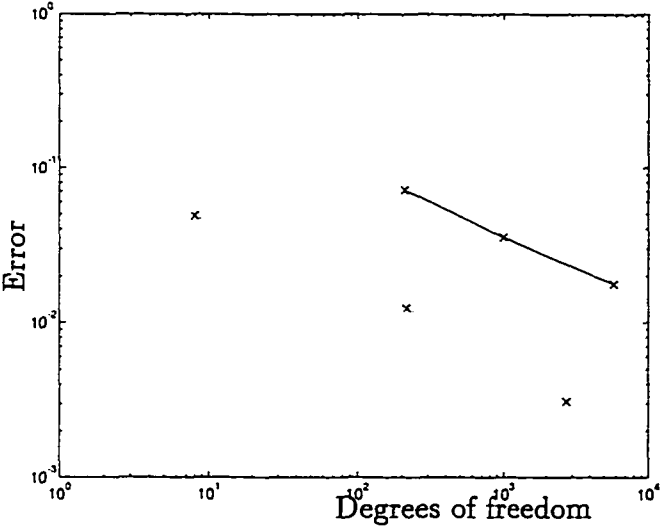
Figure 8.14. L^2-norm of the error in $\mathbf{E}_r$. The solid line is with a Neumann boundary condition, and the dashed line is with a Dirichlet boundary condition. The three points for each curve corresponds to the three meshes for the cube.
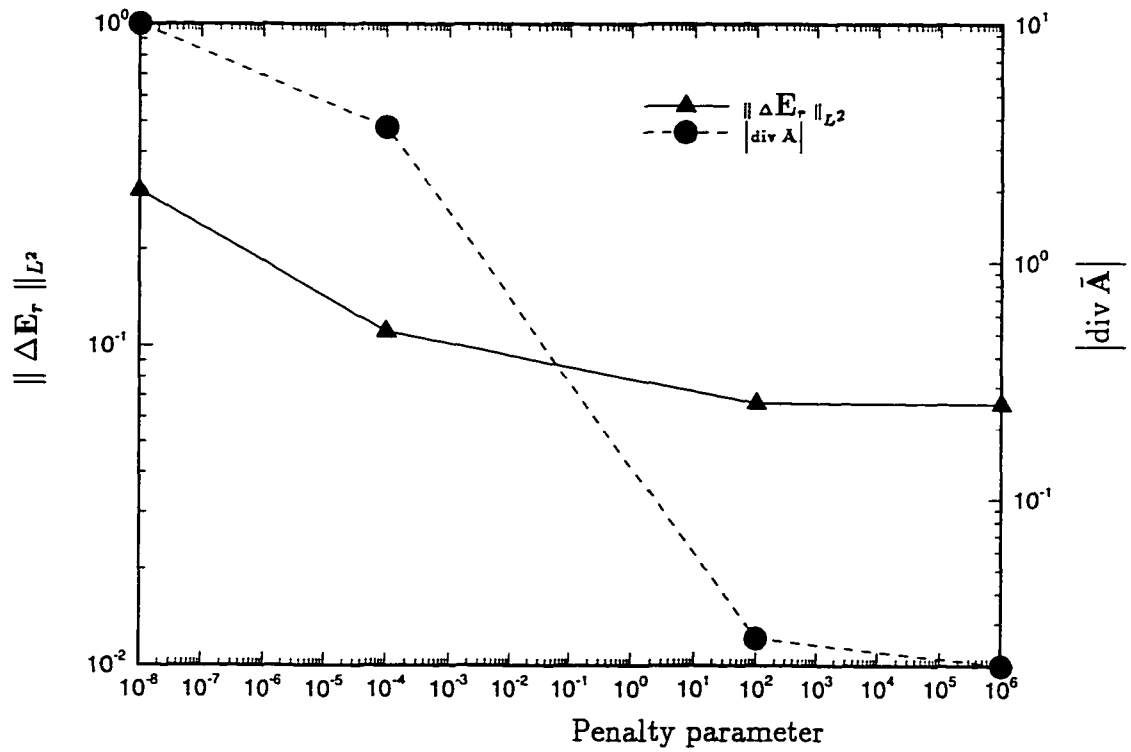
Figure 8.15. Effect of the penalty parameter. The solid line is the L^2 error norm of $\mathbf{E}_r$ (i.e., $\| \Delta\mathbf{E}_r \|_{L^2}$), and the dashed line is $|\operatorname{div}\bar{\mathbf{A}}|$.
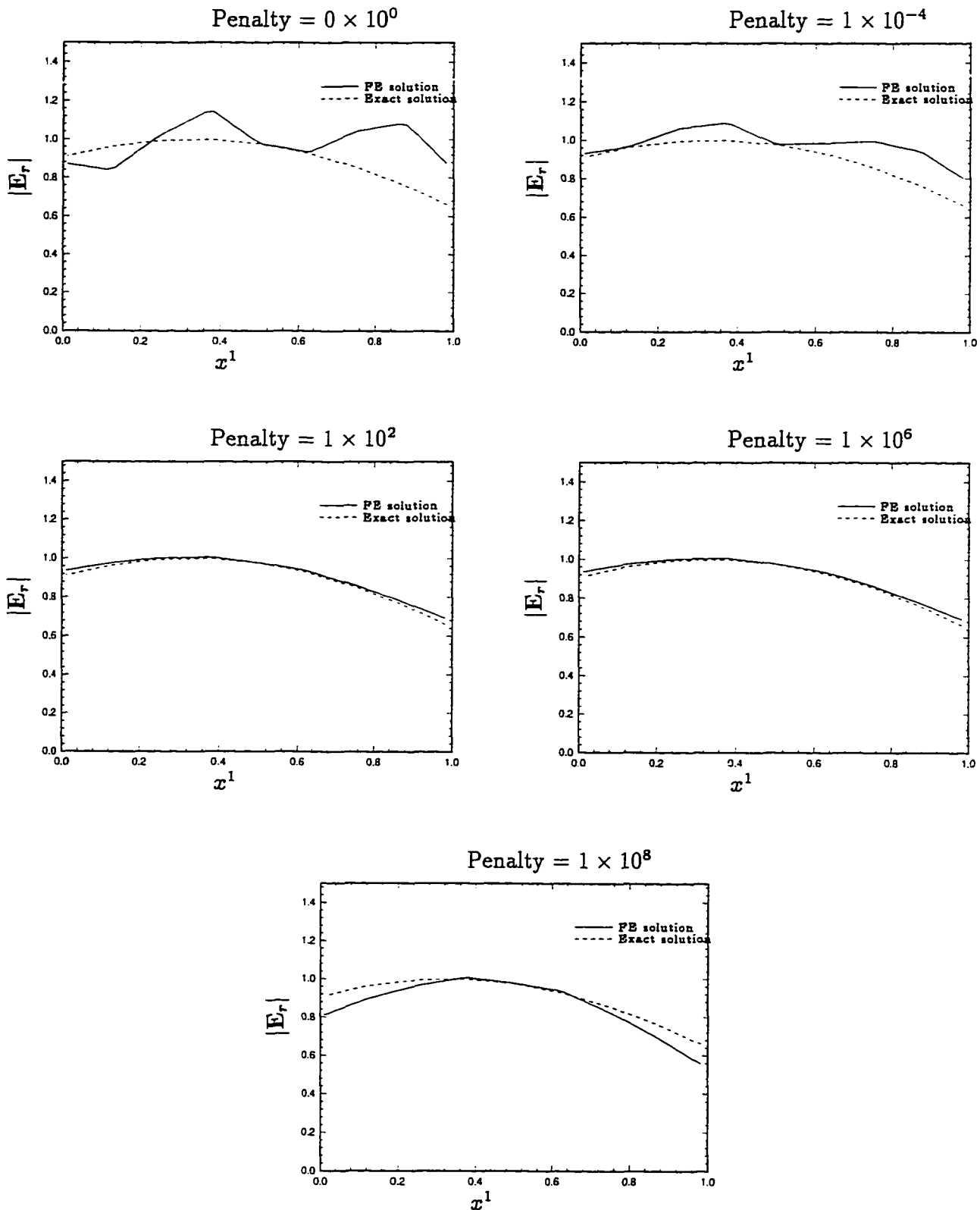
Figure 8.16.   Effect of the penalty parameter on E_r.   The field E_r is plotted along the x^1-axis passing through the center $(0.5, 0.5, 0.5)$ of the cube.   The solid line corresponds to the FE solution, and the dashed line corresponds to the exact solution.
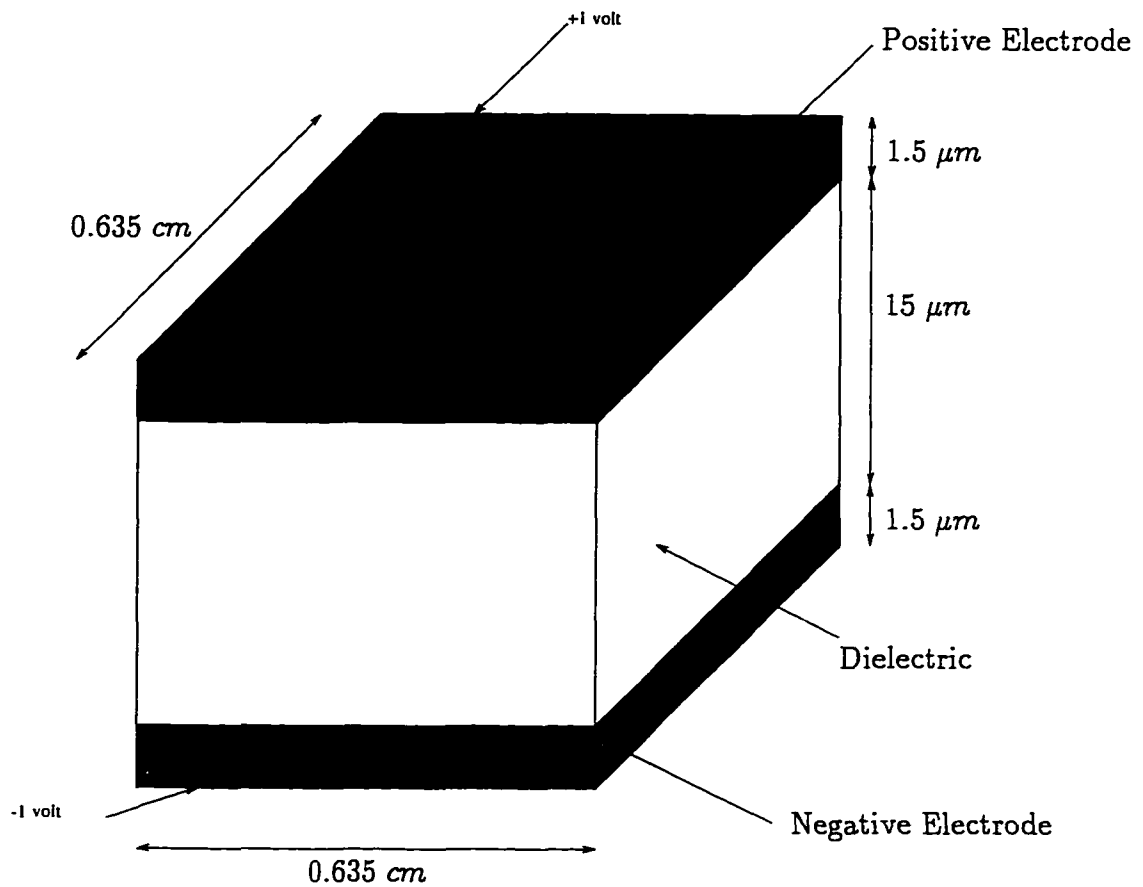
Figure 8.17. A simple parallel plate capacitor. A voltage of $+1$ *Volt* is applied to the top of the top electrode and a voltage of -1 *Volt* is applied to the bottom of the bottom electrode.
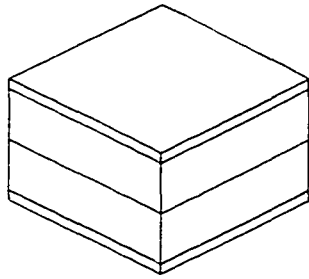
(a)
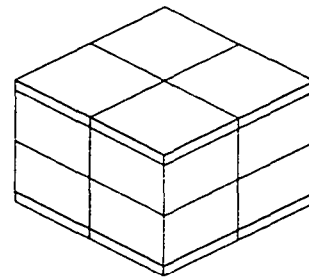
(b)
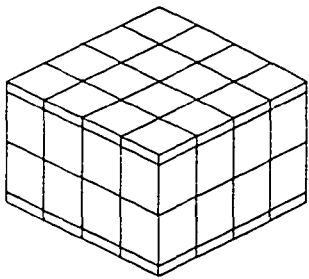
(c)
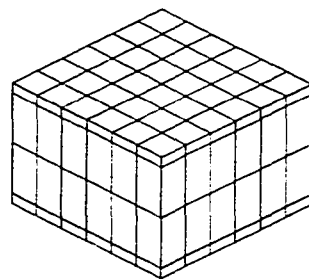
(d)

Figure 8.18. Four meshes for the parallel plate capacitor: The mesh is refined along the horizontal plane. The mesh (a) has 20 nodes and 4 elements, the mesh (b) has 45 nodes and 16 elements, the mesh (c) has 125 nodes and 64 elements, and the mesh (d) has 245 nodes and 144 elements.
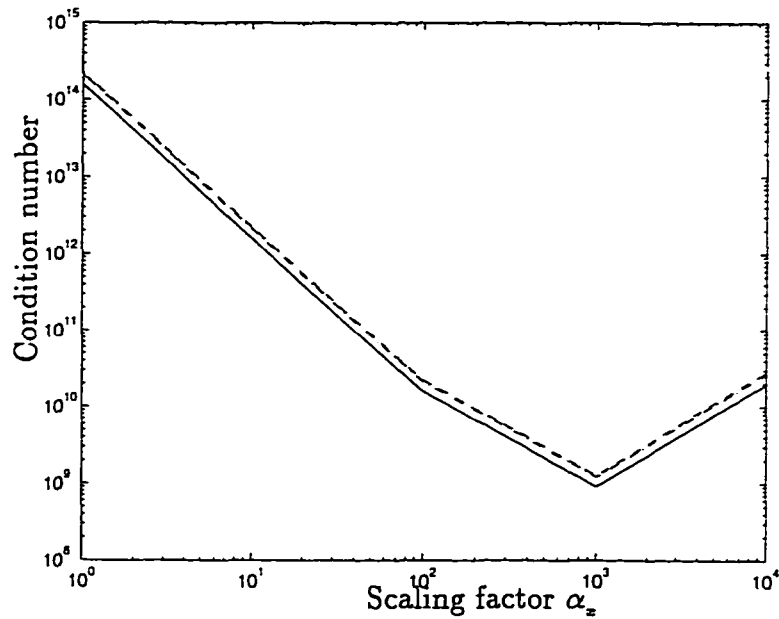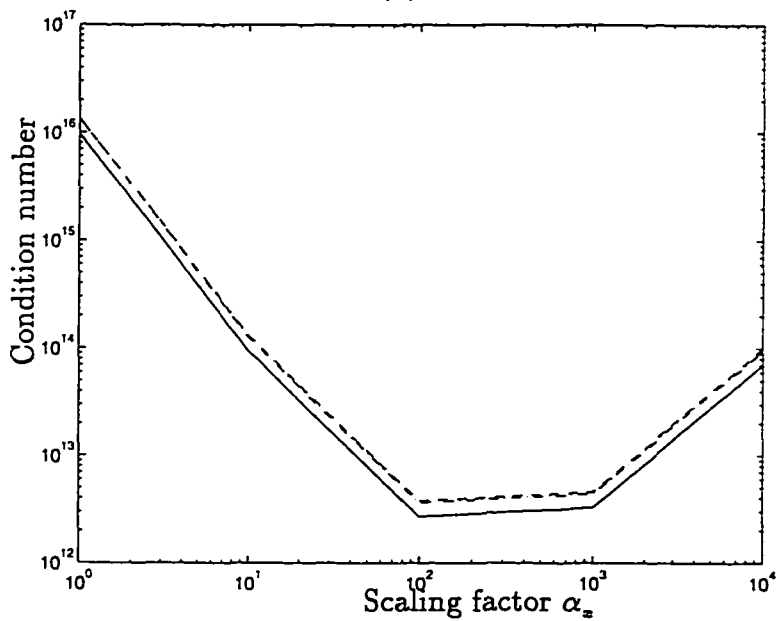
Figure 8.19. The change in the condition number with the changing mesh size and varying scaling factor α_z. The plot (a) corresponds to the transient solution, and plot (b) corresponds to the time-harmonic solution. The solid line is for mesh (a), the dashed line is for mesh (b), the dashed-dotted line is for mesh (c), and the dotted line is for mesh (d) in Figure 8.18.
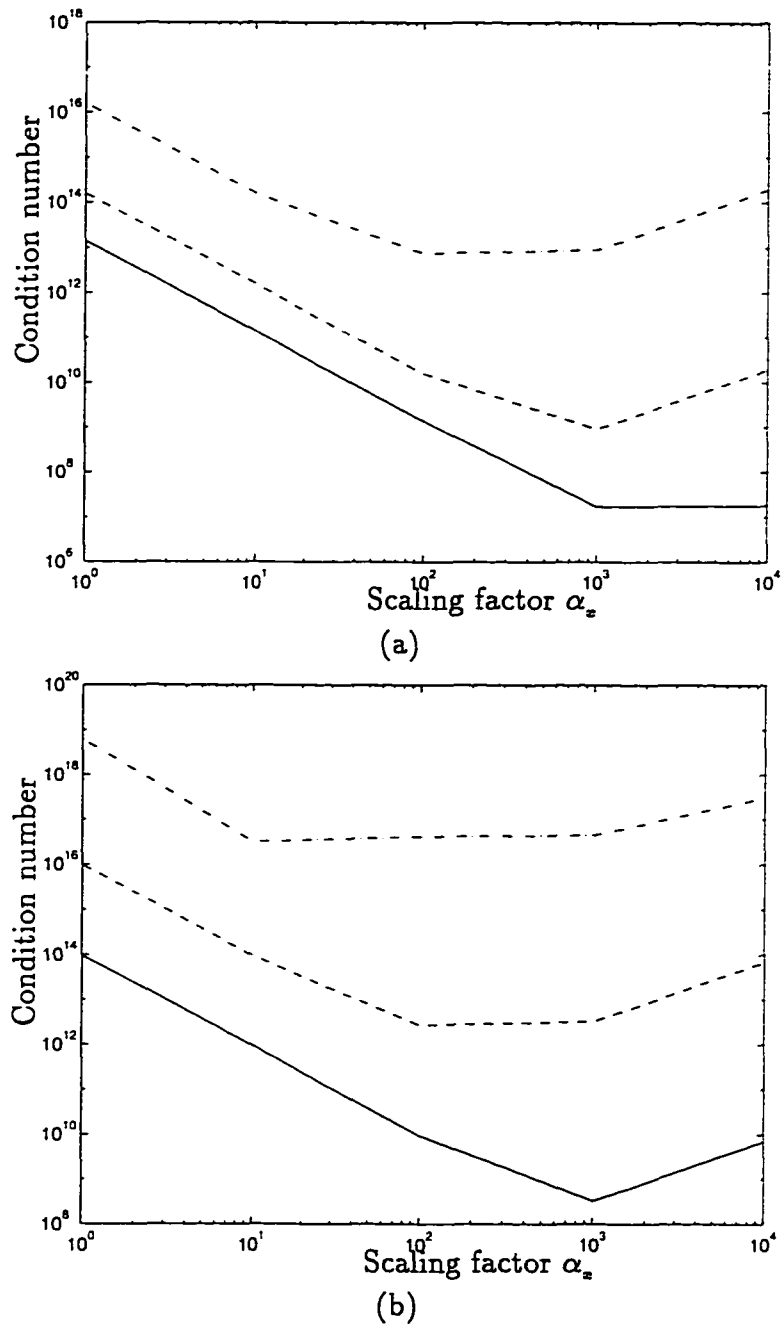
Figure 8.20. The change in the condition number with varying scaling factor α_z. The solution uses mesh (a) from Figure 8.18. For the transient solution in figure (a), the solid line is with the time step size $\Delta t_{n+1} = 2\pi/10^9$ SI units, dashed line is with $\Delta t_{n+1} = 2\pi/10^7$ SI units, and dashed-dotted line is with $\Delta t_{n+1} = 2\pi/10^5$ SI units. For the time-harmonic solution in figure (b), the solid line is with angular frequency $\omega = 10^9$ SI units, dashed line is with $\omega = 10^7$ SI units, and dashed-dotted line is with $\omega = 10^5$ SI units.
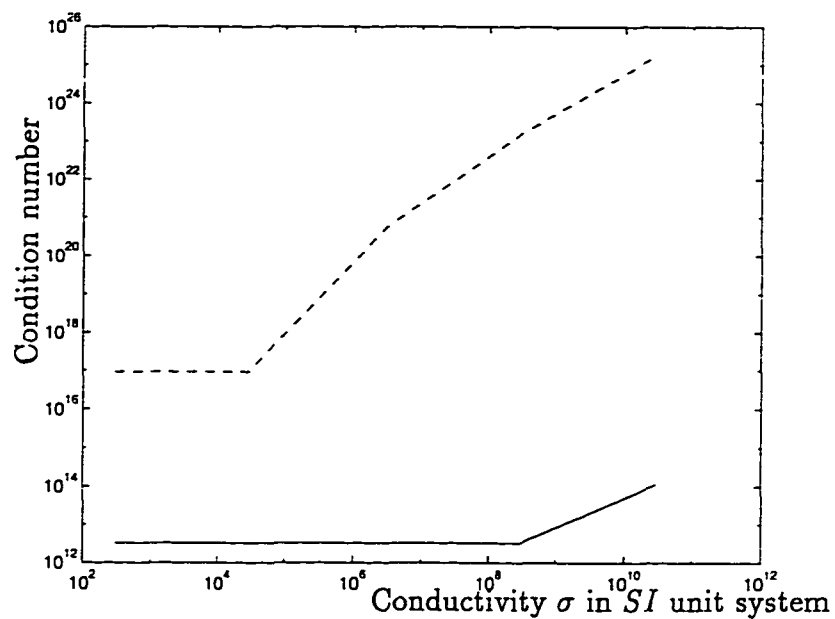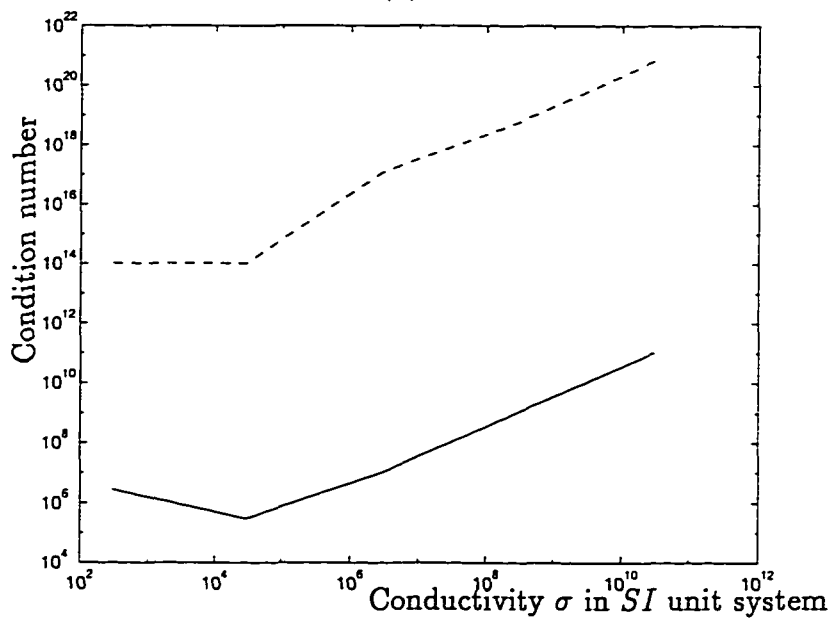
Figure 8.21. The change in the condition number with varying conductivity σ of the electrode. The solution uses mesh (a) from Figure 8.18. The top figure is at an angular frequency $\omega = 10^7$ SI units, and the bottom figure is at $\omega = 10^{11}$ SI units. The solid line is with the generalized unit system ($\alpha_x = 10^3$), and the dashed line is with the SI unit system.

Figure 8.22. The change in the relative error with varying conductivity σ of the electrode. The solution uses mesh (a) from Figure 8.18. The top figure is at an angular frequency $\omega = 10^7$ SI units, and the bottom figure is at $\omega = 10^{11}$ SI units. The solid line is with the generalized unit system ($\alpha_z = 10^3$), and the dashed line is with the SI unit system.
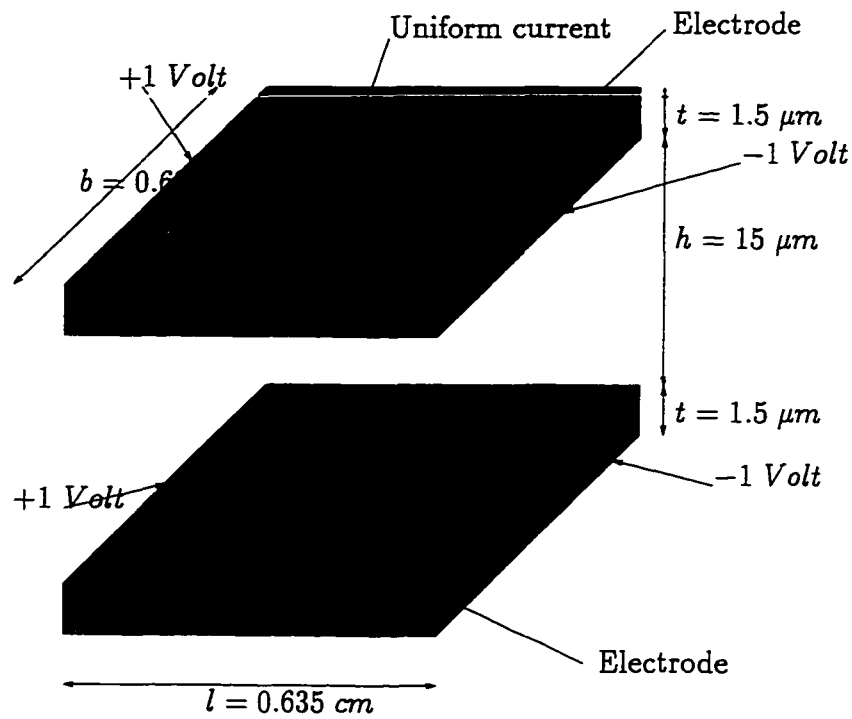
Figure 8.23. Two parallel conducting plates separated by air. Uniform current is flowing from the left end to the right end in each conductor.
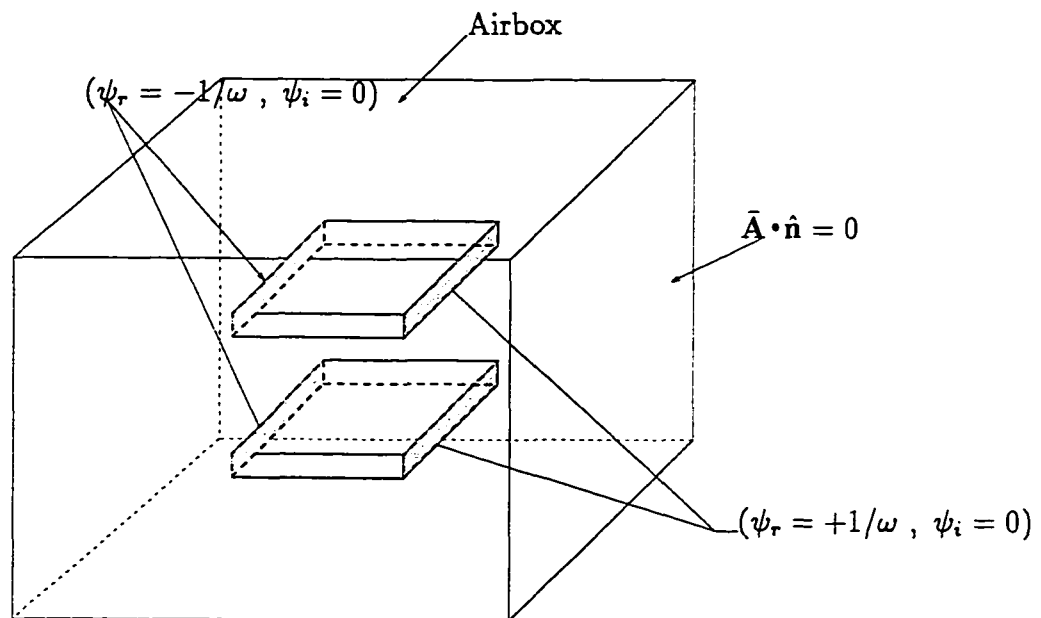
Figure 8.24. The boundary conditions and excitations imposed on the two parallel conducting plates. The amplitude of the voltage is imposed on the left and right ends of the conducting plates.
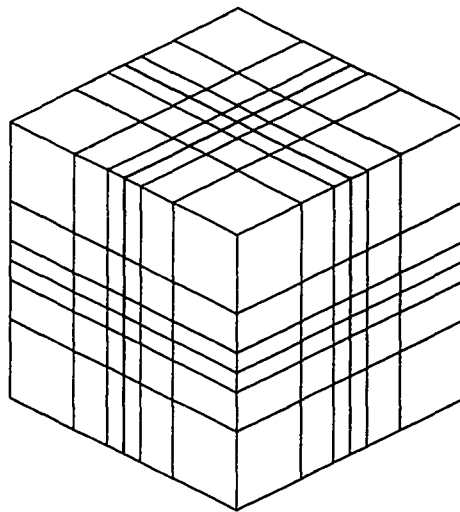
Figure 8.25. A mesh for the two parallel conducting plates: It has 972 nodes and 704 elements. The mesh for the surrounding air is generated using an exponential distribution.

CHAPTER 9
TIME-HARMONIC ANALYSIS OF MULTI-LAYER CERAMIC CAPACITORS

In this chapter, we present time-harmonic solutions to the MLCC introduced by Ngo [1990]. The resistance, inductance, and the capacitance are computed as a function of the frequency for (i) a single cell in the MLCC and (ii) a $2 \times 2 \times 3$ stack of cells. The results are compared to the circuit model proposed by Ngo [1992] and Anand [1993]. The finite element analysis effectively determines small values of the inductance. The equivalent series resistance *esr*, and the equivalent series inductance *esl*, extracted from the finite element solution, are observed to be smaller than the circuit model.

Due to the change in the behavior of the capacitor with frequency, it is necessary to choose the appropriate computational algorithm to reduce numerical ill-conditioning. Algorithm 9.1 is used to analyze capacitors below 10^5 *Hertz*, and Algorithm 9.2 is used to analyze capacitors above 10^5 *Hertz*. For Algorithm 9.2 a multiple scale technique is used to improve accuracy. In the solutions presented below, the Coulomb gauge is imposed via a penalty method and one-point reduced integration.

9.1. Choice of Computational Algorithms

The applicability of the simple RLC circuit model is limited to physical systems whose maximum linear dimension is much smaller than the wavelength of the electromagnetic wave. Figure 9.1 is an example of a typical electromagnetic wave, where Λ is the wavelength and $f = \omega/(2\pi)$ is the frequency. Remark 9.1 explains

201

the relation between the wavelength Λ and the frequency f for different materials. In other words, the physical size of the system is small enough to neglect the time needed for propagation of the electromagnetic signals. As a consequence, all the quantities in the system (i.e., the circuit) can be measured at the same time. From the power point of view, the wavelength is small enough to neglect any power loss due to radiation. A concise explanation of the approximation can also be found in Kraus [1984, p. 446] and Wangsness [1986, pp. 449–451].

The lumped parameters (R, L, and C) obtained from a FE solution is a simplification to the Maxwell equations. As the behavior of the capacitor changes with the frequency, the lumped parameters (R, L, and C) computed form a FE solution also change. Care must be exercised at higher frequencies to ensure that the dimension of the largest element in the mesh is significantly smaller than the wavelength; a thumb rule is to have the mesh size smaller than one-eighth of the wavelength.

For the MLCC proposed by Ngo [1990], the footprint of the capacitor is approximately 2.54×10^{-2} $m \times 2.54 \times 10^{-2}$ m, and the thickness is approximately 4.5×10^{-4} m. From Figure 9.2 we estimate that the simple RLC circuit model in Figure 5.1 for the capacitor is applicable to frequencies lower than 10^5 Hz. Note that at microwave frequencies (10^9 Hz and above) the circuit model could give erroneous results. The circuit models developed by Anand [1993] is an effort to increase the applicability of the circuit models to frequencies above 10^5 Hz. The circuit proposed by Ngo [1992] divides the capacitor into numerous small cells. The footprint of a single cell is 6.35×10^{-3} $m \times 6.35 \times 10^{-3}$ m and the thickness is approximately 1.8×10^{-5} m. Each of these cells are further divided into half-cells. These half-cells are modelled by a simple RLC circuit. As the dimensions of each cell is much smaller than the entire capacitor, the applicability of the circuit model

is increased to beyond $10^7\ Hz$.

Remark 9.1. The change in the wavelength of the electromagnetic wave with the changing excitation frequency for the materials used in the MLCC is given in Figure 9.2. The properties of the materials were listed in Table 7.1. The velocity of a plane wave in a conductive media at a frequency $f = \omega/(2\pi)$ is

$$v = \frac{1}{\sqrt{\mu\epsilon}} \left\{ \frac{2}{(1 + 1/Q^2) + 1} \right\}^{1/2} ,$$

where the

$$Q = \frac{\omega\epsilon}{\sigma} .$$

The dimensionless parameter Q can also be written as

$$Q = \frac{|\partial \mathbf{D}/\partial t|}{|\mathbf{J}_f|} ,$$

i.e., the parameter Q is a measure of the relative importance between the displacement current and the conduction current. For conductors $Q << 1$, and for insulators $Q >> 1$. However, note that the behavior is frequency dependent. For air and the dielectric ceramic, the velocity v inside the material is given by

$$v = \frac{1}{\sqrt{\mu\epsilon}} ,$$

and for the conductors sliver palladium and copper the velocity inside the material is

$$v = \frac{1}{\sqrt{\mu\epsilon}}\sqrt{2Q} .$$

The wavelength Λ inside a medium is given by

$$\Lambda = f\,v ,$$

where $f = \omega/(2\pi)$ is the frequency of the electromagnetic wave. The skin depth δ for a conducting material, is defined as the distance inside the material at which the

magnitude the field decreases by a factor of $1/e$. The skin depth δ is related to the wavelength Λ as follows:

$$\delta = \frac{4\pi}{\mu\omega\sigma\Lambda} \ .$$

Increasing the frequency, decreases the skin depth. See Wangsness [1986] or Kraus [1984] for a more detailed explanation on electromagnetic wave propagation.

∎

The behavior of a capacitor can be described by a combination of the following three physical processes: The current flow in the conductors (characterized by the current density $\mathbf{J}_f$) is coupled with the electrical energy stored in the dielectric (characterized by the displacement field $\mathbf{D}$) and the induced magnetic field (characterized by the magnetic field $\mathbf{H}$). At low frequencies the electromagnetic problem in the capacitor can be decoupled such that the electric field inside and surrounding the capacitor is determined first and then the induced magnetic field is calculated. This decoupling between the electric and the magnetic field is possible because the power due to electric field dominates the power due to the magnetic field.

The partial differential equations (PDEs) solved to determine lumped parameters for the time-harmonic electromagnetic problem (2.33) is the Ampere's law

$$\operatorname{curl}\bar{\mathbf{H}}_0 - i\omega\,\bar{\mathbf{D}}_0 - \bar{\mathbf{J}}_{f_0} = \bar{\mathbf{J}}_{a_0} \ ,$$

and the continuity equation

$$i\omega\left\{\operatorname{div}\bar{\mathbf{D}}_0\right\} + \operatorname{div}\bar{\mathbf{J}}_{f_0} = 0 \ .$$

Recall that the current density

$$\bar{\mathbf{J}}_{f_0} = -i\sigma\omega\operatorname{grad}\bar{\psi} - i\sigma\omega\,\bar{\mathbf{A}} \ ,$$

$$v = f\,\Lambda$$

Amplitude
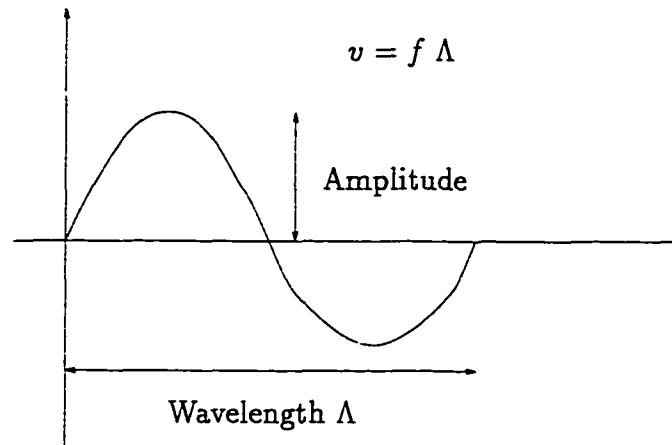
Wavelength Λ

Figure 9.1. An electromagnetic wave: The amplitude of the wave versus length at a fixed instant in time. The wave velocity v depends on the material. Inside a conductor (a dispersive medium) the amplitude of the wave is damped.
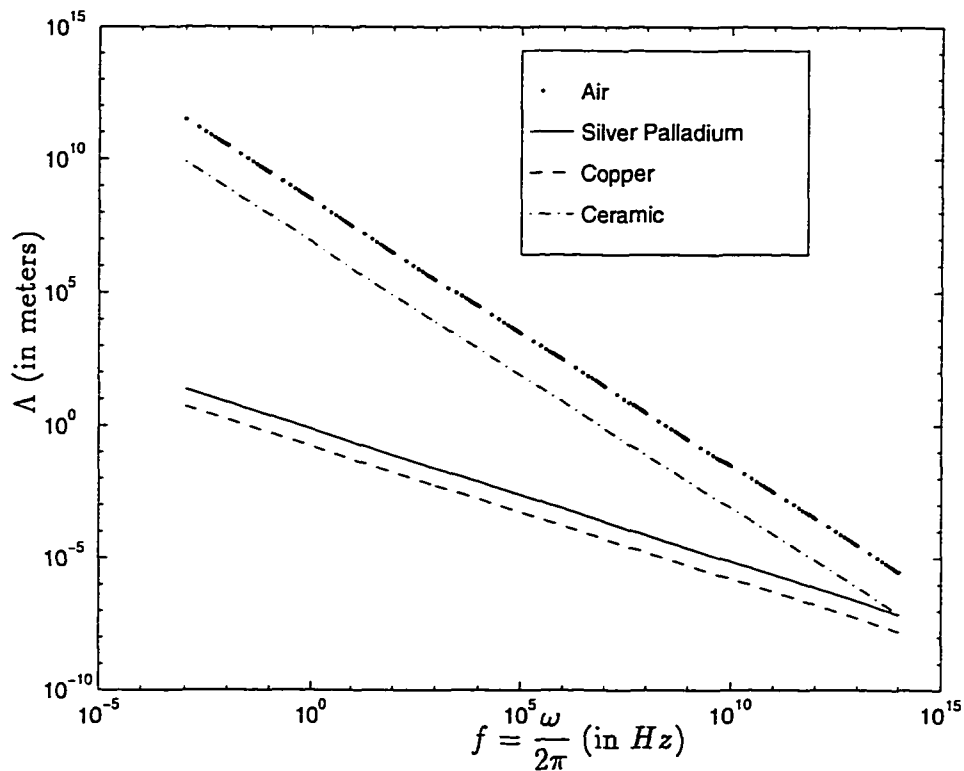
Figure 9.2. The wavelength Λ of the electromagnetic wave as a function of frequency f inside different materials.

the displacement electric field

$$\bar{\mathbf{D}}_0 = -i\epsilon\omega \operatorname{grad}\bar{\psi} - i\epsilon\omega \bar{\mathbf{A}} ,$$

and the magnetic field

$$\bar{\mathbf{H}}_0 = \frac{1}{\mu} \operatorname{curl}\bar{\mathbf{A}}_0 ,$$

are defined in terms of the magnetic vector potential $\bar{\mathbf{A}}_0$ and the time-integrated scalar potential $\bar{\psi}_0$. The conductivity σ, permittivity ϵ, and the permeability μ are piece-wise linear functions of position. Using the above potentials we rewrite the PDEs to be as follows: The Ampere's law

$$\operatorname{curl}\left(\frac{1}{\mu} \operatorname{curl}\bar{\mathbf{A}}\right) + i\sigma\omega \bar{\mathbf{A}} - \epsilon\omega^2 \bar{\mathbf{A}} + i\omega \left(\sigma \operatorname{grad}\bar{\psi}\right) - \omega^2 \left(\epsilon \operatorname{grad}\bar{\psi}\right)$$

$$= \bar{\mathbf{J}}_{a_0} ,$$

and the continuity equation

$$+i\omega \operatorname{div}\left(\sigma \bar{\mathbf{A}}\right) - \omega^2 \operatorname{div}\left(\epsilon \bar{\mathbf{A}}\right) + i\omega \operatorname{div}\left(\sigma \operatorname{grad}\bar{\psi}\right) - \omega^2 \operatorname{div}\left(\epsilon \operatorname{grad}\bar{\psi}\right)$$

$$= 0 ,$$

are solved by FE method using the appropriate boundary conditions to determine $\bar{\mathbf{A}}$ and $\bar{\psi}$. The coupling between the $\bar{\mathbf{A}}$ and the $\bar{\psi}$ potentials is decided by the Coulomb gauge

$$\operatorname{div}\bar{\mathbf{A}} = 0 .$$

In the present implementation, the Coulomb gauge is imposed via the penalty method. Inside an homogeneous material we have $\operatorname{div}\left(\sigma \bar{\mathbf{A}}\right) \equiv 0$ and $\operatorname{div}\left(\epsilon \bar{\mathbf{A}}\right) \equiv 0$. However, for regions with discontinuous material properties we cannot make such a

simplification. Hence, the PDEs to be solved are reduced to

$$
\operatorname{curl}\left(\frac{1}{\mu}\operatorname{curl}\bar{\mathbf{A}}\right) + i\sigma\omega\,\bar{\mathbf{A}} - \epsilon\omega^2\,\bar{\mathbf{A}} + i\omega\left(\sigma\operatorname{grad}\bar{\psi}\right) - \omega^2\left(\epsilon\operatorname{grad}\bar{\psi}\right)
$$

$$
+\lambda\frac{1}{\mu}\left(\operatorname{div}\bar{\mathbf{A}}\right)^2 = \bar{\mathbf{J}}_{a_0}\,,
$$

$$
+i\omega\operatorname{div}\left(\sigma\,\bar{\mathbf{A}}\right) - \omega^2\operatorname{div}\left(\epsilon\,\bar{\mathbf{A}}\right) + i\omega\operatorname{div}\left(\sigma\operatorname{grad}\bar{\psi}\right) - \omega^2\operatorname{div}\left(\epsilon\operatorname{grad}\bar{\psi}\right) = 0\,,
$$

$$
(9.1)
$$

where $\flat$ is the penalty parameter.

The large difference in the numerical values of the material properties μ, ϵ, and σ are detrimental to the numerical conditioning of the above equations. The numerical significance of each of the terms in the (9.1) can be determined only upon accurate solution. However, a simplistic approach is to examine the numerical values of the coefficients of the different terms in (9.1) for the material properties listed in Table 7.1 as a function of frequency. Figures 9.3 and 9.4 explains the numerical behavior of curl $\left(\frac{1}{\mu}\operatorname{curl}\bar{\mathbf{A}}\right)$, $\sigma\omega\bar{\mathbf{A}}$, and $\epsilon\omega^2\bar{\mathbf{A}}$ as a function of the angular frequency ω in the SI and the *generalized* unit systems, respectively. We assume that the material is silver palladium and the geometric dimensions are that of an electrode inside a single cell. The length $l = 10^{-5}\ m$, and curl $\left(\operatorname{curl}\bar{\mathbf{A}}\right) \approx \bar{\mathbf{A}}/l^2$. We observe that the numerical value for curl $\left(\frac{1}{\mu}\operatorname{curl}\bar{\mathbf{A}}\right)$ is significantly larger than $\sigma\omega\bar{\mathbf{A}}$ and $\epsilon\omega^2\bar{\mathbf{A}}$, and hence, at the frequency of interest $(< 10^7\ Hz)$ we can neglect the contributions due to $\sigma\omega\bar{\mathbf{A}}$ and $\epsilon\omega^2\bar{\mathbf{A}}$. Similar conclusions can be made for dielectric material and air. Similarly, from Figures 9.3 and 9.4 we observe that the $\sigma\omega\bar{\psi}$ term dominates the $\epsilon\omega^2\bar{\psi}$ term. We observe that at low frequencies (i.e., less than $10^7\ Hz$), the difference in magnitudes between $\sigma\omega\bar{\psi}$ term and the $\epsilon\omega^2\bar{\psi}$ term is pronounced. An approximation at low frequencies is to neglect the coupling between the $\bar{\mathbf{A}}$ and $\bar{\psi}$ terms in the continuity equation, i.e., assume $\omega\operatorname{div}\left(\sigma\,\bar{\mathbf{A}}\right) \approx 0$
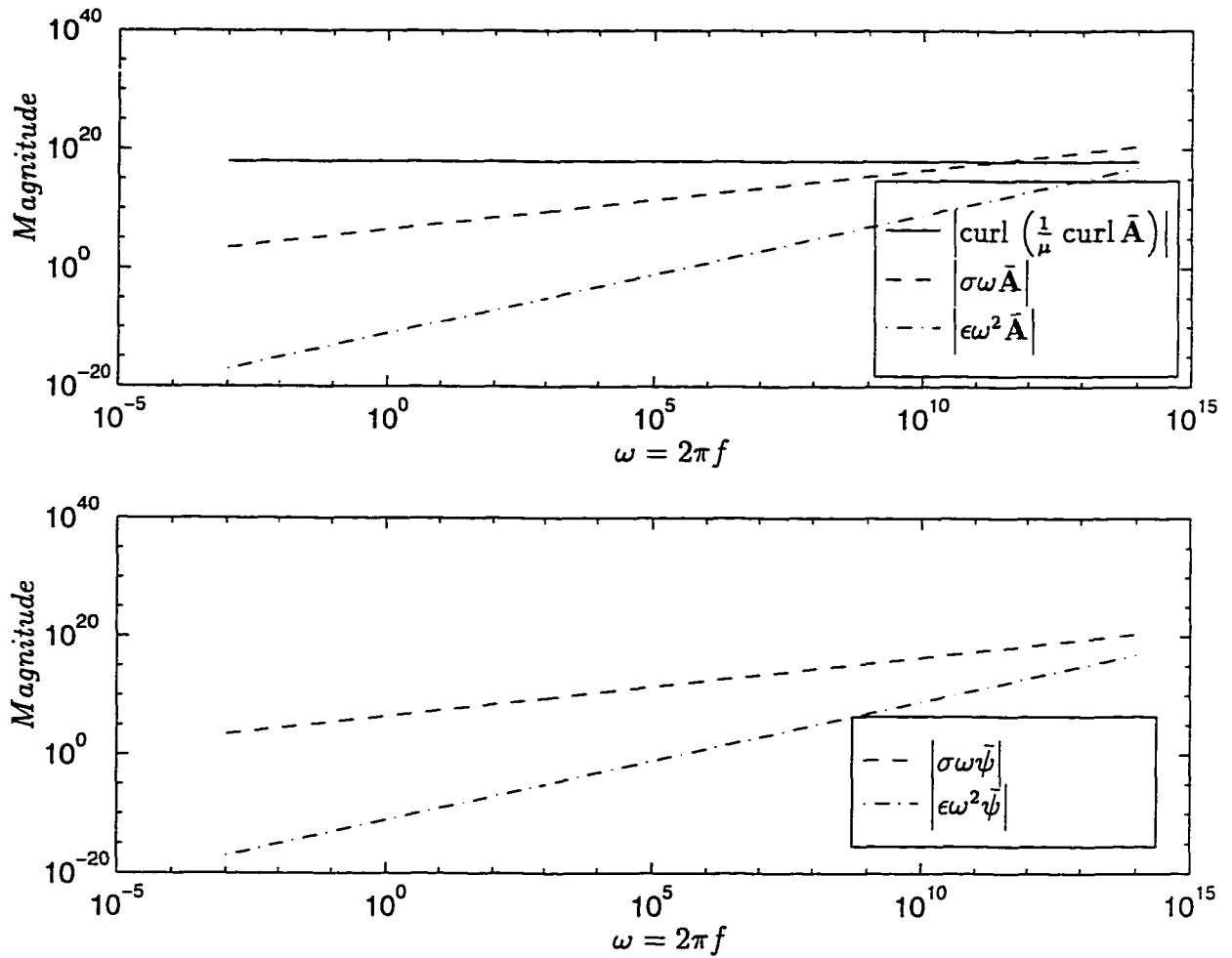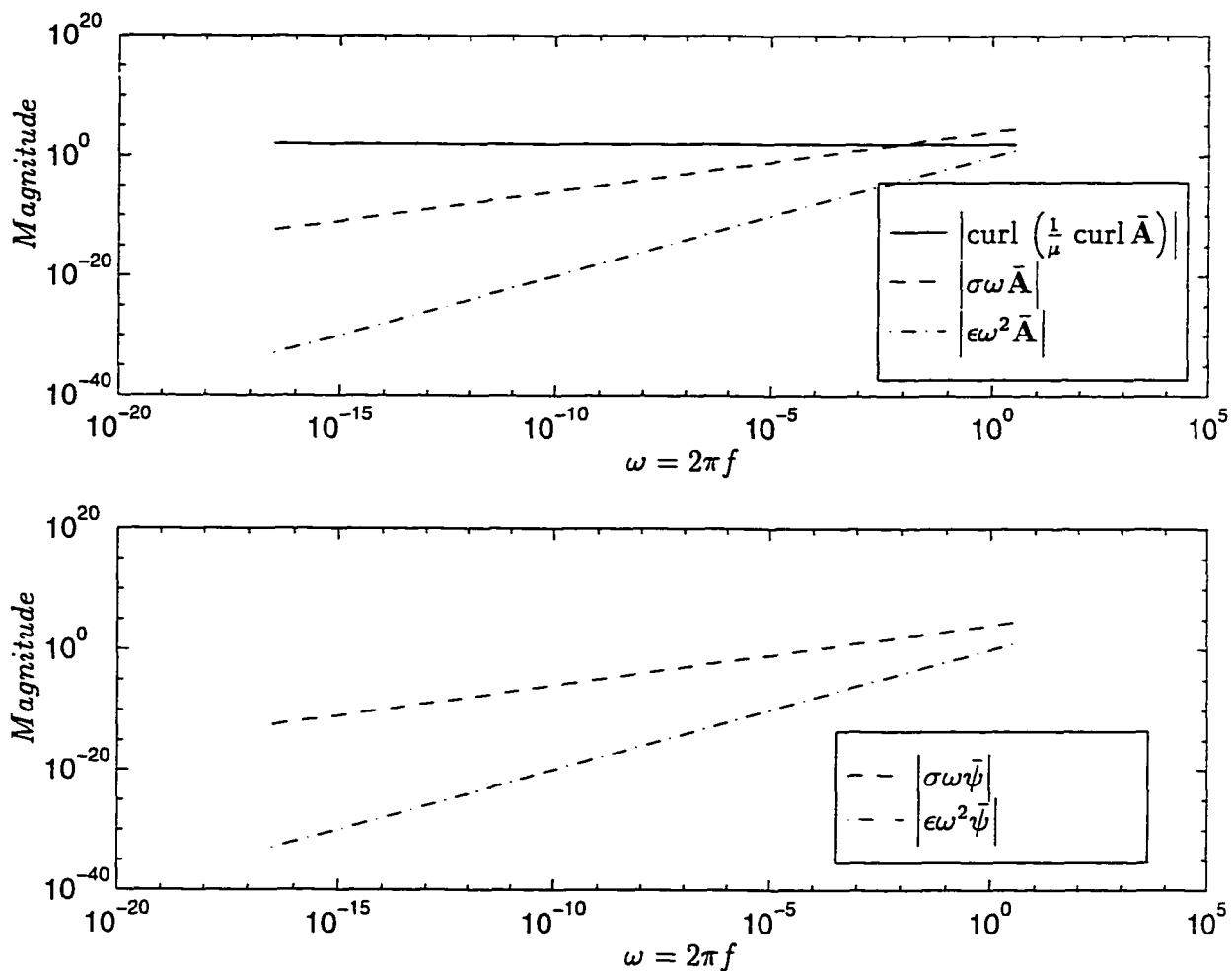
Figure 9.3. Relative magnitudes, in SI unit system, of the different terms in Ampere's law and the continuity equations inside an electrode of a MLCC.

and $\omega^2 \text{div} \left(\epsilon \bar{\mathbf{A}} \right) \approx 0$. Such an assumption implies that we neglect the effects of the eddy currents generated in the conducting parts. Recall that the eddy currents are defined to be equal to $i\sigma\omega \bar{\mathbf{A}}$.

In regards to the FE solution to the electromagnetic problem, this large difference in the magnitudes of the different terms involved in the differential equations

Figure 9.4. Relative magnitudes, in *generalized* unit system, of the different terms in Ampere's law and the continuity equations inside an electrode of a MLCC. The scaling factor is $\alpha_z = 10^3$. The frequency range is same as that used for Figure 9.3.

translates to an ill-conditioned matrix. The consequence is poor numerical accuracy and in some cases intractable matrices. We propose to alleviate the numerical ill-conditioning at low frequencies by introducing simplified algorithms. At low frequency we the electric and magnetic problems into two parts: First we solve for

the scalar potential $\bar{\psi}$, and later use the scalar potential to determine the vector potential $\bar{A}$. We neglect $\sigma\omega\bar{A}$ and $\epsilon\omega^2\bar{A}$. We introduce Algorithm 9.1 to solve electromagnetic problems at low frequency. At higher frequencies it is imperative to solve the coupled electromagnetic problem; Algorithm 9.2 solves the complete electromagnetic problem with no simplifications. However, we use a two step method improve the accuracy of the solution.

In the particular case where the permeability μ is constant inside the volume Ω enclosing the capacitor, we can make simplifications to Algorithms 9.1 and 9.2. The term

$$\text{curl}\left(\frac{1}{\mu}\text{ curl }\bar{A}\right) = \text{grad}\left(\frac{1}{\mu}\right) \times \left(\text{ curl }\bar{A}\right) + \left(\frac{1}{\mu}\right)\text{curl}\left(\text{curl }\bar{A}\right)$$

$$= \text{grad}\left(\frac{1}{\mu}\right) \times \left(\text{ curl }\bar{A}\right) + \left(\frac{1}{\mu}\right)\text{grad}\left(\text{div }\bar{A}\right) - \left(\frac{1}{\mu}\right)\text{div}\left(\text{grad }\bar{A}\right) .$$

Imposing the Coulomb gauge $\left(\text{div }\bar{A} = 0\right)$ and assuming that the permeability μ is constant, i.e., $\text{grad}\left(\frac{1}{\mu}\right) = 0$, we have

$$\text{curl}\left(\frac{1}{\mu}\text{ curl }\bar{A}\right) = -\left(\frac{1}{\mu}\right)\text{div}\left(\text{grad }\bar{A}\right) .$$

The Ampere's law in (9.1) is reduced to

$$-\left(\frac{1}{\mu}\right)\text{div}\left(\text{grad }\bar{A}\right) + i\sigma\omega\bar{A} - \epsilon\omega^2\bar{A} + i\omega\left(\sigma\text{ grad }\bar{\psi}\right) - \omega^2\left(\epsilon\text{ grad }\bar{\psi}\right)$$

$$+\lambda\frac{1}{\mu}\left(\text{div }\bar{A}\right)^2 = \bar{J}_{a_0} ,$$

$$(9.2)$$

as a consequence of the above simplification. At low frequencies we could simplify the above equation to

$$-\left(\frac{1}{\mu}\right)\text{div}\left(\text{grad }\bar{A}\right) + i\omega\left(\sigma\text{ grad }\bar{\psi}\right) - \omega^2\left(\epsilon\text{ grad }\bar{\psi}\right)$$

$$(9.3)$$

$$+\lambda\frac{1}{\mu}\left(\text{div }\bar{A}\right)^2 = \bar{J}_{a_0} .$$

Algorithm 9.1. Problem with conductors, low frequency excitation.

Step 1. Determine the scalar potential. Solve the equation

$$-i\omega \operatorname{div}\left(\sigma \operatorname{grad}\bar{\psi}\right) + \omega^2 \operatorname{div}\left(\epsilon \operatorname{grad}\bar{\psi}\right) = 0 ,$$

for the scalar potential $\bar{\psi} \in \mathbb{C}$ inside the region Ω. A voltage $(i\omega\bar{\psi})$ is specified at select points on the surface of the conductor.

Step 2. Determine the magnetic field in all the materials, i.e., the conductors, dielectric and air. Solve the equation

$$\operatorname{curl}\left(\frac{1}{\mu}\operatorname{curl}\bar{\mathbf{A}}\right) + \flat\,\frac{1}{\mu}\left(\operatorname{div}\bar{\mathbf{A}}\right)^2 = -i\omega\left(\sigma \operatorname{grad}\bar{\psi}\right) + \omega^2\left(\epsilon \operatorname{grad}\bar{\psi}\right) ,$$

for vector potential $\bar{\mathbf{A}} \in \mathbb{C}^3$ inside the region Ω. The scalar potential $\bar{\psi}$ is obtained from Steps 1. The penalty parameter $\flat$ is chosen such that the Coulomb gauge $(\operatorname{div}\bar{\mathbf{A}} = 0)$ is imposed.

∎

In the capacitor if we choose to only impose voltage and not current, then $\bar{\mathbf{J}}_{a_0} \equiv \mathbf{0}$, and hence, the above equation simplifies to

$$-\left(\frac{1}{\mu}\right)\operatorname{div}\left(\operatorname{grad}\bar{\mathbf{A}}\right) + \lambda\frac{1}{\mu}\left(\operatorname{div}\bar{\mathbf{A}}\right)^2$$

$$= -i\omega\left(\sigma \operatorname{grad}\bar{\psi}\right) + \omega^2\left(\epsilon \operatorname{grad}\bar{\psi}\right) . \tag{9.4}$$

The solution to the above equations for simple geometry of the conductor can be obtained in terms of spherical harmonics;[29] see e.g., Kellog [1953]. Hedlund and Nou [1989] uses the above simplification to solve simple magnetostatic problems. However, in the present computer implementation we choose not to include the above simplifications. This allows an extension of the present work to problems where the permeability μ is not constant. Moreover, the general case permits the use of other gauge conditions discussed in Chapter 2.

---

[29] The solution using the spherical harmonics satisfies the Coulomb gauge; see e.g., Wangsness [1986, p. 252].

Algorithm 9.2. Problem with conductors and high frequency excitation.

Step 1. Solve the equation

$$-i\omega \text{div} \left(\sigma \text{ grad } \bar{\varphi}' \right) + \omega^2 \text{ div} \left(\epsilon \text{ grad } \bar{\varphi}' \right) = 0 \ ,$$

for the scalar potential $\bar{\varphi}' \in C$ inside region Ω. A voltage $(i\omega\bar{\varphi}')$ is specified at select points.

Step 2. Solve the equations

$$\text{curl} \left(\frac{1}{\mu} \text{ curl } \bar{\mathbf{A}} \right) + i\sigma\omega \ \bar{\mathbf{A}} - \epsilon\omega^2 \ \bar{\mathbf{A}}$$

$$+ \ i\omega \text{ div} \left(\sigma \text{ grad } \bar{\varphi}'' \right) - \ \omega^2 \text{ div} \left(\epsilon \text{ grad } \bar{\varphi}'' \right)$$

$$+ \flat \frac{1}{\mu} \left(\text{div } \bar{\mathbf{A}} \right)^2$$

$$= -i\omega \text{div} \left(\sigma \text{ grad } \bar{\varphi}' \right) + \omega^2 \text{ div} \left(\epsilon \text{ grad } \bar{\varphi}' \right) \ ,$$

$$i\omega \text{div} \ \sigma \ \bar{\mathbf{A}} - \omega^2 \text{div} \ \epsilon \ \bar{\mathbf{A}} + i\omega \text{div} \left(\sigma \text{ grad } \bar{\varphi}'' \right) - \omega^2 \text{ div} \left(\epsilon \text{ grad } \bar{\varphi}'' \right) = 0 \ ,$$

for the vector potential $\bar{\mathbf{A}} \in C^3$ and the reduced scalar potential $\bar{\varphi}'' \in C$ inside the region Ω. The scalar potential $\bar{\varphi}'$ is obtained from Step 1. The total scalar potential is given by $\bar{\psi} = \bar{\varphi}' + \bar{\varphi}''$. The penalty parameter $\flat$ is chosen such that the Coulomb gauge $(\text{div } \bar{\mathbf{A}} = 0)$ is imposed. Note that the potential $\bar{\varphi}''$ is constrained to zero at all points where the voltage $(i\omega\bar{\varphi}')$ is specified.

∎

9.2. FE Model for a Single Cell

The single cell in Figure 7.3 and the surrounding box of air are discretized using hexahedral brick elements. A typical mesh including the surrounding box of air is shown in Figure 9.5. The mesh has 876 nodes and 756 elements. Figure 9.6 shows a typical mesh of the single cell without the surrounding air. Note that

increasing the number of nodes in the conductor leads to a significant increase in the number of nodes in the surrounding airbox. We study the effects of mesh refinement and the size of the airbox. We conclude that refining the mesh beyond the 876 nodes as shown in Figure 9.5 has an insignificant effect on the lumped parameters. The number of elements in the airbox does not effect the lumped parameters. However, with an increase in the size of the airbox we observe an increase in the inductance. The present computational resources limit the size[30] of the airbox to 1.0 m, i.e., approximately 1000 times the length of the conductor. In the results presented here we use an 1.0 m airbox and a mesh of 876 nodes. A voltage of +1 $Volt$ is prescribed on opposite sides of the top electrode, and a voltage of −1 $Volt$ is prescribed on opposites sides of the bottom electrode. The voltage is prescribed such that the current flow in the top electrode is perpendicular to the current in the bottom electrode. The boundary conditions are explained in Figure 9.7.

Figure 9.8 shows the current distribution inside the electrodes. It is evident that unlike the assumptions in the circuit model, the distribution of current is not linear. Figure 9.9 and Table 9.2 compare the impedance predicted by the FE solution to the impedance obtained from the circuit model proposed by Ngo [1992]. Smaller values for esr and the esl are obtained using FE analysis. This difference in the lumped parameters can be explained by the change in the current distribution.

The circuit model for the single cell is shown in Figure 9.10, and the numerical values of the components are listed in Table 9.1. The construction of the circuit model is explained in Anand [1993], however, a brief overview of the model is also presented below in Remark 9.2.

Remark 9.2. To construct a circuit model for the MLCC we divide the entire

---

[30] The size of the airbox refers to the length of the cube of air surrounding the capacitor.

Table 9.1. Numerical values for the lumped parameters in Figure 9.10 for a single cell.

Circuit parameter parameters	Numerical value (SI units)
R11_3 = R11_5 = R11_4 = R11_6	3.777×10^{-2} $ohms$
L11_3 = L11_5 = L11_4 = L11_6	2.85×10^{-10} $Henry$
C11_1	3.56850×10^{-8} $Farad$
K11_1 = K11_2	-5.64×10^{-1}

Table 9.2. Equivalent circuit parameters for a single cell of the MLCC.

Circuit parameters	Circuit model by Ngo [1992]	FE solution
esr	3.7783×10^{-2} $ohms$	3.5402×10^{-2} $ohms$
esl	1.2355×10^{-10} $Henry$	1.1995×10^{-10} $Henry$
srf	7.5509×10^{7} Hz	7.6926×10^{7} Hz
Capacitance	3.5685×10^{-8} $Farad$	3.5685×10^{-8} $Farad$

MLCC into $4 \times 4 = 16$ stacks as shown in Figure 7.1. Each stack consists of positive and negative electrodes sandwiched between the top and bottom bus; a single stack is shown in Figure 7.2. Each dielectric layer inside the stack together with its positive electrode and negative electrode is termed as a "cell." A single cell is shown in Figure 7.3. Ngo [1992] proposed a circuit model (see Figure 9.11) for each stack of cells. The numerical value of the resistance and the inductance of the circuit in Figure 9.11 depends on the number cells in each stack. To construct a circuit model for more than one stack of cells, we connect the the circuit model for each stack of cells in a novel architecture. The entire procedure is described in detail in Anand [1993].

We assume a linear distribution of current in each electrode. In Figure 7.2 we assume that the current is maximum at the edge close to the vias, and is zero at the center of the electrode. An estimate for the resistance and the inductance of each half of the electrode can be obtained assuming this linear distribution of current. Using formulae from Grover [1973] we can estimate the inductance of each half-electrode and mutual inductance between two half-electrodes. Note that the current in the positive electrode is perpendicular to the current on the negative electrode. Hence, we assume that there is no mutual inductance between the positive and negative electrodes.

The formula for the self-inductance L of each half electrode for a uniform distribution of current is given by

$$L = l \left[\log_e \left(\frac{l}{d} + \sqrt{1 + \frac{l^2}{d^2}} \right) + \frac{d}{l} \right] \quad n \ Henry \ , \qquad (9.5)$$

where the Geometric Mean Distance (GMD) d is

$$d = 0.22313 \ b \quad cm \ , \qquad (9.6)$$

where l is the length of the half-electrode, and b its width. For the single cell in Figure 7.3, $l = 0.3175 \ cm$, $b = 0.508 \ cm$, and the thickness $t = 1.5 \times 10^{-4}$ for each half-electrode. The mutual-inductance $\mathfrak{M}$ between the positive or negative half electrodes is given by the formula (9.5), where L is replaced by $\mathfrak{M}$ and the GMD d is calculated as follows.

$$\log_e (d) = \frac{h^2}{b^2} \log_e(h) + \frac{1}{2} \left(1 - \frac{h^2}{b^2} \right) \log_e \left(h^2 + b^2 \right) + 2\frac{h}{b} \tan^{-1} \left(\frac{h}{b} \right) - \frac{3}{2} \ , \quad (9.7)$$

where h is the distance separating the two half-electrodes. Note that the units for distances used in the above inductance formulas must be in $centi - meter$, and the inductance is obtained in $nano - Henry$.

The total inductance of the n half-electrode is a combination of the self-inductance of each half-electrode and the mutual-inductance between the two half-electrodes. The total inductance is calculated as follows. The matrix equation

$$
\begin{bmatrix} \bar{Z}_{1,1} & \bar{Z}_{1,2} & \cdots & \bar{Z}_{1,n} \\ \vdots & \vdots & \vdots & \vdots \\ \bar{Z}_{n,1} & \bar{Z}_{n,2} & \cdots & \bar{Z}_{n,n} \end{bmatrix} \begin{Bmatrix} \bar{I}_1 \\ \vdots \\ \bar{I}_n \end{Bmatrix} = \begin{Bmatrix} V \\ \vdots \\ V \end{Bmatrix} , \tag{9.8}
$$

is solved to determine the n currents $\bar{I}_1, \cdots, \bar{I}_n$ in half-electrode, where V is the voltage applied to the ends of the half-electrode. The entries in the impedance matrix are as follows.

$$
\bar{Z}_{i,i} = R + i\omega L \quad \text{for } i = \{1, \cdots, n\} ,
$$
$$
\bar{Z}_{i,j} = i\omega \mathfrak{M} \qquad \text{for } i, j = \{1, \cdots, n\} \text{ and } i \neq j , \tag{9.9}
$$

where the resistance of each plate is given by

$$
R = \frac{1}{3} \frac{l}{\sigma t b} . \tag{9.10}
$$

The total impedance of the stack of n half-electrodes is

$$
\bar{Z} = \frac{V}{(I_1 + \cdots + I_n)} , \tag{9.11}
$$

and the total inductance is

$$
L_{total} = \frac{Z_i}{\omega} , \tag{9.12}
$$

and the total resistance is

$$
R_{total} = Z_r , \tag{9.13}
$$

where $\bar{Z} = Z_r + iZ_i$.

To recapitulate, we divide each stack of electrodes into four half-stacks as shown in Figure 9.11. The resistance and the inductance of each of the half-stack of electrodes is obtained from the expression derived above. For example, resistance

R11_3 and inductance L11_3 corresponds to one positive half-stack. These circuit connected to the resistance and the inductance of the top and bottom bus. The expressions for the resistance and the inductance of the top and bottom bus can be obtained from the formulae listed above. The nodes 1101 and 1103 represent the east and west ends of the positive half-stacks, respectively. The nodes 1107 and 1109 represents the south and the north ends of the negative half-stacks, respectively. The capacitance C11_1 represents the capacitance of the entire stack. Note that there exists a mutual inductance between the two positive half-stacks and the two negative half-stacks. These coupling factors for the mutual inductances are represented by K11_1 and K11_2.

To construct the circuit model for a group of stacks we connect the adjacent nodes, e.g., the east end node of a stack is connected to the west end node of the adjacent stack, and so on. However, combining the stacks together requires the addition of the mutual inductance between stacks. The calculation of the mutual inductance K11_1 and the others is explained in Anand [1993].

■

9.3. FE Model for a Stack of $2 \times 2 \times 3$ Cells

The stack of $2 \times 2 \times 3$ cells and the surrounding box of air are discretized using hexahedral brick elements. A typical mesh including the surrounding box of air is shown in Figure 9.12. The mesh has 3296 nodes and 294 elements. Figure 9.13 shows a typical mesh of the stack of cells without the surrounding air. Similar to the analysis for the single cell, we use an airbox of size 1.0 m. A voltage of $+1$ $Volt$ is prescribed on opposite sides of the top electrode, and a voltage of -1 $Volt$ is prescribed on opposites sides of the bottom electrode. The voltage is prescribed such that the current flow in the top electrode is perpendicular to the current in

Table 9.3. Equivalent circuit parameters for a stack of $2 \times 2 \times 3$ cells of the MLCC.

Circuit parameters	Circuit model by Ngo [1992]	FE solution
esr	$5.828 \times 10^{-3} \; ohms$	$3.920 \times 10^{-3} \; ohms$
esl	$5.283 \times 10^{-11} \; Henry$	$4.650 \times 10^{-11} \; Henry$
srf	$3.802 \times 10^7 \; Hz$	$3.765 \times 10^7 \; Hz$
Capacitance	$2.7778 \times 10^{-7} \; Farad$	$3.5857 \times 10^{-7} \; Farad$

the bottom electrode. These boundary conditions are similar to that shown in Figure 9.7.

Figure 9.14 shows the current distribution inside the electrodes. It is evident that unlike the assumptions in the circuit model, the distribution of current is not linear. Figure 9.15 and Table 9.3 compare the impedance predicted by the FE solution to the impedance obtained from the circuit model proposed by Ngo [1992]. Smaller values for *esr* and the *esl* are obtained using FE analysis. This difference in the lumped parameters can be explained by the change in the current distribution. The difference in the capacitance is explained as follows. The capacitance in the circuit model is simply estimated by

$$\frac{10 \times 10^{-6}}{(4 \times 4 \times 27)} \times (2 \times 2 \times 3) = 2.778 \times 10^{-7} \; Farad \; ,$$

however, the capacitance from the FE analysis is computed by the accurate distribution of the scalar potential.

The circuit model for the single cell is shown in Figure 9.16, and the numerical values of the components are listed in Table 9.4; see Remark 9.2 for details regarding the circuit model.

Table 9.4. Numerical values for the lumped parameters in Figure 9.16 for $2 \times 2 \times 3$ stack of cells without the top and bottom bus.

Circuit parameter parameters	Numerical value (SI units)
All resistance	1.889×10^{-2} $ohms$
All inductance	2.834×10^{-10} $Henry$
All capacitance	6.944×10^{-8} $Farad$
Mutual inductance	Varies depending on the location of the half-stacks
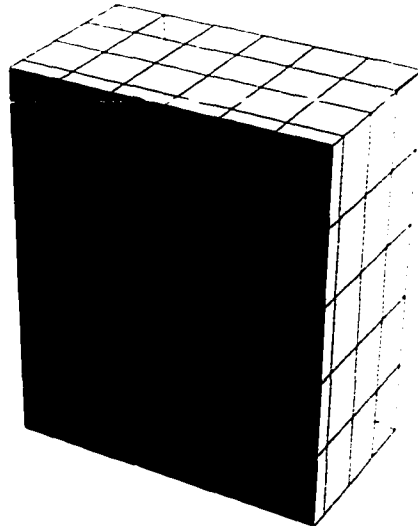
Figure 9.5. A mesh for a single cell including the surrounding air. The capacitor is sliced along a vertical plane passing through the center.
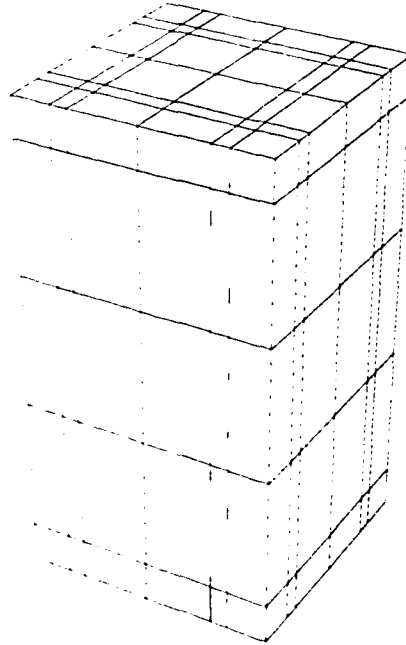

Figure 9.6. A mesh for the electrodes and the dielectric for a single cell.

Airbox

$(\psi_r = -1/\omega \; , \; \psi_i = 0)$

$\bar{\mathbf{A}} \cdot \hat{\mathbf{n}} = 0$

$(\psi_r = +1/\omega \; , \; \psi_i = 0)$
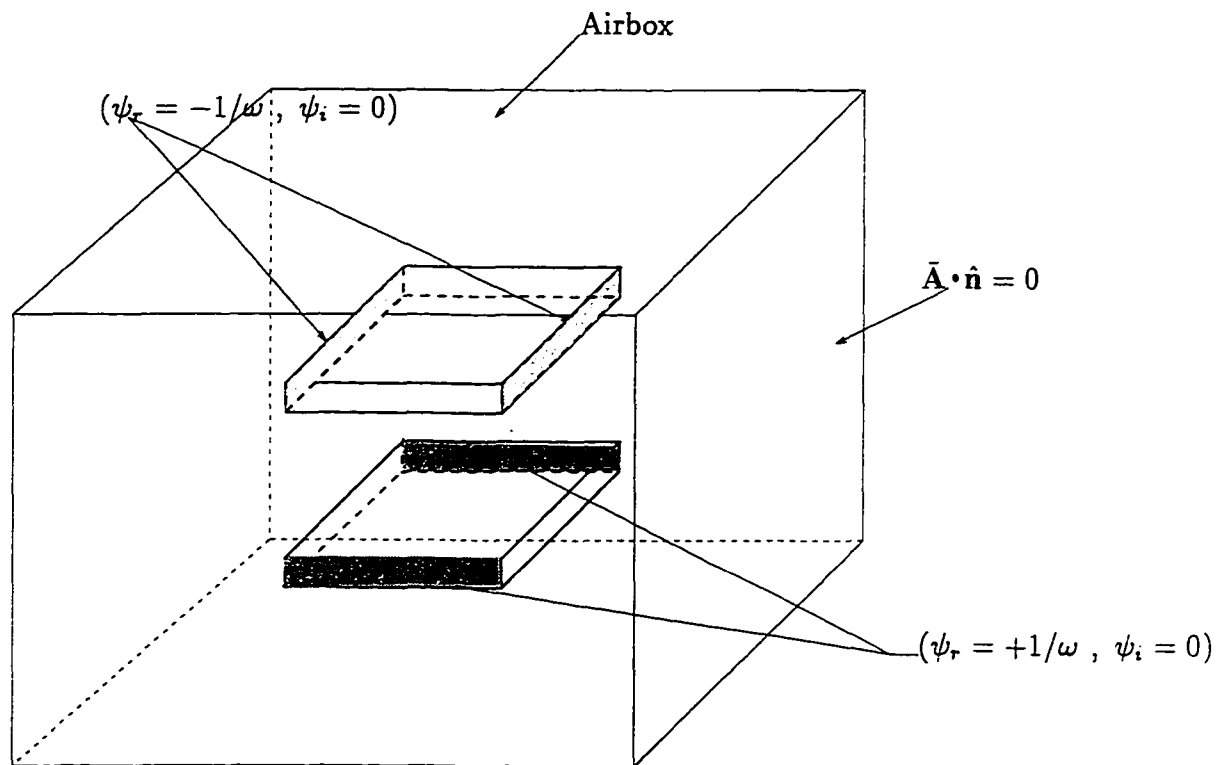
Figure 9.7. The boundary conditions and excitations imposed on the two electrodes in a single cell.
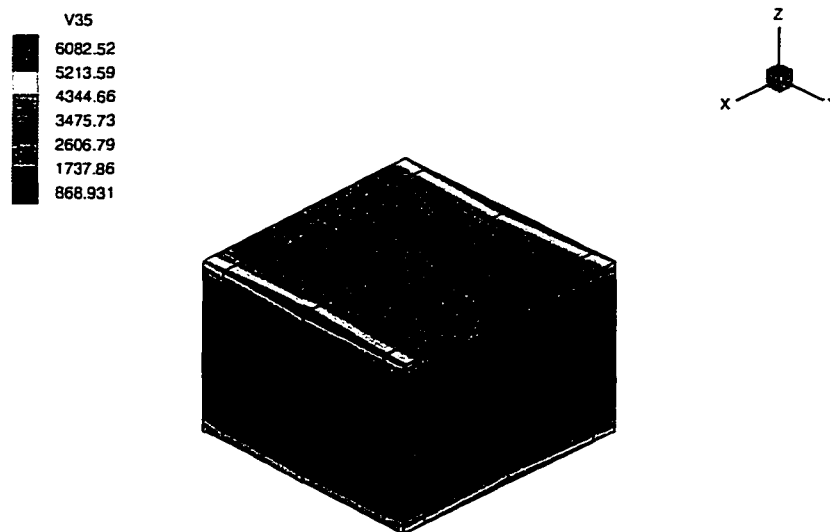
Figure 9.8. The current in the conductors of a single cell at frequency $f = \frac{10^8}{2\pi}$ Hz. We observe that the distribution of current in the electrodes is not linear. The current in the top electrode is along the x-direction, and the current in the bottom electrode is along the y-direction.
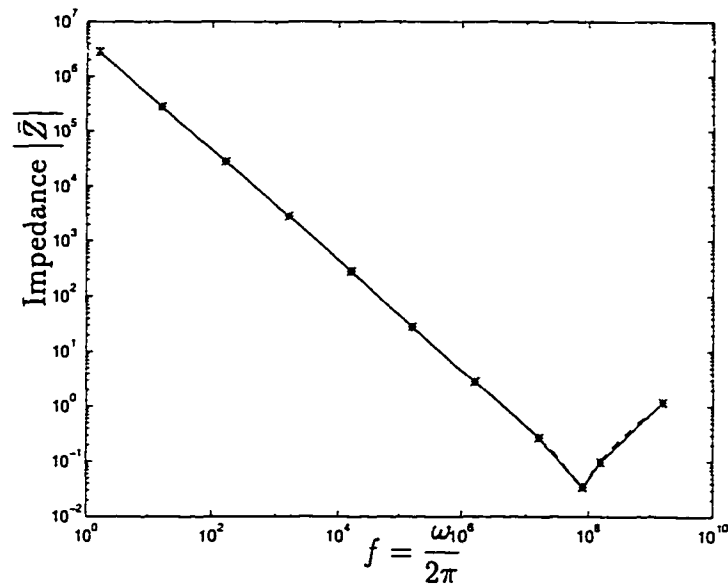
Figure 9.9. The impedance of a single cell as a function of frequency. The frequency $f = \frac{\omega}{2\pi}$ Hz. The solid line is from finite element analysis and the dotted line is from the circuit model.
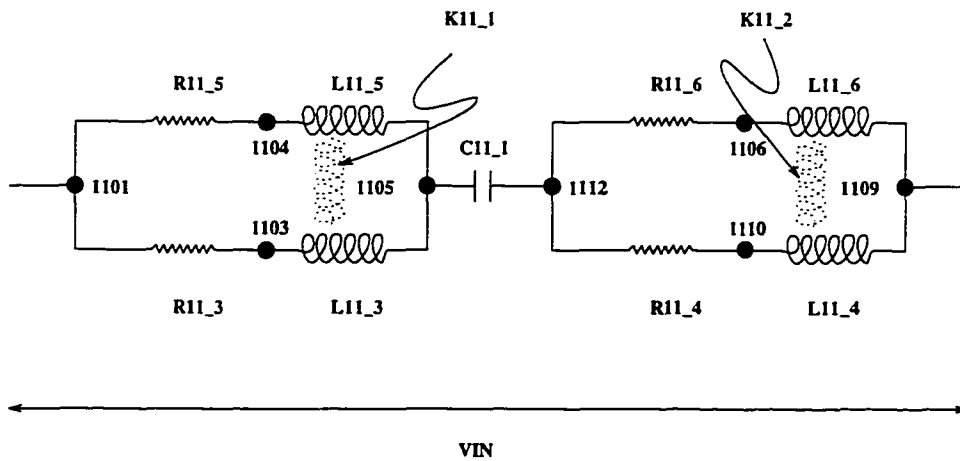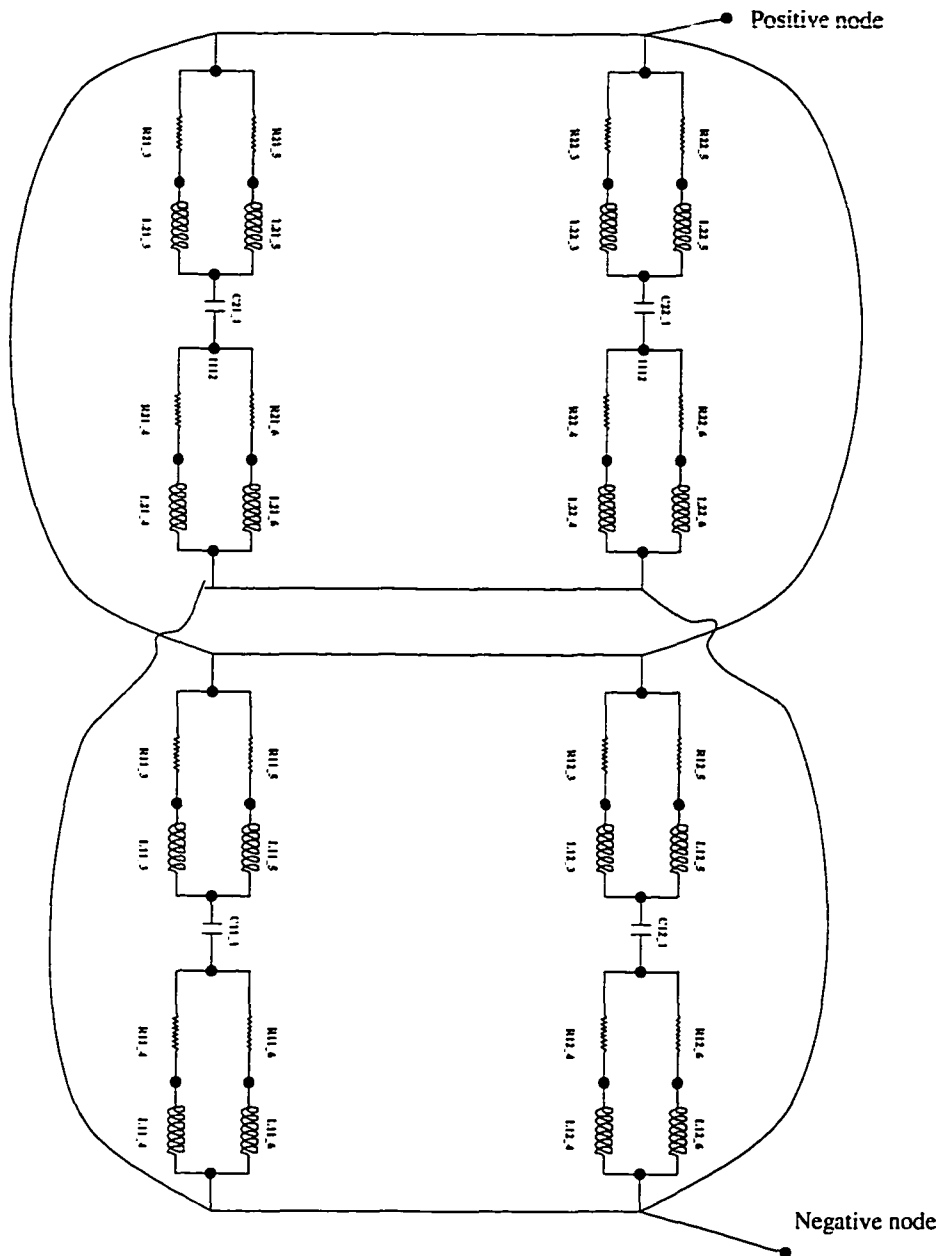

Figure 9.10. A circuit model for $1 \times 1 \times 1$ stack of cells without the top and bottom bus.
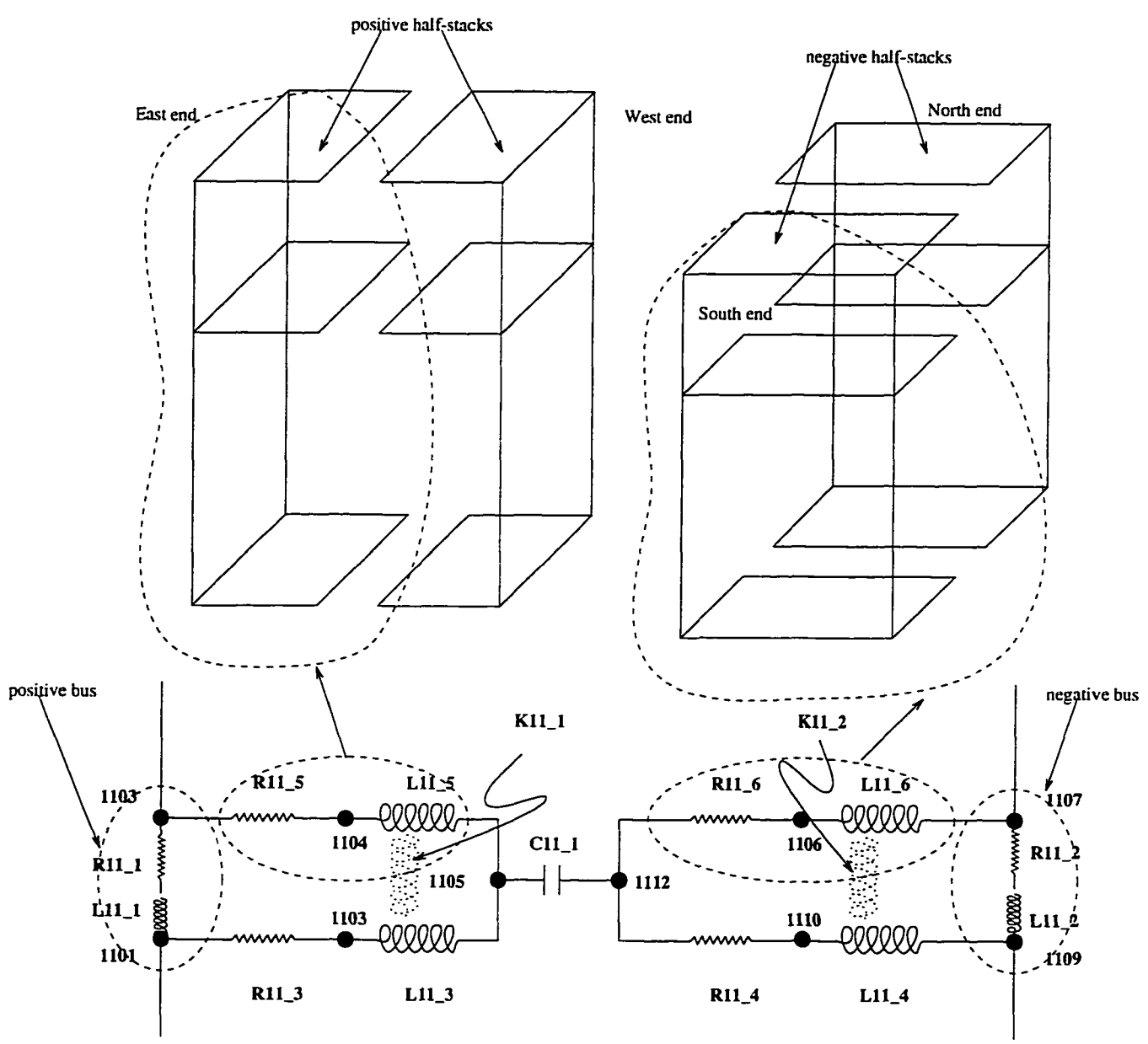
Figure 9.11. A circuit model for a stack of cells with the top and bottom bus.
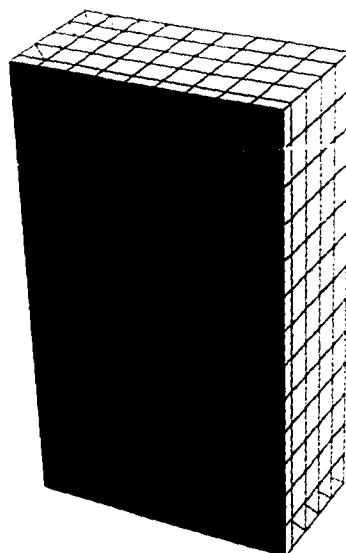
Figure 9.12. A mesh for a $2 \times 2 \times 3$ stack of cells including the surrounding air. The capacitor is sliced along a vertical plane passing through the center.
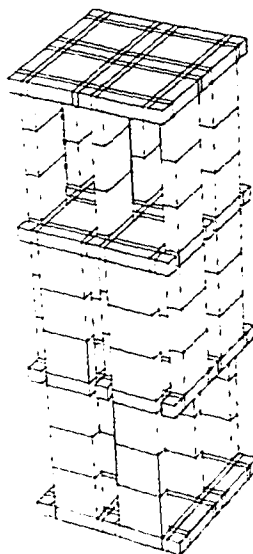
Figure 9.13. A mesh for the electrodes in the $2 \times 2 \times 3$ stack of cells.
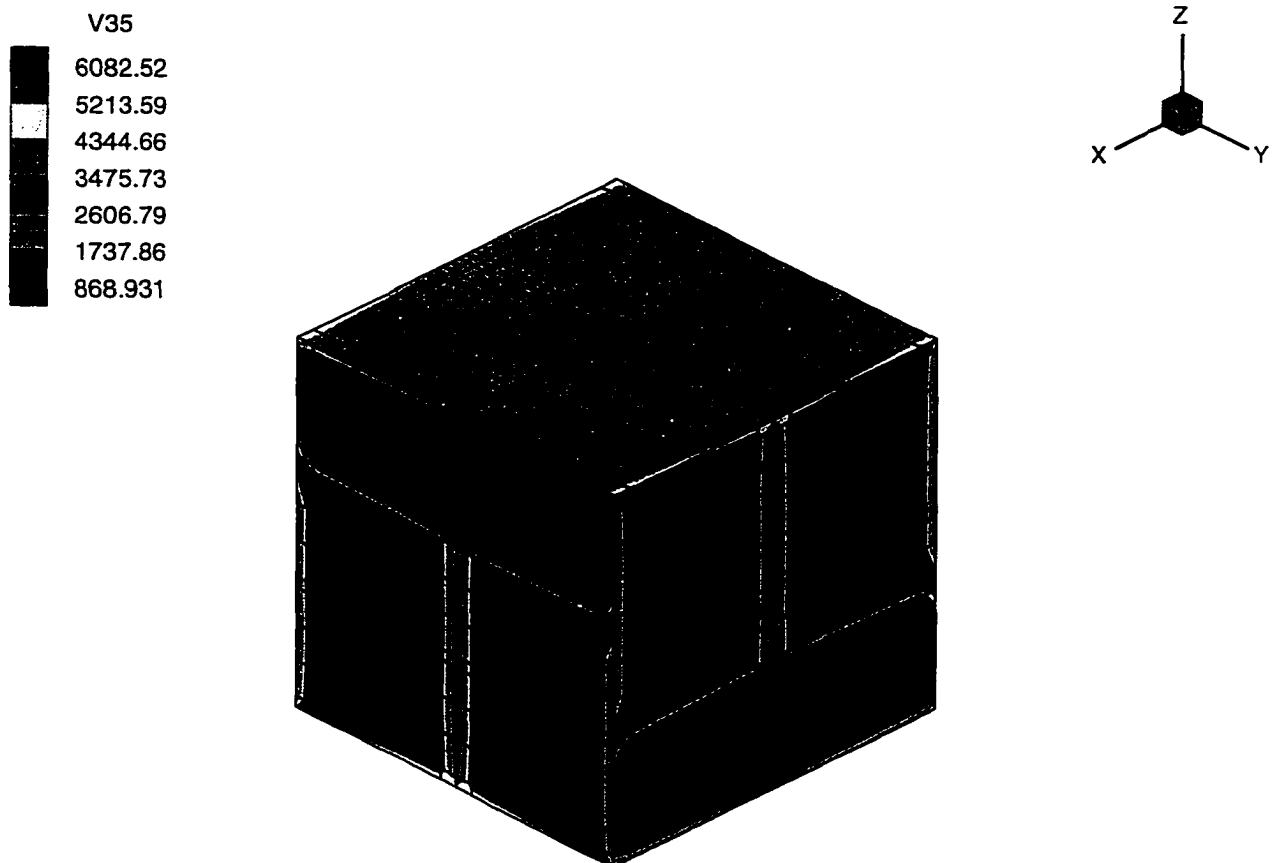
Figure 9.14. The current in the conductors of a $2 \times 2 \times 3$ stack of cells at high frequency. The frequency $f = \frac{10^8}{2\pi}$ Hz. The current in the top electrode is along the y-direction, and the current in the bottom electrode is along the x-direction.
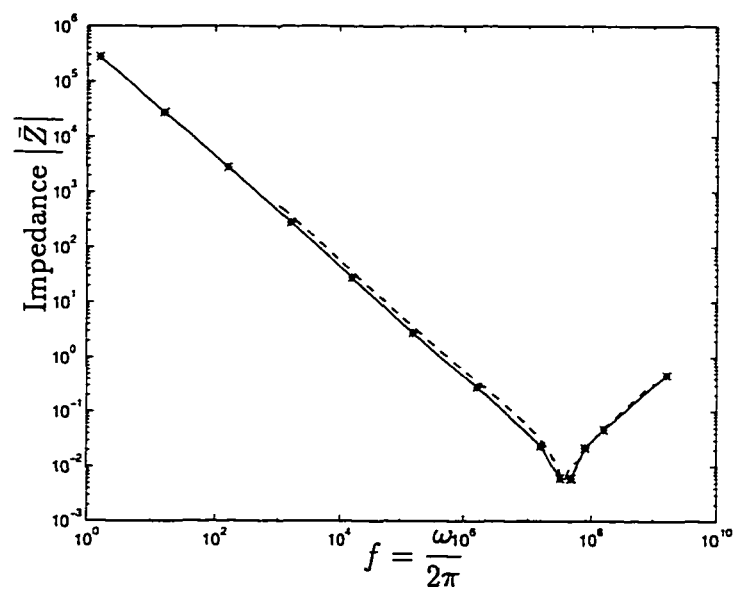
Figure 9.15. The impedance of a stack of $2 \times 2 \times 3$ cells as a function of frequency. The frequency $f = \frac{\omega}{2\pi}$ Hz. The solid line is from finite element analysis and the dotted line is from the circuit model.

Figure 9.16. A circuit model for $2 \times 2 \times 3$ stack of cells without the top and bottom bus. The mutual inductance is not shown in the above circuit.

CHAPTER 10
CLOSURE

We analyze new advanced MultiLayer Ceramic Capacitors (MLCCs) using the Finite Element (FE) method. We compute the lumped parameters—the resistance R, the inductance L, and the capacitance C—of a MLCC designed by Ngo [1990]. The behavior of the capacitor depends on the frequency of excitation. At low frequencies, the capacitive reactance dominates. At very high frequencies the inductance dominates. However, in between (from 10^5 to 10^8 Hertz), the interaction between the R, L, and C decides its behavior.

We introduce a multiple-scale technique to transform Maxwell equations from the SI unit system to a new *generalized* unit system. Scaling is useful to analyze a MLCC that has a complex geometry and a mixture of regions of finite conductivity and zero conductivity. For these miniature devices at the frequency of interest (below $10^7 ~ Hz$), in the SI unit system, the numerical values of the terms related to the electric current is substantially larger than those that are related to the other physical processes. The consequence is ill-conditioned matrices that make accurate analysis impossible.

In this work, we demonstrate that a suitable choice of the scaling parameter shifts the focus of the problem away from the dominating effect of the conductors, and as a consequence, reduces the condition number and significantly improves the accuracy. Moreover, the multiple-scale technique offers the flexibility to adjust to different geometrical shapes and material properties of the electrical components.

We use a coupled formulation with a choice of two algorithms to compute R,

229

L, C of the MLCC at different frequencies. The low frequency algorithm is used at frequencies significantly below the self-resonant frequency (srf), and the high frequency algorithm is used close to or above the srf. The srf for a 10 $\mu Farad$ MLCC designed by Ngo [1990] is in the order of 10^7 Hz. We develop a new FE code that combines the the multiple-scale technique with the two algorithms to compute accurate values for R, L, and C. Sophisticated mesh-generation routines are also developed to mesh the complicated geometrical shapes of the components that comprise the MLCC.

At zero frequency, the capacitance C of the 10 $\mu Farad$ MLCC computed using FE analysis shows a 20% difference from the experimental value. This difference is explained by changes in the geometry and the material properties during manufacturing.

At higher frequencies, the coupling between the electric and magnetic fields increases the size of the matrix equations. The available computer resources limit the time-harmonic analysis of the coupled electromagnetic problem to $2 \times 2 \times 3$ stack of cells. The results presented in this dissertation reveals the distribution of current in the electrodes: Unlike the distribution assumed by the circuit model proposed by Ngo [1992], the distribution of current is not strictly linear. The lumped parameters R and L computed using FE analysis is smaller than those predicted by Ngo [1992]'s circuit model.

The coupled formulation for electromagnetic problems, combined with newly developed mesh generation utilities, and the use of a multiple-scale technique, provides accurate analysis of advanced capacitors. This work demonstrates the efficacy of FE analysis in computing small values of inductance L. This formulation and implementation are applicable to design and analyze next-generation MLCCs and other passive electromagnetic devices.

APPENDIX A
CIRCUIT SIMULATOR

In the present work we use a circuit simulator called ACS (Al's Circuit Simulator) developed by Albert Davis, Rochester, NY (Davis [1996]). ACS is similar to SPICE, however, it is written in C++ and is a public domain software. Entire package can be obtained from `ftp://mammoth.lle.rochester.edu/pub/local/acs`. ACS provides a convenient interactive tool to simulate DC, AC, and transient circuits. It provides a "true" mixed mode simulation between analog and digital devices. The author claims that an input file for ACS can be used with SPICE, and vice-versa, with minimal changes. ACS also has a simple behavioral modeling language that allows simple description of the behavior of various components ranging from capacitors to MOSFETS.

In our present research we use the results from ACS to compare with the lumped parameters obtained from the FE solution. The the input file for ACS is similar to SPICE. For example, a simple circuit in Figure A.1 models a single stack of $1 \times 1 \times 14$ cells in a capacitor, where the geometry of each cell is described in Figure 7.3. The circuit model does not include the top and bottom bus. Hence, the behavior of the $1 \times 1 \times 14$ is slightly different from the model in Anand [1993, p. 48]. The numerical values for the resistances, inductances, and the capacitance in the circuit model are same as in Anand [1993, p. 48]; this model has been explained earlier in Chapter 9. The ACS input file `1.1.14.cells.ckt` for the circuit in Figure 7.3 is as follows.

```
*****************************************
* Input file from ACS Version 0.19:
* (Fri Feb  2 18:58:14 EST 1996)
```

231

```
*    1 x 1 x 14 stack of cells without the top and
*    bottom buses.
*********************************************

* Define the resistors
* Name    Node 1    Node 2    Value
R11`3     1101      1111      0.0034
R11`4     1112      1110      0.0034
R11`5     1101      1104      0.0034
R11`6     1112      1106      0.0034

* Define the inductors
* Name    Node 1    Node 2    Value
L11`3     1111      1105  0.31512e-09
L11`4     1110      1109  0.31512e-09
L11`5     1104      1105  0.31512e-09
L11`6     1106      1109  0.31512e-09

* Define the capacitor
* Name    Node 1    Node 2    Value
C11`1     1105      1112   0.625e-6

* Define the coupling coefficient between the inductors
* Name    Inductor 1    Inductor 2    Coupling coefficient
*                             M`ij / sqrt(L`i*L`j)
K11`1     L11`3         L11`5         -0.54214
K11`2     L11`4         L11`6         -0.54214

* Initialize the voltages
*
* Name    Node 1    Node 2    Value
VIN       1101      1109      AC 1.0
   *      AC value of input voltage
   *      This is an independent
   *      voltage source
VG        1109                0 0
   *      DC and AC value are zero

* Specify the parameters that need to be printed for AC analysis
*    VM(1101)    Magnitude of voltage at 1101
*    IR(VIN)     The real part of the input current
*    II(VIN)     The imaginary part of the input current
* The impedance is Z = VM / (IR + i*II)
.PRINT AC VM(1101) IR(VIN) II(VIN)

* Perform the AC analysis. The frequency is swept logarithmically by
* decades.
*    ¡number of points¿ = 1000
*    ¡start value¿      = 100
*    ¡end value¿        = 1000MEG
*    The keyword "Basic" makes the tabular data in standard format
*    that can be used by MATLAB
.AC Basic DEC 1000 100 1000MEG

* End; do not return to interactive mode
.END
```

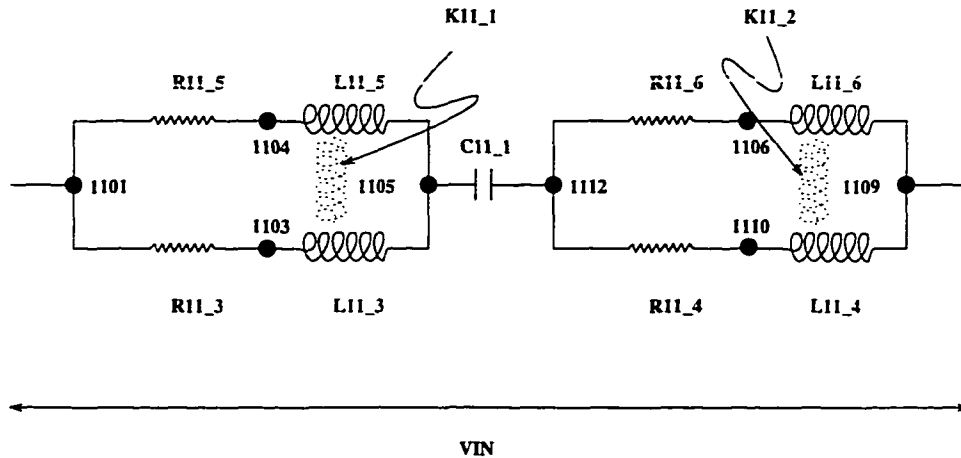The circuit simulator ACS is installed in the directory v̄inay/lib/acs. We

Figure A.1. A circuit model for $1 \times 1 \times 14$ stack of cells without the top and bottom bus.

can access the code by typing the following commands on aemes, a DEC-ALPHA machine, with OSF 2.0+ operating system.

```
% cd ~vinay/lib/acs
% acs019.dec-alpha-osf 1.1.14.cells.ckt > acs.out
```

The tabular output (ACS does not include graphics) that is saved in the file acs.out can be used in MATLAB to plot the results. A sample of the output file acs.out is as follows.

```
ACS (Al's Circuit Simulator) 0.19
Never trust any version less than 1.0
Copyright 1994, Albert Davis
ACS comes with ABSOLUTELY NO WARRANTY
This is free software, and you are welcome
to redistribute it under certain conditions.
See the file "COPYING" for details
*********************************************
#Freq    VM(1101)  IR(VIN)   II(VIN)
100.    1.      -538.4E-12 -392.7E-6
100.23  1.      -523.9E-12 -393.6E-6
100.46  1.      -523.9E-12 -394.51E-6
100.69  1.      -538.4E-12 -395.42E-6
```

```
.
.
.
986.26E+6  1.     -0.004268  1.1187
988.55E+6  1.     -0.0042484  1.1162
990.83E+6  1.     -0.0042288  1.1136
993.12E+6  1.     -0.0042094  1.111
995.41E+6  1.     -0.00419   1.1085
997.7E+6   1.     -0.0041708  1.1059
1.E+9      1.     -0.0041516  1.1034
```

A plot of the impedance versus frequency is generated using the values in the acs.out; The variation of the magnitude and the phase angle of impedance are plotted in Figure A.2. Recall that the impedance

$$\tilde{Z} = \frac{\bar{V}}{\bar{I}} = Z_r + iZ_i \ .$$

The following MATLAB code is used to generate the figure and calculates the *esr*, *esl*, ans *srf*.

```
clear all
load acs.dat

% Frequency
f = acs(:,1);

% voltage
vm = acs(:,2);

% Real and imaginary part
cr = acs(:,3);
ci = acs(:,4);

% Impedance
z = vm ./ ( cr + i*ci);

% Plot the magniude
zm = abs(z);
zp = - atan(ci./cr);

% Plot the magnitude
loglog(f,zm);
xlabel('frequency')
ylabel('Magnitude')
print -dps mag.ps
pause
```

Table A.1. Equivalent circuit parameters: For the circuit in Figure A.1, i.e., a stack of $1 \times 1 \times 14$ without the top and bottom bus.

Circuit Parameter	Analytical formula	Analytical value	From ACS
esr	R	$3.4000 \times 10^{-3}\ ohms$	$3.4000 \times 10^{-3}\ ohms$
esl	$L - \mathfrak{M}$	$1.4428 \times 10^{-10}\ Henry$	$1.4423 \times 10^{-10}\ Henry$
srf	$\dfrac{1}{2\pi\sqrt{LC}}$	$1.6762 \times 10^{7}\ Hz$	$1.6749 \times 10^{7}\ Hz$
Capacitance	C	$6.25 \times 10^{-7}\ Farad$	$6.25 \times 10^{-7}\ Farad$

```
% Plot the phase
semilogx(f,zp*180/pi);
xlabel('frequency')
ylabel('Phase angle')
print -dps phase.ps

% Calculate the esr and srf
[zz,ii] = min(abs(zp));
fprintf(1,'ESR = %19.12e \n',zm(ii))
fprintf(1,'SRF = %19.12e \n',f(ii))
n = length(z);
fprintf(1,'ESL = %19.12e \n',-imag(z(n))/2/pi/f(n))
[zz,ii] = min(imag(z));
fprintf(1,'CAP = %19.12e \n',1/imag(z(1))/2/pi/f(1))
```

The impedance for the simple circuit in Figure A.1 is given by the following formula.

$$\bar{Z} = 2\frac{R + i\omega L - i\omega\mathfrak{M}}{2} + \frac{1}{i\omega C}\ ,$$

where R is the resistance for all the resistors, L is the inductance for all the inductors, C is the capacitance of the capacitor, and $\mathfrak{M}$ is the mutual inductance between (L11_3 and L11_5), and (L11_4 and L11_6). Table A.1 provides a comparison between the values obtained from the above formula to those obtained from ACS.
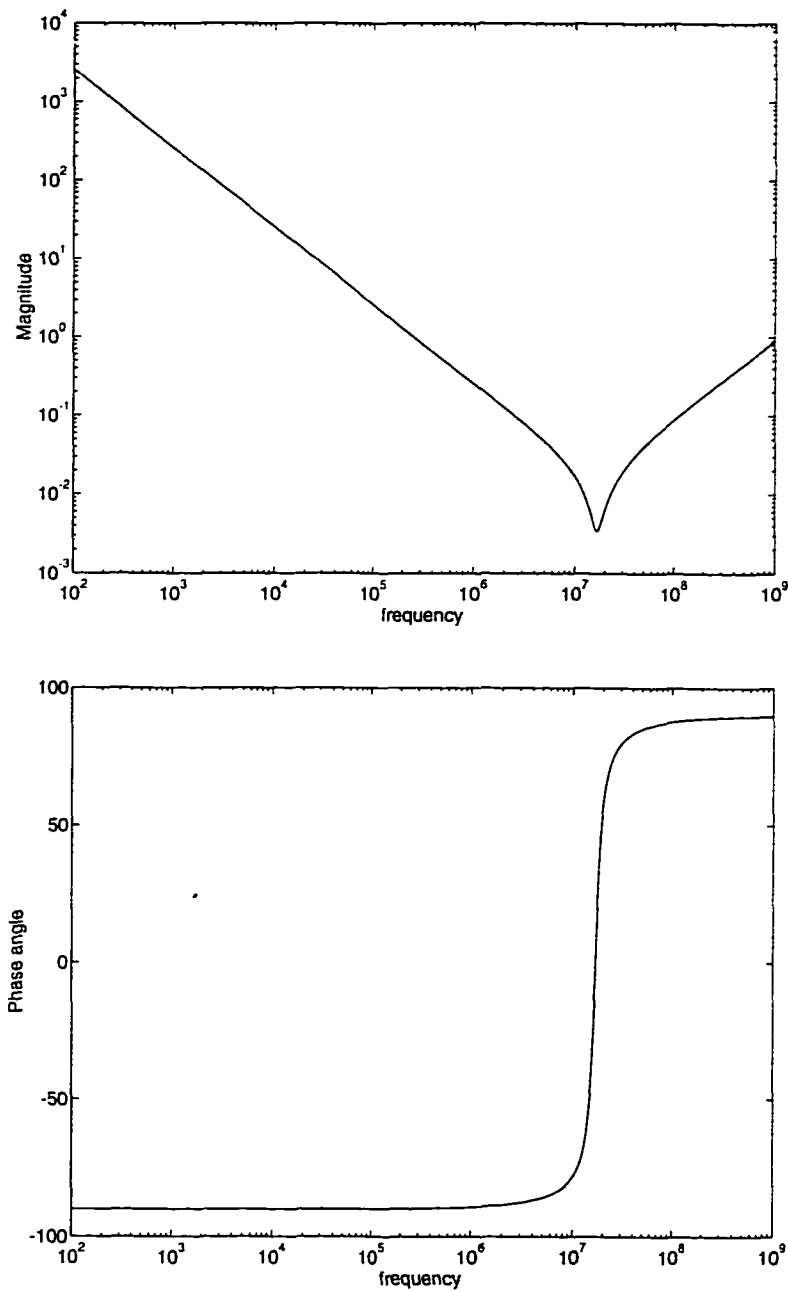
Figure A.2. The impedance versus frequency for $1 \times 1 \times 14$ stack of cells without the bus obtained using ACS. The $srf = 16.75MHz$, the $esr = 3.41 \times 10^{-3}$ $ohms$, the $esl = 1.44 \times 10^{-10}$ $Henry$, and the capacitance is 0.625×10^{-6} $Farad$.
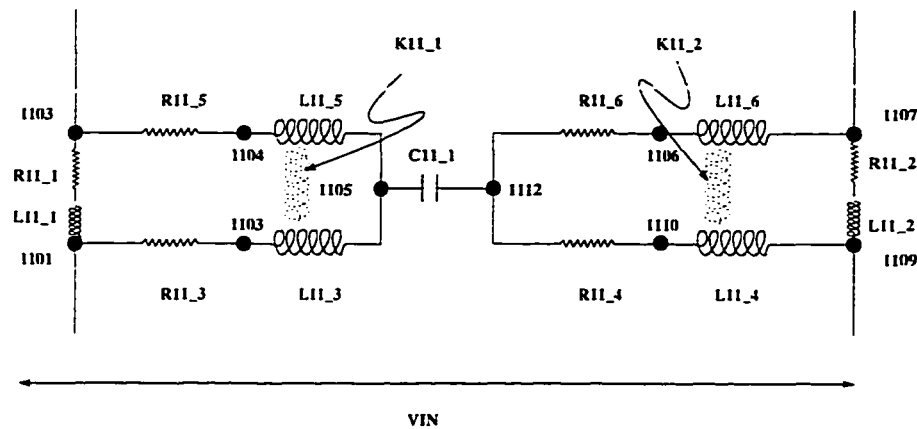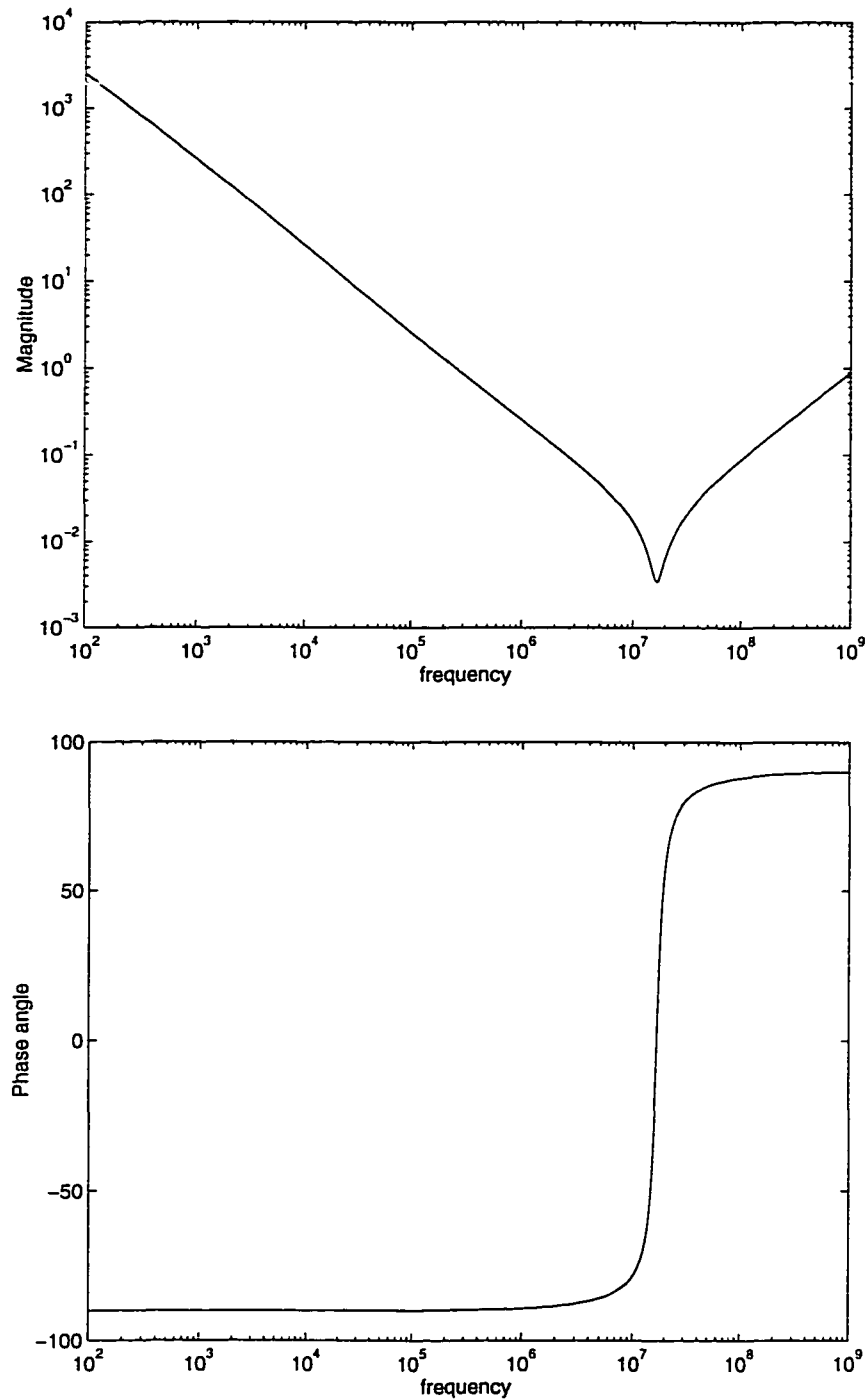
Figure A.3. A circuit model for $1 \times 1 \times 14$ stack of cells with the top and bottom bus.

The circuit in Figure A.3 is an extension to the above example: The circuit includes the top and bottom bus. Table A.2 compares the results from the ACS circuit simulator to an equivalent SPICE simulation presented in Anand [1993, p. 54]. An AC voltage is applied between nodes 1101 and 1109. Note that node 1101 is connected to node 1103, and node 1107 is connected to node 1109. Hence, the circuit parameters for the circuit without the bus is same as the one with the bus. The variation of the magnitude and the phase angle of the impedance are plotted in Figure A.4. From Table A.2 it is evident that there is a difference between the ACS results presented here and the results presented in Anand [1993, p. 54]. This difference remains to be explained.

We also construct a circuit for the entire $4 \times 4 \times 27 = 432$ cells in the MLCC. The construction of the circuit has been outlined in Remark 9.2. A detailed construction of the circuit model is presented in Anand [1993]. Once again we observe a difference between the ACS results presented here and the results presented in Anand [1993, p. 54]. Table A.3 compares the results from the ACS circuit sim-

Figure A.4. The impedance versus frequency for $1 \times 1 \times 14$ stack of cells with the bus obtained using ACS. The $srf = 16.75MHz$, the $esr = 3.41 \times 10^{-3}$ $ohms$, the $esl = 1.44 \times 10^{-10}$ $Henry$, and the capacitance is 0.625×10^{-6} $Farad$.

Table A.2. Equivalent circuit parameters: For the circuit in Figure A.3, i.e., a stack of $1 \times 1 \times 14$ with the top and bottom bus.

Circuit parameters	From ACS	From Anand [1993, p. 54]
esr	3.405×10^{-3} $ohms$	3.850×10^{-3} $ohms$
esl	1.442×10^{-10} $Henry$	1.432×10^{-10} $Henry$
srf	1.675×10^{7} Hz	1.757×10^{7} Hz
Capacitance	6.25×10^{-7} $Farad$	6.25×10^{-7} $Farad$

Table A.3. Equivalent circuit parameters: For the circuit of the complete MLCC, i.e., for $4 \times 4 \times 27 = 432$ cells and the top and bottom bus.

Circuit parameters	From ACS	From Anand [1993, p. 56]	Experimental results
esr	3.317×10^{-4} $ohms$	1.290×10^{-3} $ohms$	6.7×10^{-4} $ohms$
esl	1.827×10^{-11} $Henry$	6.957×10^{-11} $Henry$	1.480×10^{-11} $Henry$
srf	1.142×10^{7} Hz	6.030×10^{7} Hz	1.300×10^{7} Hz
Capacitance	1.0×10^{-5} $Farad$	1.0×10^{-5} $Farad$	1.0×10^{-5} $Farad$

ulator to an equivalent SPICE simulation presented in Anand [1993, p. 56]. The configuration of the example considered here, corresponds to Case 1 with contact at both sides. The esl predicted from ACS is closer to experiments, however, the esr is smaller than the experimental results. The variation of the magnitude and the phase angle of the impedance are plotted in Figure A.4; the variation of impedance presented in these figures differ from the variation presented in Anand [1993, p. 53].
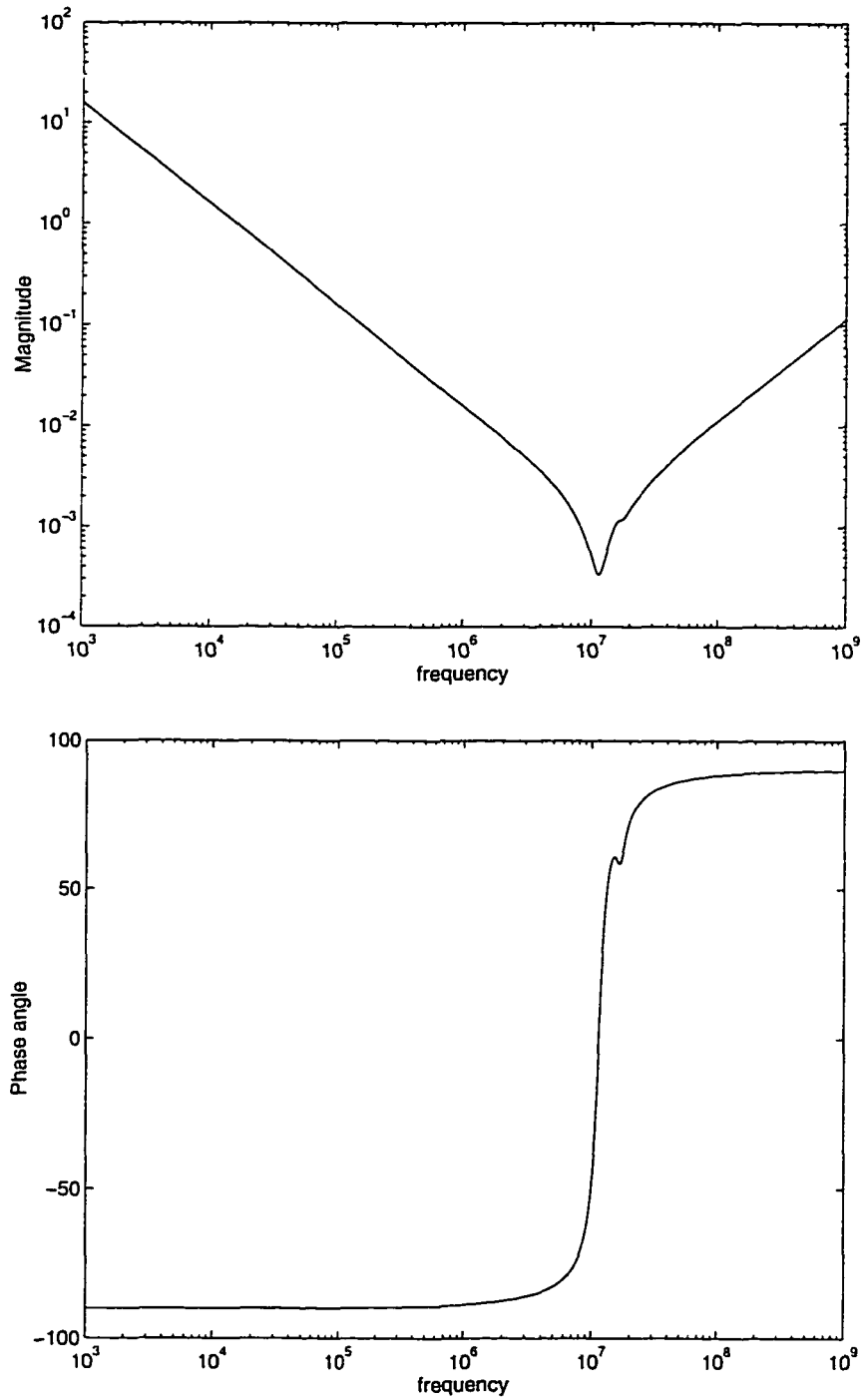
Figure A.5. The impedance versus frequency for entire 10 $\mu Farad$ MLCC, i.e., $4 \times 4 \times 27$ stack of cells with the bus obtained using ACS.

APPENDIX B
CONSTITUTIVE MODELS FOR HIGH PERFORMANCE
MATERIALS

The volume efficiency of capacitors depends on the magnitude of the permittivity of dielectric materials: The higher the permittivity, the larger the capacitance per unit volume, and hence the smaller the capacitor. Common dielectric materials employed in MLCCs today are high-permittivity ceramics based on barium titanate ($BaTiO_3$). Constitutive laws for polycrystalline ceramic $BaTiO_3$ can be obtained from constitutive laws for single-crystal $BaTiO_3$ by means of "averaging" methods such as those presented in Mason [1948], Marutake [1956], Yurkevich and Rolov [1986], etc. Thus to obtain a good model for ceramic $BaTiO_3$, it is important to obtain first an accurate constitutive model for single-crystal $BaTiO_3$ that agrees with experimental measurements at various temperatures. Accurate constitutive models are essential to maximize the various tensor properties of ferroelectrics leading toward optimal design of electrical devices. However, such an accurate constitutive model has yet to be obtained. We propose a methodology based on semi-infinite optimization to obtain accurate constitutive models for single crystal ferroelectrics for all the phases (i.e, for all temperatures).

These high permittivity dielectrics such as $BaTiO_3$ are ferroelectric. Ferroelectrics are characterized by reversible spontaneous polarization P_s,—i.e., polarization at zero electric field—and the existence of hysteresis loops in the relation between polarization P and electric field E. Ferroelectric crystals are *pyroelectric* (electrical and mechanical properties depend on temperature), *piezoelectric* (mechanical strains are linearly dependent on electric field), and *electrostrictive* (strains depend quadratically on electric field, i.e., deformation does not change by reversing

241

the electric field). The remainder of the section will focus on $BaTiO_3$.

Since the late '40s there has been considerable research to obtain constitutive models for ferroelectric material. One of the more popular methods is based on the thermodynamic phenomenological theory by Ginzburg [1946] and Devonshire [1949]. They successfully extended the basic idea of Landau's theory of phase transitions to explain the complicated sequence of phase transitions in $BaTiO_3$ and the interrelationships between the macroscopic anomalies accompanying the transitions.

$BaTiO_3$ acquires different crystal structures as temperature (denoted by θ) decreases from above the Curie temperature θ_c ($= 117°C$): cubic ($\theta \geq 117°C$), tetragonal ($117°C \geq \theta \geq 5°C$), orthorhombic ($5°C \geq \theta \geq -80°C$), rhombohedral ($-80°C \geq \theta$); see Jona and Shirane [1962, p.110]. The tetragonal, orthorhombic, and rhombohedral phases are ferroelectric. Due to the change in crystal symmetry, the direction of spontaneous polarization P_s changes with the crystal phases. In the cubic phase, $P_s = 0$. When the cubic crystal is cooled below the Curie temperature into the tetragonal phase, one of the edges of the cube, called the c-axis (3-axis), elongates, whereas the other two edges of the cube, called the a-axes (1-axis and 2-axis), shorten. In the tetragonal phase, P_s is along the c-axis (the elongated edge of the cube). Since there are 6 edges (<100> directions) of the original cube, the c-axis (polar axis) can be along any one of the six equivalent directions. Similarly in the orthorhombic phase, P_s is along one of the facet-diagonals (any one of the 12 equivalent <110> directions of the original cube), and in the rhombohedral phase along one of the body-diagonals (any one of the 8 equivalent <111> directions of the original cube). The number of non-zero components of the permittivity tensor change with the change in the direction of P_s. Most other ferroelectrics display first-order transitions, see, e.g., Smolenskii et al. [1984, p.58]. Single crystal $BaTiO_3$ also exhibits hysteresis effects Merz [1953].

The phenomenological model starts with a Taylor series expansion of the governing thermodynamic potential—the elastic Gibbs function—in terms of the independent variables. The elastic Gibbs function G_1^t, used extensively in the present work—with temperature, mechanical stress, and electrical polarization as independent primary variables—is expanded about the state with zero stresses and zero polarization. The coefficients of G_1^t are functions of temperature, and are determined based on experimentally measured properties of the crystal. The resulting model is then used to predict other properties of the crystal.

A successful phenomenological model must be able to reproduce the discontinuities of ferroelectric properties at the phase transitions, in addition to being able to represent accurately the electrical properties such as polarization and permittivity within each crystal phase. The electrical properties in the 4 phases of $BaTiO_3$, the first-order phase transitions and their associated discontinuities requires the imposition of equality and functional-inequality constraints on the coefficients of G_1^t. Thus far, ad hoc methods have been proposed to determine the coefficients of G_1^t, yielding inaccurate models that violate the constraints (Srinivas and Vu-Quoc [1992]). The consequences of these constraint violations are the large errors in the values of spontaneous polarization and of permittivity coefficients, erroneous transition temperatures, and the absence of one or more crystal phases.

We have proposed and successfully demonstrated a methodology based on semi-infinite optimization to determine the unknown coefficients of G_1^t for $BaTiO_3$ (Srinivas and Vu-Quoc [1992]). The optimal solution when used in the model accurately predicts the ferroelectric properties of $BaTiO_3$ single-crystals—phase transitions, spontaneous polarization, permittivity, etc.—over a range of temperatures in all the four phases of $BaTiO_3$.

Finding the minimum of the relative errors between the analytical and exper-
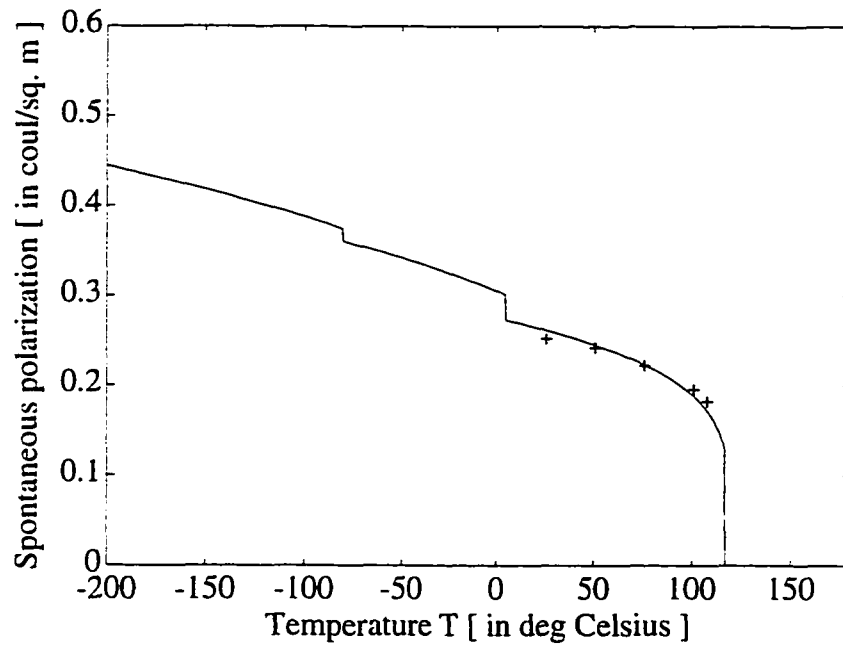
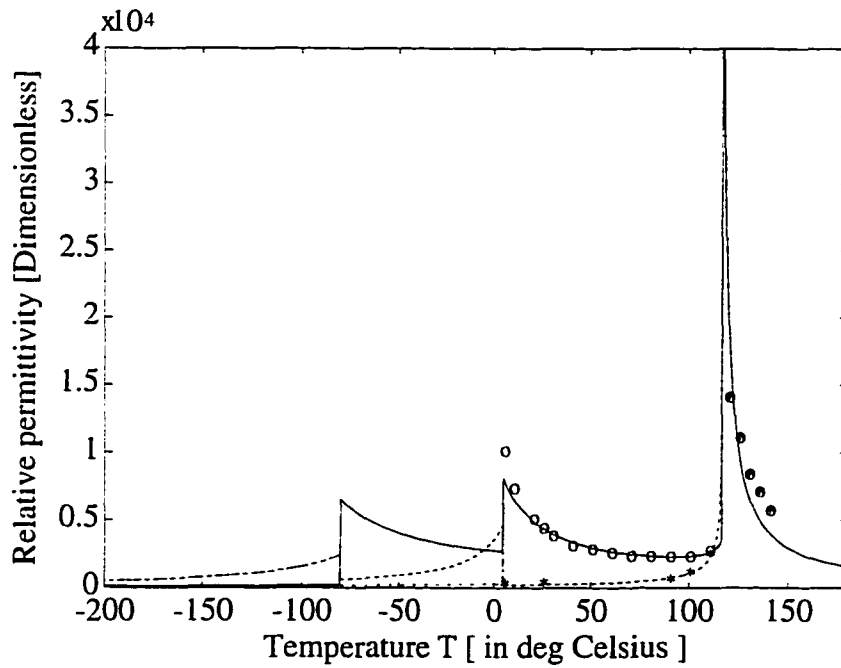Figure B.1. Spontaneous polarization vs. temperature.

Figure B.2. Relative permittivity coefficients vs. temperature at zero electric field.

imental values, subjected to functional constraints, is a *semi-infinite optimization* problem, which refers to optimization problems having a *finite* number of design parameters and an *infinity* of constraints, which are in general nonlinear equality and/or inequality constraints. A functional constraint, which depends on a continuous independent parameter in addition to a finite set of design parameters, can be thought of as equivalent to an infinity of constraints. Let $x \in \mathbf{R}^n$ represent the design parameters, whose number (n) is finite; $f: \mathbf{R}^n \to \mathbf{R}$ the objective (or cost) function; $g_i: \mathbf{R}^n \times \mathbf{R} \to \mathbf{R}$, for $i = 1, \cdots, l$, the l functional inequality constraints; and $h_j: \mathbf{R}^n \to \mathbf{R}$, for $j = 1, \cdots, m$, the m equality constraints. A functional constraint $g_i(\mathbf{x}, y) \leq 0$ for all $y \in Y_i \subset \mathbf{R}$, where Y_i is a compact interval in $\mathbf{R}$, can be thought of as equivalent to an infinite number of constraints. The following statement

$$\min_{\mathbf{x} \in \mathbf{R}^n} \{ f(\mathbf{x}) \mid \quad g_i(\mathbf{x}, y) \leq 0 \ \forall y \in Y_i \subset \mathbf{R} \ , \ \text{for } i = 1, \cdots, l$$
$$h_j(\mathbf{x}) = 0, \ \text{for } j = 1, \cdots, m, \ \} \ ,$$

$$(\text{B.1})$$

in which the functions f, g_i, for $i = 1, \cdots, l$, and h_j, for $j = 1, \cdots, m$ are assumed to be locally Lipschitz continuous, is a *semi-infinite optimization* problem. Here, f, g_i, h_j are functions of the coefficients of the elastic Gibbs function. These coefficients are assumed in the present work to be polynomial functions of the temperature y and the design parameters $\mathbf{x}$. The objective function $f(\mathbf{x})$ defined to be the error between the analytical and the experimental values in the permittivity coefficients and in spontaneous polarization. The functional-inequality constraints enforce the appropriate crystal phase in each temperature region. The equality constraints enforce the first-order phase transitions at the transition temperatures. Note that due to the presence of the equality constraints in B.1, there are several difficulties encountered in its solution, which are discussed in Srinivas and Vu-Quoc [1995].

In Vu-Quoc and Srinivas [1994], we demonstrate the success of the semi-infinite

optimization based methodology by obtaining a simple phenomenological model for the cubic and tetragonal phases of $BaTiO_3$. In Vu-Quoc and Srinivas [1996], we have obtained, for the first time, a model for all the four phases of $BaTiO_3$. A substantial difference, of over 500% is observed between the overall relative errors from the models obtained using the existing methods and that obtained using the proposed methodology. Figures B.1 and B.2 show the remarkable agreement of the optimal model (represented by solid and dashed lines) with the experimental data (represented by '+', 'o', and '*') over all the four phases.

The proposed methodology offers an approach to "design" general phenomenological models for ferroelectrics with a virtually unlimited flexibility for generalization not available hitherto. The optimal model obtained is simple, i.e., uses only a few design parameters by assuming the coefficients of the elastic Gibbs function to be either constants or linear functions of temperature. Unlike the ad methods used in the past, the proposed methodology does not restrict one to such a simple model. Furthermore, despite the disagreement on the experimental values of $BaTiO_3$ crystals sometimes found in the literature, we emphasize, however, that the proposed methodology to develop phenomenological models for $BaTiO_3$ crystals in particular, and for ferroelectric crystals in general, based on semi-infinite optimization approach can be applied to any set of experimental values. Also it is noted that the proposed methodology can be generalized for application to tungsten bronze ferroelectrics Cross and Neurgaonkar [1992], and to ferroelastic materials such as $KH_3(SeO_4)$, TeO_2, V_3Si, $SrTiO_3$, and to ferroelectric-ferroelastic materials such as KH_2PO_4 and $BaTiO_3$ (see Toledano, Fejer and Auld [1983]).

REFERENCES

Albanese, R. and Rubinacci, G. [1990], Magnetostatic field computations in terms of two-component vector potentials, *International Journal for Numerical Methods in Engineering* **29**, 515–532.

Anand, V. [1993], Lumped parameter model for a multilayer matrix capacitor, Master's thesis, University of Florida, Gainesville, FL.

Barnes, J. L. and Lomax, R. J. [1977], Finite-element methods in semiconductor device simulation, *IEEE Transactions on Electron Devices* **ED-24**(8), 1082–1089.

Bernadou, M., George, P. L., Hassim, A., Joly, P., Laug, P., Perronet, A., Saltel, E., Steer, D., Vanberborck, G. and Vidrascu, M. [1986], *MODULEF: A Modular Library of Finite Elements*, INRIA, France.

Bossavit, A. [1989], Simplicial finite elements for scattering problems in electromagnetism, *Computers Methods in Applied Mechanics and Engineering* **76**, 299–316.

Bossavit, A. [1990], Solving maxwell equations in a closed cavity, and the question of spurios modes, *IEEE Transactions on Magnetics* **26**(2), 702–705.

Brauer, J. R., Larkin, L. A., MacNeal, B. E. and Ruehl, J. J. [1991], New nonlinear algorithm for finite element analysis of 2D and 3D magnetic fields, *Journal of Applied Physics* **69**(8), 5044–5046.

Brown, M. L. [1982], Calculation of 3-dimensional eddy currents at power frequencies, *IEE Proceedings, Part A* **129**(1), 46–53.

Carpenter, C. J. [1977], Comparison of alternative formulations of 3D magnetic field and eddy current problems at power frequencies, *IEE Transaction* **124**, 1026–1034.

Cendes, Z. J., Weiss, J. and Hoole, S. R. H. [1982], Alternative vector potential formulations of 3d magnetostatic field problems, *IEEE Transactions on Magnetics* **18**(2), 367–372.

Ciarlet, P. G. [1987], Finite element approximation theory, *in* H. Kardestuncer, ed., *Finite Element Handbook*, McGraw Hill, New York, chapter 4.

Cook, R. D., Malkus, D. S. and Plesha, M. E. [1989], *Concepts and Applications of Finite Element Analysis*, 3rd edn, John Wiley and Sons, New York.

Courant, R. and Hilbert, D. [1962], *Methods of Mathematical Physics, Volume 2*, John Wiley & Sons, New York.

Cross, L. E. and Neurgaonkar, R. R. [1992], Phenomenological analysis of tetragonal tungsten bronze ferroelectrics, *Journal of Materials Science* **27**, 2589–2594.

Davis, A. [1996], *ACS (Al's Circuit Simulator) Users Manual*, Rochester, NY. Can be obtained from `ftp://mammoth.11e.rochester.edu/pub/local/acs`.

DeFrancesco, R. [1996], Low-tech wonders, *in* L. Ruskeyer, ed., *Louis Ruskeyer's Wall Street*, 1101 King St, Suite 400, Alexandria, VA 22314, p. 11.

Emson, C. R. I. [1988], Methods for the solution of open-boundary electromagnetic-field problems, *IEE Proceedings, Part A* **135**(3), 152–158.

Eringen, C. A. and Maugin, G. A. [1990], *Electrodynamics of Continua-I: Foundation & Solid Media*, Springer-Verlag, New York.

George, P. [1991], *Automatic Mesh Generation*, John Wiley & Sons, Baffins Lane, Chichester; West Sussex, England.

Golub, G. H. and van Loan, C. F. [1987], *Matrix Computations*, 1st edn, The Johns Hopkins University Press, Baltimore.

Gratkowski, S. and Ziolkowski, M. [1992], A three-dimensional infinite element for modelling open-boundary field problems, *IEEE Transactions on Magnetics* **28**(2), 1675–1678.

Grover, F. W. [1973], *Inductance Calculations*, Dover Publications, New York.

Hammond, P. [1981], *Energy Methods in Electromagnetism*, Clarendon Press, Oxford.

Hammond, P. [1982], Use of potentials in calculation of electromagnetic fields, *IEE Proceedings, Part A* **129**(2), 106–112.

Hedlund, R. and Nou, P. [1989], An assessment of current finite element formulations in computational magnetostatics, Technical report, University of Florida, Gainesville, FL 32611.

Hoole, S. R. H., Rios, R. and Yoganathan, S. [1988], Vector potential formulations and finite element trial functions, *International Journal for Numerical Methods in Engineering* **26**, 95–108.

Hughes, T. J. R. [1987], *The Finite Element Method*, Prentice-Hall, Inc., Englewood Cliffs, NJ.

Imhoff, J. F., Meunier, G. and Sabonnadiere, J. C. [1990], Finite element modelling of open boundary problems, *IEEE Transactions on Magnetics* **26**(2), 1228–1231.

Jackson, J. D. [1962], *Classical Electrodynamics*, Wiley, New York.

Johnson, C. [1987], *Numerical Solution of Partial Differential Equations by the Finite Element Method*, Cambridge University Press, New York.

Jona, F. and Shirane, G. [1962], *Ferroelectric Crystals*, The Macmillan Company, New York.

Kellog, D. O. [1953], *Foundations of Potential Theory*, Dover Pub. Co., New York.

Kikuchi, F. [1987], Mixed and penalty formulations for finite element analysis of an eigenvalue problem in electromagnetism, *Computers Methods in Applied Mechanics and Engineering* **64**, 509–521.

Kraus, J. D. [1984], *Electromagnetics*, 3rd edn, McGraw-Hill, New York.

Langford, J., Srinivas, V. and Vu-Quoc, L. [1995], Finite element modelling of advanced multilayer ceramic capacitors using clesm modulef., Technical report, Aerospace Engineering, Mechanics & Engineering Science, University of Florida, Gainesville, FL 32611.

Lee, P. [1993], A lagrange multiplier method for the interface equations from electromagnetic applications, *SIAM Journal of Numerical Analysis* **30**(2), 478–506.

Lee, R. L. and Masfen, N. K. [1990], A mixed finite element formulation for maxwell's equations in time domain, *Journal of Computational Physics* **88**, 284–304.

Lerch, R. [1990], Simulation of piezoelectric devices by two- and three-dimensional finite elements, *IEEE Transaction on Ultrasonics, Ferroelectrics, and Frequency Control* **37**(2), 233–247.

Lowther, D. A. and Silvester, P. P. [1986], *Computer Aided Design in Magnetics*, Springer-Verlag, New York.

MacNeal, B. E., Brauer, J. R. and Coppolino, R. N. [1990], A general finite element vector potential formulation of electromagnetics using a time-integrated electric scalar potential, *IEEE Transactions on Magnetics* **26**(5), 1768–1770.

MacNeal, B. E., ed. [1989], *MSC/EMAS Modellling Guide*, The MacNeal-Schwendler Corporation, Los Angeles, CA.

MacNeal, B. E., ed. [1992], *MSC/EMAS Application Manual*, The MacNeal-Schwendler Corporation, Los Angeles, CA.

Marutake, M. [1956], A calculation of physical constants of ceramic barium titanate, *Journal of the Physical Society of Japan* **11**(8), 807–814.

Mason, W. P. [1948], Electrostrictive effect in barium titanate ceramics, *Physical Review* **74**(9), 1134–1147.

Maugin, G. A. [1980], The method of virtual power in continuum mechanics: applications to coupled fields, *Acta Mechanica* **35**, 1–70.

Mayergoyz, I. D. [1993], Some remarks concerning electromagnetics potentials, *IEEE Transactions on Magnetics* **29**(2), 1301–1305.

McDonald, B. H. and Wexler, A. [1972], Finite-element solutions of unbounded field problems, *IEEE Transactions on Microwave Theory and Techniques* **MTT-20**(12), 841–847.

Merz, J. W. [1953], Double hysteresis loop in $BaTiO_3$ at the Curie point, *Physical Review* **91**(3), 513–517.

Mesquita, R. C. and Bastos, J. P. A. [1992], An incomplete gauge formulation for 3d nodal finite-element magnetostatics, *IEEE Transactions on Magnetics* **28**(2), 1044–1047.

Monk, P. [1992], A finite element method for approximating the time-harmonic maxwell equations, *Numerische Mathematik* **63**, 243–261.

Monk, P. [1993], An analysis of Nédélec's method for the spatial discretization of Maxwell's equations, *Journal of Computational and Applied Mathematics*.

Morisue, T. [1993], A comparison of the coulomb gauge and the lorentz gauge magnetic vector potential formulations for 3d eddy current calculations, *IEEE Transactions on Magnetics* **29**(2), 1044–1047.

Morweiser, W. and Meunier, G. [1994], The characterization of passive multilayer componenets by electromagnetic field computation, *IEEE Transactions on Magnetics* **30**(5), 3012–3015.

Morweiser, W., Meunier, G. and Salze, H. [1994], Computer-aided design of passive multilayer components using electromagnetic field computation, *IEEE Transactions on Components, Packaging and Manufacturing Technology–Part A* **17**(3), 338–343.

Moulson, A. J. and Herbert, J. M. [1990], *Electroceramics: Materials, Properties, Applications*, Chapman & Hall, New York.
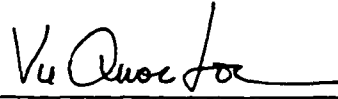
Nakata, T., Takahashi, N., Fujiwara, K. and Shiraki, Y. [1990], Comparison of different finite elements for 3-d eddy current analysis, *IEEE Transactions on Magnetics* **26**(2), 434–437.

Ngo, K. D. T. [1990], 'Multilayer capacitor suitable for substrate integration and multimegahertz filtering', *United States Patent.* Patent No. 4,949,217.

Ngo, K. D. T. [1992], 'Lumped parameter model for a multilayer ceramic capacitor', *Private Communication.*

Penman, J., Grieve, M. D. and Wilson, A. F. [1986], On the solution of open boundary field problems using the finite-element method, *IEE Proceedings, Part A.*

Prymak, J. and Martin, A. [1989], Customizing multilayer ceramic capacitor chips, *Electronic Engineering Times* pp. 57–88.

Ramahi, O. M. and Mittra, R. [1991], Finite element solution for a class of unbounded geometries, *IEEE Transactions on Antennas and Propogation* **39**(2), 244–250.

Ren, Z., Bouillault, F., Razek, A. and Verite, J. C. [1988], Comparison of different boundary integral formulations when coupled with finite elements in three dimensions, *IEE Proceedings, Part A* **135**(8), 501–507.

Sabonnadiere, J. L. C. [1987], *Finite Element Methods in CAD: Electrical and Magnetic fields*, Springer-Verlag, New York.

Sarjeant, W. J. [1990], Capacitors, *IEEE Transactions on Electrical Insulation.*

Silvester, P. P. and Ferrari, R. L. [1983], *Finite Element for Electrical Engineers*, Cambridge University Press, New York.

Simkin, J. and Trowbridge, C. W. [1979], On the use of the total scalar potential in the numerical solution of field problems in electromagnetics, *International Journal for Numerical Methods in Engineering* **14**, 423–440.

Smolenskii, G. A., Bokov, V. A., Isupov, V. A., Krainik, N. N., Pasynkov, R. E. and Sokolov, A. I. [1984], *Ferroelectrics and Related Materials*, Gordon and Breach Science Publishers, New York.

Srinivas, V. [1992], In search for a phenomenological modal for single-crystal barium titanate that agrees with experiments: A semi-infinite optimization approach, Master's thesis, University of Florida, Gainesville, FL.

Srinivas, V. and Vu-Quoc, L. [1992], Toward an accurate phenomenological model for all 4 phases of barium titanate that agrees with experiments: A semi-infinite optimization approach, Technical Report AeMES-TR-92-1-03, Aerospace Engineering, Mechanics & Engineering Science, University of Florida, Gainesville, FL 32611.

Srinivas, V. and Vu-Quoc, L. [1995], Accurate phenomenological models for all four phases of $BaTiO_3$ via semi-infinite optimization, *Ferroelectrics* **163**, 29–57.

Stratton, J. A. [1941], *Electromagnetic Theory*, McGraw-Hill, New York.

Toledano, P., Fejer, M. M. and Auld, B. A. [1983], Nonlinear elasticity in proper ferroelastics, *Physical Review B* **27**(9), 5717–5746.

Vu-Quoc, L. and Srinivas, V. [1994], A new methodology to obtain accurate models for ferrolectrics with application to $BaTiO_3$, *IEEE Transactions on Dielectrics and Electrical Insulation* **1**(2), 196–212. Erratum: *IEEE Transactions on Dielectrics and Electrical Insulation*, Vol. 1, No. 4, p. 757.

Vu-Quoc, L. and Srinivas, V. [1996], Semi-infinite optimization formulation to obtain accurate phenomenological models for all phases of ferroelectric-ferroelastic crystals, *IEEE Transactions on Ultrasonics, Ferroelectrics, and Frequency control* **43**(1), 176–190.

Wangsness, R. K. [1986], *Electromagnetic Fields*, 2nd edn, Wiley, New York.

Williamson, S. and Chan, E. K. C. [1993], Three-dimensional finite element formulation for problems involving time-varying fields, relative motion, and magnetic saturation, *IEE Proceedings, Part A* **140**(2), 121–128.

Yurkevich, V. E. and Rolov, B. N. [1986], Thermodynamic model of phase transitions in ferroceramics, *Ferroelectrics* **68**, 265–273.

Zienkiewicz, O. C. and Taylor, R. L. [1989], *The Finite Element Method*, 4th edn, McGraw-Hill, New York.
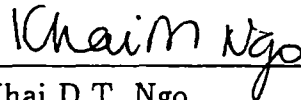
BIOGRAPHICAL SKETCH

Vinay Srinivas was born on July 7, 1968, in Hassan, India. He received his Bachelor of Technology in aeronautical engineering from Indian Institute of Technology, Bombay, India, in 1989. In 1992, he was awarded a M.S. degree in aerospace engineering at University of Florida for his thesis work on the development of a new methodology based on semi-infinite optimization for obtaining accurate models for ferroelectric materials. Since then he has been pursuing a Ph.D. degree in engineering mechanics at University of Florida. His research interests include computational electromagnetics, optimization, and finite element methods.

253

I certify that I have read this study and that in my opinion it conforms to acceptable standards of scholarly presentation and is fully adequate, in scope and quality, as a dissertation for the degree of Doctor of Philosophy.
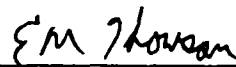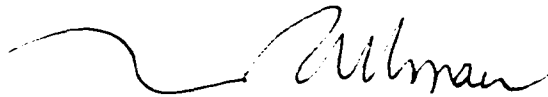
_____

Loc Vu-Quoc, Chairman
Associate Professor of
   Aerospace Engineering, Mechanics,
   and Engineering Science

I certify that I have read this study and that in my opinion it conforms to acceptable standards of scholarly presentation and is fully adequate, in scope and quality, as a thesis for the degree of Doctor of Philosophy.

_____

Khai D.T. Ngo
Associate Professor of
   Electrical and Computer Engineering

I certify that I have read this study and that in my opinion it conforms to acceptable standards of scholarly presentation and is fully adequate, in scope and quality, as a dissertation for the degree of Doctor of Philosophy.

_____

Ewen M. Thomson
Associate Professor of
   Electrical and Computer Engineering

I certify that I have read this study and that in my opinion it conforms to acceptable standards of scholarly presentation and is fully adequate, in scope and quality, as a dissertation for the degree of Doctor of Philosophy.
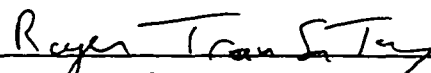
Martin Uman
Professor of
   Electrical and Computer Engineering

I certify that I have read this study and that in my opinion it conforms to acceptable standards of scholarly presentation and is fully adequate, in scope and quality, as a dissertation for the degree of Doctor of Philosophy.

Nicolae Cristescu
Graduate Research Professor of
   Aerospace Engineering, Mechanics,
   and Engineering Science

I certify that I have read this study and that in my opinion it conforms to acceptable standards of scholarly presentation and is fully adequate, in scope and quality, as a dissertation for the degree of Doctor of Philosophy.
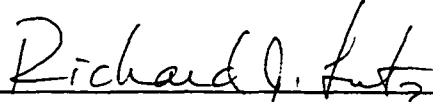
Roger Tran-Son-Tay
Associate Professor of
   Aerospace Engineering, Mechanics,
   and Engineering Science

This dissertation was submitted to the Graduate Faculty of the College of Engineering and to the Graduate School and was accepted as partial fulfillment of the requirements for the degree of Doctor of Philosophy.

May 1996

Winfred M. Phillips
Dean, College of Engineering

Karen A. Holbrook
Dean, Graduate School